AERODYNAMICS OF HIGH PERFORMANCE TURBINE BLADING

P.I. KING

MERTON COLLEGE

OXFORD

MARCH, 1986

A thesis submitted for the degree of Doctor of Philosophy
at the University of Oxford

Department of Engineering Science
Parks Road
Oxford

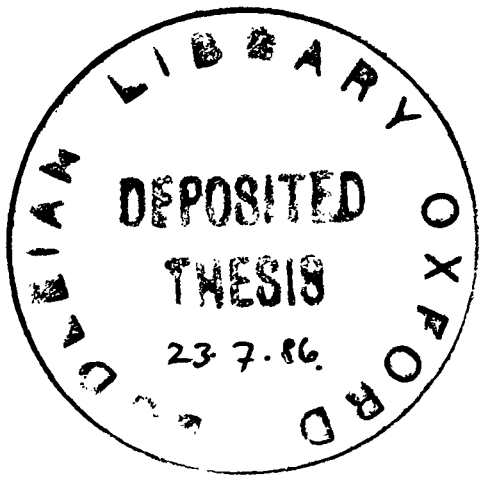

TO MY BELOVED CATHERINE

AERODYNAMICS OF HIGH PERFORMANCE TURBINE BLADING

P.I. King, Merton College

A thesis submitted for the degree of Doctor of Philosophy
at the University of Oxford, March, 1986

ABSTRACT

A major addition to European research facilities is the Oxford University Engineering Laboratory (O.U.E.L.) blowdown tunnel which can provide full-scale Reynolds and Mach number simulations on large and small models of turbine stage components. The facility was designed to provide extended aerodynamic capabilities to complement the existing heat transfer research in the Isentropic Light Piston Tunnel (ILPT) at O.U.E.L. The blowdown tunnel will be used for fundamental investigations of the boundary layers and flow fields around turbine blades in a linear cascade. The study of these flow fields is necessary for the prediction of heat transfer rates and for the optimisation of materials and cooling schemes required to improve gas turbine efficiencies.

As a commissioning exercise measurements were made on cascades of similar geometry to those which had been previously tested in the ILPT and in other European facilities in order to compare results and analyse differences which occur due to the influence of tunnel geometry. Measurements made on various rotor profiles identified regions on the suction surface where surface pressure data is sensitive to the various types of exit plenums and exit pressure gradients.

A second phase of work included measurements and a theoretical study of the boundary layer on a large-chord turbine rotor profile. Measurements on the pressure surface of the blade suggested the presence of secondary longitudinal vortices which rapidly lose an identifiable structure towards the trailing edge. On the suction surface, boundary layer measurements were compared with theoretical models, and it was shown that current numerical models of compressible turbulent boundary layers approximately correspond with the data. An adjunct to the boundary layer work was research on the use of a hot-wire anemometer, intended for future boundary layer measurements, and for which calibration laws and temperature effects were studied.

ACKNOWLEDGEMENTS

The work for this thesis was performed at the Osney Laboratory of the Department of Engineering Science, Oxford University. The funding for the development of the blowdown tunnel, the commissioning work and the subsequent research was provided by the Science and Engineering Research Council and Rolls-Royce Ltd. whose support and advice is gratefully acknowledged. A debt is also owed to a large number of people at the Osney Laboratory.

Thanks is especially given to Dr. N.C. Baines and Professor D.L. Schultz who guided the research and provided helpful suggestions and sound advice. They also provided a detailed reading of the text and offered many suggestions which improved the final draft.

During the period of the research valuable assistance was offered by Dr. M.L.G. Oldfield and Dr. T.V. Jones, and the writer is grateful for their time and effort.

The day-to-day operation of the blowdown tunnel was supported by John Allen who assisted in all phases of the author's research and whose untiring efforts helped the experimental programme remain on course.

Daily discussions occurred with other students in the laboratory, and this created a stimulating environment. R.J.G. Norton, F.G. Horton, D.J. Doorly, and D.G. Henshaw are thanked for their support and encouragement.

Thanks is given to the workshop group for manufacturing support, and a special thanks goes to Tom Norman who seemed always to respond instantly and expertly to the author's requests.

Many others of the Osney Laboratory staff contributed to the author's research; Keith Walton, Kevin Grindrod and Trevor Godfrey are thanked.

Finally, there are no words to adequately express my feelings for C.L.K., who brings sunshine to those around her.

C O N T E N T S

C O N T E N T S

(continued)

C O N T E N T S

(continued)

P R I N C I P A L N O T A T I O N

The most commonly used symbols are defined below. In some cases the defining equations are given, and in some cases, where the symbols have more than one meaning, an explanation is provided. Symbols which appear only briefly in the text and which only serve to clarify a particular statement are defined within their context.

A	Coefficient in King's law; used also as surface area
A^*	Sonic throat area
atm	One standard atmosphere, 1.01325×10^5 Pascals
AVDR	Axial-velocity density ratio
B	Coefficient in King's law
BTU	British thermal unit
bar	1×10^5 Pascals
C	Coefficient in King's law; degrees Celsius; constant in wall-wake law, eqn.3.6
C_f	Friction coefficient, eqn.3.2
c	Chord
cax	Axial chord
c_p, c_v	Specific heat at constant pressure and volume, respectively
d	Hot-wire diameter
E	A law-of-the-wall function defined in eqn.5.19
eff	compressor efficiency
F	Reynolds number per meter, eqn.5.11
f	A function of Mach number defined in eqn.5.6
ft	feet
G	A hot-wire parameter defined in eqn.4.5
G_{δ_2}	Goertler number, eqn.5.8
G_{tr}	Value of Goertler number at flow transition
H	Boundary layer shape factor, eqn.3.3
Hz	Frequency, $seconds^{-1}$
h	Heat transfer coefficient; hot-wire end-conduction factor, eqn.4.12
hp	Horsepower
i_w	Hot-wire electrical current
J	Joules
K	Acceleration parameter, eqn.5.4; Von Karman constant, 0.4; degrees Kelvin

K_i	A function which indicates conformity to 2-D flow, eqn.6.3
k	Thermal conductivity
k_f	Thermal conductivity of the fluid
kg	Kilograms
k_t	Turbulent conductivity
L	Hot-wire length
L/D	Length-to-diameter ratio
l	Turbulent mixing length
lbm	Pound mass (English system)
M	Mach number; prefix representing $1x10^6$
m	Meter; a function of Mach number, eqn.3.8
$\dot{m}$	Mass flow rate
mf	Mass fraction
min	Minutes
mm	$1x10^{-3}$meters
Nu	Nusselt number
Nu_e	Effective Nusselt number, eqn.4.13
Nu_f	Free-convection Nusselt number
n	Exponent in King's law
P	Pressure
Pr	Prandtl number
Pr_t	Turbulent Prandtl number, eqn.3.15
R	Gas constant; radius of curvature, eqn.5.8; degrees Rankine
Re	Reynolds number
$R_{w,a,o}$	Hot-wire resistance: general, at ambient temperature, at 0^oC, respectively
$R_{c,co}$	Cable excess resistance and offset resistance, respectively
R_{pr}	Prong resistance
R_T	Bridge arm resistance
R_v	Decade resistance
r	Recovery factor, eqn.5.16; prong temperature factor, eqn.4.16
Sp	Pressure surface length
s	seconds; blade surface distance
T	Temperature
T_f	Film temperature
Tu	Turbulence intensity, u'/U
T_w	Hot-wire temperature
U	Freestream velocity

UV	Ultra-violet
u	Local mean velocity
u'	Fluctuating streamwise velocity
u^*	Van Driest equivalent velocity, eqn.3.7
u_τ	Friction velocity
$V_{b,bo}$	Bridge-top voltage: with flow and at zero flow, respectively
v'	Fluctuating normal velocity
W	Coles' wake function, eqn.3.9
w	Cascade relative velocity
X/M	Non-dimensional distance behind a bar grid, distance/bar spacing
x	Blade coordinate
y	Boundary layer normal direction; blade coordinate
β	Cascade relative flow angle
γ	Ratio of specific heats, c_p/c_v
δ	Boundary layer 99% thickness
δ_1	Displacement thickness, eqn.3.4
δ_2	Momentum thickness, eqn.3.5
η	Turbine total-to-total efficiency
μ	Dynamic viscosity
μm	Microns ($1x10^{-6}$m)
ν	Kinematic viscosity
Π	Profile parameter, eqn.3.6
ρ	Mass density
τ	Shear stress
Ω	Ohms

SUBSCRIPTS

aw	Adiabatic wall
cas	Cascade
e	Freestream
ej	Ejector
ej_1	Ejector one, annular
ej_2	Ejector two, discrete nozzles
ex	Cascade exit plane
g	Gas
in	Compressor inlet

o	Stagnation condition or total condition
out	Compressor outlet
reg	Regulator
s	Supply valve; isentropic state
stdn	Static pressure at the cascade exit
supply	Valve upstream of regulator
t	Tank
tank	Valve upstream of the working section plenum
th	Theoretical
tr	Transition
w	Wall (surface) location
x	Axial direction
1	Upstream of the cascade
2	Downstream or exit plane
∞	Infinity

CHAPTER I

INTRODUCTION

1.1 CENTRAL ISSUES IN THIS THESIS

The investigations reported in this thesis concern two main topics. Firstly, the development, commissioning, and initial testing of a new blowdown wind tunnel at the Oxford University Engineering Laboratory (O.U.E.L.). Secondly, the initial tests on a large chord version of a highly loaded, high-pressure rotor blade, profile 'B22', previously tested in the Isentropic Light Piston Tunnel (ILPT) by NICHOLSON(1981).

The development of the blowdown tunnel is the result of efforts of the Oxford turbomachinery group (led by D.L.Schultz, M.L.G.Oldfield, and T.V.Jones) to add new, large-scale capabilities in aerodynamic research on turbine section components to complement those already existing in heat transfer and smaller scale aerodynamic testing in the ILPT.

The period over which the work in this thesis took place spanned the time when the new blowdown tunnel was in its final construction stages. Of necessity then, the major portion of this author's work was devoted to the design, calibration, and functional testing of various components of the tunnel. These tasks included such subjects as the design and installation of the second ejector system, the calibration of the high pressure valves, the design of the measurement systems, and the writing of miscellaneous computer software.

The first efforts in commissioning the tunnel were focused on the inlet flow conditioning system. This is a vital area of the tunnel and considerable time was spent correcting deficiencies in flow uniformity and cascade periodicity. These efforts were to pay off later when experimental

models were interchanged and setting up time was reduced.

An important series of tests following the inlet studies were the studies on profiles previously tested in either the ILPT or in other facilities in Europe. These tests were intended to verify previous data and to identify any tunnel-induced characteristics in the data. The blowdown cascade is a major addition to European research facilities, and it was thus important that its performance be checked against other similar cascades. Thus, a nine-blade version of the B22 profile tested in the ILPT by Nicholson was studied in the new tunnel. Also tested was a transonic turbine cascade, the VKI-1, a profile designed at the Von Karman Institute and previously tested at DFVLR, Braunschweig. This latter series of tests produced a large amount of data of which only a small portion appears in this thesis. The results of the VKI-1 tests deal specifically with differences in data between the two tunnels involved, the O.U.E.L. blowdown tunnel and Braunschweig high-speed cascade tunnel.

The last work in the blowdown tunnel performed by the author was the initial testing of a large chord version of the profile, B22, a model for which the use of the full capabilities of the tunnel had been intended. These tests were concerned with the measurement of fine-grid surface pressure data and the examination of boundary layer behavior on both surfaces of the airfoil. Included with the boundary layer tests is theoretical and numerical work on boundary layer theory.

Finally a last phase of work reported in this thesis are the efforts to update in the O.U.E.L. capabilities to perform hot-wire velocity measurements in the new blowdown facility. The use of hot wires in a transient test environment under conditions of sub-atmospheric pressures and compressible flow regimes complicate the calibration procedures, and thus a systematic examination of the important independent variables was carried out. These studies, conducted in a low speed wind tunnel under

standard environmental conditions, may be of value for further studies in the blowdown tunnel. The results of the hot wire work are reported in chapter four.

All of the work mentioned above brought into play an examination of principles involving the fluid dynamics of turbomachinery and the application of test data to the successful design of turbine components. The following sections of this chapter are, therefore, devoted to aspects of turbine performance and the testing of turbine components in facilities such as the O.U.E.L. blowdown tunnel.

1.2 THE ROLE OF THE TURBINE IN JET ENGINES

Consider the ideal gas generator (Brayton cycle), figure 1.1, the thermodynamics of which are common to all turbomachines. The cycle consists of four processes: a) adiabatic compression, b) heating at constant pressure, c) adiabatic expansion (with work extracted), and d) heat rejection at constant pressure, usually taking place in the atmosphere.

That portion of the cycle devoted to work extraction is performed by the turbine, a component currently at the focal point of extensive research. The work performed by this component is done by removing kinetic energy from hot, expanding gases which have flowed from the combustion chamber into a stationary nozzle just ahead of the turbine rotor. Up to 75% of all the fuel energy added to the air flowing through the engine is used by the turbine to drive the compressor and accessories.

Turbine performance has a major effect on engine performance in two ways. The first concerns its ability to convert energy available at the turbine entrance into shaft work. Losses from such phenomena as profile drag resulting from skin friction and boundary layer separation, shock losses (in the case of transonic turbines), coolant mixing losses, secondary flows and leakages all combine to lower the total pressure and

temperature below that caused by the extraction of shaft work alone. These losses are accounted for in the total-to-total efficiency defined as,

$$\eta_{tt} = (T_{o4}-T_{o5})/(T_{o4}-T_{o5s}) \qquad \ldots 1.1$$

The temperatures in equation 1.1 correspond to those in figure 1.2.

A second major impact on engine performance is the value of turbine entry temperature (TET), the average gas temperature at the inlet to the first stator vane. The maximum allowed TET is constrained by blade materials and blade cooling effectiveness. The benefit to engine performance of a high value of TET is seen by examining two competing aircraft mission requirements, not necessarily on the same aircraft.

The first is the cruise portion of the mission where low fuel consumption is required. OATES(1984) has shown that fuel consumption decreases (thermal efficiency increases) for a given flight Mach number when the compressor pressure ratio is increased. For a fixed TET however, this limits fuel addition and thus reduces specific thrust (thrust/air mass flow rate). An increased TET would avoid the larger and heavier engine needed to recover thrust at the increased pressure ratio.

A second mission requirement is encountered by tactical fighter aircraft, i.e., a requirement for a high specific thrust at a given compressor ratio and flight Mach number. A higher TET in this case would allow for increased fuel addition and a gain in specific thrust (and total thrust). Newer designs for tactical aircraft have also taken advantage of increased TET's to allow higher compressor pressure ratios for better fuel economy in the cruise phase of a tactical mission. It should be noted that an engine designed for the high specific thrust needed for, say, an escape manoeuvre would be over-powered for the cruise portion of the flight. So, in practice, afterburning is used to achieve short-duration bursts of very high values of specific thrust.

Current values of TET range up to approximately 1700K. For example, the Pratt & Whitney JT9D turbofan engine used on the Boeing 747 aircraft has a TET of 1645K (DRING and HEISER(1978)). Above a value of about 1200K, however, turbine blades must be cooled, and thus the rise in TET has stimulated research in blade cooling technology. This has created an attendant research interest in detailed boundary layer flows with the aim of producing reliable prediction techniques for local heat transfer coefficients and coolant mixing dynamics.

New cooling technology will concentrate on specific problems (notably the regions near the blade leading and trailing edges) with an emphasis on less (or even no) coolant mass usage and lower mixing losses. This will require a thorough understanding of internal passage flows and external, interactive effects of coolant injection with downstream boundary layer behavior. It is the need to understand better the boundary layer on a turbine blade in general that provided the impetus for the development of the new O.U.E.L. blowdown tunnel for large chord model testing.

1.3 TURBINE RESEARCH

1.3.1 Turbine Loss Mechanisms

Much current turbine research is concerned with three of the major loss mechanisms: (a) uncooled or baseline aerodynamic losses, (b) aerodynamic losses from coolant mixing, and (c) thermodynamic losses of total temperature (available work) due to coolant injection.

Uncooled losses are those associated with an irreversible fall in the total pressure in three regions in the turbine: (1) around the blade profile, (2) at the endwalls (hub and tip), and, as one group, (3) all those other regions where, because of mechanical/structural gaps the flow can exit and re-enter the main stream.

Profile losses are those due to skin friction, boundary layer

separation, base pressure deficit (form drag), and shock formation. These losses depend mainly on the shape of the profile (the shape being designed to meet certain lift distribution requirements or to conform to structural constraints). These baseline losses will exist in cooled or uncooled turbine stages and are the type for which 2-D cascade testing can yield valuable design information.

Endwall and leakage (or parasitic: DRING and HEISER(1978)) losses arise from three-dimensional geometrical effects and are also influenced to a large degree by turbine rotation. For example, in the hub region at the leading edge there is formed a vortex, the horse-shoe vortex, whose axis is aligned with the flow direction and which wraps around the leading edge of the blade. This vortex will occur in either a static or rotational environment and much interest has risen in its effect on the main passage flow (LANGSTON et al.(1978) and SIEVERDING(1984)). In a static environment vortices such as this sweep fluid toward the suction surface leaving behind a boundary layer which is thinned and skewed. The vortices also mix with the main flow, especially in a design with small aspect ratio, and cause fluid to be transported between streamtubes in the meridional plane (and thus possibly corrupt the assumption used in the design of the profile). In a rotating environment the initial boundary layer formation is skewed (DRING and HEISER(1978)), and there is a further influence due to the radial pressure gradient. Static studies are useful in understanding the basic mechanism of formation of these vortices, but rotational effects must inevitably be introduced to understand the effect on tip/hub unloading and mainstream mixing losses.

Leakage losses occur in several locations. In the tip region of an unshrouded rotor gases flow from the pressure surface to the suction surface between the tip and casing, causing a mixing loss. Also, in the circumferential gaps between rotor platforms, in the gaps between labyrinth

seals on unshrouded rotor casings, and in the space between rotating discs there are regions where gases can leave the main flow and return downstream causing further mixing losses. The study of these loss mechanisms require the centrifugal effects of a rotating turbine stage.

The second major source of aerodynamic losses, (b) above, occurs in cooled turbine designs. Cooling air injected into the flow to protect the blade surface interrupts the natural boundary layer formation and can adversely affect the profile losses. Also, as a result of coolant mixing with the main stream flow, total pressure losses occur, reducing the availability of kinetic energy conversion in the exhaust stream. Both convective cooling and film cooling losses are amenable to study on a stationary, 2-D cascade (SCHULTZ et al.(1977)), but for the study of specific profile designs and cooling schemes it would make sense to utilize the rotating stage for a complete simulation of radial pressure-induced mixing effects (cf. SUO(1978)).

Thermodynamic losses referred to at the beginning of this section stem from injected coolant which reduces the total temperature of the main flow, and thereby causes a loss in weight-specific work capability. Unlike the analysis of losses in total pressure from coolant mixing, however, thermal losses are readily calculated and in general do not require specialized testing other than to determine how the mixing process itself is affected by such phenomena as secondary flows and rotation.

A discussion of losses should not be completed without mentioning that freestream turbulence plays an important role in all of the above loss mechanisms. There is room for an extensive amount of research on this subject, and the linear cascade would seem to be the natural instrument for this research. Fundamental studies with closely controlled variables would be required so that such processes as transition, pressure gradient effects and surface curvature effects could be more readily understood and

predicted.

1.3.2 Dynamic Similarity Requirements in the Turbine Cascade Test

Ideally, tests performed to examine the flows in turbomachinery should simulate the pressure/temperature environment of the actual engine flow as nearly as possible. The properties of the test gases (thermal conductivity, specific heat, etc.) should also exhibit the same pressure-temperature dependencies as the gases in the actual flow environment. For experiments in other than actual flow conditions the experimental data are still applicable to engine flows if certain similarity parameters are maintained. The principal feature of similarity testing is that competing gas effects are made to occur in proportion to their occurence in the actual engine environment. The correct parameters are revealed from the non-dimensional forms of the conservation equations and non-dimensional boundary conditions, and they influence the use of experimental results. The required similarity parameters are listed in the following table.

Similarity Parameters Required in Turbine Testing

Geometry (model shape and roughness)	x/c, y/c
Reynolds Number	Ux/ν
Prandtl Number	$\mu c_p/k$
Eckert Number, or equivalently,	
Mach Number	$U/\sqrt{\gamma RT_e}$
Specific Heat Ratio	γ
Temperature Ratio	T_w/T_e
Freestream Turbulence (intensity and scale)	Tu, l/c
Boundary Conditions:	
Nusselt Number (see the discussion below)	
Various Coolant-to-Gas Temperature Ratios	

The Grashof similarity parameter (buoyancy effect) is ignored.

From the momentum and energy equations come the requirements for equality in Reynolds number, Prandtl number and Eckert number (and Grashof number, which is neglected) for flows involving viscous effects and variable temperature (cf. WHITE(1974)). For flows at approximately adiabatic conditions the Eckert similarity condition reduces to required equality in Mach number and specific heat ratio. For flows where heat transfer at the blade wall is important then the Eckert number will include the wall-to-freestream temperature ratio. If heat transfer at the wall is a free variable, i.e., not a specified quantity, then the Nusselt number is an outcome of the experiment, like the skin-friction coefficient, and not a constraint requiring control by experimental setup. Finally, if film cooling is used then ratios involving coolant temperature, mass flux, and momentum flux are introduced. See DANIELS(1979) or COLLADAY and STEPKA(1974).

The freestream turbulence shown in the table above is currently the subject of research at various institutions, and its effects on turbine passage aerodynamics are not fully understood. Least understood are the effects of the scale of the turbulence, the integral lengths of the mean flow and the microscale, or lengths associated with small-scale dissipation, and their influence on the friction and heat transfer occurring at the surface of the blade. Further, until more is known about turbulence scale effects in the engine, simulation of this effect in the cascade test cannot be done.

It was assumed that, at least in the early years of operating the new blowdown tunnel, experiments would focus on aerodynamic effects attributable to cascade geometry, i.e., profile and form drag and

shock/boundary-layer phenomena. Thus, aerodynamic measurements reported in this thesis concern turbine profiles which were uncooled and on which aerodynamic phenomena, at approximately adiabatic conditions, were of primary interest. The variables from the table above requiring similarity include, therefore, all values except for the temperature ratio, T_w/T_e.

Most of the parameters from the table above are accurately simulated. Simulation of the Reynolds number and Mach number is the main feature of the blowdown tunnel. The Prandtl number is a free variable, but its value (roughly 0.71) will not differ appreciably from the value for combustion products (approximately 0.75). The correct turbulence intensity is introduced via a bar grid located upstream of the cascade, and the scale of the turbulence, as suggested above, remains a free variable. Thus, all parameters will be approximately simulated except for the specific heat ratio, which for air (1.4) is approximately 9% lower than the value for combustion gases (approximately 1.27). Fortunately, the effect of differing specific heat ratios is weak. For example, using the value for air as 1.4 and the engine mixed-out gas value as 1.27, it can be shown that for a freestream Mach number equal to 0.5, say, the difference in static-to-total pressure ratios is about 1.5%. For a Mach number of 1.15 this difference is about 5%. The change in Mach number across a normal shock is negligibly different for the two cases, less than 0.25% for an upstream Mach number equal to 1.15. Also the Prandtl-Meyer angle differs only by about 0.12^{o}. This weak dependence on specific heat ratio implies that important flow effects (shocks, expansions, friction drag, etc.) which occur in transonic turbines can be accurately simulated in the static test using room air as the test gas.

For the design of a new cascade model the similarity parameters can be used to solve simultaneous equations to obtain operating pressures and temperatures. An example of the use of these ideas is given in section 1.4,

below, where the power advantages of transient testing are discussed.

1.4 TRANSIENT CASCADE TESTING

1.4.1 Power Advantages: Stationary Cascade

A transient test facility, such as the O.U.E.L. ILPT or blowdown tunnel, has a major cost advantage over a continuous flow facility. The lower power required in transient testing results in a simpler design with less expensive construction costs and reduced operating expenses. For example, consider the power that would be required to drive the current blowdown tunnel in a continuous mode with the large chord B22 model installed (this is a reasonable question since with the tunnel now in place one would only modify the existing configuration for continuous flow). Operating the tunnel as a blowdown the cascade air temperature is roughly room temperature with inlet stagnation pressure at 0.42bar. For continuous operation a compressor system would be required, which would have the additional effect of heating the air upstream of both cascade inlet and ejector(s) (presumably the compressor would provide air for both). The use of heated inlet air would require a higher stagnation pressure (higher than 0.42bar) in the working section (since Reynolds number/pascal decreases with increased temperature at constant Mach number). However, by allowing the air to enter uncooled a loss-producing cooling system would not be needed. Indeed if the cascade inlet temperature was sufficiently high the pressure at the cascade exhaust would be increased to a value that could be obtained without the need for downstream ejector flow. The inlet temperature required for this last condition can be calculated assuming the exhaust pressure to be 0.7atm (the tunnel will self-pump with an exhaust pressure of approximately this value). Based on an isentropic exit Mach number of unity and a Reynolds number of 2×10^6 based on true chord and exit Mach number, the required inlet temperature is 725K. A high-pressure axial

flow compressor operating between atmospheric pressure and temperature and 725K would require an overall pressure ratio of approximately 19 (assuming 85% efficiency and needing perhaps 12 stages) to reach this temperature (combustion heating will not be considered), reaching an exhaust pressure which would have to be throttled down to the desired value of 1.35atm. This rather extreme case is avoided if the inlet air is cooled. With cooled air at the cascade inlet, ejector pumping would be required to reduce the exit static pressure, but high-temperature strucural problems would be avoided. It is of interest (at least academically) to calculate the power required for both cases, heated and cooled cascade inlet air.

Assume a compressor outlet pressure of 20atm for the uncooled case. If the compressor inlet temperature and work efficiency (85% will be used for all examples) are known the outlet temperature (or pressure ratio) can be calculated from (cf. HORLOCK(1966)),

$$T_{out}-T_{in}= (1/eff)(T_{out\ ideal}-T_{in}) \qquad ...1.2$$

which reduces to

$$T_{out}/T_{in}= 1 + (1/eff)(P_{ratio}^{(\gamma-1)/\gamma}-1) \qquad ...1.3$$

In this case the compressor outlet air would be at a temperature, T_{out}=740K. As previously noted, a throttling valve would also be required to reduce the main flow stagnation pressure at the cascade inlet to 1.35atm. Assuming a cascade throat area of 0.08m^2 the required mass flow would be 16kg/s. The power required to drive the compressor ($\dot{m}c_p\Delta T$) would be 7.56MW.

For the second case, if the gas is cooled upstream of the cascade and the ejector system used for reducing the cascade exit pressure then the compressor pressure ratio is reduced to approximately 10 (based on ejector

data). If cooling reduced the cascade inlet temperature to 285K (this could be problematic) the mass flow for a stagnation pressure of 0.42bar would be 8kg/s through the cascade and a similar amount through the ejector. From equation 1.3, T_{out} becomes 600K and the required power to drive the compressor would be 5.1MW, 2.4MW less than using hot compressed gases with no ejector flow.

Neither of the above schemes, however, lends itself to the economy required in a university environment. Considering economy alone, the most sensible system is an intermittent tunnel fed from a high-pressure reservoir. A simple calculation will show that in operating the blowdown for, say, seven seconds the high-pressure reservoir can be replenished in about 20 minutes by a 90hp compressor operating with overall efficiency of 50% and delivering 5kg/min.

One of the main disadvantages in using a continuous flow system in a stationary cascade is the inability to utilize the cascade flow to recover and re-use a portion of the input power. It should be possible then to show that in the case of a fully annular, rotating stage, a power take-off to help drive the compressor will result in less auxiliary power required than that for the stationary cascade. This will be demonstrated in the following section.

1.4.2 Power Required for a Rotating Stage

Consider the use of a fully annular turbine stage (one vane and rotor) to perform heat transfer experiments in a continuously running, closed-loop tunnel in which full engine simulation is required (except, perhaps, for simulation of specific heat ratio which cannot be modelled economically in a non-combusting, continous flow operation). Choose for convenience engine parameters simulated by EPSTEIN et al.(1984) at the Massachusettes Institute of Technology where a turbine cascade of

Rolls-Royce design is currently being tested. Then for a given vane chord size of 59mm all variables are established once a coolant temperature is selected. In this example two cases are of obvious importance; (1) room temperature coolant air and (2), room temperature blade.

In the first case assume the coolant to be at a temperature of 295K. Simulating the engine gas-to-coolant temperature ratio of 2.25 requires the inlet gas total temperature to be 665K. The turbine exit total temperature then scales as the engine temperature ratio 1280/1780 (=0.72) which yields a value of 478K at the turbine exit. With a Reynolds number of 2.7×10^6, a vane chord of 59mm and an exit Mach number of approximately unity, the isentropic turbine inlet total pressure must be 8.3atm. Using the engine total pressure ratio 4.5/19.6 (outlet to inlet) yields a value of 1.9atm for the cascade exit. Finally, mass flow requirements are scaled using appropriate values of pressure, temperature, and chord to yield a value of 25kg/s, scaled down from the engine value of 49kg/s. Assuming gas parameters at the compressor outlet to match the turbine inlet values and a compression efficiency of 85%, the required power input to the compressor and the available power output of the turbine are calculated to be 6.37MW and 4.7MW respectively. Tunnel circuit losses would contribute approximately 0.5MW if the tunnel energy ratio (cf. RAE and POPE(1984)) was assumed to be five, and there would be some additional power required to pump the cooling air. The net work required from an external source would then be approximately 2.17MW, considerably smaller than the power required to run the stationary cascade (although of different scale) considered earlier.

The power required to run a rotating cascade can be reduced further if the choice is made to maintain the blade at a room temperature value. Although this adds a non-trivial task of continuously cooling and pumping low-temperature coolant fluids this may be a worthwhile problem to tackle

if the power savings are substantial. Thus, choosing a blade temperature of, say, 295K and using the engine gas-to-wall temperature ratio of 1.6 (EPSTEIN et al.(1984)) the turbine inlet and outlet total temperatures are calculated to be 472K and 340K, respectively. From the Reynolds number, $2.7x10^6$, the turbine inlet total pressure is 5.5atm and then, from the engine pressure ratio, the turbine exit total pressure is 1.26atm. Using similarity parameters a new mass flow is calculated to be 19.7 kg/s. Finally, using equation 1.3, one calculates the interesting result of 292K for the gas temperature at the inlet to the compressor. The new values of compressor input power and turbine output power are found to be 3.56MW and 2.61MW, respectively. Estimating circuit losses at 0.27MW yields the total power required from an external source to be 1.22MW, slightly more than 1/2 the power required to drive the system with room temperature coolant. This example indicates a significant power reduction from the previous case but, with a required coolant temperature of 210K pumped at a rate of approximately 2.5kg/s, it may not yield a realizable design. Power requirements must be weighed against complexity of design as well as initial capital outlay and other economic factors, all of which increase the risk beyond that reasonable for a university undertaking.

There does not seem to be much interest amongst engine manufacturers for testing in the middle-ground between linear cascades and fully annular, rotating cascades (e.g. stationary sector cascades) and so one must inevitably review the capabilities of the university to provide relevant data for full engine design using equipment that can be run within the small (by comparison) operating budget of the university. In this spirit one must return to the idea of utilizing the capabilities of the 2-D linear cascade as the only practical way for the university to participate in this process. METZGER(1983) summarizes the situation by suggesting that, in general, industry is best suited for engine testing while the university

can best apply its resources to large geometric scale investigations; the role of government should be to support and coordinate those activities. At the moment this does not limit university research as there is an abundance of fluid dynamics not yet understood for which the the use of linear cascades is the only sensible means of investigation.

1.4.3 The Role of the Two-Dimensional Linear Cascade

The stationary, linear cascade seems best suited for large-model experiments in research aimed at understanding fundamentals of flows in turbomachinery. Also any flows which are only weakly three-dimensional can be effectively studied on the linear cascade. This would include, for example, the study of coolant flow from a centre-span hole on the suction surface of a turbine rotor (see DRING et al.(1980)). Any flow situations which are not yet predictable computationally are also candidates for linear cascade research. These include rotor flows with transonic exit conditions and/or cross-channel shock/boundary layer effects with surface reflections and coolant flow interactions.

The effect of high freestream turbulence can be easily studied in the linear cascade where the effects of pressure gradient and curvature can serve as independent parameters. This problem is even more interesting now in view of the recent work of KRISHNAMOORTHY(1982) who was able to induce high levels (18% to 21%) of freestream turbulence and measure strong variations of heat transfer on the pressure surface, a result not seen (or believed) previously. Also the effects of turbulence scale and/or frequency spectrum are not well understood and lend themselves to investigation in the linear cascade. The unpredictable effects of freestream turbulence in general was regarded by BROWN and MARTIN(1974) as an unsolved yet primary ingredient in affecting heat transfer in flows with transition regions and adverse pressure gradients. If such effects are to be isolated and

understood a systematic investigation with carefully controlled parameters is required. A large-chord model used in a linear, 2-D cascade again seems to be the appropriate vehicle.

The O.U.E.L. blowdown tunnel was constructed with the above ideas in mind. A 300mm chord model of a high-pressure, transonic turbine rotor blade was constructed for studying the boundary layer phenomena occurring on the highly curved pressure surface of the blade. Details of the new tunnel, its commissioning, and the preliminary results of tests on the large chord B22 profile follow in subsequent chapters.

1.5 SUMMARY OF CHAPTERS

Following is a brief summary of the remaining chapters.

Chapter two discusses the experimental apparatus and includes a few of the operating features of the blowdown tunnel not previously discussed by BAINES et al.(1982) and BAINES et al.(1984).

In chapter three the experimental programme is outlined and background theory is discussed. This chapter includes a discussion of events leading up to the cascade tests done as part of the commissioning exercise and includes a summary of the numerical codes used for a comparison with cascade data. A discussion of boundary layer theory relating to the measurements on the large-chord profile, B22, is also provided.

In chapter four the results of hot-wire experiments are reported. Included is a brief summary of hot-wire heat transfer theory and a discussion of hot-wire response laws currently used in calibration procedures. Results of measurements of temperature effects are also reported.

Chapter five presents the experimental results obtained for the commissioning exercise, which includes surface pressure data from three

cascades. Also included in this chapter are the results from the first boundary layer measurements on the large-chord blade.

In chapter six, extended discussions of some of the important results from chapter five are given.

The major conclusions drawn from all the experiments are presented in chapter seven.

Two appendices provide supplemental information. In appendix A, a sample calculation for setting the valves and ejectors for a blowdown run is given. Appendix B presents the theory on the numerical smoothing techniques used in the boundary layer studies.

CHAPTER II

EXPERIMENTAL APPARATUS

2.1 THE O.U.E.L. BLOWDOWN FACILITY

2.1.1 Principal Features

Many of the features of the new O.U.E.L. blowdown wind tunnel have been described elsewhere (BAINES et al.(1982)). GOSTELOW(1984) shows two views of the facility including the overall layout and the test section with the 100mm B22 cascade installed. This chapter will therefore be limited to a brief description of a few of the important tunnel components and their operation.

In figure 2.1 is shown a schematic of the blowdown tunnel. Certain pressures and locations have been labeled for future reference. A distinguishing feature of the tunnel is the operator's ability to vary independently cascade Reynolds number and Mach number. This is accomplished by controlling cascade inlet total pressure, P_o, and discharge jet pressure, P_{ex}, using upstream gate valves and in-line tandem ejectors located downstream of the working section plenum. Operation of the ejectors is described in section 2.1.3.

All tunnel air is fed from a high-pressure storage tank through a 12in valve (labeled stop valve in figure 2.1), normally fully open. Cascade mass flow, and hence total pressure, is established by the openings set in the supply valve and tank valve and by the pressure set in the regulator. The regulator is a variable orifice flow meter designed to maintain the driving pressure for the cascade and ejectors at a fixed (adjustable) value. An example of a setting up procedure with sample calculations can be found in Appendix A.

The air reservoir has a capacity of $31m^3$ and is usually pressurized

to a maximum of 27atm at room temperature (on special occasions, when significant mass flow is required, the reservoir is charged to 31atm). A full charge of air amounts to roughly one ton in weight of which up to 25% is normally used during any one run. During reservoir emptying, full regulation and steady flow are maintained in the working section. It is useful to note that all cascades of similar span use roughly the same amount of air regardless of chord size due to the inverse relationship between cascade flow and ejector flow for models of varying chord. This is clearly illustrated in figure 2 of BAINES et al.(1982).

The maximum allowable pressure in the working section plenum is constrained by structural considerations to be 4atm. Since model size and total pressure are inversely related (for a constant Reynolds number and Mach number) and since large chord models are of primary interest in this work, the total pressure constraint is not a limitation.

Some cascade models, because of smaller scale, require that downstream pressure be above atmospheric pressure. For this mode of operation a downstream choke (butterfly valve) is provided and is removed from the tunnel when not in use.

The total running time of the tunnel is composed of three segments, the starting transient, the steady flow portion, and the stopping transient. The starting transient is normally of two to three seconds duration, varying with model size, valve sequencing, and ejector requirements. The duration of the steady flow portion is controlled by the operator and is determined by balancing data acquisition requirements with available air supply. Data acquisition time can be minimized by such measures as the close-coupling of transducers. If, however, there is a requirement for traversing behind wakes or through boundary layers then acceleration limits on stepper motors become the limiting factor as certain trajectories are impossible in a fixed amount of time. Air supply can be

the limiting factor if two ejectors are required to achieve low downstream pressures. Once the variable orifice regulator reaches its stop (maximum opening) driving pressures fall and further maintenance of steady flow through the cascade is impossible. Considering all of this the data acquisition window can be sustained for approximately two seconds. The stopping transient itself is of no importance other than for considering the proper sequencing of shut-off valves to prevent blow-back into the working section from atmospheric pressure. The total run duration is, thus, approximately seven seconds.

Total temperature must be monitored to insure Reynolds number similarity. This temperature falls during the starting transient but remains steady during the regulated portion of the run. Thus with pressures and temperature constant in the working section the cascade mass flow is constant even in the face of falling pressure and temperature in the air reservoir. Experience indicates a drop of six to seven degrees Kelvin during the transient start-up with little variation from run to run. Thus Reynolds number is a repeatable quantity from run to run as is Mach number.

2.1.2 Test Section

The cascade model is located in a cylindrical tank which, during a tunnel run, is a sealed plenum as shown in figure 2.2. Air is introduced into the tank through an eight-inch feed pipe which is capped and drilled to provide a shower-head distribution. Air flows around the cascade support structure to the cascade entrance duct which is located near the ceiling of the tank. The entrance duct is rather short, and the inlet air must be directed into side plates and a flow straightener in order to obtain uniformity and a low turbulence level.

The working section (test section is used synonymously) can accommodate cascade models up to 300mm span and 1m in pitchwise dimension,

though a cascade of this size would exacerbate entrance flow problems. The effective entrance duct length is approximately 1m, so, in practice, models are usually designed to be about 500mm or less in pitch direction. This provides an L/D ratio (duct length to hydraulic diameter) of about 2.5, still quite short for obtaining developed flow at the cascade entrance plane.

The chord dimension of the cascade model is limited only by the minimum number of passages required for uniform and periodic flow at the entrance plane and by the ejector capacity for reducing the exhaust plane static pressure low enough for large chord models. In this regard it is noted that a 300mm chord blade cascade has been successfully tested at full-scale Reynolds and Mach numbers.

Other test section features include inlet liners which can be rotated to study off-design incidence effects. In practice this necessitates a change of flow conditioning apparatus which is normally fitted to the entrance duct about 400mm upstream of the cascade. The catcher (moulded from fiberglass) located downstream of the cascade accepts an off-centreline flow of plus or minus 10^{o} and thus avoids sudden contraction losses. With this momentum conserving device in place the exhaust will evacuate naturally down to about 0.8atm without ejector boost.

Schlieren windows are located on the tank sidewalls for flow visualization. The centre of the windows are eccentrically located in portholes and by rotating the windows the accessible visual field of the cascade may be increased. All windows (tank and model) are manufactured from optical quality glass.

Electrical pressure transducers are mounted in a sealed aluminium box attached to the lower support structure. The lower face of this structure deflects flow away from the box. The transducer box is vented to atmosphere via flexible pressure lines fed through sealed access ports in

the tank walls. Electrical cables are taken out through these same ports.

Flow conditioning is achieved through the use of a honeycomb flow straightener, one or two screens attached to the face(s) of the honeycomb, and, when required, a mono-plane bar grid for turbulence generation.

An example of a turbulence grid constructed for the large chord B22 cascade is one designed along the lines of a unified theory developed by NAUDASCHER and FARELL(1970). To produce a turbulence value (u'/U) of 5% a bar grid of 12.7mm diameter and 30mm centre spacing was built and placed 350mm upstream of the centre blade leading edge. This led to an X/M value of 11.6 which according to HINZE(1975) should produce homogeneous turbulence. The design formulation used correlated closely to the data of BAINES and PETERSON(1951) and to the more recent data of BLAIR et al.(1981).

This completes a general description of the working section of the blowdown tunnel. More details on specific cascades tested for this thesis are described later in chapter five.

2.1.3 Ejectors

A unique operational feature of the blowdown tunnel is the capability to adjust downstream cascade exit pressure independently of cascade inlet total pressure. This is done by adjusting the throat areas and driving pressure of the two ejectors. BAINES et al.(1984) describe the theory of the tandem ejector system and show the magnitude of the pressure ratios that can be attained with the ejectors running simultaneously (their figures 9 and 11). The purpose of this section will be to supplement their report with information of an empirical nature derived from operating experience with the tunnel.

The sections which follow deal with (a) practical limits on the regulator pressure, (b) a quantified comparison of individual ejector

pressure ratios, (c) ejector driving pressure as a function of regulator pressure, and (d) diffuser pressures downstream of the ejectors.

(a) First from figure 2.1 note that the driving pressure for both ejectors is the regulated pressure. The pressure selected to drive the ejectors must be selected from a range of pressures for which the regulator can provide sufficient mass flow for uniform pressure regulation.

There is a maximum practical limit on regulator pressure and this value can be calculated if the valve upstream of the regulator, the supply valve, is considered choked for the duration of the run. This is not an absolute requirement, but, if not approximately true, steady regulation may cease at an inconvenient time in the run.

To calculate the maximum regulator pressure one notes that the reservoir, which feeds the supply valve, can be considered to be emptying at approximately constant mass flow rate. For constant mass flow the reservoir pressure decreases exponentially from flow start (1) to flow stop (2) according to the fraction of original mass lost from the reservoir. That is,

$$P_{s2}/P_{s1} = (1-mf)^{\gamma} \qquad ...2.1$$

The quantity mf is the ratio of total mass flow out to initial mass in the reservoir. If, for example, the maximum reservoir pressure is 31atm (455psi, and this is an upper limit) then for a 17% drop in mass, say, the supply pressure drops to 23.8atm (350psi). For the supply valve to remain approximately choked the regulator pressure just downstream of the supply valve should ideally be limited to 12.6atm (185psi). That is,

$$P_{reg} = P_{s2}/1.89 \qquad ...2.2$$

The value 1.89 is the isentropic pressure ratio at unity Mach number. In practice P_{reg} can be significantly higher, say 14atm (205psi). This can be explained by examining the variation of A^*/A versus pressure ratio. From isentropic tables it can be seen that at choked conditions a drop in pressure ratio of as much as 10% results in only a 0.5% change in A^*/A. Thus, even with the higher (14atm) regulator pressure (and thus lower pressure ratio across the supply valve) the supply valve is still approximately choked.

(b) For the purpose of setting valve openings prior to a run it is necessary to know roughly what fraction of the total pressure ratio established by the ejectors running in tandem is attributable to each ejector.

Consider the pressure ratio for the first (annular) ejector to be defined as the ratio of the static pressure in the cascade exit freestream to the pressure at the first diffuser exit downstream of the first ejector, P_2/P_{o4}. The subscripts refer to stations shown in figure 2.1. Next, P_{o4} is roughly equal to the static pressure at station 6 if subsonic flow exists at the diffuser entrance. If this is not the case, e.g. because of excessive ejector mass flow, ejector pumping deteriorates severely. See BAINES et al.(1984) for a discussion of this effect. For the second (discrete jet) ejector it is convenient to define the relevant pressure ratio as the ratio of freestream pressure at the injection point to the pressure at the second diffuser exit, i.e., P_6/P_{o7}. It is usual to consider P_{o4} approximately equal to P_6. From Baines et al., op cit., performance curves 9 and 11, ejector one establishes a lower pressure ratio because of the inherently better mixing achieved in annular injection. If the pressure ratio for the second ejector is an arbitrary value, x, i.e.,

$$P_6/P_{o7} = x \quad (4 \text{ nozzles open}) \qquad \ldots 2.3$$

then a fair approximation for the first ejector is,

$$P_2/P_{o4} = 0.75x \qquad \ldots 2.4$$

Knowledge of the above ratios is important in conserving run times during the setting-up phase in a new cascade test. Equations 2.3 and 2.4 hold when the four discrete nozzles of ejector two are fully open. Normally these nozzles are fully open (or at least in a fixed position) to take advantage of the accurate screw thread adjustment on ejector one.

(c) Upstream of the ejectors, ball valves throttle the flow and in combination with the ejectors form an in-line, two-throat pipe system. Thus the driving pressure for the ejectors is less than the regulator pressure and is a function of the amount of opening of the ejector. Although both ejectors are always choked it is not possible to calculate an accurate value of choked-flow area because of a non-unity discharge coefficient. The values of pressure ratio, P_{ej}/P_{reg}, as a function of A^* have been experimentally determined, however, and these results absorb the discharge coefficient.

For the first (annular) ejector a 5th order curve fit through calibration data yields the desired result. The coefficients are included in Appendix A and used in the example setup. For the second (discrete) ejector only one data point was acquired as this ejector is normally run with four nozzles fully open. This results in $P_{ej2}/P_{reg}=0.75$.

(d) It is commonly (and fairly accurately) assumed that the total pressure downstream of each ejector (running singly) in the diffuser exit is approximately atmospheric. Given the dynamic head of the main streams, however, one attains a slightly better initial (pre-tuning) setup by using

values between 1.02 and 1.06 atm for these pressures. This can be seen in the example setup calculated in Appendix A.

2.2 DATA ACQUISITION

2.2.1 Hardware

The data acquisition system for the blowdown tunnel evolved mainly from the experience gained in transient testing in the ILPT, SCHULTZ and JONES(1973) and SCHULTZ et al.(1977). The hardware configuration is shown in figure 2.3 and is intended to support the measurement of total, static, and differential pressures using (a) stationary probes mounted internal to cascade blades and (b) moving probes mounted in a traversing mechanism downstream of the cascade. Other physical quantities which can be measured in the tunnel include total temperature in the cascade inlet, boundary layer profiles and turbulence using hot wires, and, in planning for the future, skin friction coefficients using thin film heat transfer gages, cf. JONES(1977).

The system shown in figure 2.3 is centred around a dedicated PDP 11/24 minicomputer utilizing the RT-11 operating system. The 64-channel, 12-bit A/D convertor is capable of acquiring electrical signals at roughly 33kHz for one channel or 300Hz for 64 channels, 200 readings per channel. Dual floppy disc drives provide for the archiving of run setup information and raw data onto discs for permanent storage. The system is controlled from a high-resolution VT100 Retro-Graphics terminal which is also used to display the A/D input levels prior to the run and to plot results after the run.

Signal preconditioning is accomplished using in-house CAS-8 amplifiers which are fitted with low pass, anti-aliasing filters whose cutoff frequencies can be changed via capacitors accessible internally. Signals can also be acquired in analog fashion using the combination of

in-house GT-8 galvanometer amplifiers (OLDFIELD(1975)) and a multichannel UV recorder.

Pressures are measured in either an absolute or differential mode using National Semi-conductor LX1610D pressure transducers. For use in the blowdown tunnel these semi-conductor transducers are removed from their as-received casing and encapsulated in Araldite epoxy resin for robustness. Measurement errors are minimized by calibrating the entire chain of transducer, signal conditioning amplifier and A/D converter as a single unit over the range of pressures expected. If the transducers are used in the differential mode this calibration includes a determination of common mode rejection ratio (see NICHOLSON(1981) for details). Whenever changes in electrical wiring entail changing channel connections or CAS-8 amplifier sensitivities or whenever test pressure ranges change, the entire measurement chain is recalibrated.

For wake and boundary layer traversing a four-axis traversing mechanism is employed. The traverse platform is driven by stepper motors in two directions through gear boxes and lead screws while the control arm, attached to the platform, can simultaneously raise and rotate a probe support. A total of four stepper motors provide the motion, each controlled by a dedicated Intel 8035 microprocessor. The spatial locus of the probe support is calculated by computer software and downloaded to the microprocessors prior to the run. A time delay is added to the time-distance trajectories to allow for steady state flow in the tunnel. (Some trial-and-error is inevitable). Use of the traverse includes using close-coupled miniature Endevco pressure transducers mounted in the probe support to minimize signal attenuation and lag.

Hot wire measurements are made using a 55D series, Disa constant temperature anemometer (CTA). The signal mean level is relayed either to the computer via the normal CAS-8 signal conditioning chain or to an

eight-channel transient recorder. The fluctuating component of the signal is anti-alias filtered, amplified by an AC amplifier and relayed to the same transient recorder. Each channel of the transient recorder is capable of acquiring 4096 data points at a maximum rate of 2MHz.

To start the tunnel one channel of the computer A/D is used to energize a relay which initiates the opening sequence of events. Adjustable delay timers are connected to shuttle valve relays which are activated to open pressure lines to pneumatic ball valves. Other timers allow for triggering an oscilloscope, a spark generator for schlieren photography and a pulse generator used to trip the transient recorder. These same timers cause the shuttle valves to reverse their positions at a preset time in order to stop the tunnel.

2.2.2 Software

The software system used in the blowdown facility is a derivative of the system developed for the ILPT, OLDFIELD et al.(1978). The blowdown tunnel operating software developed by BAINES(1983) retains the modular concept developed earlier. That is, data acquisition is partitioned into activities common to all users and portions which are dependent on the specific model.

The software package is highly interactive and features a top-down (hierarchial) structure leading from a menu-driven selection of major activities down to detailed input for each activity. Three major modules comprise the software system. These include the setup program, the signal acquisition program and the data processing program. Peripheral segments allow for pre-run A/D inspection, post-run raw data examination and plotting of raw data or processed results. Each of these software components is explained in more detail by Baines, op cit.

For each run only two new files are created. One is the runsheet

(setup) file listing transducer connections, calibration data and tunnel hardware configuration (valve settings, sequencing, etc.). The second file created is the raw data file in time-voltage format. If processed results are required later for on-screen viewing or in hardcopy form the processing portion of the tunnel operating software is accessed via menu selection and the two files created for the run are used together to create a results file which can be listed down on the line printer. The runsheet file and raw data file are archived on floppy disc after each run.

Software for calibrating transducers is separate from the main tunnel operating software and follows methods outlined by OLDFIELD(1978) and NICHOLSON(1981). Other separate software include programs for processing frequency-dependent data via the fast Fourier transform (FFT) and inverse FFT for auto-correlation. These programs are used mainly in conjunction with hot wire experiments.

2.2.3 Run Setup

Assigning valve openings and ejector settings prior to a run requires a knowledge of the hardware operating system as well as calculations of mass flow through the system. The most complex setup procedure occurs when a new build is installed in the tunnel and uncertainties exist about such aerodynamic quantities as the aerodynamic throat area of the cascade. Usually there is also a decision to be made concerning the choice of using one or two ejectors.

Operating experience with the blowdown tunnel has provided a systematic approach in determining each new setup configuration for the tunnel. In Appendix A an example of the setup calculations for the large-chord B22 cascade is shown. This cascade required the use of tandem ejectors to lower the cascade exit pressure, and so this example will provide guidance for the most complex of any case likely to be encountered

by a tunnel operator.

2.3 B22 PROFILES

Two versions of the B22 profile were tested as part of the work in this thesis. The two profiles, the 100mm and 300mm chord versions, are scaled-up versions of the profile tested by NICHOLSON(1981). A view of the profile is given in figure 2.4. The coordinates of the blade are included in Nicholson's report and are omitted here for brevity.

The B22 profile is a mid-section rotor profile of high-reaction design. The profile features a high turning angle, approximately 110^{o}, and thus is designed for high specific work.

Testing on this profile by NICHOLSON(1981) indicated the presence of secondary flow phenomena on the pressure surface requiring further study. The large chord (300mm) version was built in order to examine and characterize the scaled-up boundary layers, specifically on the pressure surface, and to provide detailed blade surface pressure measurements. On the other hand the 100mm chord version is intended for further studies in wake losses and incidence effects (as well as serving as a commissioning model for the new blowdown tunnel).

The blades were instrumented internally with hypodermic pressure tubing, brought out flush with the blade surface. The locations of the pressure taps on the 100mm chord blade are identical in scaled location to the B22 rotor tested by NICHOLSON(1981); his report should be consulted for tapping locations. The 300mm chord blade, however, was instrumented in more detail, and the locations of tappings on this blade are shown in figure 2.4 and table 2.1.

2.4 VKI-1 CASCADE

The VKI-1 cascade used for commissioning tests in the O.U.E.L.

blowdown tunnel was loaned to the Department of Engineering Science by DFVLR, Braunschweig. The cascade consists of seven hub-section rotor blades of 100mm chord and 300mm span. The VKI-1 profile was designed at the Von Karman Institute in the early 1970's and was intended to test design methods existing at the time. Details of the design are presented by KIOCK et al.(1985). Only one significant modification was installed for the Oxford tests, that of the use of shutter plates in the end passages to facilitate the tuning of the cascade. (The cascade, as used in the Braunschweig tests, utilized curved vanes in the end passages, KIOCK et al., op cit.).

CHAPTER III

EXPERIMENTAL PROGRAMME

3.1 DEVELOPMENT AND COMMISSIONING OF A NEW BLOWDOWN FACILITY

As outlined in chapter two, prior to performing measurements to obtain new data in the O.U.E.L. blowdown tunnel it was necessary to conduct a series of commissioning trials to determine the operating characteristics for the various stages of the tunnel. For example, initial tests included calibration of the gate valves located just upstream of the regulator and just upstream of the plenum. The former, or supply valve, controls the flow of primary air to various sections of the tunnel (see figure 2.1). The latter, or tank valve, controls the air flow into the plenum.

The 100mm cascade proved to be an ideal vehicle for establishing tunnel running characteristics and performance standards since inlet and exit pressures were easily set up and were repeatable. The aspect ratio (span/chord) of the 100mm build was three, and thus sidewall boundary layer effects or other secondary flow effects were of insignificant proportions. This was verified using oil dot flow visualisation. Thus the through-flow area was a stable value for the calibration of ejectors and gate valves.

Calibration of a gate valve entails the determination of the theoretical value of choked flow area as a function of valve setting. This was done using the known flow area of the 100mm cascade as a reference and equating the product $P_o A^*$ for the valve and cascade (mass conservation with assumed iso-energetic flow).

Performance characteristics of the first and second stage ejectors were obtained on as as-required basis. That is, data were obtained by trial-and-error setting up for each new build until sufficient data were

accumulated to estimate the performance curves. This subject is treated in more detail in chapter two.

The cascade inlet proved to be the region of the tunnel where a major effort was expended. Lacking a long inlet duct to facilitate uniform flow at the entrance to the cascade, the working region required a careful measurement of inlet and exit periodicity prior to performing blade surveys.

A number of factors can influence periodicity and flow quality in a short inlet duct. Of major concern in this case was the severe turning of plenum air into the duct brought about by the proximity of the inlet liners to the ceiling of the plenum. Another was the question of need and type of flow conditioning apparatus such as turbulence-damping screens and the honeycomb flow straightener. The attempt to resolve these questions resulted in a considerable development effort utilizing a perspex scale model built especially for smoke visualization studies.

Also included in the inlet investigation was a study of the effect of pitchwise location of the inlet liners on periodicity. The location of the liners proved to be a major influence on the mass flow in the end passages and the dominant factor in the shape of the blade stagnation streamlines. (This end effect is discussed in some detail by PIANKO(1975)). Changing the liner position for these tests proved to be a time consuming task, however, and so another approach was adopted. Thin, adjustable shutter plates were attached to the end portion of either liner and this allowed one to adjust by trial and error the air flow in each end passage. The results of all of the above studies are detailed in chapter five.

3.2 B22 100MM TESTS

3.2.1 Background and Planned Tests

The B22 100mm chord cascade is a nine-blade cascade (seven flow

passages were used in testing) constructed in order to extend and complement aerodynamic studies initiated by NICHOLSON(1981) who tested a seven passage cascade of similar design but smaller (about half) scale.

The B22 profile used in the 100mm cascade was designed from primarily aerodynamic considerations and intended to minimize losses while providing high work output at high turning angle (approximately 110^{o} total turning) and with little or no separation. It was of interest then to verify the capabilities of this profile. The initial tests done in the new blowdown tunnel were the first of a series of tests designed also to study the effects on pressure distribution of incidence, Mach and Reynolds number variations.

Of further interest was the determination of profile losses using the new wake-traversing equipment purchased for the blowdown tunnel. Nicholson had found in his tests on the B22 profile that shock-boundary layer interactions at exit Mach numbers slightly below design value caused significant aerodynamic losses. The pressure profiles in the trailing edge region also showed a tendency for the flow to diffuse or decelerate to a lower exit velocity. This latter point is mentioned here because one aspect of the new studies on this profile was the investigation of the extent to which Nicholson's data corresponded to similar measurements in a different tunnel in which tunnel geometry could influence in a slightly different way the flow field in the region near the trailing edge.

It was also shown in Nicholson's work that at design exit Mach number there were regions on the blade where surface Mach number measurements did not correspond well with values from a numerical time-marching code. His data also indicated an upstream shift in the location of sonic velocity on the suction surface, an effect expected only with a higher incidence angle. Anomalies such as these would, it was hoped, be explained in comparing data obtained from the 100mm cascade tested in

the blowdown tunnel.

Data obtained in these new series of tests would also need to be compared with predictions. Results of prediction codes used by Nicholson were used in this thesis for comparing data obtained in different facilities. The predictions used were, first, the results of a streamline curvature code developed by Rolls-Royce and second the results of a time marching code written by DENTON(1975). Interpretation of experimental results in light of numerical predictions can only be done, however, when there is an understanding of the principles upon which the codes are based. Thus what follows is a brief discussion of the streamline curvature and time-marching methods. Later another code used extensively in the boundary layer work done for this thesis, STAN5, will be discussed.

3.2.2 Synopsis of Streamline Curvature Method

The flow through an actual turbine rotor passage experiences a radial pressure gradient due to rotational effects. This effect is absent in a linear cascade. One desires the results of linear cascade testing, however, to be applicable to the actual engine operation. One way of achieving this is by designing a 2-D test profile based on the trajectory of gas particles over the actual blade, i.e., spatial coordinates derived from the radially varying trace of the curved streamline projected onto the surface of the blade in the actual passage. OATES(1978) describes this as unwrapping the meridional surface in order to obtain a two-dimensional flow field. A 2-D design could then be made using the capabilities of a 3-D prediction code.

The utility of a prediction code which accounts for radial effects is then two-fold. In the first case the program can be used to generate the profile shape if, say, a particular velocity distribution is prescribed. In the second case predictions of blade surface pressures can be compared with

the cascade data, a process which validates and improves the code's usefulness.

Streamline curvature numerical methods account for radial effects. They are essentially based on the work of SMITH(1966), although he credits TRAUPEL(1942) and WU(1950) as first proposing the scheme. Smith derived and first published the exact equations for radial pressure equilibrium in a rotating frame of reference. His results for radial pressure variation accounted for centripetal acceleration, meridional streamline radius variation and blade thickness (blockage effect).

The method is so named because the radius of curvature of the meridional streamline is a dependent variable and calculated independently using a numerical interpolation scheme (see HORLOCK(1966)). The essence of the computational procedure is to start with an estimated flow field pattern, calculate a new velocity field, and compute new streamline patterns, from which come new radial derivatives to be used for the next iteration. Typically the flow field is calculated by marching spatially from leading to trailing edge (see CARUTHERS(1976)). Complete flow fields are iterated until a convergence criterion is met. Variations on this approach can be found in the literature (WILKINSON(1970), DAVIS(1976), and KLEIN(1977)).

Various assumptions common to the streamline curvature method include neglected viscous effects (thin boundary layer) and isentropic flow (modelled mathematically using the irrotationality condition). The resulting governing equations for steady, inviscid, compressible flow allow a stream function approach (c.f., KATSANIS(1968,1969)) and are of the elliptic type requiring boundary conditions to be specified around the entire envelope or control surface of the flow. The above assumptions naturally limit the accuracy of the calculations in flows with shocks unless those shocks are weak (irrotationality condition). The streamline

curvature method is stable also for supersonic flows for which the equations become hyperbolic in form, but again accuracy is best in a shockless flow.

The streamline curvature results shown in this thesis were produced from a code employed by Rolls-Royce which utilizes a method developed by Stuart (GOSTELOW(1984)). The main feature of the method is the use of a full orthogonal grid and the incorporation of an indirect/direct design system. The code also includes boundary layer calculations. The streamline curvature predictions used for comparisons in chapter five are from an earlier derivative of the current Rolls-Royce code.

The assumption of steady, inviscid flow in the streamline curvature method simplifies the mathematics but limits the application of the code to flows of an elliptic or hyperbolic character, i.e., flows for which velocities and pressures in the flow field are either dependent on both upstream and downstream boundary conditions or characterized by solutions which are uniform along characteristic directions. When regions of both types are in close proximity (as with a shock wave) the method loses its capability to converge to a solution. The time-marching approach to the solution of the governing conservation equations, however, allows numerical calculation through these regions.

3.2.3 Synopsis of Time Marching Method

As stated above a flow field with mixed subsonic and supersonic regions poses numerical difficulties for methods like the streamline curvature method or any method which employs a straightforward stream function approach to the solution of the steady, inviscid, compressible flow equations. This problem is partially solved (shock dissipation is still difficult to model) in the use of a parabolized, time-marching method, however, where mixed conditions, normally elliptic or hyperbolic in

spatial coordinates, are eliminated in favour of equations which are parabolic in the time dimension. The equations retain identical form in both subsonic and supersonic regions and thus offer the advantage that flows with shocks can be calculated.

A time-marching calculation is identical to the calculation that would be made of a steady flow field with a step change in boundary conditions. In that case if the new boundary conditions were steady the entire flow field would eventually assume a steady character. In practice a guessed flow field is specified, representing the initial steady flow, and then new boundary conditions are specified, representing the state to which the perturbed flow must evolve.

The time-marching method in theory can 'capture' shocks since the governing equations are the same conservation equations used to calculate the Rankine-Hugoniot jump equations. In practice this requires very small mesh sizes (large computing time) and so shocks are usually smeared over several meshes. (A fairly new scheme developed by DENTON(1982) adds a dissipative correction term and has improved the shock capturing capability of the method).

Two approaches to writing the governing equations can be found. First is the integral form as in the method of MCDONALD(1971) and second is the differential form in the method of GOPALAKRISHNAN and BOZZOLA(1972) as reported in FARN and WHIRLOW(1977). (The differential form has been used earlier in external flows (MORETTI and ABBETT(1966)). For further discussion see ANDERSON(1982).

GOSTELOW(1984) suggests that the integral form is simpler to operate and interpret. It was also this form to which DENTON(1975) made his improvements and which later NICHOLSON(1981) used for comparisons with his data. Because those numerical results are also employed in this thesis it is of interest to highlight some of the more important aspects of the

scheme.

The basis of the time-marching method, as in other numerical schemes, is to partition the flow area into an orthogonal grid. The integral form of solution then involves writing the conservation equations for any one area formed by a quadrilateral of orthogonal grid lines. Each conservation equation includes a flux term integrated over the surface boundary of the quadrilateral and an unsteady term with properties evaluated at the centre of the quadrilateral. Some specific points of the updating and time-stepping process are given below.

Boundary conditions are specified at the upstream inlet plane to include total temperature, pressure and flow angle. At the outlet plane pressure is specified and held constant during the calculations. (Outlet flow angle is a byproduct of the calculations). Then starting with the guessed flow field all densities are updated via the continuity equation by calulating an integrated mass flux, say ρU, and dividing by the known (old) velocity, U. Local temperature is then calculated using the adiabatic, steady flow energy equation (which is inexact for the early calculations), and a new local pressure is found from the perfect gas law. Finally, the velocities are updated using the momentum equation and the process repeated for the next time step.

As with all numerical methods there are considerations of a purely computational nature which must be taken into account. These will not be discussed here. A discussion of such things as mesh formulation, differencing schemes, stability, damping, convergence criteria, etc., can be found in the literature, eg. CASPAR(1982).

3.3 VKI-1 CASCADE TESTS

It is appropriate when commissioning a new wind tunnel to compare results from other tunnels. As mentioned earlier the tests on the 100mm

chord B22 profile allowed comparison with data on a model of different scale tested in the ILPT. The testing of the VKI-1 profile, however, afforded an opportunity to test identical hardware to that previously tested in the high speed cascade tunnel at the DFVLR in Braunschweig and allow a direct tunnel-to-tunnel comparison.

The VKI-1 profile is a high-turning, turbine rotor hub section designed at von Karman Institute and also tested there. The results of these tests were presented in a VKI lecture series (SIEVERDING(1973)). Subsequently the profile was tested at DFVLR, Goettingen, LEHTHAUS(1975), and DFVLR, Braunschweig, KIOCK(1980).

For each of the three facilities a cascade was constructed from the VKI-1 profile but in each the chord size and aspect ratio were tailored to the particular facility. The coordinates of the profile along with a more complete discussion of the cascade builds and the four tunnels taking part in the tests on this profile are presented by KIOCK et al.(1985).

The experimental work reported in this thesis is from a portion of the complete data collection and for brevity includes only the results obtained in the Oxford and Braunschweig tunnels. This is most relevant to the commissioning process because of the use of identical cascade hardware.

The scope of the preliminary tests in the Oxford tunnel were limited to inlet and exit periodicity checks and blade Mach number distributions. Neither the downstream traversing equipment nor the schlieren system were in place in the Oxford blowdown tunnel in their final form, and hardware additions to the tunnel were underway at the same time.

Some major differences in the Oxford and Braunschweig tunnels are mentioned now and discussed further in chapter six. First is the length of the inlet ducts, 900mm in the Oxford tunnel and 1500mm in the Braunschweig tunnel (KIOCK et al.(1985)). The boundary layer growth and duct velocity profiles are thus expected to be different owing to differences in

streamwise flow development.

Both facilities utilize boundary layer suction upstream of the end passages but in a slightly different way. End passage flow in the Braunschweig tunnel proceeds past curved end pieces while in the Oxford tunnel end passage flow experiences sudden expansion past sharp-edged shutter plates. This would seem to indicate a difference in Reynolds number dependency in the end passages in the two tunnels and a difference in the ability to tune the inlet to correct level of inlet Mach number and correct incidence angle in the two tunnels. This is elaborated on in subsequent chapters, five and six.

Finally, a most important difference in the two tunnels is the method of exhausting the exit flow. The Braunschweig tunnel is a continuous running, open-return facility enclosed entirely in a large plenum chamber, thus making it a hybrid closed-return tunnel. The exhaust from the cascade expands suddenly into the large plenum and recirculates to the tunnel entrance induced by the pressure difference between tunnel entrance and exit (cf. HOHEISEL(1977) or OLDFIELD(1980)).

The Oxford blowdown tunnel, on the other hand, exhausts the flow into a small exit chamber from which it is directed via a bell-mouth to the downstream ducting. In this case shock and expansion systems may interact in the exit plane in quite a different way than in the Braunschweig tunnel. However, these effects are minimized in this case because of the fairly large distance between cascade exit plane and exit chamber walls. It is also important to note that differences which would normally occur in exit flow in a tunnel using ducted flow as opposed to one using free exhaust or dump diffusion flow are mitigated in this case because of what amounts to effectively closed-return flow in the Braunschweig tunnel.

The major objective of the preliminary Oxford tests was to obtain, compare, and analyze differences in blade Mach number distributions. This

resulted in an understanding of characteristic tunnel effects.

Results of a prediction code written by LEHTHAUS(1977) will be compared to the results from the two facilities. This will help to narrow the reasons for any differences that occur in the data.

Flow conditioning appartus, measurement equipment, signal conditioning instrumentation, and the data acquisition system used in the tests have been described elsewhere and involve only that needed for measuring blade static pressures, upstream total pressure and duct sidewall static pressures. A pitot rake with attached yaw meter was used to measure inlet incidence.

3.4 LARGE CHORD B22 PRESSURE SURFACE

One of the primary reasons for building the large chord turbine profile was to study secondary flow effects, specifically the effects of surface curvature on the boundary layer on the pressure surface. Anomalous effects had been seen by NICHOLSON(1981) who noted in hot film traces on his smaller version of the B22 profile that heat transfer fluctuations on the pressure surface possessed characteristics of both laminar and turbulent flow. If this dual nature can be described as the boundary layer maintaining itself in a transition-like state, the transition of flows on concave surfaces is naturally an important phenomenon needing further testing.

The transition mechanism on a surface of high concave curvature seems to be dominated not entirely by Tollmein-Schlichting (T-S) instabilities familiar to the zero-curvature surface or the convex surface. TANI(1969) suggests that the concave wall induces a spanwise variation of boundary layer thickness which modifies the development of travelling T-S waves. Today there is universal agreement that the transition process is three-dimensional in nature, manifested in streamwise running vortices

arising from centrifugal instabilities.

Several investigations have focused on determining the location, size and spacing of these vortices, and with good results, but as yet no theory exists which can predict those characteristics. Additionally, these investigations have been successful in correlating results with stability analyses by SMITH(1955), for constant curvature, or TOBAK(1971), for bounded curvature, but, as yet, no results of a predictive nature have come about.

The transitional nature of a boundary layer on a concave surface is identified with the Goetler number, equation 5.8, which ties together momentum Reynolds number and curvature. This parameter takes on two ranges of values in the literature depending how transition is identified.

First is the value which identifies a neutral stability or imminent growth of instabilities, i.e., that imperceptible beginning of transition associated with the aforementioned stabilitiy analyses of Smith or Tobak. The value of the Goertler for this case number was first put at 0.32 by SMITH(1955) for zero-pressure-gradient flow and later revised upward to 0.46 by FLORYAN and SARIC(1982).

RAGAB and NAYFEH(1981) calculated the effect of pressure gradient on the Goertler number using the Falkner-Skan similarity flows (SCHLICHTING(1978)). Their results showed an increase in Goertler number for flows with positive pressure gradient indicating a delay in the onset of transition. The opposite effect occurred for negative pressure gradient. These calculations and those of Smith above were for constant curvature, a geometry not often found on modern-day turbine profile designs.

TOBAK(1971) calculated the neutral stability Goertler number for flows on surfaces of varying curvature by patching curves of constant radius with straight line segments attached to either side of the arc. His calculations indicate that the Goertler number must be at least 0.58 to

initiate growth of flow instabilities. Thus there seems to be no general agreement as to what might constitute a lower bound on the value of Goertler number. Indeed, HALL(1983) suggests that a minimum may not exist. His numerical simulations indicate that the formation and subsequent amplification of longitudinal vortices is related to how the initial disturbances arise (for example, tunnel-caused instabilities) and where in the flow, relative to a starting reference point, the disturbances are introduced. This would seem to indicate that the nature of the interaction of the vortices with the mean flow is somehow dependent on the upstream history of boundary layer. In particular his results suggest that the farther upstream an instability occurs the less likely are Goertler vortices to be triggered downstream (i.e., dampening will preclude amplification).

A higher range of Goertler number is associated with the observance of gross transitional effects. LIEPMANN(1945) suggested a range of values from six to nine depending on the freestream turbulence level (the lower value corresponding to higher turbulence). These values were obtained from observed transition in a water channel of moderately high curvature. WINOTO et.al.(1979a,b), also in tests in a water channel, report a scattering of values between seven and 13.

In earlier data of LIEPMANN(1943) obtained in a water channel of smaller curvature (larger radius) the transition point was observed to occur at a Goertler number of 7.3. Liepmann's subsequent explanation (for the value being lower than nine) suggests a non-uniqeness of the value of transition Goertler number. He explained that as curvature decreases transition is due less to Goertler instability and more to T-S-like instabilities. This suggests that transition on a concave surface may not always be accompanied by observable longitudinal vortices.

The coexistence of longitudinal vortices and travelling T-S waves

was confirmed by HAN et al.(1979) in smoke flow visualization on a large-chord turbine blade. They observed an initial Goertler vortex formation which broke down under the action of T-S instabilities. Their stated Goertler number for transition was unity. There appears to be a wide range of values of this parameter reported in the literature. KEMP(1977) reports values from five to six for his experiments on two turbine profiles. MARTIN and BROWN(1979) indicate a value of three for transition on a turbine blade. All observers agree, however, that the transition location and thus the value of transition Goertler number is sensitive to pressure gradient and level of freestream turbulence. What seems not to be addressed is how the observed events are influenced by peculiarities of the tunnel itself.

The extent to which tunnel effects may influence the formation of identifiable cross-stream variations was pointed out in the flat plate work of KLEBANOFF and TIDSTROM(1959). They found that the formation of instabilities occurring upstream of the transtion point was influenced by the cleanliness of the anti-turbulence screens. Given this and Hall's conclusions it may be expecting too much of a phenomenological, correlative parameter like Goertler number to be a precise indicator of transition.

In this research one experimental objective was to attempt to identify a coherent vortex structure on the pressure surface of the large-chord B22 profile. The measurement methods were all of a pressure-measurement type including spanwise traverses with a flattened pitot tube to detect velocity gradients.

Various methods of flow visualization were tried on the pressure surface in an attempt to identify a near-surface structure in the flow. First the surface was coated with a mixture of napthalene and methyl alcohol as MCCORMACK(1970) had done in observing secondary flow through deposition of the napthalene in streamwise running striations. Second, a

mixture of titanium dioxide and diesel oil was used in a dot pattern in an attempt to locate a transition or separation region on the pressure surface. Finally, flourescent paint was brush-painted on the surface. With this method secondary flow will cause shear patterns which can be seen under ultraviolet light.

For these tests (and the follow-on tests on the suction surface) a parallel-bar turbulence grid was utilized to produce a turbulence level calculated to be 5.5% (u'/U) at the entrance of the cascade.

A second objective was to obtain boundary layer profiles at various locations on the pressure surface. For reasons explained later these surveys were limited to two positions near the trailing edge.

3.5 LARGE CHORD B22 SUCTION SURFACE

The first flow characteristics to be studied on the large chord B22 profile were the boundary layer profiles at various locations along the blade surface. As this was also the first experience with measuring boundary layers in the blowdown tunnel these measurements provided the opportunity to refine and modify methods for transient testing. The results of these tests also provided data for comparisons with Rolls-Royce codes and with STAN5, the 2-D viscous code discussed in section 3.6.

The flow on the suction surface of a turbine airfoil is generally turbulent over most of the surface, and boundary layer growth is greatly influenced by the curvature of the blade surface. BRADSHAW(1973) analyzed the flow over curved surfaces and from his results one can conclude that in general the convex curvature found on the suction surface will cause the mixing length and hence the thickness of the turbulent boundary layer to be reduced in comparison to that found on a flat surface. However, a contradiction to this can be found in ducts of low aspect ratio and in rotating ducts as reported by SHARMA and GRAZIANI(1982). In these cases

secondary influences arise in the form of cross-channel pressure gradients caused (in the non-rotating case) by the vortices which form on the end walls (passage vortex). Sharma and Graziani were able to show that thicker boundary layer data could be correlated with STAN5 results when a modification was made to the code to account for end wall effects. It was of interest then in the current study to determine the shape of the profiles in the large chord build, which had an aspect ratio (span/chord) of unity.

It was desired that the design of the large chord cascade provide for flow that would be two-dimensional and free from the effects of low aspect ratio. Thus, one of the first tests done on this build was to run a series of surface flow visualization tests using oil dot patterns applied to the suction and pressure sides of the centre, instrumented blade. The results of this would then also indicate the reliability of the unmodified (i.e., not including end-wall effects) version of STAN5 for comparisons with experimental data. For this thesis it was concluded that for 2-D flow the unmodified version probably provides as good a numerical comparison as is currently available. Section 3.6 has further details on this subject.

The importance of studying curvature effects bears directly on the heat transfer problem of a turbine blade. Prediction and design techniques must incorporate an adequate modeling of surface curvature effects to anticipate correctly wall temperatures. As far as the accuracy of predictions incorporating curvature effects, RODI and SCHEURER(1983) suggest that as yet none of the curvature models currently available is completely reliable for all types of flows. The curvature effect on heat transfer was demonstrated in the experiment of THOMANN(1968) who showed the effect of wall curvature in a zero-pressure-gradient, compressible flow. His results indicated a decrease in the Stanton number (non-dimensional heat transfer coefficient) when the curvature was convex and an increase in

the heat transfer coefficient when the curvature was concave. One would then expect a reduced heat transfer coefficient on the suction surface and an increase on the pressure surface in comparison with flat plate results.

The flow on the B22 suction surface undergoes transition and experiences large curvature and significant pressure gradients simultaneously. In the region available to a pressure probe (x/s=0.3 to 1) in the initial series of tests reported in this thesis, however, the flow is less influenced by these factors. Thus, thicker boundary layers are expected than on the corresponding location on the pressure surface, which experiences an accelerating flow field.

The presence of thicker boundary layers on the suction surface afforded the opportunity to validate measurement techniques required for high speed, transient testing. The use of a flattened pitot tube, for example, would yield more information on the boundary layer profile by virtue of its proportionately smaller fraction of boundary layer thickness.

Once velocity profiles are obtained there are several techniques which can be employed to determine the degree of conformity with known wall-wake laws and to calculate skin friction coefficient. The first includes the use of the Von Karman momentum integral.

If profiles are obtained at closely-spaced intervals along the surface the compressible form of the Von Karman momentum integral relation can be used to find skin friction. The required relationship is (see SCHLICHTING(1979)),

$$d\delta_2/dx + (2-H-M_e^2)(\delta_2/U_e)dU_e/dx = C_f/2 \qquad \ldots 3.1$$

where

$$C_f/2 = \tau_w/(\rho_e U_e^2) \qquad \ldots 3.2$$

and

$$H = \delta_1/\delta_2 \qquad \ldots 3.3$$

The integral thicknesses δ_1 and δ_2 are defined for compressible flow,

$$\delta_1 = \int_0^\infty (1 - \frac{\rho U}{\rho_e U_e}) dy \qquad \ldots 3.4$$

$$\delta_2 = \int_0^\infty (\rho U/\rho_e U_e)(1-U/U_e) dy \qquad \ldots 3.5$$

Equation 3.1 is an approximation for compressible flows as it ignores static pressure variation through the boundary layer (which according to WHITE(1974) is particularly important even in low Mach number supersonic flows).

The density variation needed for equations 3.4 and 3.5 can be calculated if temperature variation is known through the boundary layer. This quantity was not measured in the initial suction surface tests so a temperature profile according to the Crocco-Buseman relation (see equation 5.15) was used. This relation yields values approximately equal to those calculated from an adiabatic assumption. The assumption of adiabatic flow can be used with good accuracy for the subsonic to transonic Mach numbers encountered on the rear portion of the suction surface.

Calculation of the skin friction coefficient in equation 3.1 follows after the velocity profiles have been measured and a suitable relationship found for the velocity profile in the region from the wall out to the first data point. This is problematic and can cause considerable error in the integral thicknesses in equations 3.4 and 3.5 if a poor approximation for this region is made. For example, a straight line approximation can yield an error in displacement thickness (eqn.3.4) of 15%

if the boundary layer is thin (say 1.5mm). Chapter five has more on the attempt to use this method (unsuccessfully) with data obtained from the suction surface.

A second method of obtaining skin friction coefficient (by inference rather than by direct calculation) is through the use of a modified wall-wake law. One modification used with some success is outlined by MATHEWS, CHILDS, and PAYNTER(1970) and is a method which essentially supplements the work of VAN DRIEST(1951) and MAISE and MCDONALD(1968). The final form of this wall-wake law is equation 3.6.

$$u^*/u_\tau = (1/K)\ln(yu_\tau/\nu_w) + C + \Pi W(y/\delta)/K \qquad \ldots 3.6$$

where u^* is the generalized velocity due to VAN DRIEST(1951) which, for an adiabatic (or more exactly iso-energetic) flow, is

$$u^* = (U_e/m^{1/2})\sin^{-1}(m^{1/2}U/U_e) \qquad \ldots 3.7$$

with m given by

$$m = [1/2(\gamma-1)M_e^2]/[1+1/2(\gamma-1)M_e^2] \qquad \ldots 3.8$$

The wake function $W(y/\delta)$ is due to COLES(1956) and assumes the convenient mathematical form,

$$W(y/\delta) = 2\sin^2(\pi y/2\delta) \qquad \ldots 3.9$$

The value of the constant C in equation 3.6 is taken to be 5.1 and the Von Karman constant is 0.4. The constant Π in equation 3.6 is a profile parameter dependent on streamwise location (it varies with pressure gradient).

A later modification to equation 3.6 is reported by SUN and

CHILDS(1973) to include an exponential term forcing the shear stress (mean velocity gradient) to zero at the boundary layer edge. Their results do not appear to differ significantly from those in the use of equation 3.6 and this author chose to use the form given in equation 3.6.

The wall-wake law given by equation 3.6 contains three undetermined values, u_τ , δ , and Π . The last of these, the profile parameter, can be eliminated by evaluating equation 3.6 at the boundary layer edge ($y=\delta$). The equation resulting from this process contains two coefficients, u_τ and δ which can be determined using a least-square curve fitting method. Further details of this process can be found in chapter five.

The skin friction coefficient is then found from u_τ according to

$$C_f/2 = (u_\tau^2 \rho_w)/(U_e^2 \rho_e) \qquad ...3.10$$

The method of finding skin friction coefficient outlined above yields best results for flows with only mild pressure gradients and should yield reasonable results for the trailing edge region of the B22 profile at M_{design} conditions for which the acceleration profile is fairly flat (but not zero).

The discussion so far has been concerned with usual law-of-the-wall relationships in the inner and overlap regions of a compressible-flow boundary layer. Since the flow condition in the blowdown is approximately adiabatic, it is also of interest to examine the degree of conformance with an adiabatic wake defect law (or outer law) derived by MAISE and MCDONALD(1968). Their correlation from data is

$$(u_e^* - u^*)/u_\tau = -2.5\ln(y/\delta) + 1.25(2-W) \qquad ...3.11$$

where the constants 2.5 and 1.25 result from a curve fit through data and W is the Coles wake function. Variables superscripted * are defined as in

equation 3.7.

Deviations from zero pressure gradient in the actual flow will cause some discrepancy with the above defect law. The defect law is an 'outer' law and since the wake portion of a turbulent boundary layer is more susceptible to pressure gradient effects than is the near-wall region the defect law will be less precise when pressure gradient is important (see CEBECI and SMITH(1974)).

The pressure gradient also influences the boundary layer thickness. If, for example, the flow tends to accelerate, the magnitude of local fluctuations, which tend to remain constant (Taylor's 'frozen' turbulence), cause a reduced local turbulence intensity and thus a reduction in the thickening rate. By comparison one expects qualitatively a thicker boundary layer on the suction surface where, in general, acceleration is much less than that on the pressure surface.

As suggested earlier, in compressible flows with pressure gradient, conformity with inner laws of the wall derived from zero-pressure-gradient flows become less satisfactory. There are trends, however, that are repeatable and these are discussed by WHITE(1974). One of these trends relevant to boundary layer data obtained in the blowdown tunnel is concerned with the effect of wall temperature.

Near the wall, but outside the viscous sublayer, a lowered temperature (compared with the freesream recovery temperature) tends to result in a more full profile, i.e., one in which the velocity at a particular height is greater than would occur for a warm wall. Conditions in the blowdown tunnel favour a neutral to warm wall condition. The total temperature of the flow is normally about five degrees Kelvin lower than the wall temperature, which results in a ratio of T_w/T_{aw} of approximately 1.03.

Adiabatic flow was assumed for the running of the 2-D, viscous flow

program, STAN5. Thus the calculated velocity profiles are expected to be somewhat more full than the measured experimental data, especially in the mid to outer regions of the boundary layer. Since warm walls also tend to reduce the skin friction coefficient (see the data in WHITE(1974)) it is expected that STAN5 would slightly overpredict these values. The STAN5 code was used extensively in this thesis work and what follows is a description of the program.

3.6 STAN5

STAN5 is a computer program written to calculate wall friction and heat transfer coefficients for 2-D and axisymmetric flows. It was written by CRAWFORD and KAYS(1976) and based on a finite-difference scheme developed by PATANKAR and SPALDING(1967,1970). The program will calculate, in addition to those parameters stated above, velocity profile, (in both x,y and inner coordinates, y^+,u^+) integral thicknesses, acceleration parameter and other parameters. The primary inputs include surface wall temperatures (or an adiabatic wall with a given free stream enthalpy), a surface velocity distribution and a starting boundary layer profile, u vs. y.

At a minimum the program solves the time-averaged momentum equation. If compressibility and/or heat transfer is important the user can elect to add the energy equation plus any diffusion equation of his own.

The finite difference equations for a 2-D viscous flow result in equations which are parabolic in form. This allows a space-marching routine to be used in which downstream variables are calculated from upstream derivatives.

As usual a closure model is needed for the Reynolds stress term, $-\overline{\rho u'v'}$, and this can be calculated in different ways depending on user input. In any case the governing differential equations are recast into

laminar-like form by relating the Reynolds stress term to the y-velocity derivative through the use of a turbulent or 'eddy' viscosity according to

$$- \overline{\rho u'v'} = \mu_t (\partial U / \partial y) \qquad ...3.12$$

Thus, an effective viscosity is inserted into the equations and is the sum of the molecular and eddy viscosities.

$$\mu_{eff} = \mu + \mu_t \qquad ...3.13$$

The method of calculating eddy viscosity is selectable from basically two turbulence models, the mixing length model (sometimes called the zero-equation model, cf. NALLASAMY(1985)), and the turbulent kinetic energy equation (one-equation model). In referring to results reported in the literature most users of STAN5 employ the mixing length model since it is straightforward to use and gives results similar to those of the turbulent kinetic energy method.

In the mixing length model the eddy viscosity in equation 3.12 is related to the mean velocity gradient via the mixing length, l.

$$\mu_t = \rho l^2 \left| \frac{\partial U}{\partial y} \right| \qquad ...3.14$$

The mixing length remains as the variable which must be modeled in order to close the system of equations. This variable is calculated throughout the flow field with the aid of empirical information (see CRAWFORD and KAYS(1976)).

If fluid property variations are required or heat transfer calculations are desired the time averaged energy equation becomes a new independent equation which must be solved. This introduces a new parameter requiring a closure model, the turbulent heat flux. This parameter is

modeled using a turbulent conductivity which, with eddy viscosity, can be formed into a turbulent Prandtl number,

$$Pr_t = c_p \mu_t / k_t \qquad \ldots 3.15$$

As in the method used for the momentum equation, the energy equation is recast into a laminar-like form which includes an effective Prandtl number formed with the molecular and turbulent values. The closure for the resulting system of equations includes an empirical relationship to link turbulent Prandtl number with eddy viscosity. Thus, the unknown fluctuating fluxes are both tied to mixing length.

As mentioned earlier one required input is a boundary layer profile at the starting surface position. For airfoils this problem has been alleviated by GAUGLER(1981) who added a subroutine to calculate a boundary layer profile on a cylinder. This author modified the subroutine so that the stagnation point on the cylinder can be a variable input; otherwise this location must always be the starting surface position, x=0, necessitating a shift in surface locations for any change in the stagnation point location.

It is of interest to discuss how STAN5 handles important flow parameters such as pressure gradient, streamwise curvature, freestream turbulence and transition.

Pressure gradient is calculated via the velocity gradient (recall that velocity is an input, not surface pressure) and modifies the effective thickness of the viscous sublayer. This is accomplished through an empirical relationship that increases or decreases the value A^+ used in the Van Driest damping function, a function which modifies the mixing length near the wall. For example, a favourable pressure gradient will increase A^+ and thereby increase the sublayer thickness. A large favourable pressure gradient could cause the sublayer to grow and overwhelm the entire boundary

layer, resulting in relaminarization.

Streamwise curvature is accounted for in the program through the use of a factor which modifies the value of the mixing length. This factor uses the vorticity term, U/R, in a surface curvature correlation developed by the authors of the program but which is based on the bouyancy concept discussed by BRADSHAW(1973). This concept likens centrifugal effects to a pressure gradient which develops in a stratified atmospheric boundary layer. For example, if the input file to STAN5 includes values for concave curvature, such as on the pressure surface of a turbine blade, the program will calculate an increased mixing length except very near the wall (where u goes to zero).

The third of the parameters mentioned above, freestream turbulence, is a user-specified value which, in the version of STAN5 used by this author, had no effect on mixing length. Its only effect was in the determination of transition Reynolds number.

Transition in STAN5 is calculated from a choice of correlations, all of which will yield reasonable starting locations for transition but tend to underpredict transition length (GAUGLER(1981)). As an option to the use of the program as a prediction tool the operator can specify a transition location or a particular transition momentum Reynolds number and use the program to correlate experimental data (as GAUGLER(1985) has done).

Results of the use of STAN5 in various facilities has been reported by GAUGLER(1985a). In general the program will yield reasonable results for heat transfer coefficient if transition is properly modeled. Transition modelling is as yet problematical, however, and the use of the current version as a prediction tool has limitations.

An anomaly pointed out by GAUGLER(1985b) is the failure of STAN5 to yield best agreement with data obtained from transient facilities. This is in evidence in Gaugler's 1985a paper for the data of SCHULTZ et al.(1977)

and of CONSIGNY and RICHARDS(1982) at their higher turbulence level. Reasons for this anomaly are unknown.

It is of benefit here to clarify the use of some of the input parameters so that others may readily use the program and to mention some of the more important results of changing the parameters.

The current version of STAN5 will calculate the initial boundary layer profile if the leading edge can be characterised as a cylinder with stagnation point at x=0. This author modified the calling subroutine to include the variable XSTPT, the x location of the stagnation point, so that experimentation with moving this point could be facilitated. This change also required some other minor modifications, notably in the calculation of the arc length on the leading edge circle and in the change in surface length for Reynolds number calculation from XU to XU-XSTPT.

If one uses enthalpy as an input boundary condition (enthalpy or heat flux can be used) one must calculate the values from known wall temperature(s) using the table of properties in subroutine PROP2. Input values of enthalpy are those measured from a reference state and are not the value $c_p T$.

The use of the turbulent kinetic energy equation (one equation model) to calculate mixing length does not produce substantially different results from the more simple zero equation model and further can cause specious results if input parameters are not carefully chosen. The lack of difference in the two cases is probably due to the fact that neither model allows for a streamwise dependent dissipation rate (or length scale).

As discussed by GAUGLER(1981) STAN5 can predict the onset of separation (the friction factor goes to zero), and if this occurs the input surface velocity distribution must be modified by the user. The program cannot calculate through a separated region and so one must run the program a second time with a specified transition Reynolds number or a specified

location of transition.

In applications with small temperature differences the use of a constant wall temperature will yield results similar to adiabatic wall conditions. This author chose the latter because it more closely approximates the actual flow conditions.

The selection of the number of transport equations is controlled by the variable NEQ. The value 2 (momentum plus energy) is the most usual input (GAUGLER(1985b)). But this important input variable can be a source of confusion. In general it should be given a value of two. This will cause both the momentum and energy equations to be solved and will require only one wall boundary condition (the FJ(J,M) variable). If TYPBC is taken as one, enter values of FJ(J,M) equal to the wall enthalpy. With TYPBC equal to two enter those values as energy flux (zero for adiabatic flow). Enter all values using the English system (lb-ft-s). Surface distances and leading values should be entered in feet, velocities in ft/s, and wall enthalpy in BTU/lbmR.

3.7 HOT WIRE ANEMOMETRY

It was planned early in the design of the new blowdown facility to utilize its size and capabilities for experiments with large models and to perform detailed investigations into boundary layer phenomena.

The hot wire anemometer is an appropriate instrument for these studies. Its small size allows for fine spatial resolution of mean and fluctuating parameters in the boundary layer and it presents only a small blockage to the flow. Considerable time was spent developing a methodology of calibration and use of hot wires for the new blowdown tunnel but with only mixed results.

The results, however, are important to future experiments in the

blowdown tunnel, and for this reason alone must be reported. In the interest of compactness, the results of this work, along with background information, theory, and test objectives, are all presented in chapter four.

CHAPTER IV

HOT-WIRE ANEMOMETRY

4.1 INTRODUCTION and PURPOSE OF EXPERIMENTS

One of the features of the blowdown tunnel is its capability for full-scale Mach and Reynolds number simulations on large models. The large-chord B22 profile was the first of these large models tested. For tests on this model the hot-wire probe was selected for use in detailed boundary layer surveys. Before starting these tests, however, some study of the hot-wire system was required. This chapter is concerned with the results of this study.

One major problem involved with the use of a hot wire concerns the calibration of a probe which responds non-linearly to changes in the phenomenon of interest and non-trivially to changes in properties of the environment. A second problem is that certain specifications on probes and associated instrumentation cannot be verified and, thus, parametric studies of the probe system are difficult. Ultimately the user will abandon his search for universal laws (since they cannot easily be put into practice), and, instead, study the behaviour of his particular system from a functional standpoint.

The study of hot wires in this chapter was divided into three categories. The first is concerned with heat transfer mechanisms. This topic is important in understanding the significance of changes in such variables as wire temperature and gas temperature and in establishing a relationship between the measured quantity, voltage, and the phenomenon under study, velocity or temperature. The second category deals with hardware, i.e., details of the wire and anemometer system: electronic circuitry, hot-wire resistance, amplifier feedback system, zero-flow power,

etc. These hardware-related characteristics will emphasize the need for empirically-determined adjustments to theoretical heat transfer laws for the hot wire. The third category deals with calibration and response laws. This final topic is concerned with the derivation of system-dependent mathematical relationships. One finds that the behaviour of a particular wire can be reliably predicted only after considerable calibration and that, in general, the responses of a mixed group of hot wires are not accurately predictable from basic heat transfer laws. Part of this is due to the influence of random aeroelastic behaviour of a hot wire (cf. PERRY(1982)). Other influences include the geometry-dependent and velocity-dependent temperature distributions in the wire which tend to induce variations in end conduction to the prongs, in turn creating virtual velocity signals (LARSEN and BUSCH(1974)). For application in the blowdown tunnel, the calibration of a hot-wire is further complicated by the reduced mean temperature and mean pressure accompanying transonic flow over a large-scale turbine blade.

4.2 BACKGROUND INFORMATION AND THEORY

The usefulness of a hot wire is due to its change in temperature (and resistance) in response to a cooling external flow. For a constant temperature anemometer (CTA) system a change in wire cooling results in a change in voltage and current in the wire in order to maintain the sum of wire and support (prong) resistance at a constant value (this is discussed in more detail in section 4.3.3). It is desireable to relate the change in voltage to the cooling effect caused by a change in gas temperature or velocity. Other variations in the flow, such as changes in pressure and concentration, humidity, and compressibility, can also modify the heat transfer occurring in the hot wire. The successful use of a hot wire hinges on knowing the response of the hot wire to these factors individually and

its behaviour in varying flow conditions. It is with this in mind that a brief discussion on hot-wire heat transfer mechanisms is presented in the following section, 4.2.1.

4.2.1 Heat Transfer: The Infinite Cylinder Model

The heat transfer model most analyzed in the past was that of a long cylinder for which conduction heat loss at the ends is zero. If the cylinder is maintained at a constant temperature through heating from an electrical current, internal heat generation is balanced by forced convection cooling. This may be expressed as

$$i_w^2 R_w = hA(T_w - T_g) \qquad \ldots 4.1$$

where subscripts w and g are for wire and gas, respectively. The symbols h and A represent the heat transfer coefficient and surface area of the cylinder, respectively. Radiation losses, which are two orders of magnitude smaller than convection losses, are usually ignored.

The heat transfer coefficient, h, can be written as $k_f Nu/d$. Thus, with $A = \pi dL$, the heat balance can be recast in the form,

$$i_w^2 R_w = \pi k_f L Nu(T_w - T_g) \qquad \ldots 4.2$$

where Nu is the Nusselt number and k_f is the thermal conductivity of the fluid (usually evaluated at either the film temperature, $T_f = (T_w + T_g)/2$, or freestream temperature, T_g).

It is convenient to express the heat balance of equation 4.2 in a form which explicitly includes the bridge voltage, designated here as V_b (see figure 4.3 also). The bridge voltage is the quantity which usually is measured and correlated in hot-wire response laws. The transformation of equation 4.2 is aided by replacing the wire current, i_w, with its equivalent value,

$$i_w = V_b/R_T \qquad ...4.3$$

The value R_T represents the sum of bridge series resistance, cable resistance, prong resistance, and wire resistance. (See figure 4.3). By substituting equation 4.3 into 4.2 the heat balance equation becomes:

$$V_b^2 = \pi k_f L R_T^2 (T_w - T_g)(1/R_w) Nu \qquad ...4.4$$

It is convenient to combine all terms dependent on T_w, T_g, and geometry in one function, G. That is,

$$G = \pi k_f L R_T^2 (T_w - T_g)(1/R_w) \qquad ...4.5$$

This allows a simple relationship between voltage and Nusselt number.

$$V_b^2 = G \cdot Nu \qquad ...4.6$$

For fixed wire parameters and a constant k_f, the function G is constant; thus, for an infinite wire it is possible to relate Nusselt number to measured voltages. If one uses a high overheat, defined as the ratio of hot-to-cold wire resistance, R_w/R_a, (a value typical of the overheat ratio used with the 55P11 probe and 55D01 CTA is 1.8), the value of G with T_g=285K is approximately

$$G \approx 15 \qquad ...4.7$$

Bridge voltage, V_b, for a velocity of 30m/s is approximately 5.5v, thus the magnitude of the Nusselt number is approximately two.

Though compact, the form of equation 4.6 may include in both terms, G and Nu, the effects of wire and gas temperatures. This is due to the functional dependence of the Nusselt number on such quantities as Reynolds number and Prandtl number which are sometimes evaluated at the film temperature, T_f. One of the objectives of the research reported in this

chapter was to examine the effect of wire temperature and gas temperature on the Nusselt number with a view to deriving an analytical form relating voltage fluctuations to velocity and temperature fluctions. However, a complicating effect, that of heat loss to the prongs, occurs when the wire is finite in length. This topic is discussed further in section 4.2.3.

4.2.2 Nusselt Number Correlations for the Infinite Cylinder

The Nusselt number, Nu in equation 4.6, has been the subject of much study. The most widely discussed and/or accepted correlations will be briefly reviewed in this section. All of the correlations concern theory and data centred around cylinders of large aspect ratio (large L/D) and thus represent results which, inevitably, must be modified for practical hot-wire use. Nominally, a large aspect ratio would be of order 2000 whereas for practical hot wires this value is likely to be around 200, a value for which the wire temperature distribution and hence the end conduction becomes significant (cf. the data of CHAMPAGNE et al.(1967)).

KING(1914) is credited with the original theoretical contribution to heat transfer effects on convectively cooled cylinders. His theoretical solution involved the use of a potential flow velocity distribution, however, and has limited applicability. The form of his experimental correlation has endured, however, and has served as the basis for formulations in use today. King's result can be summarized as

(KING'S LAW) $$Nu = A + BU^{1/2} \qquad ...4.8$$

The values of A and B in equation 4.8 depend on wire diameter and temperature as well as on fluid properties, and U is the freestream velocity.

King's Law tends to overestimate the Nusselt number, and COLLIS and WILLIAMS(1959) suggest that King's original data contained some systematic

errors. Thus, while the precise values of A and B in equation 4.8 may no longer be of interest, the form of equation 4.8 continues to be the working model for theoretical analyses.

It should be noted that equation 4.8 is a two-term correlation. There are several one-term correlations (e.g. HILPERT(1933)) which apply to heat transfer on cylinders at high Reynolds numbers. Hilpert's correlation does not provide the accuracy for calculating the sensitivities needed in hot-wire work and is not widely accepted.

Subsequent to KING's(op cit.) work KRAMERS(1946) revised the coefficients in King's law to include an explicit dependence on Prandtl number. Kramers' expression is widely accepted and appears extensively in theoretical analyses:

(KRAMERS) $$Nu = 0.42Pr^{0.2} + 0.57Pr^{0.33}Re^{0.5} \qquad ...4.9$$

In a later development COLLIS and WILLIAMS(1959) showed experimental data on hot wires of large aspect ratio which suggested a deviation from the usual square-root law, as in equations 4.8 and 4.9, in favour of one with a variable exponent on the Reynolds number. This exponent would have two values for two different velocity ranges, the ranges joined at the point of the onset of wire vortex shedding. The Collis and Williams correlation also includes a temperature loading factor which apparently accounts for the change in wire temperature distribution due to changes in wire mean temperature. The form of their relationship is

(COLLIS and WILLIAMS) $$Nu = (A + BRe^{n})(T_f/T_g)^{0.17} \qquad ...4.10$$

where n=0.45 for Reynolds numbers less than 44 (onset of vortex shedding) and n equals 0.51 for larger Reynolds numbers. The values of A and B are 0.24 and 0.56 (lower Re range) and supposedly are independent of wire temperature. COLLIS and WILLIAMS(op cit.) evaluated all gas properties at

the film temperature.

One important result of Collis and Williams' work was that their data confirmed the idea that the exponent in King's law should be regarded as a calibration constant dependent on wire particulars and only roughly equal to 0.5. Nowadays, with the temperature loading factor in equation 4.10 absorbed in the coefficients A and B, the modern version of King's law is written in the variable-exponent form,

(KING'S LAW: MODERN FORM) $$Nu = A + BRe^{n} \qquad ...4.11$$

Other relationships for Nusselt number can be found (cf. INCROPERA and DEWITT(1981)) and they all mainly relate to results from data on heat transfer for infinite cylinders. The effect of end conduction to the wire supports in a wire of finite length, however, reduces the practical value of the above correlations. This feature is discussed further in the next section, 4.2.3

4.2.3 The Finite-Length Hot-Wire Model

The primary effect of finite wire length is to cause heat conduction to the end supports (prongs) resulting in a significant portion of the voltage required to heat the wire appearing as a virtual fluid dynamic cooling signal. The end-conduction loss is partly responsible for the inconsistencies in many of the empirical response laws developed over the years. The theoretical analysis of the finite-wire heat transfer problem with end conduction is problematical. This is due, in part, to the fact that prong temperature is a boundary condition, and its magnitude depends on such factors as prong geometry, probe orientation, and flow effects, all of which combine to preclude specifying accurate boundary counditions.

Even if an accurate heat transfer model existed, probe dynamics

would probably invalidate the results. PERRY(1982) shows that under aerodynamic loading heated wires distort, sag, and buckle. His photographs indicate locations on the wire where hot spots arise and move in response to varying stream velocities, altering the wire shape and temperature distribution. In spite of these practical difficulties it is of interest to examine the results of a simplified heat transfer analysis in order to identify parametric groupings which are important in determining the resulting heat transfer and response law of the hot wire.

LARSEN and BUSCH(1974) performed an analysis of the finite-wire heat transfer problem, and their results are probably as accurate as can be found anywhere in the literature. The prong temperature they used for the end boundary condition was estimated from the pioneering data of CHAMPAGNE et al.(1967) whose infra-red measurements indicated that in certain instances prong temperatures can be 60^{o}C higher than the ambient gas temperature. Larsen and Busch showed that results for wire temperature distribution depend largely on prong temperature and on the form of the assumed Nusselt number law, which, in their case, was taken to be the KRAMERS(1946) relation, equation 4.9. The results of their analysis indicated that for low velocities, say 1m/s, end conduction losses accounted for 26% or more of the total heat loss. At higher velocities (15m/s was the highest velocity calculated) the end conduction reduced to values of order 15%, dependent on velocity. BRADSHAW(1971) quotes similar values for the case where the prongs are at the ambient gas temperature. The end-loss values given by CHAMPAGNE et al.(op cit.) actually show a strong dependence on L/D ratio, the fractional value of end conduction varying in inverse proportion to this ratio, but with end-conduction losses slightly lower than those in the Larsen and Busch calculations. Further, it should be noted that Larsen and Busch's results overpredict the mid-wire temperature compared with CHAMPAGNE's (op cit.) measurements. This

discrepancy is typical of the problems occurring in theoretical calculations as also reported by others (cf. COMTE-BELLOT (1975)).

The conclusion drawn from the Larsen and Busch analysis is that for a given wire at a fixed temperature, the velocity-dependent end-conduction can increase the wire's internal power generation disproportionately to the effect of cooling velocity. Thus, a wire not calibrated for extremely low velocities will indicate an apparent increased velocity. The results of the Larsen and Busch analysis would also indicate that any theoretical relationship between the bridge voltage and a Nusselt number formulation based on the results of large-aspect ratio wires must somehow be modified by an end-conduction term which depends on velocity, wire geometry and wire temperature. Thus, it appears that a simple relationship such as equation 4.6, which has been much analyzed, can only be accurate over an extended velocity range if the Nusselt number is considered to be an effective Nusselt number representing the wire power consumed in two mechanisms, forced convection and end conduction. The wire term, G (equation 4.5), and Nusselt number, Nu, must be inextricably coupled by a modifier to account for the velocity-dependent end-conduction. Finally, it is interesting that the effect of increased end conduction at low velocities is not mentioned (or perhaps is considered negligible) by researchers concerned with wall-proximity effects where velocities approach zero and where there is reported an apparent (false) increase in velocity as the wire nears the wall (cf. OKA and KOSTIC(1972), HEBBAR(1980), and BHATIA et al.(1982)).

4.2.4 Heat Transfer Summary: A Working Model

A working model for heat transfer must include (at least implicitly) the effects of end conduction which becomes more significant as the flow velocity decreases. The understanding of low-velocity heat transfer behaviour is also important in that popular forms of response laws

(discussed in section 4.4) usually contain a term deemed independent of velocity (the 'A' term in King's law). However, this velocity-independent term is often associated with free convection at zero velocity (cf. AL'OMAR and BAKHTAR(1970)). For the practical (finite length) hot wires used in the current study, however, it is suggested that this term is virtually independent of free convection effects.

In assessing the magnitude of free convection or mixed free and forced convection, one usually compares Grashof number and Reynolds number. There is no universal agreement on the relative magnitudes of these parameters though a concensus arises that Grashof number must be of significant proportions in comparison with the Reynolds number. For the purpose of calculating a value of Grashof number which would indicate the presence of free convection or mixed convection, two criteria have appeared, both having individual merit. The first (cf. INCROPERA and DEWITT(1981) has the form $Gr \geq Re^2$. This form is secured on a theoretical footing since the term Gr/Re^2 appears in the non-dimensional form of the Navier-Stokes momentum equation. The second form is due to COLLIS and WILLIAMS(1959) and is suggested from the results of their experiments: $Gr \geq Re^3$. Since $Gr < 1$ for a hot wire, the second criteria allows for a larger Reynolds number at the onset of mixed convection and is the more conservative of the two. A calculation for the case of a 5 μm diameter wire at a temperature of 500^{o}C yields a Grashof number of roughly $1x10^{-6}$. For a Reynolds number of 0.01 (Collis and Williams' criteria) the flow velocity is approximately 0.05m/s (2in/s). Thus, only a small stream velocity is required to preclude the free convection heat transfer mode.

Many experimenters, in spite of the foregoing analysis, have used the zero-flow power consumption as a parameter in constructing a response law (cf. BRUUN(1976), though later he suggests alternatives: BRUUN(1979)). Unquestionably, the zero-flow bridge voltage (designated as V_{bo}) is related

to conduction and free convection at zero flow. The model to be offered now, however, suggests omitting this term when considering hot-wire response functions.

Guided by the results of LARSEN and BUSCH(1974) one can estimate the end conduction loss at zero velocity (for L/D=250) at roughly 1/3 the total heat production in the wire, with free convection accounting for the other 2/3 (radiation loss is negligible). According to the value of Gr/Re^2 given above, at a low flow velocity the free convection term will disappear, but end conduction will continue to dissipate heat. As the flow velocity increases end conduction is reduced (according to LARSEN and BUSCH, op cit.) but remains a significant loss mechanism. The magnitude of the end conduction will depend on the L/D ratio, and one would expect, as suggested earlier, that the end conduction effect would cause the Nusselt number to reflect this dependence. For comparison, the data of BAILLE(1971), as shown by COMTE-BELLOT(1975), indicates a strong dependence of Nusselt number on L/D, the Nusselt number decreasing for larger values of L/D at constant Reynolds number. It is possible that for smaller values of L/D (increased Nusselt numbers), BAILLE's(op cit.) data is showing some effect of increased end conduction. It is also possible that the temperature loading factor of COLLIS and WILLIAMS(1959), the value 0.17 in equation 4.10, is influenced by a small, velocity-dependent end conduction factor (they used large-aspect-ratio wires and estimated a 3.6% loss, worse case). This would imply that other experimenters might arrive at different temperature loading factors for various probe lengths. Indeed, this is the case (cf. KOCH and GARTSHORE(1972)). The list of different temperature loading factors reported by BRUUN(1975) points out the variability that can be found.

One can summarize the results of the foregoing discussion in a loss diagram as shown in figure 4.1. The forced convection and end conduction

losses are shown as the primary loss mechanisms. This model suggests that the zero-velocity free convection loss should be neglected at all velocities, except near zero, and further implies that if zero-power consumption is used as a calibration parameter it will only weakly correlate data where, at finite velocity, forced convection is the dominant effect. Thus, the response equation (4.6) could be recast to reflect end conduction dependence on wire parameters and Nusselt number, viz.,

$$V_b^2 = G \cdot h \cdot Nu \qquad \ldots 4.12$$

where the function, h, is simply the ratio of total heat production in the wire to the forced convection loss. The value of h will be larger than unity for low-aspect-ratio wires (roughly equal to 1.15 for velocities greater than 15m/s (BRADSHAW(1971)) and will have a value approaching 1.35 as the velocity nears zero (LARSEN and BUSCH(1974)). The function h depends roughly on the inverse square-root of the Nusselt number (see BRADSHAW's(op cit.) analysis), and over a small velocity range h changes slowly (a result which fortuitously allows for accurate response laws over those same velocity ranges). In general, the function, h, cannot be isolated from the Nusselt number so it is more convenient to absorb h in the Nusselt number and recast 4.12 in the form,

$$V_b^2 = G \cdot Nu_e \qquad \ldots 4.13$$

where the function Nu_e is an effective Nusselt number. (Henceforth, the subcript e will be dropped, which should not cause confusion). Because of the intractable form of equation 4.13, the emphasis in hot-wire anemometry has shifted from attempts at predicting the hot-wire response theoretically to the more empirical, functional approach (BRUUN(1979)) using simplified response laws of the type shown in equation 4.11 (King's law, modern form). Hot-wire users have achieved great success using the empirical approach;

however, the onus has fallen on the user to become familiar with the characteristics of his particular system. The remainder of this chapter is devoted to the results of experiments in a similar pursuit by this author.

4.2.5 Scope of Experiments

The experiments conducted for this chapter were concerned mainly with determining an appropriate response law for the hot-wire system described in section 4.3. Of concern were the effects of zero-flow power consumption on the form of the response law and the effects of changes in wire temperature and freestream temperature on the output voltage of the anemometer system. Another objective was to determine the certainty with which a response law developed from a limited range of velocities could be applied to an extended range of velocities. Finally, the results of initial studies in the blowdown wind tunnel to determine the frequency spectra of turbulent fluctuations are reported.

4.3 EXPERIMENTAL APPARATUS and PROCEDURES

4.3.1 General Description of Apparatus

All experiments were carried out in a low-speed (0-50m/s), open circuit wind tunnel. A schematic diagram of the experimental setup is shown in figure 4.2.

Hot-wire signals for all tests were provided by a Disa 55P11 miniature, single-wire, platinum-plated, tungsten probe. Eight probes in all were tested, each with a diameter of 5 μm (according to manufacturer's specifcations) and all having an average length of 1.25mm (L/D=250). The tunnel speed for most experiments varied from 20m/s to 45m/s and resistance ratios (R_w/R_a, hot resistance/cold resistance) varied from 1.2 to 1.8. Reynolds numbers based on wire diameter ranged approximately from 2 to 15. The probes were held in place by a Disa 55H22 right-angle probe holder and

mounted such that the long axis of the probe (not the wire) was aligned with the flow direction. Inclination of the wire to the tunnel centreline direction was set visually at zero degrees (previous tests in the tunnel indicated negligible flow angularity).

Probe output was monitored by a Disa 55D01 constant temperature anemometer (CTA). The CTA was equipped with adjustable gain, controls for input/output bias voltage variation, induction compensation and bandwidth control, all accessible on the front face. Bridge voltage was measured using a calibrated digital voltmeter with 4.5 digit accuracy. Between the CTA and voltmeter was a lowpass RC filter having a cutoff (-3db) frequency of 2Hz. An oscilloscope also monitored bridge output in order to detect closed-loop feedback oscillations in the CTA bridge circuit.

Wind speed was calculated from total and static pressures measured using a pitot-static tube and a 5:1 ratio inclined manometer. The pitot-static tube was mounted with its sensing ports three inches below the wire and in the same vertical plane.

Test section temperature was monitored via a single K-type (chromel-alumel) miniature thermocouple and Comarc digital thermometer. The thermocouple projected through the top wall of the tunnel to approximately 175mm (seven inches) above the hot-wire probe. A change in temperature of more than $1^{o}C$ during any run was cause for discarding the data.

4.3.2 Wire Temperature

In order to study the parametric behaviour of the CTA system, the wire temperature, wire resistance, and gas temperature must be known. The wire temperature is calculated by inverting the relationship,

$$R_w = R_o(1+a_1T_w+a_2T_w^2) \qquad ...4.14$$

where R_o is the wire resistance at $0^{o}C$, T_w is the wire temperature in ^{o}C,

and a_1 and a_2 are temperature coefficients which account for non-linear variations in resistance. If T_w equals the ambient air temperature then R_w becomes R_a. Temperature coefficients given by BRUUN(1975) were found to agree well with ambient temperature measurements and were subsequently used for the high temperature calculations. These coefficients are

$$a_1 = 0.00385/^oC$$

$$a_2 = 1.1x10^{-6}/(^oC)^2$$

The next section discusses the methods used to determine the resistances needed for equation 4.14.

4.3.3 Wire Resistance

In attempting to ascertain the wire resistance one encounters the major source of uncertainties in the use of hot wires. These uncertainties are involved mainly with the uncertain knowledge of prong temperature and the fact that the CTA is essentially a constant resistance device in which wire temperature may vary slightly if the gas temperature changes. This effect is discussed further below and is in accordance with the findings of BRUUN(1975).

In figure 4.3 is shown a schematic of the bridge circuit used in the 55D01 CTA. As shown in the figure a 20:1 resistance ratio was used for the experiments. The hot-wire resistance is basically established by the variable decade resistor, R_v. The zero-ohms adjuster is intended to offset the cable resistance which remains at its room temperature value. The maximum zero-offset available on the the 55D01 CTA is 0.54ohms, slightly less than the resistance of the particular cabling used in the experiments. Thus, it was necessary to monitor the excess cable resistance, labeled R_c in figure 4.3. The portion of the cable resistance offset by the zero-ohms adjuster (0.54ohms) is labeled R_{co}.

The resistance value on the decade resistor is set manually prior

to the run. The resistance sum, wire plus prong, is then maintained at a constant level by the feedback amplifier which amplifies and inverts the bridge-unbalance voltage. The amplifier maintains the bridge-top voltage, V_b, at a value designed to so heat the wire, increasing (or decreasing) its resistance, as to nullify the bridge-unbalance voltage. This operation would be inherently unstable without the presence of a small unbalance voltage (input bias) applied to the amplifier input terminals.

As can be seen in figure 4.3 the decade resistance equals the sum of three resistances:

$$R_v = R_w+R_{pr}+R_c \qquad ...4.15$$

In this expression R_v is the decade resistance value and the subscripts w, pr, and c refer to the wire, prongs and excess cable resistances, respectively. The value of R_c is measured prior to the run using a shorting plug as shown in figure 4.3. With R_v and R_c held constant during the run the information known with certainty is the sum R_w+R_{pr}.

According to LARSEN and BUSCH(1974) the prong temperature can be estimated from the data of CHAMPAGNE et al.(1967) if one knows the wire temperature and gas temperature:

$$T_{pr} = T_g + r(T_w-T_g) \qquad ...4.16$$

where r is a factor which depends on probe geometry and cooling velocity and which, according to LARSEN and BUSCH (op cit.), varies between the values 0.2 and 0.3.

It is of interest to estimate the uncertainty in wire temperature which comes about due to the uncertainty in r. Using the value 0.25 for r and a typical set of probe parameters (resistance ratio=1.8, T_g=10°C, R_c=0.05 ohms, R_v=7.5 ohms) one finds from equations 4.14, 4.15, and 4.16 that T_{pr}=70°C and T_w=245°C. If r=0.0 for these same conditions T_w=255°C, a

difference of 10 degrees. If the gas temperature changes, one can calculate, for the same overheat, a wire-to-gas temperature sensitivity of -0.1, i.e., a fall of 10 degrees in gas temperature will result in a rise in wire temperature of one degree. Thus, one can conclude that the wire temperature is significantly uncertain at high overheat. Since T_w changes when the mean gas temperature changes (and even when the cooling velocity changes because of the change in prong temperature), the functional dependence of the wire voltage on changes in freestream temperature is difficult to predict. Fortunately the thermal inertia of the prongs is sufficiently high that turbulent temperature fluctuations have no effect on the mean prong temperature. For lower overheat ratios the uncertainty in T_w is less. For example, if the resistance ratio is reduced to 1.25 the uncertainty in T_w, due to the uncertain value of r, is zero.

4.3.4 Zero-Flow Heat Transfer

Zero-flow heat transfer consists of free (natural) convection and end conduction which occurs at the wire-prong junction. The relative magnitude of these two modes of heat transfer is dependent on probe geometry and is considered here separately as a system parameter, somewhat under the control of the user via the decade resistance setting. The magnitude of the two modes of heat transfer can be estimated by calculating the free convection loss from correlations found in the open literature for an infinite cylinder and subtracting the result from the measured total heat loss to obtain the end loss. This is done by noting first that

$$\% \text{ End Conduction Loss} = 100 - \% \text{ Free Convection Loss} \qquad \ldots 4.17$$

Using the definition for G from equation 4.5, equation 4.17 reduces to

$$\text{Fractional End Condition Loss} = 1 - Nu_f/(V_{bo}{}^2/G) \qquad \ldots 4.18$$

where Nu_f represents the Nusselt number for free convection and V_{bo} is the zero-flow, bridge-top voltage. A correlation for the Nusselt number was taken from INCROPERA and DEWITT(1981) and due to CHURCHILL and CHU(1975) (a complex power-law expression omitted here for brevity).

End conduction was calculated for probe four (evaluating all gas properties at the film temperature), and the results are shown in figure 4.4. The end condition is plotted versus driving potential, T_w-T_g, and is seen to decrease from approximately 40% at low temperature differences (low overheat) to approximately 30% at higher overheats. These results are roughly in accord with the calculations of LARSEN and BUSCH(1974) and exhibit the same trend as the data of CHAMPAGNE et al.(1967). The latter's data show that higher overheats cause the temperature distribution along the wire to be more uniform, with the temperature gradients more confined to the region near the prongs. Although a more complete model for zero-flow heat transfer cannot be offered, the results shown in figure 4.4 support the suggestion made earlier of increasingly larger end conduction losses at velocities approaching zero.

4.3.5 Wire Contamination

Early tests with various hot wires were not repeatable. It was discovered that a run duration of only 20 minutes in the closed laboratory environment was sufficient to contaminate the wires and significantly reduce the CTA voltage output. This effect is illustrated in figure 4.5. For the test results shown in the figure, three consecutive runs were made under identical conditions of ambient gas temperature and wire resistance. For the first and third runs the wire was pre-cleaned (stirred gently in methanol). For the second run the wire remained uncleaned. The squared-voltage-response for the uncleaned wire was reduced by roughly four to six percent. All data accumulated prior to this finding were discarded.

Similar discrepancies have since been reported by MARTINEZ-VAL et al.(1982). Their data shows that in addition to contamination-caused mean velocity errors, there also occurs a reduced sensitivity to fluctuating velocity, with the acquired surface film on the wire reducing the penetration depth of cooling perturbations.

4.3.6 Nusselt Number Calculations

For parametric studies, one calculates the effective Nusselt number from the bridge-top voltage according to equation 4.13, which includes the parameter, G. As shown in equation 4.5, the parameter G contains the thermal conductivity of the fluid, k_f. One must choose a reference temperature at which to evaluate thermal conductivity, and usually the choice is among gas temperature, film temperature, or some other reference temperature which may more suited for various flow conditions (e.g., recovery temperature). Further, when Nusselt number is correlated with Reynolds number and Prandtl number, similar choices must be made. In the case of heat transfer dominated by the forced convection mode, it would seem natural to use the film temperature in calculating fluid properties. However, this choice does not necessarily cause the data to collapse on a single curve, and, thus, the experimenter must inevitably try other reference temperatures. For the studies presented in this chapter the choice of reference temperature will be noted for each particular case.

4.4 EXPERIMENTAL RESULTS

4.4.1 Comparisons with Correlations for Long Cylinders

KRAMERS(1940) suggested the relation shown in equation 4.9 which correlates data for forced convection heat transfer from long cylinders at low Reynolds numbers. COLLIS and WILLIAMS(1959) offered the later version shown in equation 4.10 which included a temperature loading factor and the new exponent, n=0.45. Hot-wire data is shown in comparison with these formulations in figure 4.6. The Nusselt numbers for the hot wire were calculated using equation 4.6, with all properties evaluated at the film temperature. The computed wire temperature for the tests was 405K, and the gas temperature was 292K.

As shown in figure 4.6, for low Reynolds numbers the wire response data lie above the theoretical correlations for long cylinders. As the Reynolds number is increased the data cross the correlations and lie below the theoretical curves. The slope of the data appears near that of the Kramers correlation (square-root law) at lower Reynolds numbers but smaller than the slope of the Collis and Williams correlation (0.45 law) at higher Reynolds numbers. The trends shown in figure 4.6 were observed in all wires tested. It was found that the use of a two-term correlation, as in equation 4.11, to describe the behaviour shown in figure 4.6 leads to inconsistencies in the response equations. This is discussed next.

4.4.2 King's Law: Two-Term Correlations

BRADSHAW(1971) suggests that the exponent in King's law, equation 4.11, should be determined empirically by curve-fitting the data accumulated during the calibration process. While this is feasible if the velocity range is small, for an extended velocity range it poses a dilemma in that various exponents can be found which reasonably correlate the

calibration data. As shown in figure 4.7, the data of figure 4.6 can be correlated with both a '0.4' law and a '0.5' law (as well as with other exponents within and outside those limits). Both of the straight lines through the data in figure 4.7 have a correlation coefficient greater than 0.999. Thus, the accuracy of mean velocity data is not sensitive to the exponent used; however, the slopes of the curves, which determine the sensitivity of the wire to cooling fluctuations, can differ significantly.

In figure 4.8 is shown the hot-wire system sensitivity, $\partial V_b/\partial Re$ as calculated numerically from the data in figure 4.7 and analytically from the two response laws shown in figure 4.7. The raw-data sensitivity follows the '0.4' response law at low Reynolds numbers but oscillates (still nearer the '0.4' law) at higher Reynolds numbers. The oscillation is due to the imprecision in numerical differentiation (which is aggavated by reduced system sensitivity). Thus, whether the data best fits a '0.4' law or perhaps a '0.45' law is not clear. Other probes tested yielded similar results, viz., more than one exponent fitted the mean data. The exponents were found to vary from 0.2 to 0.55 depending on the probe used. Similar difficulties were reported by PERRY and MORRISON(1971) who further demonstrated that, if one designated the coefficient, A, in King's law to be the zero-flow voltage (squared), the use of a constant-exponent (independent of velocity) response equation would never yield the correct system sensitivity over an extended velocity range.

Alternative attempts by researchers to derive an extended-range response equation include allowing the exponent to vary with velocity (cf. ELSNER and GUNDLACH(1973)) or allowing the coefficients, A and B, in equation 4.11, to vary (such as implicitly suggested by BRUUN's(1970) analysis). Though these methods lead to greater accuracy there is no inherent gain in accuracy over other mathematical forms for the response equations which may be more easily mathematically manipulated and less

cumbersome in use when calibrating the hot wire.

4.4.3 Higher-Order Response Equations

From the discussion above it is clear that any hot-wire response equation designed to correlate data from a finite-length hot wire must include a minimum of three free coefficients to allow for intercept, slope and curvature of the data. However, two-term correlations (which satisfy the three-degree-of-freedom criteria) appear imprecise with respect to system sensitivity, especially over extended velocity ranges. A remedy was suggested by van der HEGGE ZIJNEN(1956) who added a third term, CRe, to the King's law response equation, equation 4.11. (In principle, there is no reason to exclude any number of terms, so an n^{th} order polynomial is equally as valid). For use with constant properties, SIDDALL and DAVIES(1972) report great success with the simplfied version of the three-term correlation,

$$V_b^2 = A + BU^{1/2} + CU \qquad \ldots 4.19$$

The coefficients A, B, and C are considered constant for a given hot-wire system. The coefficient, C, is usually of small magnitude and is considered a correction term. The correlation equation given by equation 4.19, while allowing for good calibration accuracy, still does not remove the disadvantage of including in three coefficients an implicit dependence on such things as wire temperature, gas temperature, pressure, etc. Thus, the study of system parametric behaviour remains difficult, and there is no new understanding of the physics of the heat transfer process. Nevertheless, calibration is simplified by removing the need to search for a best-fit exponent. The three-term correlation has been applied to the probe data of figure 4.6 and is shown in figure 4.9.

In general, the three-term correlation in equation 4.19 was found

superior to the two-term correlation both in fitting the raw data, as shown in figure 4.9, and in fitting the system sensitivity, as shown in figure 4.10. BRUUN(1971) showed that a three-term correlation fitted his data with good precision over the velocity range, 15m/s to 150m/s, in spite of his designating the coefficient, A, to be equal to zero-flow voltage (squared). Allowing the coefficient, A, to be a line-fitted value, this author was able to fit Bruun's data over the extended range, 0.8m/s to 150m/s, demonstrating the inherent capability of the three-term correlation to allow for curvature of the slope of the data. This author also found that fitting a straight line to the derivative of equation 4.19, i.e. $d(V_b^2)/dU$ versus $U^{-1/2}$, resulted in more accurate coefficients and allowed for a full-range correlation to be determined from an intermediate range of data. Thus, for constant-property flows, the use of equation 4.19 allows the results from a calibration over a limited velocity range acquired, say, in a low-speed wind tunnel, to be extrapolated outside the range of calibration.

4.4.4 Temperature Effects

It is not unusual for the gas temperature during a run to be different from the temperature existing for the hot-wire calibration. This temperature difference can be a result of a change in the ambient temperature in the case of an open-circuit tunnel or, in the case of the blowdown tunnel, a result of the combined effects of a fall in total temperature during the run and a high-speed flow expansion over a transonic turbine blade. Changes in mean gas temperature will also influence the wire temperature by changing the prong temperature (recall that the sum of wire resistance plus prong resistance is the quantity maintained constant by the CTA system). It is of interest, then, to determine the temperature sensitivity of the CTA system to changes in the mean gas temperature and/or

the wire temperature.

From dimensional reasoning it is appropriate to study the behaviour of the Nusselt number as it relates to non-dimensional groups such as Reynolds number, Prandtl number, Knudsen number, probe aspect ratio, orientation, etc. For a given hot-wire system, this group of parameters reduces reasonably well to Reynolds number since Prandtl number is a weak function of temperature, and the other parameters remain constant. Arguably, slip flow can be important, resulting in what is known as the temperature jump, a discontinuous temperature change from the wire to the gas. Calculations for wires of the diameter (5μm) used for the experiments herein result in Knudsen numbers of order 0.02. Using the results of the kinetic theory of gases (cf. the expression in WHITE(1974)) and values of Reynolds and Mach numbers typically occurring in this hot-wire work (M=0.1, Re=4, say), one can calculate the temperature jump to be approximately 20^{o}. This temperature drop would then reduce the film temperature by 10^{o}. The certainty in the result of a calculation of this type is impossible to assess, however. The best approach would be to minimize changes in slip-flow effects by maintaining the temperature loading, T_w-T_g, as near as possible to the value existing during calibration. Failing that, one must have sufficient information on temperature effects to correct the data. If slip flow effects are ignored, the relationship to be studied has the form,

$$V_b^2/G = Nu(Re) \qquad ...4.20$$

Then using a three-term correlation, a practical hot-wire response equation has the form,

$$V_b^2/G = A + BRe^{1/2} + CRe \qquad ...4.21$$

The above form is similar to the one proposed by van der HEGGE ZIJNEN(1956). Note that the values G and Re both contain gas properties

which must be evaluated at a designated reference temperature.

The effect of changes in wire temperature were studied by varying the decade resistance values for various values of freestream velocity. These results are shown in figure 4.11 for a constant gas temperature of $4.2^{o}C$. It was found that the use of thermal conductivity evaluated at the mean gas temperature, T_g=$4.2^{o}C$, decoupled the dependence of Nusselt number on wire temperature except for low overheats (where, as suggested from the results shown in figure 4.4, end conduction can increase to a large fraction of the total heat production in the wire). This appears to be new information on hot-wire behaviour. The usual method of evaluating the thermal conductivity at the film temperature resulted in correlations similar to those shown by BRUUN(1975) where for a constant velocity the Nusselt number decreases as wire temperature increases.

It would seem that the study of temperature effects could be reduced to the study of the temperature loading, T_w-T_g (or T_w-T_g/R_w), and, thus, be reduced to the study of the results of figure 4.11 alone. However, as will be shown, this was found to produce inconsistent results.

Changes in gas temperature generally result in increased power as shown in figure 4.12 where the bridge voltage is seen to increase with decreased gas temperature for any velocity. The changes in gas temperature were due to changes in atmospheric temperature on the same day. For the two cases shown in figure 4.12 the wire temperature, as calculated by methods described earlier, differed by approximately $1.7^{o}C$ at a magnitude of $201^{o}C$, a 0.4% variation in absolute temperature. Reducing the data to the functional form of equation 4.20 resulted in the correlation shown in figure 4.13. Gas properties for the Reynolds numbers in figure 4.13 were evaluated at the gas temperature, whereas the thermal conductivity was evaluated at the film temperature. This combination of temperatures is most often used by researchers as it accounts for variable gas properties and

conveniently decouples the Reynolds number from wire temperature. Other combinations of temperatures were tried but failed to correlate the data as well as shown in figure 4.13. Even so, there is a slight (1%) systematic deviation in the reduced data indicating that changes in gas temperature affect the Nusselt number in a slightly different manner from changes in wire temperature alone. BRADSHAW(1971) suggests that data such as that shown in figure 4.13 will never collapse onto a single curve without using a temperature loading factor as was done by COLLIS and WILLIAMS(1959) in their experiments on large-aspect ratio wires. Nevertheless, the results shown in figure 4.13 are encouraging and indicate the merit of further experiments to identify the effect of imposing a temperature loading factor on the correlations.

Other researchers have tackled the temperature problem in different ways. BEARMAN(1971) used a simple temperature loading analogy to correct the coefficient, A, in the two-term, King's law equation (equation 4.11). A similar analysis by this author failed to yield the desired accuracy. The empirical approach used by KANEVCE and OKA(1973) yields results which are system-dependent but which capture the spirit of hot-wire use, viz., one must calibrate and understand the particular system in use.

4.4.5 Measurements of Frequency Spectra

The initial use of hot wires in the O.U.E.L. blowdown tunnel was limited to the measurement of frequency spectra since flow environmental effects on the mean hot-wire response were as yet undetermined. Of interest, at first, was the determination of the frequency range in which the majority of fluctuating energy was contained. The large-chord, B22 profile served as the cascade model for these tests with the intention of following the initial spectra measurements with detailed mean and fluctuating velocity measurements in the boundary layer at various

locations on the blade surface. Each of the hot-wire probes used was calibrated in the low-speed, open-circuit wind tunnel prior to use in the blowdown tunnel so that flow environment effects could be simultaneously observed.

Data were collected using a transient recorder (see chapter two) sampling 4096 data points per channel at a rate of 200kHz. The fluctuating portion of the CTA bridge output signal was bandpass filtered prior to measurement by the transient recorder using a Barr&Stroud filter with low and high -3db points set at 1kHz and 75khz, respectively, the higher value intended to prevent aliasing of the measured signal. Polaroid photographs of oscilloscope traces were made during each run to ascertain the presence of CTA bridge oscillations; and whenever any change was made to the measurement setup the still-air frequency response of the anemometer was re-measured using a 1kHz square-wave signal obtained from a variable-frequency oscillator. Typical magnitudes of cutoff frequency for the anemometer ranged between 16kHz at low frequency gain settings (gain = 3 on the DISA 55D01 CTA) and 40kHz at higher gain settings (gain = 5).

Post-run processing was accomplished using software specially prepared by this author and utilizing the fast Fourier transform (cf. BRIGHAM(1974)) to reduce raw voltage signals. Output from this software included results of squared-signal (power) versus frequency.

Oscillations in the anemometer system during runs in the blowdown tunnel proved to be a significant problem. These oscillations were typically of order 100kHz with an amplitude of roughly 0.05 volts. Although bandpass filtering removed these high-frequency components it was necessary to determine the influence of bridge oscillations on the remaining signal levels. Typical frequency spectra obtained at location x/s=0.83, tapping 37 on the suction surface of the large-chord blade (see figure 2.4) are shown in figure 4.14. Oscillations occurred in runs 1351 and 1352. Indications of

oscillations, though not certain, occurred in run 1349. (The height of the probe, measured prior to each run, is also indicated adjacent to each trace in figure 4.14). Note that the apparent falloff in energy at low frequencies is due to the bandpass filtering process. In runs 1354 and 1355 a different probe was used, and no oscillations occurred, suggesting that the occurrence of oscillations somehow depends on probe geometry.

Close examination of figure 4.14 suggests that for runs with oscillations there exists an apparent oscillation-induced enhancement of measured energy at frequency levels near 5kHz and a re-enhancement of the signal beginning at approximately 35kHz. The energy levels in this latter region will have been appreciably attenuated by the CTA system, however. Also, the low-frequency energy levels (around 4kHz) for runs without oscillations appear to be somewhat broader than for those runs with oscillations. All of these effects are small, however, and more testing would have been required to confirm the foregoing conclusions.

The range of frequencies containing significant levels of fluctuation can be seen in figure 4.15a. The data shown were acquired at location x/s=0.566, tapping 49 on the blade suction surface. For the runs shown in figure 4.15a the probe cutoff frequency, as measured in still-air, was 40kHz. It can be seen that the major energy levels occur at frequencies below approximately 10kHz, with smaller energy levels detectable up to roughly 20kHz.

The 99% boundary layer thickness at tapping 49 is approximately three millimeters (see chapter five). Thus, the probe heights (1mm and 2mm) shown in figure 4.15a are situated in the wake region of the boundary layer, and higher frequency levels are expected to be of interest at probe heights nearer the blade surface.

In figure 4.15b is shown the results of measurements made upstream of the cascade in the inlet region between the bar grid and cascade

entrance plane where the Mach number is approximately 0.3. These results indicate that most of the turbulent energy is contained in frequencies below 10kHz. This would suggest a connection between the frequency content of freestream turbulence and that which occurs in the wake region of the blade surface boundary layer.

Finally, preliminary calculations (not included here) indicate that mean voltage levels occurring during the foregoing runs are well-correlated with corrections made to the Nusselt number (equation 4.20) accounting for changes in temperature and pressure from those (ambient values) occurring during calibration of the hot-wire probes. This warrants further testing to determine whether corrections to wire temperature accounting for prong resistance and corrections for rarefied gas effects (temperature jump due to small wire diameter) would reduce the data sufficiently to permit the establishment of an analytical relationship between fluctuating voltage and the fluctuations in velocity (or Reynolds number) and temperature.

4.5 DISCUSSION and CONCLUSIONS

Many considerations involved with the use of hot wires in the blowdown cascade need further investigation. These include the effects of the changes in pressure and the effect of flow compressibility. Of interest also are the effects of wire inclination and orientation, which are involved with measurements with crossed wires and the measurement of fluctuating signals in the presence of velocity and temperature fluctuations. The effect of temperature and pressure changes and compressibility effects are particularly relevant to measurements made in the low-pressure, high-speed environment experienced by large-chord models in the blowdown tunnel. The study of pressure effects are difficult and time consuming, however, in that this effect cannot be studied in a constant-pressure environment using a low-speed, open-circuit wind tunnel.

Certain attempts to introduce pressure effects in the coefficients in King's law (cf.AL'OMAR and BAKHTAR(1970) via the pressure term in the Reynolds number and the Grashof number have not been sufficiently tested.

Compressibilty effects have been studied empirically by KOVASZNAY(1950) who was able to correlate hot-wire data for transonic and supersonic flow conditions. Kovasznay used King's law, a temperature loading factor, and a suitable choice of reference temperature for evaluating viscosity and thermal conductivity, and was able to reasonably collapse his data onto a single curve, but his results seem highly system dependent and not related to any rigorous heat transfer laws. The results of Kovasnay's efforts again point to the need for an extended calibration exercise to determine the response laws for a particular hot-wire system.

It appears that in boundary layer studies, where velocities are significantly reduced from freestream values, corrections for gas temperature and pressure (i.e., Reynolds number effects), using the G function defined earlier for Nusselt number correlations, may yield good results if the correct reference temperature can be determined. It is possible that accounting for slip flow effects, where the film temperature is reduced, may reduce the one percent deviation in gas temperature effects noted earlier in this chapter. In compressible flow the local gas temperature will depend on viscous dissipation and local heat conduction (Prandtl number effects). If the local temperature can be estimated for boundary layer flows, say, by using the Crocco-Buseman relationship (cf. WHITE(1974) and the discussion in chapter five), it is possible that the functional form shown in equation 4.20 may yield a suitable correlation after all.

The frequency spectra measurements conducted in the blowdown tunnel on the large-chord, B22 profile indicate that information from fluctuating flow is contained mainly in the spectral region up to 10kHz, with

components up to 20kHz reduced by roughly one order of magnitude. Measurements in these frequency ranges are within the capabilities of the instrumentation available in the O.U.E.L. Even with uncalibrated hot wires, however, one can obtain valuable information concerning freestream turbulence effects and energy dissipation in the boundary layer.

Finally, the work reported in this chapter clearly only addresses limited cases of hot-wire use. As PERRY(1981) remarks, even if one could find a response law for the straight wire one is left with the problem of probe orientation and inclination, both of which alter the flow field around the wire and render the response laws specific only to one's particular experimental setup.

CHAPTER V

EXPERIMENTAL RESULTS

5.1 COMMISSIONING TESTS

5.1.1 Inlet Tests

5.1.1.1 Flow Conditioning

As previously noted the eight-passage B22 blade (100mm chord) served as a commissioning model for the new blowdown tunnel. NICHOLSON's(1981) results on the B22 profile were taken as the standard allowing that small differences might exist due to differences in the two tunnels (Blowdown vs ILPT) especially in the downstream expansion regions.

Initial tests in the tunnel consisted of spanwise and pitchwise pressure surveys to establish uniformity and periodicity and measurements of angular incidence. ERWIN and EMERY(1951) discussed the criteria for 2-D flow in tests on their compressor and turbine cascades. A primary concern is that equal pressures, velocities, and incident flow angles should exist at corresponding spanwise locations. They found that for turbine profiles (favourable pressure gradient) these conditions are less a function of blade aspect ratio (span/chord) than of flow uniformity in the entrance duct. Their blade pressure distributions were nearly identical for blade aspect ratios of 0.83 and 3.3. (However, this was not true for the compressor blades which they tested). These results agree with the later measurements of Bolcs, Fransson, and Ridah as reported in WOOD(1980). Recall that the aspect ratio for the 100mm chord turbine cascade used in the commissioning tests is three (300mm span).

The original as-built inlet displayed considerable non-uniformity

of flow. In figure 5.1a the as-built assembly is shown. In the lower portion of the figure the results of a survey of stagnation pressures across the inlet conducted in the spanwise direction are illustrated. The reference pressure for these tests was the plenum tank pressure.

A small amount of scatter existed from run to run but clearly the variation across the span indicated a velocity defect in the centre of the inlet duct. This was also accompanied by separation regions on the semi-circular contraction pieces fixed to the side plates and in the upper regions on the long liner, near the entrance of the inlet duct. This was verified by the movement of oil dots applied in those regions.

For these studies a multi-pitot probe rake was constructed with a 45^{o} wedge yaw probe in the centre rake position. The yaw probe proved to be useful in determining qualitatively the presence of large scale, low frequency turbulence which caused unsteady fluctuations in the flow incidence angle. The computer software time-averaged the yaw pressure signal and calculated a 95% confidence limit in the measurement thereby assigning a numerical "quality" value to the turbulence effects. The scatter in the signal for the clean inlet, i.e., with no flow conditioning apparatus installed, was 168% of the mean value, a cause for concern.

A methodical approach was undertaken to identify sources of flow distortion and turbulence. This was aided by the construction of a small scale model of the inlet for smoke visualization studies. These studies led to modification of the inlet hardware.

First the sideplate-to-ceiling gap, figure 5.1a, was increased from 120mm to 200mm to reduce the severe turning and shearing of the air entering from the plenum into the inlet duct. This was helped by replacing the semi-circular entrance pieces with ones of elliptical shape. The design of the elliptical shape was after the work of ROUSE and HASSAN(1949). Their

paper provides empirical design criteria for achieving a continuous pressure drop and avoiding a severe adverse pressure gradient in the inlet transition section of a wind tunnel. The two measures stated above eliminated the separation zones on the sideplates and liners.

There remained in the inlet an unsteadiness and centre pressure deficit which were thought to be independent of any other part of the tunnel inasmuch as the frequencies of fluctuations in the yaw signal were of order 1000Hz, much higher than the oscillations in the driving pressure or of frequencies associated with resonance in the delivery piping system. The flow visualization model indicated a region of separated flow at the top of the plenum centred over the inlet duct where the incoming streams mix. The confluence of the streams created a wake-like shear zone which was convected down the duct leading to lateral velocity fluctuations observed on the yaw meter traces. This was corrected by modifying the plenum, as described below.

A curved guide vane (cusp) was fitted to the top of the plenum to smoothly divert the lateral momentum of air down into the duct, figure 5.2. In doing so the region of violent mixing was reduced to the small wake shed off the trailing edge of the cusp. This wake would either dissipate rather quickly or be greatly attenuated by the addition of a gauze screen in the inlet duct. The addition of the cusp reduced the scatter in the yaw trace by a factor of five and reduced the variation in stagnation pressure to within 0.5% (figure 5.2).

The cusp could only redirect the spanwise mixing of the airstreams entering the duct over the sideplates so it was necessary to install a honeycomb flow straightener to remove the pitchwise flow instabilities. For this purpose a four-inch deep aluminium honeycomb of 3/8 inch cell size (L/D=12) was installed. This sort of device reduces lateral velocities with

minimum pressure drop. The choice of honeycomb size in this case was dictated by availability but according to RAE and POPE(1984) the honeycomb should have a minimum L/D of 6 to 8 (no maximum is indicated). This would seem to indicate the desirability of developing a full velocity profile within the cells.

The honeycomb loss coefficient, K, (defined as the non-dimensional pressure loss, $\Delta P_o/(1/2\rho U^2)$ was calculated to be approximately 0.6. Rae and Pope give a value of 0.2 for an L/D of 6. Thus the value 0.6 seems reasonable then given twice the L/D and an approaching flow with considerable spatial distortion.

The effect of the flow straightener itself on the inlet flow was determined by running without the cusp or any gauzes installed. The reduction in stagnation pressure variation was not appreciable, but the yaw fluctuation was reduced by a factor of 18.

Wire gauzes fitted to either face of the honeycomb completed the flow conditioning apparatus installed in the inlet. Gauzes reduce streamwise variations by flattening the transverse pressure profile. This can be seen by observing that because the loss coefficient, which relates pressure drop to dynamic head, is approximately constant, regions of high velocity will dissipate proportionately more energy and experience a larger drop in velocity and pressure.

The gauze used was of 36% solidity which according to MEHTA(1984) is low enough to avoid causing instabilities (and thereby defeating its purpose). The pressure drop coefficient was 1.3 for one gauze and 2.5 for two. These values agree with those given by ANNAND(1953) as reported by Mehta for a gauze of 28 mesh, 0.007 inches diameter wire.

The combined effects of cusp, flow straightener and gauzes reduced the fluctions in yaw to about 1% of the pre-flow conditioning value and

resulted in a total pressure variation (post-tuning, fig.5.5) of about 1% throughout the cascade entrance plane. This was deemed of adequate quality to reduce turbulence to an estimated value of less than 1%. There remained in the inlet a spanwise flow distortion quite unrelated to flow conditioning but instead to the end blade passage flow. This is the subject of the next section which deals with 'tuning' the inlet.

5.1.1.2 Cascade Periodicity -- Inlet Uniformity

Ideally the pressure distribution across the cascade entrance plane should simulate as nearly as possible that which would develop with an infinite array of blades, i.e., a periodic pressure distribution of period equal to one pitch. Periodicity in the inlet (or lack of it) affects local incidence and passage mass flux and thereby alters blade Mach number distributions and boundary layer development. Inlet periodicity also affects exit conditions even in supersonic exit flow by modifying the end passage flow, the boundary of which serves as a reflecting surface for trailing edge shock and expansion waves.

Periodicity in the case of the blowdown tunnel is achieved largely by controlling the flow into the end passages (see PIANKO(1975)). This is because of two developments which have a major effect on pitchwise periodicity. The first is the duct sidewall boundary layer growth. The displacement effect on the liners can cause the flow to accelerate. Also, because the liners are of different length, this can lead to asymmetrical boundary layer growth. Boundary layer growth enhances the distortion due to the second effect, an asymmetrical streamline flow into the end passages.

If streamlines in the end passages are distorted from those theoretically in the midpassages of an infinite blade array, pressure distortion is communicated across the entire entrance plane. For example,

if one duct wall (or liner) were to be solidly adjoined to the pressure side of the end blade, the stagnation streamline would be directed into the end passage and distort the flow as in figure 5.3a. Similarly, at the wall adjacent to a suction surface less than full acceleration at the leading edge will lead to a blockage effect in that passage. The result in the inlet of combining these effects would be an incorrect inlet Mach number level, incorrect incidence, or both of the above.

One common method of controlling inlet periodicity is to bypass flow at the end blades, c.f. HOHEISEL(1974) and WOOD(1980). The bypass flow can be controlled by varying suction to a fixed gap or as in the case of the O.U.E.L. blowdown by varying the size of the gap, a more economical procedure as flow is drawn off passively without the need for an external vacuum source. The suction is applied by the pressure differential between the cascade entrance and exit planes. Using this technique one can tune the inlet to a uniform velocity periodicty with correct magnitude. Once the tuning is complete for a particular exit condition only minor adjustments in shutter gaps may be needed for high exit Mach number flow. The configuration used is shown in figure 5.3b. The liners have been fitted with moveable shutters to vary the bypass area. It was found important that the shutters be sharp-edged to remove Reynolds number effects and allow a free expansion into the passage. The powerful effect of varying the bypass flow is shown in figure 5.4. (The pressure tapping locations shown are spaced at one blade pitch so variation within passages is not indicated.)

Final P_o measurements for the tuned cascade inlet plane are shown in figure 5.5. The measurements were taken at five pitchwise locations centred on the instrumented passage. The variation in stagnation pressure across the inlet plane, save for one location, was less than 1%. One pitch location, A, was situated near the flow straightener. Near the sidewall the

stagnation pressure was higher by about 1% having not had sufficient flow length to quite mix out. This was not considered a serious discrepancy given the good uniformity overall.

5.1.1.3 Exit Flow Uniformity

One objective in cascade testing is to provide for an exit flow which is periodic across the exit plane and which is free from spurious tunnel influences. One method used (in other tunnels) to obtain outlet periodicity is to control outflow angle through the use of tailboards (also, see PIANKO(1972)). Tailboards are not used at O.U.E.L. for two reasons. First, without perfect alignment (alignment is not known a priori) they tend to cause a pressure gradient normal to the flow direction, altering the cascade tangential direction pressure gradient and effectively acting as a mixing duct. Second, without proper suction they cause in transonic flow an exit plane distortion by introducing spurious shock wave or expansion fan reflections into the exit flow region. (Slotted tailboards, as described in the work of Bolcs et.al. by WOOD(1980), can be useful in continuous flow tunnels where time is allowed for tuning the downstream flow conditions).

The blowndown tunnel uses instead a free jet exhausting into a small exit chamber. This jet is surrounded by a relatively stagnant air mass with pressure equal to the jet pressure and which forms a shear layer allowing for wave reflections of unlike sign to occur. Regardless of the method of exhaust gas evacuation, however, it is difficult in a linear cascade to provide the exit conditions which would occur in the engine. Thus each build must be carefully tested for tunnel-caused influences prior to aerodynamic tests on the blade itself.

In the blowdown tunnel each cascade build is pressure tapped on the

downstream sidewalls to check for exit flow periodicity. The results for each build in this thesis are presented in the appropriate sections throughout this chapter. To aid in obtaining uniformity in all O.U.E.L. builds the walls at either end of the cascade blades have a machined step just downstream of the exit plane to allow a sudden expansion in the spanwise direction. This expansion complements the expansion occurring in the pitchwise direction. What occurs overall is a rapid, constant-pressure mixing out of the flow which promotes uniformity and allows for repeatability from run to run.

The blowdown exhausts the cascade flow into the downstream duct via a small plenum followed by a catcher which recovers the dynamic head of the exhaust jet creating a streamwise pressure gradient unlike that in the other tunnels discussed in this thesis. Results of tests to be shown later indicate that a pressure gradient in the duct type of exhaust may present a different boundary condition than would occur in the dump diffusion type of exit condition found in the Oxford ILPT and the free expansion exit found in the Braunschweig cascade tunnel. From these same tests it also appears that exit conditions may be coupled to inlet flow uniformity and Mach number level even at transonic conditions. This is discussed more in chapter six where it is suggested that differences in the results of tests in various tunnels bear some correlation with differences in evacuating the downstream flow.

5.1.1.4 Flow Angularity

In the blowdown tunnel inlet duct liners (guide vanes) are preset to the desired inlet angle (e.g. 42.75^{o} for the B22 profile). Because of the relatively short length of the duct it is necessary to ensure proper inlet angles by surveying the incidence angle across the front face of the

cascade prior to a series of tests. Results of measurements on the first commissioning model, the 100mm B22 profile, are shown in figure 5.6 for the cascade design condition. These tests were done using a 45^{o} wedge yaw meter located in positions A through E as shown in figure 5.6 and indicate uniformity within 1^{o}. The slightly lower angle at A and larger angle at E are due to the expanded area occurring downstream of the flow straightener. In the instrumented passage where the streamline curvature is least the flow conforms to the preset angle of the liners.

5.1.2 B22 100mm Chord Cascade

5.1.2.1 Inlet/Exit Periodicity

Inlet and exit Mach number surveys were performed using tapping locations as shown in figure 5.7. A fine grid of sidewall tappings spanned the instrumented passage for a distance of one pitch on either side and were located at both the inlet and exit locations on the cascade. Three conditions of interest were measured and designated as M-, Md, and M+ respectively. These represent averaged exit Mach numbers of 0.73, 0.969, and 1.2 for the centre, instrumented passage. The results of the upstream and downstream surveys are shown in figure 5.8.

A calculation based on a pitch of 84.02mm and a geometrical throat of 31.72mm yields for an inlet angle of 42.75^{o} an isentropic Mach number of 0.316 for the inlet at choked conditions. This agrees closely with the measured value of 0.32 at Md. These results are similar to those of NICHOLSON(1981) for the B22 blade and they also demonstrate good periodicity for the cascade at the M_{d} condition. They also indicate that good accuracy in calculating the inlet Mach number can be obtained using both an isentropic calculation and the ideal throat, the smallest distance between suction and pressure surface, when boundary-layer displacement

effects are not too great. The displacement thickness was estimated at 2mm on each wall (based on turbulent flow over a flat plate), and this amounts to a reduction in duct area of about 2%. A compensating effect in this case, also, is the boundary-layer displacement thickness growth in the blade passage which tends to cause the isentropic area ratio to remain roughly constant. Similar comments were made by LEHTHAUS(1975) in his calulation on the VKI-1 profile, where, too, his inlet duct was rather short. Calculations for long ducts can lead to misleading values for inlet Mach numbers, however (cf. KIOCK et al.(1985)).

The inlet Mach numbers shown in figure 5.8a indicate that for the M+ condition the centre passage Mach numbers are larger by about 3% than for the design condition. This effect needs further investigation (including the effects of inlet sidewall and endwall boundary layer displacement thickness and aerodynamic throat variability), but as discussed later this high Mach number average is possibly due to the inlet incidence being slightly lower than the value preset by the liners, 42.75^{o}.

The Mach number variations across the inlet also indicate that for numerical predictions of cascade flow the boundary condition of uniform flow should be held only at a significant distance upstream of the cascade- at least one axial chord but better two axial chords upstream.

The exit Mach number distribution, figure 5.8b, exhibited good periodicity. It was not possible, however, to examine the cascade exit region for shock or expansion reflection problems. Since this was a commissioning exercise occurring during final stages of tunnel modifications the traversing gear and schlieren system were not in place. This temporarily leaves an incomplete description of the downstream flow field.

5.1.2.2 B22 100mm Chord Pressure Distributions

Results of blade Mach numbers for the 100mm B22 rotor blade are shown in figures 5.9 and 5.10. Differences on the pressure surface reflect the influence of the choked passage at the Md and M+ condition compared to the unchoked passage at the M- condition. On the suction surface, up to the aerodynamic throat, the Mach numbers are similar, a result expected when the cascade is choked.

At transonic exit Mach numbers marked differences begin to occur on the suction surface at x/cax = 0.54, just upstream of the geometric throat which was measured to be at approximately x/cax = 0.6. At this location (x/cax=0.54) the flow is sensitive to slight changes in downstream pressure since it is here that the flow is bounded on one side by a solid wall, the suction surface, and by a shear layer on the other side formed by the trailing edge wake shed off the pressure surface of the adjacent blade. The geometry of the effective duct formed in this way is sensitive to the angle and spreading rate of the shear layer. If the shear layer is roughly parallel to the suction surface a flow analogous to critical Fanno flow may develop where at sonic velocity closely spaced weak normal shocks and expansions occur as a result of the competing effects of favourable pressure gradient and zero area expansion. In critical Fanno flow the location of the shock system also is extremely sensitive to back pressure, cf. JOHN(1969). The analogy only goes so far, however, since in a duct with solid walls reflected waves are of the same sign as the incident waves, whereas waves reflected off a shear layer (pressure boundary) change sign. One could see by sketching this out that with a solid/shear layer boundary, intersecting shock-expansion waves will be interspaced with an alternating shock-shock, expansion-expansion wave system, a slightly different arrangement to that occurring in critical Fanno flow.

One can see in the schlieren photographs of the B22 profile by NICHOLSON(1981) a shock-expansion system similar to that just described above for the transonic exit condition, Md. The suction surface trailing edge is angled to the mean flow by approximately 2.5^{o} which is also approximately the semi-angle of the wake shed at the trailing edge of the adjacent blade. As mentioned earlier at the time of these blowdown tests schlieren photography was not available to verify conditions of the 100mm B22 exit flow field. This work would be a valuable addition to the existing pressure surveys.

For the M+ condition there is a rather rapid expansion to Mach 1.23 on the pressure surface near the trailing edge as the flow accelerates to match downstream flow conditions. The fan from this expansion impinges on the suction surface and promotes localized flow acceleration. This fan accounts for the Mach number increase at x/cax = 0.54. and is not an unexpected occurrence, cf. figure 1.17 in HORLOCK(1966).

At the trailing edge the difference in Mach numbers on the suction and pressure surfaces indicates that recompression shocks necessary for downstream flow equilibration occur off the blade in the downstream trailing wake region.

5.1.2.3 Comparisons With ILPT Data and Numerical Predictions

The results of tests on the 100mm B22 profile are plotted against the results of NICHOLSON(1981) obtained in the Isentropic Light Piston Tunnel (ILPT) in figures 5.11, 5.12, and 5.13. These comparisons are made only to better understand the characteristics of the blowdown tunnel since the ILPT, designed mainly for heat transfer measurements, cannot provide the detailed aerodynamic measurements available in the blowdown tunnel.

It can be seen in figures 5.11, 5.12, and 5.13 that on the pressure

surface there is reasonable agreement for all exit conditions. Agreement on the suction surface is not as good. In addition, the results seem to indicate that in the ILPT an aerodynamic throat was formed upstream of that for the 100mm blade at approximately x/cax = 0.4 versus 0.54 for the 100mm blade. This suggests that there may be differences in incidence angles for the two builds. Experience with the large-chord cascade, discussed later in section 5.2, indicates that even with the inlet guide vanes set at the correct incidence angle, a mistuned inlet, e.g. where inlet pressure periodicty is skewed, will cause a shift in throat position and an increase in suction surface Mach numbers.

In figures 5.12 and 5.13 it can be seen that on the 100mm blade at Md and M+ there is an expansion (acceleration) occurring in the trailing edge region on the suction surface which does not agree with what appears to be a diffusion occurring in the ILPT data in the same region. One possible reason for this may be that the comparisons are for different exit conditions, a discrepancy caused by the method of specifying exit Mach number in the two tunnels. For the Nicholson B22 cascade, exit Mach number is based on a sidewall pressure measured downstream of the free expansion step at a location 0.78 chord aft of the cascade exit plane. For an indicated exit Mach number of 0.96 the spatial average of Mach numbers on his build near the trailing edge plane (measured from tappings at 0.336 chord downstream) is approximately 0.91. For the same quoted exit Mach number on the 100mm cascade the near-exit (0.61 chord downstream) spatial average of Mach numbers is 0.96, five percent higher. Thus it appears that what is designated Md in figure 5.12 actually amounts to a 5% difference in spatially averaged Mach numbers. This problem will be resolved later when the 100mm cascade is tested with schlieren flow visualization.

Another possible reason for the difference in trailing edge

diffusion is a difference in the back pressure field caused by differences in geometry and the method used in exhausting the exit flow. The dump diffusion exit of the ILPT may be sensitive to back pressures in a slightly different way than the hybrid (as GOSTELOW(1984) calls it) duct diffusion exit in the blowdown tunnel. At transonic flow conditions the cascades tested are sensitive to back pressures. It is in this range that shocks and expansion fans form, reflect off end passage shear flows and propagate across the exit into the free stream. Differences in exit-plenum geometry can play an important (and undesired) role in wave reflection and measurably influence the exit flow. Combined with this are differences in the character of the shear flow in end passages which too are principally determined by the tunnel configuration and which can alter the reflection system just described. Further, if only the definition of exit Mach was root cause of the noted differences in blade Mach numbers then by iterating the blowdown back pressures eventually a blade pressure distribution would occur identical to the results from the ILPT. This iteration occurred during the setup stages for transonic flow conditions on the 100mm blade without the trailing edge Mach numbers ever matching ILPT data identically. (A similar state of affairs was apparent in the VKI-1 tests reported in section 5.1.3). An important concern then is how one can best interpret and utilize data from different tunnels. This issue will be discussed further in chapter six.

Also shown in figures 5.11, 5.12, and 5.13 are the results of predictions used by Nicholson compared with the experimental results from the 100mm B22 profile. The prediction codes, which were outlined in chapter three, are the streamline curvature method derived from an early version of the Rolls-Royce CODIB (GOSTELOW(1984)) and a time-marching prediction, developed by DENTON(1975), which solves the Euler equations.

As noted by NICHOLSON(1981) the streamline curvature method experiences some difficulty in convergence at higher Mach numbers. This is due in part to the streamline flux term ρU which is double valued at a Mach number of unity and secondly to the numerical inconsistencies inherent with an algorithm composed for an elliptic flow field which is then applied to flows hyperbolic in form (i.e. flows in which properties are defined along characteristic lines in the flow field). Thus, reasonable agreement occurred in subsonic regions especially on the pressure surface, excepting the M- condition where over the last 30% of the blade surface the predictions were high due to a difference in exit Mach numbers (0.8 for the prediction versus roughly 0.73 for the data).

On the suction surface results from the streamline curvature method were not as good. There was some fair agreement with the 100mm chord data at the design condition but the Mach numbers were underpredicted in the flow expansion region on the last 25% of the blade surface. At the M+ condition the Denton method could only predict the trend in the data because of the limited shock capturing capabilities (coarse grids) built into the available version of the code (since improved by DENTON(1982)).

Nicholson's numerical results using the early Denton code as shown in figures 5.11 to 5.13 show a slightly better fit with the 100mm data in the region x/cax= 0 to 0.75 except at higher exit Mach numbers where experimental data from the two tunnels are the most inconsistent. The pressure surface was underpredicted for all exit conditions.

The above comparisons say more about the state of numerical codes and flow modelling than they do about differences that exist in the data from two tunnels. More must be learned about flow sensitivities to tunnel boundaries and changes induced by end passage flows before a numerical code can be expected to predict behaviour in the most sensitive of flow regimes,

sonic and near-sonic conditions. For good reliability of predictions the pressure field at the control volume boundary must be matched to the actual flow. Often used is a downstream boundary condition with homogeneous flow at constant pressure equal to, say, the back pressure at one chord or so downstream of the cascade. This resulting lack of pressure gradient induces, numerically, a flat plate flow which may differ from the actual flow. For example, the blowdown tunnel at Oxford could have a significant favourable pressure gradient in the exhaust region due to the effect of the ejector system. This effect must be included in the flow model as even in transonic flow the end passage flow is likely to remain subsonic and very much dependent on the back pressure. As pointed out earlier the reflections off the end passage shear layer influence the state of the flow downstream of the cascade and thus indirectly influence the state of the flow on the blade in the downstream region. This is discussed further in chapter six.

5.1.3. Results of Tests on the VKI-1 Cascade

5.1.3.1 Upstream and Downstream Surveys

Upstream and downstream surveys were completed in only a limited sense in that direct tapping-for-tapping comparisons with Braunschweig data were not available. The scope of the testing was reduced to surveying only a sufficient number of locations to insure uniformity of the flow at the cascade entrance. The inlet was fitted with shutters at the end passages and repeated runs were made to arrive at a tuned inlet. The resulting Mach number level in the inlet with choked passage flow was 0.252, about 3% lower than the value obtained at Braunschweig, 0.26. A reason for this difference given by KIOCK et al.(1985) is that the displacement thickness in the longer (Braunschweig) duct accelerates the flow due to the reduced effective cross-section.

Downstream surveys in the blowdown were minimal and done mainly to ascertain a method of comparing exit conditions with those in the Braunschweig tunnel. Because of differences in describing downstream Mach number at the two locations it became a hit-or-miss exercise to replicate both the exit conditions and blade surface Mach numbers. In the end data was generated which overlapped Braunschweig data and thus provided comparisons for many exit conditions.

Braunschweig data is quoted based on two types of exit conditions measured downstream of the cascade. The first is based on a theoretical expansion (or diffusion) to the plenum pressure, equation 5.1.

(Braunschweig)
$$M_{2th} = f\left(\frac{P_{plenum}}{P_{01}}\right) \qquad \ldots 5.1$$

The second is based on the results of a pressure traverse in the exit region and indicates an averaged downstream Mach number. This mixed out value is given by equation 5.2.

(Braunschweig)
$$M_2 = f\left(\frac{P_2}{P_{02}}\right) \qquad \ldots 5.2$$

The plenum pressure is lower by about 4% than the mixed out pressure, P_2, so $M_2 < M_{2th}$ for this cascade.

Oxford has no direct comparison as the exit conditions there are based on an isentropic flow calculation using upstream total pressure and static pressure downstream of the expansion step, equation 5.3.

(Oxford)
$$M_2 = f\left(\frac{P_{stdn}}{P_{01}}\right) \qquad \ldots 5.3$$

As will be shown later the use of equation 5.3 to define exit Mach number produced results similar to those for Braunschweig's M_2.

5.1.3.2 Reynolds Number Effects in Transonic Flow on the VKI-1 Cascade

These results were acquired early in the VKI-1 testing programme and are presented to demonstrate the effects of Reynolds number notably on the suction surface of the VKI-1 cascade when the exit Mach number is near 1. Blade pressure surveys were acquired for two Reynolds numbers $2x10^6$ and $8x10^5$. Tests run at the higher Reynolds number had a reduced coverage of pressure tappings as KIOCK(1980) had already shown that in the upstream portions of the blade Mach number values are insensitive to Reynolds number variation. His tests stopped at $Re=1x10^6$ so these results will add to existing information on the VKI-1 profile.

Though many runs were done with high Reynolds numbers at transonic exit conditions only two are presented here, selected for their agreement in exit Mach number (the isentropic pressure ratio, equation 5.3, was identical in both cases). This data is shown in figure 5.14 and indicates a Reynolds number effect occurring in the region on the blade from x/c = 0.56 to 1 for an exit Mach number of 0.96.

The primary effect indicated in figure 5.14 is that with a higher Reynolds number the shock on the suction surface appears to move forward to a location farther upstream. The subsequent suction surface expansion occurs at higher Mach numbers and the base pressure (indicated by a pressure tapping at the base of the trailing edge circle) is lower (higher indicated Mach number). The base-pressure-tapping Mach number is calculated as a matter of convenience, but this Mach number may differ from the freestream Mach number just outside the wake separated off the blade at that point.

The boundary layer on the pressure surface will be thicker for the case of a lower Reynolds number, but the situation on the suction surface is not so clear. It is known that the high favourable pressure gradient on a turbine blade can induce relaminarization of a turbulent boundary layer and can, under the right conditions, create a different shock-boundary layer interaction to that which would occur otherwise with a fully developed turbulent boundary. An indicator of the likelihood of this occurring is the acceleration parameter K, JONES and LAUNDER(1972), which combines an accountability of boundary layer momentum and free stream pressure gradient,

$$K = \nu/(U^2)(dU/dx) \qquad \ldots 5.4$$

where U is the free stream velocity and x is the surface length.For a variety of accelerating, laminarizing flows this factor takes on a value near 3×10^{-6} (JONES and LAUNDER, op cit).

It is convenient to recast equation 5.4 in terms of Mach number, total temperature and total pressure combined with Sutherland's formula taken from KUETHE and CHOW(1976),

$$K = \frac{(dM/dx)T_o}{47760P_oM^2f(f^2+110/T_o)} \qquad \ldots 5.5$$

where the factor f is defined for convenience as,

$$f = (1+ \frac{\gamma-1}{2} M^2)^{-1/2} \qquad \ldots 5.6$$

The constant 47760 in equation 5.5 is arrived at by using the ratio of specific heats, γ , equal to 1.4, the gas constant for air, R, equal to 287J/kgK, and a reference viscosity for air of 1.784×10^{-5}kg/ms at T=288K.

In the case of a static turbine rotor cascade the use of upstream total pressure in place of local total pressure yields good accuracy. A calculation for K for the low Reynolds number flow in the vicinity of the throat is 1.8×10^{-6}. This value is somewhat lower than the Jones and Launder criteria for relaminarization, but it is high enough to regard this flow as potentially laminarizing and the boundary layer as potentially a thinning one. One could provisionally conclude that a lowering of the overall Reynolds number in an accelerating flow may not produce a thicker boundary layer, since, as shown by equation 5.5, K is inversely proportional to Reynolds number whereas the thickness of a turbulent boundary layer (on a flat plate) tends to scale as Reynolds number to the -1/7 power (WHITE(1974)). Thus, as the Reynolds number decreases the acceleration parameter increases faster than the tendency of the boundary layer to thicken, the relaminarizing effect offsetting, or possibly overwhelming, the turbulent boundary layer.

Up through the higher Reynolds numbers tested by Kiock there was no shift in shock location on the suction surface such as occurred in the Oxford data. Recent measurements by Kiock (BAINES et al.(1985)) indicate that at design Reynolds number, 0.8×10^{6}, laminar flow exists up to the point of shock impingement on the suction surface followed by a laminar-to-turbulent flow transition region. The Oxford data for a Reynolds number of 2×10^{6} in figure 5.14 suggest the possibility of an earlier transition to turbulent flow corresponding to the upstream location of the shock impingement. One possible reason for this is that the effect of the change in Reynolds number is to cause a change in thickness of the trailing edge wake. From the argument in the previous paragraph, the boundary layer may thicken for the higher Reynolds number. The recompression shock from the pressure surface trailing region may then

strike the suction surface at a more oblique angle, reducing the shock strength (smaller total pressure loss). Since the back pressure is decoupled from upstream pressures (supersonic flow) a stronger expansion could occur as shown in figure 5.14.

As with results on the 100mm B22 profile one cannot rule out the additional conclusion that differences occurring at transonic conditions are due to shock reflection differences induced by differing tunnel hardware and exit flow patterns. It is clear, however, that in the Oxford blowdown tunnel it is of paramount importance that the correct Reynolds number be established to insure correct Mach number distribution and to arrive at valid loss data.

5.1.3.3 VKI-1 Cascade Data Compared for Two Tunnels

Only the important results of comparisons between Braunschweig data and Oxford data are presented here. KIOCK et al.(1985) presents comparisons among data obtained in four tunnels (three cascade builds) and in BAINES et al.(1985) a more complete subsonic and transonic comparison between Braunschweig and Oxford. The data to be presented here also includes comparisons with a prediction code.

As mentioned earlier the tests at Oxford were on the same cascade hardware as tested at Braunschweig. Thus what follows can be considered a direct comparison of tunnel data and the influences of the tunnel on the data.

Shown in figures 5.15 and 5.16 are a partial set of two runs in the Oxford tunnel compared with data from KIOCK(1980). The blade tappings were located on pressure and suction surfaces in adjacent passages so the following discussion assumes good passage-to-passage uniformity. The two Oxford runs shown in figure 5.15 overlap the Braunschweig data for

comparison purposes as it was not possible to match exit conditions exactly. Also pressure surface data for Oxford's M_2=0.93 and M_2=0.96 was identical and so for clarity only one set of pressure surface data is shown.

Data from the two tunnels agree rather well over most of the blade surfaces including the location of the stagnation point on the pressure surface. The Oxford data is slightly lower on the pressure surface near the trailing edge including the trailing edge base tapping at x/c=0.997 which indicates a higher base pressure by about 15% for the Oxford runs. However, this discrepancy disappears at lower exit Mach numbers, as seen in figure 5.16, and so one suspects that the trailing edge expansion-recompression region must differ in the two tunnels when transonic conditions prevail.

In comparing the transonic flow cases the suction surface shock appears to be located slightly more downstream in the Oxford tunnel. The local peak in Mach number occurred consistently at x/c=0.6 as compared with 0.56 in the Braunschweig tunnel. Such differences can occur if the outlet flow is less turned since in that case the shock off the pressure surface wake will impinge at a location farther downstream on the suction surface.

The transonic flow field over the suction surface from x/c=0.52 to the trailing edge is dominated by a complex set of circumstances. A schlieren photograph from a different build tested at Gottingen (KIOCK et al.(1985)) confirms the presence of shock formation on the suction surface just aft of x/c=0.6 although it appears in the data in figure 5.15 that the shock is smeared by the subsonic boundary layer which senses the impending pressure rise. However, as noted by LEHTHAUS(1975) the smearing may also be caused by unsteady oscillation of the shock.

One can argue that pressure fluctuations in the trailing edge vortex street could induce or enhance shock oscillations. The schlieren

referred to above indeed shows the shock boundary at the wake shear layer to be in a highly oscillatory state as evidenced by the inability of the camera to stop the motion. The presence of large-scale structure in the wake would account for this phenomenon but this scale is not always visible. Measurements by NARAYANAN(1982) indicate that in high speed flows large-scale coherent structures exist but can be masked by small-scale random fluctuations. In some high speed flow situations, however, the large-scale structure is quite visible, MATALLEBI and NORBURY(1981) in GOSTELOW(1984).

Unsteady pressure oscillations in the exit flow field which induce oscillations upstream may not appear in two tunnels testing the same cascade. With open-jet tunnels, downstream pulsations cannot be prevented from propagating upstream. In a ducted system, however, the exit flow can be accelerated, drastically reducing the upstream penetration of pressure fluctuations. This principle has been employed for many years in transonic tunnels by installing a sonic throat downstream of the test section to remove shock buzzing, GOETHERT(1961). The catcher and ejector system quite possibly may alleviate downstream unsteadiness but this question must remain open pending more testing.

Reducing unsteadiness in the exit region, if such were the cause of smeared shocks, would lead to a sharper definition in the Mach number distribution. The reduced back pressure needed for the Oxford 0.96 run and the appearance of a steeper Mach number gradient as shown in figure 5.15 tend to support this idea, but more testing is certainly required to settle this point.

In subsonic exit flows, figure 5.16, tunnel-dependent flow effects become less noticeable. As shown in the figure surface Mach numbers are in good agreement although exit conditions differed slightly. The trends in

the diffusion on the suction surface are identical. The only (unresolved) discrepancy is at one location on the pressure surface, x/c=0.36, where the Oxford data indicates a higher Mach number. It is reasonably concluded that the two facilities will produce similar results for subsonic flow conditions.

The experimental data can be compared to predictions made by LEHTHAUS(1977) in his dissertation at Braunschweig. He used a time-marching approach assuming an inviscid, irrotational flow field and utilizing the MCDONALD(1971) grid formulation. As usual with this approach dissipation must be added artificially or not at all. In this case none was added, and thus only weak shocks ($M < 1.3$) with corresponding small entropy increases could be accurately simulated. Only the case for M_2=0.87 will be used as this is the only prediction data near an Oxford test case. The results of the prediction are shown in figure 5.17 compared with two Oxford runs, M_2=0.89 and 0.76.

It appears in figure 5.17 that at M_2=0.87 (Lehthaus) the prediction shows the flow already to be critical with sonic speed surpassed at x/c=0.48 and a weak shock downstream on the suction surface. Agreement with experimental data is good except in the last 40% of the suction surface. Here the predicted Mach numbers lay between the results of the two experimental sets of data. It appears the flow on the suction surface may not be correctly modelled in this region perhaps due to incorrect simulation of the expansion-recompression which occurs at the pressure surface trailing edge and which influences suction surface flow or because of the way the exit flow responds to the exhaust regions in different tunnels. The prediction boundary conditions impose a constant static pressure with zero pressure gradient one axial chord downstream of the cascade exit. As shown in figure 5.17 this leads to a rapid expansion over

the last 10% of the blade whereas the data show a recompression occurring.

Finally, good agreement occurred with the Oxford data not only in the stagnation region and at x/c=0.36 but also on the pressure surface which as mentioned earlier did not match the Braunschweig value there.

5.2 LARGE CHORD TESTS

Tests on the large chord (300mm) version of the B22 profile comprised the first use of the new blowdown tunnel to obtain new experimental data on the B22 profile. The large chord cascade consisted of three blades (two passages) of 300mm span (unity aspect ratio). The centre, instrumented blade contained 73 pressure tappings which would allow a fine measurement grid at the leading and trailing edges.

The objective of the large chord tests included ensuring the efficacy and viability of a two-passage transonic turbine cascade. This could be done by establishing good agreement with previous aerodynamic data obtained in the ILPT and obtained on the 100mm B22 cascade in the blowdown tunnel. A second objective was to perform preliminary detailed investigations of the boundary layer especially on the pressure surface where the character of the boundary layer is least understood.

5.2.1 Inlet and Exit Surveys: Periodicity

Inlet and exit surveys were accomplished using tapping locations shown in figure 5.18. A turbulence grid designed to produce 5.5% streamwise turbulence intensity was installed just behind the honeycomb and gauze. Details of the grid can be found in chapter three.

In figure 5.19 are the results of inlet and exit Mach number surveys. Three upstream surveys are shown in order to demonstrate the correlation between the shape or skewness of the distribution and the centre passage inlet angle. The run numbers are shown with inlet angle shown in parenthesis.

The effect of lower incidence is to increase Mach numbers toward the long liner location (see figure 5.18). The opposite effect occurs when

the incidence is high as shown by the results for run 1195 in figure 5.19.

These curves also represent varying exit conditions from subsonic to transonic. It is noteworthy that the untuned inlet of run 337, where the exit flow was subsonic and the inlet incidence was low, shows a higher average inlet Mach number than the near choked flow for the higher exit Mach number. Thus caution must be exercised when using only the inlet Mach number average as an indicator of correct inlet conditions, especially since the higher value (due to a badly mistuned inlet flow) may agree with the expected theoretical value. This point is discussed further in chapter six, section 6.2.

By the use of various tuning configurations it could be shown that altering the inlet incidence angle via the shutter bypass flow gave good agreement in blade distribution with prior builds (Nicholson's B22 and the 100mm blade). It was then realized that the disagreement on the upstream blade locations of those two builds was probably due mainly to incidence differences.

The ability to tune for various conditions on the large chord cascade proved its viability as a cascade to be used for further testing. The tuning configuration settled on (producing the values shown in figure 5.19 for runs 1194 and 1195) left the incidence slightly high (43.8^{o} at the centre blade with the liners set at 42.75^{o}) but produced reasonable comparisons with the earlier tests on the B22 profile at M_{d}.

All of these surveys utilized sidewall tappings spanning two pitches in the cascade inlet plane and 1.5 pitches at the cascade exit. A pitot rake with yaw meter attached was used for incidence measurements. (for location A, figure 5.19, the yaw meter was very close to the turbulence grid and produced invalid results). However, it was learned during the inlet tests that the pitot rake distorts the flow due to its

proximity to the cascade inlet plane so all subsequent Mach number surveys were carried out using a small pitot tube in the inlet for measuring the reference stagnation pressure.

Downstream exit Mach numbers are shown for three conditions ranging from subsonic to critical flow. As can be seen in figure 5.19 periodicity is identifiable even on this large two-passage cascade.

5.2.2 Large Chord B22 Mach Number Distribution

Results from two runs (1190 and 1192) with nearly identical exit Mach numbers are plotted together in figures 5.20a and 5.20b. The distributions are plotted against %chord and %surface length respectively. Tappings 13, 42, and 56 were not measured. (Tapping locations are shown in figure 2.4).

Tapping 1 shown in figure 5.20b represents the location on the leading edge circle 42.75° around from the axial direction and would be the theoretical stagnation location of an undisturbed streamline running parallel to the inlet liners. The actual stagnation streamline, however, is farther around the leading edge towards the pressure surface and appears to be near tapping 3, x/s=0.016.

Near the leading edge at tapping 72 there is a sharp velocity acceleration followed by a sharp deceleration, an occurrence not observed on previous builds. It is not known whether this is a phenomenon previously undetected due to course measurement grids or whether, perhaps, it is an artifact related to the blend point location on the large chord profile.

The location of tapping 72 relative to tapping 3 (the possible stagnation point) is 13.2mm in surface length (measured) which corresponds to about 93° of circular arc on the leading edge circle. Schlieren photographs indicate a small laminar separation-reattachment bubble at

tapping 72 which is interacting with the surface blend point located between tapping 72 and 71. The blend point is a location where the curvature changes value in a very short distance and can induce an almost discontinuous and thus unstable change in radial (surface normal) pressure gradient near the blade surface.

Farther along the suction surface downstream of the throat the distribution is extremely flat with a gradual diffusion occurring toward the trailing edge. There is a perturbation in the distribution at x/s=0.504 not seen before and which indicates the appearance of a weak shock at the location x/s=0.48. This does not appear to emanate from the trailing edge region of the adjacent blade. There is also another shock at about tapping 48 which arrives from the trailing edge of the adjacent blade and whose pressure rise is smeared through the subsonic boundary layer. This gives the appearance of a gentle diffusion as seen in figure 5.20b.

The trailing edge tapping, 27, is located in the base pressure region and usually has a Mach number calculated for convenience only. But because the flow has diffused to subsonic speed in this case that tapping does indicate the freestream Mach number at the trailing edge.

Finally, it is noted that on the pressure surface just downstream from the leading edge between tappings 10 and 15 the Mach number distribution is very flat, simulating flat plate flow .

5.2.3 B22 Profile Comparisons from Three Builds

Early runs on the large build (prior to 1190) indicated an inlet incidence which was high by an estimated two degrees. The location of the sonic point on the suction surface was farther upstream near x/cax=0.4 (a similar location to that of the Nicholson B22 profile). One earlier run, 1182, is shown in figure 5.21, with ILPT run 2211 superimposed. Differences

between the large chord earlier and later runs at lower incidence are seen mainly in suction surface data upstream of the throat. At this point there is a clear indication that incidence is an important parameter in locating the aerodynamic throat.

An aerodynamic throat which moves forward with higher incidence may induce an early separation on a highly cambered airfoil, and there is some evidence of this possibility shown in figure 5.22 where on the large chord results (run 1190) a very flat profile exists between x/cax=0.45 and 0.55 on the suction surface. (Subsequent boundary layer measurements did not, however, confirm the presence of a separated region).

The data shown in figure 5.22 represent the conclusion of the preliminary commissioning efforts on the blowdown tunnel. The data for M_d from three builds are represented, one ILPT and two for blowdown cascade runs.

In general, the agreement is better than expected especially in view of the uncertainties surrounding the validity of data obtained on a two-passage cascade. The ability to tune that cascade must remove any doubts and instill confidence in continuing further experiments on that build. There were, however, differences in the data which need discussing.

In view of early incidence tests on the large chord build it seems reasonable now that the higher Mach numbers upstream of the throat in the ILPT 2211 data are due primarily to inlet angle differences. The measured incidence for the 100mm cascade was 42.75^{o} and the suction surface data for this build are in accord with the large chord (43.8^{o}) data in the region upstream of the throat.

Differences in the downstream regions are believed to be associated with tunnel geometry differences. The large chord data are thought to be influenced by the presence of the traverse gear which manifests its

presence as a pressure blockage. This creates a downstream pressure gradient similar to that existing in the exhaust region of the ILPT prior to the installation of the downstream throat. The similar diffusion in the downstream regions for the ILPT and large chord data seem to bear this out though the matter merits further investigation. The 100mm data show an expansion in the downstream region reflecting perhaps the effects of unimpeded duct flow. (The 100mm data was obtained prior to the installation of the traverse mechanism).

A final comparison of data from the three builds is shown in figure 5.23. This data is for exit Mach numbers higher than critical and of slightly different values for the three builds. The large chord data is from the earlier tests (prior to 1190) where the incidence was higher. The 100mm data was obtained from what is now thought to be a slightly low incidence in the instrumented passage at M+. The upstream values of Mach number on the suction surface are in accordance with earlier arguments concerning incidence. Thus these data emphasize the importance of adjusting periodicity for correct inlet flow. Major conclusions cannot be drawn concerning differences in downstream flow because of the different exit Mach numbers. It is observed though that, as occurred with the data at the M_d condition, downstream trends in the flow are similar for the large chord and ILPT data.

5.2.4. Large Chord Pressure Surface

The pressure surface is, for the most part, a concave surface where secondary flow phenomena are of interest. These secondary flows, Goertler vortices, are a boundary layer phenomenon and influence transition, cf. SCHLICHTING(1979) and BROWN and MARTIN(1981).

Surveys on the pressure surface of the large chord B22 profile

included attempts at flow visualization and spanwise pressure measurements at various locations on the blade. Most surveys were done downstream of tapping 17, x/s=0.44, (x/cax=0.577), as this was the farthest reach of the traverse system, and at tapping 26 near the trailing edge. The upstream surveys were in a region of high curvature on the pressure surface.

The curvature on both surfaces is plotted in figure 5.24. The values were calculated from a file of coordinates supplied by SCRIVENER(1980) for the B22 profile. Finite differencing programs were written to calculate curvature according to equation 5.7 (cf. GOODMAN(1967)),

$$1/R = \frac{y''}{(1+y'^2)^{1.5}} \qquad \ldots 5.7$$

The data were smoothed using a convolution function borrowed from digital filter theory. The function was the Hanning filter and is discussed by KING and OLDFIELD(1985) in appendix B. Other filters (quadratic-cubic, moving least-square polynomial, and running average) yielded similar results but were discarded for reasons discussed by KING and OLDFIELD(op cit.).

In figure 5.24 the constant radius regions at the leading and trailing edges and the blend points are omitted so that the smaller scale at intermediate locations is better defined. Curvature calculations made at the blend point regions indicated a step change in curvature as suggested earlier.

The pressure surface appears to consist of a nearly constant radius of curvature just aft of the leading edge preceding a rise to maximum curvature at x/cax=0.24. Following the point of maximum curvature and moving downstream there appears to be a series of regions consisting of decreasing curvature patched with regions of constant curvature proceding to x/cax=0.84. At this point there is a sudden decline in curvature. This

region may be influencing the slight disagreement that occurred between the large chord data and the ILPT data on the pressure surface. It is possible that curvature influences on flow will be more dramatic on the large chord blade since sudden changes in curvature (designed in) will tend to be less blended out than would occur on a smaller blade.

The likelihood of Goertler-like flow characteristics on the pressure surface is suggested by the value of the parameter G_{δ_2}, the Goertler number, which depends on the momentum thickness Reynolds number and radius of curvature in the following way:

$$G_{\delta_2} = Re_{\delta_2}(\delta_2/R)^{1/2} \qquad ...5.8$$

As discussed in chapter three this parameter can take on two ranges of values. The first, associated with the imperceptible beginning of flow instability where characteristic wavelengths form and begin to be amplified, is dealt with in the stability analysis of, e.g., SMITH(1955). A neutral stability is usually discussed where for a value of the Goertler number less than 0.34 flow instabilities are damped out. FLORYAN and SARIC(1982), in more recent calculations, show that this value should be closer to 0.46. A higher range of values are reported in experiments to indicate a more definite change from the laminar state, where large, measurable disturbances occur. In those experiments involving turbine blades a Goertler number between 3 and 7 seems to be a popular choice. As LIEPMANN(1945) pointed out, however, the transition Goertler number is not a constant but will vary. Thus, between the extremes of flat plate transition (G_{δ_2} =0) and transition on a surface of large curvature the physics of the process indicate a coupling of Tollmien-Schlichting waves and Goertler vortices (see HAN(1982)), and the possibility of a range of transition Goertler numbers. Refer to section 3.4 for an extended

discussion.

The momentum thickness used to calculate the Goertler number for the B22 profile, Md condition, is shown in figure 5.25. In the figure are shown the results of a laminar boundary layer calculation. The laminar condition seems relevant to this analysis as will be made clear subsequently. Also shown in the figure are the results of Rolls-Royce finite-difference predictions which apparently indicate a transition to a turbulent-like flow as evidenced by the larger downstream values.

The laminar calculation was accomplished using the method of THWAITES(1949), a one-parameter utilization of the von Karman integral. The integral is reduced to a first order, linear differential equation as a result of Thwaites' discovery of a linear relationship between the friction coefficient and shape factor. The resulting relationship for momentum thickness is given by

$$\delta_2^2 = \frac{0.45\nu}{U^6} \int_0^x U^5 dx \qquad \ldots 5.9$$

For a given velocity distribution this expression is numerically integrated from the stagnation point to the location of interest. From the large chord B22 distribution, figure 5.20b, the stagnation point was assumed to occur between tappings 2 and 3, at x/s=0.0112.

Equation 5.9 can be recast in a more useful form when dealing with surface Mach number values. Using the definition for local Mach number one obtains,

$$\delta_2^2 = \frac{0.45Sp}{F(M)(Mf)^5} \int_0^{x/s} (Mf)^5 d(x/s) \qquad \ldots 5.10$$

where f is given in equation 5.6 and Sp is the true pressure surface length (328.9mm for the large chord blade). F(M) is Reynolds number per meter,

$$F(M) = U/\nu \qquad \ldots 5.11$$

which can be expressed in terms of M, P_o, and T_o using Sutherland's formula.

$$F(M) = 47760(P_o/T_o)(Mf)f^2(f^2+110/T_o) \qquad \ldots 5.12$$

The constant 47760 comes about as noted in equation 5.5.

In figure 5.25 the laminar calculation begins to deviate from the finite-difference calculations at about x/s=0.05. One transition criterion which agrees with the location shown is due to FOREST(1977). The transition is expressed as a critical Goertler number.

$$G_{tr} = 9 \exp(-17.3u'/U_e) \qquad \ldots 5.13$$

The value u'/U_e represents a streamwise turbulence value. Note that for zero turbulence that equation 5.13 predicts a transitional Goertler number of 9. This would agree with the low-turbulence value obtained by LIEPMANN(1945) (in a duct of constant radius), but is slightly higher than values reported in the literature for some turbine profiles (cf. KEMP(1977) and HAN(1982)).

With the turbulence grid in and an expected turbulence level of 5.5%, G_{tr}=3.47. This value will occur at approximately x/s=0.057, which is near tapping 6. For zero turbulence the transition value (G_{tr}=9) would occur at x/s=0.092, just upstream of tapping 8. The traverse probe could only reach to about x/s=0.44 (x/cax=0.57), and so it is of interest in future testing to determine whether coherent structure could exist at this location and what physical length scales might be observed.

According to the results of KEMP(1977) and HAN(1982) the extent to which secondary flow is observable is dependent on the location of breakup

of the flow into a turbulent-like random structure. Kemp was able to see coherent structure visually (using the china-clay technique) downstream to x/c=0.7. Here his flow became muddled in a developing turbulent flow, retaining, however, velocity profiles less full than expected for a turbulent flow. He claimed that the high acceleration on the pressure surface prolonged a laminar-transitional state in the boundary layer.

BROWN and MARTIN(1981) suggest that flow acceleration on the pressure surface, quantified by the factor K defined in equation 5.4, is a major influence on the state of the boundary layer preceding and during a transitional phase. They conclude that if K is large enough (greater than $2.5x10^6$) the boundary layer will remain laminar far downstream of the calculated transition region.

The acceleration factors for the large chord B22 profile are shown in figure 5.26. On the pressure surface a high acceleration begins at about x/s=0.38. Accelerations of the magnitude shown in figure 5.26 can be expected to thin the boundary layer, stretch the streamwise vortical flow, and even minimize the effects of freestream turbulence (cf. KEMP(1977). KEMP's(op cit.) boundary layer profiles downstream of initiation of the secondary flow did not fill out to the fullness of a turbulent profile. In fact, the flow on his PVD blade separated, reattached as a laminar-like boundary layer, and persisted as such on the downstream portion of the pressure surface. Thus, the evidence suggests that a transition criterion which neglects acceleration, freestream turbulence, or even the physics of flat surface transition, will be of greatest accuracy only in regions where very high curvature dominates the character of the flow and, furthermore, that turbulent profiles calculated from, say, an integral relationship will overpredict momentum thickness.

Attempts at flow visualization on the large chord B22 profile

failed to produce incontrovertible evidence of secondary flow though the use of fluorescent paint indicated fine, streamwise striations, spaced at about 1mm, running to the trailing edge. Attempts at napthalene deposition yielded similar results. In both cases, however, the spacing appeared too regular to be attributed to secondary flow.

At the trailing edge of the blade three flow conditions will preclude the appearance of a regular pattern of flow. First is the inevitable breakdown of the coherent structure into a turbulent flow. The only reported occasions of a persistent Goertler flow are on surfaces of constant radius with low freestream turbulence, obviously not the case here. In fact, if the flow arriving at the concave curvature is already turbulent, JEANS and JOHNSTON(1982) report that no visible, cell-like vortex structure will ever exist, although the boundary layer profiles will be unlike the full profiles of a turbulent flow over a flat or convex surface. Thus turbulence destroys visualization of the secondary flow phenomenon.

A second mitigating circumstance is the possibility of a meandering secondary flow. WINOTO et al.(1979a) reported this occurrence in their experiments in a constant curvature water channel. Their later experiments did not provide evidence of this phenomenon, nor has any other experimenter expressed this as a problem in flow visualization (though KEMP(1977) stated this as a possibility for the cause of the eventual breakup of the coherent flow).

Finally there has been a suggestion from BROWN and MARTIN(1981) that the spanwise wavelengths grow with increasing streamwise distance. To the author's knowledge there has been no conclusive experimental evidence produced to support this conclusion though stability theory does not deny the possibility, allowing for magnification of selected wavelengths based

on momentum thickness.

A final attempt at flow visualization using oil dots applied to the pressure surface showed little or no movement at Md conditions. The possibility of separation and subsequent reattachment on the pressure surface cannot be ruled out (though this condition was not observed on the smaller scale cascade tested in the ILPT).

Following the attempts at flow visualization, boundary layer surveys were conducted to isolate effects due to secondary flow phenomena. A flattened pitot tube was used for these measurements, with width-to-height ratio of about 12. The Reynolds number based on slot height (0.1mm) was usually in the region of 600 which, according to BRYER and PANKHURST(1971), will produce negligible error.

Wall proximity effects, according to Bryer and Pankhurst, will cause a pitot tube reading to be low as the tube approaches the wall. The additive correction is small as long as the ratio of tube height to tube diameter is greater than about one. This was the case for the tests on the large chord blade.

It was observed also that results of a moving spanwise traverse with probe immersed in the boundary layer at constant height must be cautiously interpreted. Probe bounce and/or vibration will cause a pressure signal not unlike that expected from the sought-after secondary flow phenomena. This proved to be a non-trivial problem with pressure surface surveys.

In figure 5.27 are the results of a moving spanwise pressure survey at location x/s=0.44, with probe 0.5mm above the blade surface. The survey spanned a distance of 20mm, 10mm to either side of centre, with speed approximately 20mm/s (1000 samples were acquired at a rate of 1000Hz). Added to the figure is a dashed line to emphasize an apparent oscillation

of mean pitot pressure, the oscillation having wavelength of order 1.3mm, increasing slightly across the span. These oscillations appear to be caused by the expected secondary vorticity since later runs with various size boundary layer trips upstream of the probe caused the oscillations shown in figure 5.27 to vanish. However, these results must be considered as provisional.

Other investigators (see chapter three) have also identified coherent structure. Reported values of wavelength on a turbine blade range from 1.2mm to 16mm and appear to be related to local curvature (and perhaps to streamwise distribution of curvature). In looking at all reported results, including cases of constant curvature, wavelengths tend to diminish with higher curvature (TANI's(1969) measurements using large radii are in apparent opposition to this). Most investigators report that once established, the wavelengths are invariant with changes in freestream velocity, a most curious result and one suggesting that tunnel hardware may play a role in establishing the particular wavelengths which are eventually amplified. Invariance of wavelength with radius of curvature has also been reported but only in cases of constant duct radius(cf. MCCORMACK et al.(1970) and WINOTO(1979b)).

Similar spanwise surveys performed downstream of x/s=0.44 failed to show any clear evidence of a cell-like secondary flow. Various types of probes were used (opposed-tube yaw meter, rotated flattened pitot tube) all producing similar negative results. Results from each run were run through a computer program, written by this author, which performed autocorrelation calculations based on the use of the fast Fourier transform. The autocorrelation calculations indicated the absence of a spanwise dependent structure.

These (negative) findings are in accord with the results of

KEMP(1977) and HAN(1982) who also found that at some point downstream of the observance of Goertler vortices the flow broke down into a less coherent, turbulent-like flow.

It is clear from all of the foregoing that identifying the nature of secondary flow structure on concave-curved surfaces and, further, understanding the physics of the phenomena, call for a more extensive investigation with systematic variation of the relevant geometrical and flow parameters. It is clear that a surface possessing varying radius of curvature affects the flow in a more complex way than does one of constant curvature.

Boundary layer profile measurements were made difficult by the traverse system which for these initial tests exhibited a significant backlash. By preloading the probe arm in one position against a specially built support, however, it was possible to obtain boundary layer surveys point by point, one per run. This was clearly an unsatisfactory situation and was abandoned after a few attempts at acquiring a velocity distribution near the trailing edge. The thinness of the boundary layer (the 99% thickness was about 1.5mm) also caused probe bounce to be a serious detriment to obtaining valid data.

However, the data that was collected is shown in figure 5.28. The tests were conducted near the trailing edge near tapping 26, x/cax=0.987. The data were acquired in the form of Mach numbers (calculated from measured pressures) and were converted to velocity ratios using the relationship,

$$U/U_e = M/M_e(T/T_e)^{1/2} \qquad \ldots 5.14$$

where the subscript e identifies the boundary layer edge value. T can be calculated from the Crocco-Buseman relationship (WHITE(1974)),

$$T = T_w + (T_{aw}-T_w)U/U_e - rU_e^2/2c_p \qquad ...5.15$$

The subscripted temperatures refer to wall temperature and adiabatic (recovery) wall temperature, and r is the recovery factor ($Pr^{1/3}$ was used). The adiabatic wall temperature is defined as

$$T_{aw} = T_e + rU_e^2/2c_p \qquad ...5.16$$

The method of finding U/U_e is an iterative procedure since the required temperature in equation 5.14 is a function of the unknown velocity ratio in equation 5.15 and 5.16. An accurate approximation (less than 0.5% error) exists if the freestream and wall temperature are similar (they typically differed by about 6^oC in the blowdown tests).

$$U/U_e \cong Mf/M_e f_e \qquad ...5.17$$

The value f is defined in equation 5.6. Equation 5.17 was used in all subsequent calculations of velocity ratio for both the pressure surface and suction surface.

The 99% thickness determined from the measurements near the trailing edge was about 1.5mm. Predictions from two sources (KIRBY(1983) and the program, STAN5) indicate a value of about 2mm in this region. However, the data shown in figure 5.28 must be considered provisional. The data for tapping 21, for example, has considerable uncertainty (perhaps as much as 30%) in y-location due to probe backlash.

There is a clear indication though that the boundary layer profiles may not be as full (turbulent-like) as the predicted values. In KEMP'S(1977) work neither the laminar nor turbulent profile calculations matched the data downstream of transition. The data showed a laminar-like

profile which persisted along the pressure surface to the trailing edge, a condition which is believed to exist in this case.

In view of the thin pressure surface boundary layer and the problems with backlash and vibration the continuation of tests on the large chord pressure surface was postponed for a later investigative effort. The remainder of the experimental work to be reported here concerns work done on the large chord suction surface. This work includes the measurement of boundary layer profiles and frequency content of the fluctuating velocities using a hot wire, the latter being reported in chapter four.

5.2.5 Large Chord Suction Surface

Boundary layer profile measurements on the suction surface of the large chord B22 profile constitute the first data collected of this type in the O.U.E.L. transient tunnels. The suction surface boundary layer growth is affected by such conditions as surface curvature and flow conditions near the transition region. The pressure data presented earlier coupled with (unpublished and provisional) schlieren photographs indicated the presence of a separation-reattachment bubble between tappings 72 and 71 (see figure 2.4), a region where the free stream velocity decreases rapidly and possibly initiates turbulent flow. The farthest reach upstream of the traversing probe is well downstream of the transition region, however, at tapping 61.

In figure 5.26 is shown the acceleration parameter, K, defined earlier. From about tapping 68 on, x/s=0.08, this parameter is less than 2.5×10^{-6} and diminishes toward zero farther downstream. One can expect then that flow characteristics will be dominated more by freestream turbulence, surface curvature, and compressibility effects rather than by streamwise pressure gradient.

The curvature on the suction surface is large between tappings 65 and 53, in the range of x/cax=0.1 to 0.6, as can be seen on figure 5.24. The effect of this parameter in an otherwise nearly zero-pressure-gradient flow should be part of a future investigation.

Measurements of boundary layer profiles on the suction surface were accomplished with the use of a flattened pitot probe attached to the probe arm of the computer-driven traverse mechanism. Data acquisition windows usually were of the order of one to two seconds, sufficiently short that the time response of the probe and associated tubing could alter (attenuate or amplify) the pressure signal.

It was necessary to determine the time response of the system empirically especially since theoretical calculations from different sources indicated an unrealistically short time constant. The probe system was tested empirically by reversing the traverse direction through the boundary layer in alternate runs. This created in one case, moving from freestream to wall, an emptying or evacuation of mass from the probe, while in the second instance the probe was filled. Only when the data was repeated could the measurement be considered valid.

The primary influence on the response time (for a given, fixed time window) was the width of the slot opening in the flattened pitot tube end. Tests were conducted with a range of openings from 0.05mm to 0.3mm. Profile data disagreed sharply for the narrow openings. Further, for reasons involving flow in the tubing system, it was not appropriate to simply average the results of a backward and forward measurement.

Mass flow in the tubing system is dependent on a number of effects (Reynolds number, sudden contractions/enlargements, tubing entrance losses, etc.) which influence the internal flow in the tube in ways which are nonlinear and asymmetric with respect to internal flow direction. By

calculating displacement thickness from to-and-fro surveys it was found that filling and emptying were not symmetric processes-- biased pressures did not distribute evenly about a mean true pressure. Only when the probe slot opening was made sufficiently large did these processes become symmetric.

As a probe is made larger to improve time response, however, one must consider the effect of finite probe dimensions on flow blockage and distortion, especially near the wall region. GRANT(1978) gives design criteria for the case when the boundary layer profile is approximated by a wake with parabolic stagnation pressure distribution. His data show that to avoid an error equal to 5% of the pressure drop (stagnation pressure drop from freestream to wall), the probe thickness must be less than 1/5th the boundary layer thickness. Strictly speaking this blockage criteria holds in a free wake (no wall). However, this seems a reasonable design goal for these experiments as long as the probe is sufficiently far from the wall. As discussed earlier, Reynolds effects are avoided if the probe is one or more diameters above the wall. Thus for boundary layers of thickness greater than 1.5mm, a flattened pitot tube of height 0.3mm or less, maintained at a height of 0.3mm or more above the wall, should yield valid pressure measurements.

The probe height settled on was 0.3mm, a value suitable for all locations except at upstream tapping 61 where the probe was slightly larger than desired for the 0.8mm thick boundary layer which occurred there.

For all boundary layer measurements it was necessary to correct for a probe offset of 0.2mm, the distance to the probe centreline when touching the wall. Also the data was numerically smoothed using a 31-point Hanning filter function (the details of which can be found in appendix B). The length of the smoothing function was chosen as a compromise between gaining

smooth data and losing end points truncated during the smoothing process. The results of the surveys are shown in figures 5.29 to 5.41.

The data, which must be considered provisional at this point, can be seen to be somewhat scattered in the region where the velocity gradient is rapidly changing. This is due to the measuring procedure which included running the traverse at a constant velocity through the boundary layer. Future measurements should include a varying velocity schedule to obtain highest accuracy near the wall.

Also shown in figures 5.29 to 5.41 are results of STAN5, a program which calculates a 2-D boundary layer flow field. A synopsis of this program can be found in chapter three.

The STAN5 results, by comparison, generally indicate a somewhat smaller 99% thickness and a less full (more laminar-like) profile. The predicted profiles agree fairly well with the experimental data except at the locations indicated by tappings 54, 56, 58, and 61, the worst agreement occurring with tapping 56, figure 5.37. The differences seen at tapping 56 appear to be due to a position error of about 0.3mm, but this cannot be verified without further testing. The STAN5 predictions also show a sharp break near the boundary layer edge. This is due to a calculational inability to fashion large asymptotic runouts of the velocity profile.

The utility of boundary layer data is in the extraction of information concerning skin friction coefficient. This information is obtained if one can calculate the friction velocity, u_τ, (c.f. equation 3.14) from either 1) direct measurements at the wall or from 2) wall-wake laws formulated from correlations with boundary layer data. In this case, lacking data from direct wall measurements, one could only resort to the latter method.

Two attempts were made to calculate friction velocity. The first

centred on using the compressible form of the momentum integral equation as outlined in chapter three. To use this method one calculates the displacement thickness, equation 3.4, for locations along the blade surface. In order to perform this calculation one must curve-fit velocity profile data in the region between the wall and first data point. Curve-fitting this data, however, is problematical. A straight line fit is an obvious choice but may yield errors up to 15% in displacement thickness. This was verified by using results generated by STAN5. One could compare the results of a calculation on a truncated velocity profile produced by STAN5 with the values output by the program for a full profile. Calculations of this type showed that the accuracy involved with curve-fitting the data near the wall could not be validated and so this method was abandoned.

The second attempt to calculate friction velocity had been used with success by OM, VIEGAS and CHILDS(1985) and MATHEWS and CHILDS(1970). This method involved utilizing a least square fit to the wall-wake law for compressible flow given by equation 3.6 .

To use this method one eliminates the wake profile parameter by evaluating the law at the boundary layer edge. The resulting equation has the form,

$$u^* = (u_\tau/K)\ln(yu_\tau/\nu_w) + 5.1u_\tau + E\sin^2(\pi y/2\delta) \qquad ...5.18$$

The value u^* is the Van Driest equivalent velocity defined in chapter three, equation 3.7 . E is a function defined for convenience as

$$E(\delta,u_\tau) = u_e^* - u_\tau/K\ln(\delta u_\tau/\nu_e) - 5.1u_\tau \qquad ...5.19$$

One then solves for values of u_τ and δ which minimize the standard

deviation (or rms error). This is done by substituting each of the 600 or so experimental data pairs of U and y into equation 5.18 with assumed values of u_τ and δ and calculating the root mean square of the deviation. This process is repeated over u_τ , δ space so that a surface plot of rms deviation vs u_τ vs δ is obtained. The minimum rms deviation on this plot identifies the values u_τ and δ .

Using the results of the foregoing calculations one can plot the data as shown in figures 5.42 to 5.54. In these figures the boundary layer data are recast in the inner variable form similar to u^+ and y^+ but with u^* replacing U. Shown also in figures 5.42 to 5.54 is the adiabatic, zero pressure gradient form of the compressible law of the wall due to VAN DRIEST(1951). The experimental results exhibit only fair agreement with this inner law. In general the most interesting difference is the slope in the inner region which for the data is larger than 2.5, the reciprocal of the Von Karman constant. Also in the wake region the data exhibit the usual tendency to deviate from the logarithmic inner law.

Using the same values of friction velocity and boundary thickness the data can be plotted in the form of a velocity defect function and compared with the velocity defect law according to MAISE and MCDONALD(1968), equation 3.11. Results of this comparison are shown in figures 5.55 to 5.58.

The data shown in figures 5.55 to 5.58 indicate a reasonable agreement for tappings 32 to 52 which are in a region on the suction surface where the boundary layer is thickest and thus where probe interference has the least effect. The data do not quite reach zero value at the boundary layer edge. This is due to the least-square optimization which minimizes a function over two-variable space for an inner law and may not produce the best value for either variable for an outer defect law.

The theoretical defect law shown in figures 5.55 to 5.58 was arrived at by MAISE and MCDONALD(1968) by curve fitting data obtained in adiabatic, zero pressure gradient flow. The experimental data from the suction surface should be expected to deviate then in regions where flow acceleration is significant. Indeed the worst agreement occurs for tappings 60 and 61 which are in a region of higher acceleration (see also figure 5.26).

The results shown for tappings 54, 56, and 58, as with previous comparisons, show a large deviation from theoretical laws. Reviewing again figure 5.26, these tappings are located in a region, x/s=0.4 to 0.6, where erratic changes in acceleration parameter may be due to the weak shock wave impinging at the surface location x/s=0.5, near tapping 52. This shock-boundary layer effect and its effect on a velocity defect law merits further investigation.

The friction velocity can be used to estimate a skin friction coefficient according to equation 3.10. This was done for these provisional boundary layer data and values ranging up to 15% higher than those calculated by STAN5 were found. It is difficult to draw conclusions from this in view of the earlier discussion on the turbulence modelling included in STAN5.

This concludes the chapter on experimental results obtained in the new O.U.E.L. blowdown tunnel. Other results of studies on hot wire use, obtained mainly in the low-speed open circuit wind tunnel located elsewhere in the building, are presented collectively in chapter four.

It is intended that all of these experimental results be used to identify further testing in the new blowdown tunnel and point to a refinement in measurement techniques which can be used successfully in future testing.

CHAPTER VI

DISCUSSION OF RESULTS

6.1 UPSTREAM FLOW CONDITIONING IN THE NEW BLOWDOWN TUNNEL

The inlet to the new blowdown tunnel presented unique entrance flow problems. The small reservoir surrounding the inlet to the working section along with the rather short entrance duct to the cascade led to a centreline velocity defect. Severe turning of the flow into the duct created a sheared flow which could not properly mix out to a homogeneous, low turbulence condition in the short distance to the cascade entrance plane.

The inlet to a cascade working section must provide for a uniform flow and allow for some form of turbulence management. From the experience with the blowdown tunnel the optimum inlet will reduce shear flow into the inlet by providing a properly curved (elliptical) entry bellmouth and will have sufficient clearance between the plenum wall and duct entry walls to allow for a flow which approximates that from an infinite plenum. Any residual sheared flow can be attenuated or even eliminated by the addition of screens and a honeycomb flow straightener.

The introduction of a honeycomb flow straightener may increase the level of the upstream Mach numbers while the addition of screens has the opposite effect. These two devices, honeycomb and screens, are necessary, however, to achieve reduced turbulence and smooth out any entrance plane pressure distortion, a necessary condition for providing the proper incidence angle to the cascade model.

It was important to identify needed inlet modifications early in the commissioning programme first, because it had been assumed (hoped) that uniform, low turbulence flow could be established in the as-designed inlet

without the need for mechanical devices, and secondly, had this study not been undertaken, each new user of the tunnel would have had to provide certain peculiar modifications for his own build. The final configuration of the inlet in the new blowdown tunnel provides the required flow quality at the entrance to the cascade model. The addition of honeycomb and screens is consistent with the practices of many tunnel users in controlling flow uniformity and managing turbulence levels.

6.2 ENTRANCE AND EXIT PLANE UNIFORMITY

There is little in the way of data on this subject in the literature outside of Oxford results. Apparently most investigators either have no problems in this area or simply do not report results of inlet/exit uniformity.

It is an accepted fact that good blade-to-blade periodicity should exist. Further it is expected that a correctly-constructed multi-passage cascade will yield experimental results similar to those of an infinite array of blades. The ideal is that the tunnel itself should impose little or no constraint on a flow which would occur freely past a cascade of blades. The study of the entrance/exit plane uniformity on the new blowdown tunnel was meant to confirm these assumptions and to determine a method of controlling periodicty at both upstream and downstream boundaries of the cascade model.

As shown by the results given in chapter five the inlet and exit uniformity are coupled by the flow in the end passages of the cascade model. Even for an eight-passage cascade an inlet flow survey must include measurements of velocity (Mach number) above the end passages since although apparent flow uniformity may exist in the centre passages the overall level of Mach numbers in those passages may be in error. This is demonstrated by comparing blade surface Mach numbers on the 100mm B22

profile with a tuned inlet against those with an untuned inlet, figure 6.1. As can be seen in figure 6.1 for an exit Mach number of 0.97 significant differences occurred on the aft portion of the suction surface. For the untuned inlet the flow in the trailing edge region tended to diffuse or recompress whereas for the tuned flow there occurred an expansion (acceleration) in this same region. For the untuned inlet the average value of the inlet Mach numbers was higher by about 6% (0.335 vs 0.316).

There was also an apparent forward (upstream) shift in the location of sonic speed from x/cax=0.55 to 0.4. A shift upstream in the throat location was observed to occur when the incidence is higher than the angle set by the liners. Higher incidence could also be accompanied by a separation bubble just aft of the high curvature portion on the blade suction surface.

In the O.U.E.L. blowdown tunnel it is possible to tune the inlet to achieve an acceptable periodicity and correct inlet Mach number level by varying suction at the end passage locations. This is done by varying the gap between the end blade and a sharp-edged shutter plate attached to the movable liner. The gap is adjusted (trial and error) until the end passage flow is sufficient to level the end passage Mach numbers with the duct-centre values. These end value Mach numbers are quite sensitive to gap size while only much smaller movements in Mach number occur in the duct-centre values.

A check on proper tuning can be done by comparing the measured inlet Mach numbers with those calculated in ideal flow (geometric throat, isentropic flow). However, this must be done with an understanding of the end passage flow. The end passage flow can be subsonic even for a generally transonic exit condition and so the average value of A^* for the cascade will not be the measured throat value. Thus the average Mach number across the entire inlet will in general not correspond to the theoretical value.

An improperly tuned inlet can cause the average inlet Mach number to be higher than tuned conditions for choked flow. This can be seen in figure 5.19 for run 337. A mistuned inlet distribution also explains the M+ condition on the 100mm B22 build which had an average inlet Mach number level about 3% higher than the tuned (choked) condition at M_d. A close examination of figure 5.8a discloses a skewness in the inlet Mach number distribution for the M+ flow caused by the short liner shutter too far open. This decreased the incidence at the instrumented passage resulting in low suction surface values. This problem was not recognized at the time and could explain why cascades tested in different facilities show varying inlet Mach numbers, cf. KIOCK et al.(1985).

In measuring the inlet angles using a pitot rake with yaw meter, one must be aware that the rake exerts a local effect on the near passage(s). If the initial cascade setup is badly mistuned the rake may cause a localized correction to the flow and indicate the correct inlet angle. Upstream wall tappings should be used to indicate a nearly tuned inlet prior to making incidence measurements.

To verify the correctness of inlet velocities a fine grid measurement across one passage will yield the theoretical value of inlet Mach number if the cascade is properly tuned. This theoretical value, as the results on both the 100mm B22 cascade and the VKI-1 cascade show, is fairly insensitive to curvature of the sonic line within the passage. Thus a tuned inlet will allow the flow to seek a natural level proper for the particular geometry, i.e., a flow in which the streamlines curve in conformance with the potential flow field of an infinite cascade array and not to an unnatural tunnel-imposed condition.

One can correlate outlet flow angle with differences in the suction surface Mach numbers using the axial velocity-density ratio (AVDR). This is a measured value and is arrived at by averaging the mass flux over a unit

distance at both inlet and outlet and dividing the result.

$$AVDR = \frac{\rho_2 V_{x2}}{\rho_1 V_{x1}} \qquad ...6.1$$

This can also be written in terms of the inlet and outlet angles,

$$AVDR = \frac{\rho_2 w_2 \cos \beta_2}{\rho_1 w_1 \cos \beta_1} \qquad ...6.2$$

A value of one is an indicator of uniform 2-D flow. Values different from one indicate an over- or underturning of the exit flow. GOSTELOW(1984) discusses the correlation of deviation from 2-D flow with AVDR and shows that for a given inlet incidence the exit angle deviation from uniform 2-D flow can be a large mutiple of the deviation of AVDR from one. That is

$$\beta_2 - \beta_{2\text{-}2D} = K_i(AVDR-1) \qquad ...6.3$$

where β_2 is the exit flow angle measured from the axial direction and K_i is a function of the inlet angle. K_i can be a large value in the case of a turbine rotor profile at high incidence.

If the outlet angle changes several effects can occur. One effect is to induce a change in the angle between the shear boundary formed by the trailing edge wake and the flow on the farside suction surface, i.e. an alteration of the effective flow area expansion angle at the exit. A subsequent change in the streamwise area gradient can change a flow from one which tends to diffuse to one which tends to expand. Thus inlet distortion can be related to downstream flow expansion by a change in the inlet incidence angle.

A discrepancy in trailing edge wake angle can also have an effect in transonic flow by altering the pattern of the expansion fan and shock wave emanating from the pressure surface trailing edge. This fan impinges

on the suction surface in the trailing edge region downstream of the throat and its strength (pressure drop) corresponds to the required pressure drop from trailing edge condition to the free stream value downstream of the cascade, cf. HORLOCK(1966). The expansion fan can create a situation where the reduced pressure on the suction surface caused by the fan and its reflections from the trailing wake shear surface compete with the positive pressure gradient required for the suction surface flow to recover to a subsonic or near-sonic exit velocity. The positive pressure gradient would then be effectively cancelled resulting in a flat plate-like flow over a portion of the suction surface. This is a possible cause of the somewhat flat velocity profile on the Nicholson B22 profile at M_d. On the other hand the strength of the oblique shock from the pressure surface recompression which strikes the suction surface also affects the suction surface Mach number distribution by interacting with the expansion fan system just described and thus the two effects are coupled.

Even with no discrepancy in the trailing edge wake angle the expansion fans (and shocks off both pressure and suction surface) are affected by reflections off the end passage shear layers. These reflections change sign at the shear layers and propagate back across the exit plane altering the pressure recovery required by the shocks and expansion fans. In accordance with arguments put forth in the preceding paragraph the entire flow field back to regions on the suction surface will be affected, and thus even in transonic flow the exit conditions will be coupled to the character (speed, jet spreading rate in the unbounded portion, turbulence level, etc.) of the subsonic end passage flow. This implies that care must be taken in achieving the proper inlet flow especially in the end passages.

6.3 COMPARISON OF CASCADE DATA IN DIFFERENT TUNNELS

It was suggested earlier that the method of exhausting exit flow in

different tunnels may be correlated to differences in Mach number distributions especially at transonic exit conditions. Two types of downstream diffusion were mentioned in the experimental results-- dump diffusion as found in the ILPT at Oxford and the linear cascade tunnel at Braunschweig (but with a major difference to be discussed later) and duct diffusion, a version of which is used on the new blowdown tunnel at Oxford.

The dump diffusion used on the ILPT entails exhausting the test gas to a large reservoir. Momentum dissipation occurs downstream as the flow dumps to a stagnant air mass which rises slightly in pressure during the run (the dump system hardware has since been modified). Because the subsonic flow in the end passages is sensitive to downstream pressure the dump pressure is able to modify this flow and accordingly the characteristics of the shear layer adjacent to the transonic flow in the neighboring passage. The form of this modification should be the subject of further experimental studies. Nevertheless, it is not difficult to conclude that if the shear plane which reflects expansion and shock waves back into the exit region is capable of being modified then so can the character of the exit region be modified. This implies that ILPT cascade data can differ slightly (and did) from data obtained in the blowdown tunnel for transonic exit conditions.

The exit momentum in the blowdown tunnel exhausts to a small chamber (which is quite capable of reflecting shock waves). From the small exit chamber the flow is routed to a catcher. The function of the catcher is to collect the momentum of the downstream exit flow and channel it to the downstream exit duct. The important difference from the ILPT in this arrangement is the downstream pressure environment which affects the end passage flow. This environment can be one of constant pressure or consist of a spatial gradient in back pressure which is capable of exerting a slightly different influence on the end passage flow.

An additional consideration concerning tunnel-to-tunnel differences is the fact that the small exhaust chamber in the blowdown tunnel may be capable of influencing the tangential pressure gradient just downstream of the cascade thereby introducing a slight skew to the trailing edge wakes. This would in turn alter the character of the flow field by slightly redirecting the reflections of waves off the wake shear surfaces. Recent schlieren photography (BAINES(1986)) has verified the presence of a variation in skew between wakes and further work is proceeding to correct this problem.

The Braunschweig linear cascade tunnel is considered a dump diffusion type of tunnel but with one difference from the Oxford ILPT. In the Braunschweig tunnel the exhaust gases dump directly to the plenum with no intervening duct. Thus the exit flow experiences an unconstrained expansion with the plenum pressure capable of exerting now a different influence than that in either the ILPT or the blowdown. It is apparent from the data presented in chapter five, however, that this last type of diffusion may be similar to the Oxford blowdown tunnel in the effect it has on suction surface Mach numbers in the range of transonic exit conditions. Two factors make the Braunschweig tunnel exit conditions more like the blowdown than like the ILPT.

First, suction is applied to the flow just upstream of the end passages (see HOHEISEL(1977)). The amount of suction appears to be governed by the inlet-to-plenum pressure ratio, a method not dissimilar in principle to the method employed in the Oxford blowdown tunnel wherein the suction is established by the inlet/exit pressure ratio. The end passage flow in the Braunschweig tunnel is guided, however, which would introduce a Reynolds number dependency not found in the end passage flow of the blowdown tunnel with its free expansion across a sharp edged plate. This could cause a difference in the end passage shear layers.

A second similarity in the two tunnels concerns the spatial pressure gradient in the exhaust area. The Braunschweig tunnel recirculates the exhaust gas back to the tunnel inlet. This would tend to induce a back pressure gradient of similar dimensions (but not directionality) to that occurring in the blowdown.

In comparing data from different cascades, including the experimental data gathered for this thesis, one can summarize the causes of differences in the data. For example, differences in inlet incidence will cause early (upstream) differences in both pressure surface and suction surface data. If incidence is correct the major differences likely to occur will be in suction surface data downstream of the throat. In transonic exit flow the suction surface will be sensitive to the method of exhausting the gas and to the downstream geometry and the flow there could show a tendency to recompress or expand. In subsonic exit flow tunnel exhaust influences will be minimal if all else is correct.

Thus, in the B22 comparisons the low incidence at M+ for the 100mm blade is in evidence. At the same time high incidence (accompanied with forward movement of the sonic line) may be the cause of high suction surface Mach numbers in a portion of the ILPT data.

Data suggests that a tuned condition must be considered tuned only for a small range of exit conditions. Hence a cascade will yield incorrect upstream blade pressures if assurances are not made that a tuned condition exits. The 100mm cascade appears to have been well tuned for M- and M_d conditions while the large chord was slightly mistuned (high incidence) at M_d. The large chord data may have also suffered effects of the presence of the downstream traverse mechanism causing a similar diffusion on the suction surface as experienced by the NICHOLSON(1981) B22 build in the ILPT.

The large chord cascade will be particularly sensitive to

reflections occurring in the exit chamber and perhaps in a different way than the 100mm cascade. Shock and expansion waves from the centre blade can easily reflect into the subsonic end passage flow, alter the bypass flow, and thereby change the incidence at the entrance of the instrumented passage. Thus, changes in exit geometry (such as a repositioning of the traverse mechanism) could hinder repeatability. Indeed failure to repeat pressure conditions was a problem experienced in the early testing on the large chord cascade.

6.4 LARGE CHORD PRESSURE SURFACE

The state of the boundary layer on the pressure surface of a turbine blade must be known to predict adequately friction losses and heat transfer coefficient. As yet there has not appeared a complete physical model which includes the secondary flow phenomenon and which is capable of being expressed in a satisfactory mathematical model.

Two classes of experiments dealing with the longitudinal vortex structure appearing on concave surfaces have appeared in the literature. The first deals with constant curvature, e.g. TANI(1969), WINOTO(1972), MCCORMACK(1970), and others. Only a few (three to this author's knowledge) have been concerned with the state of the boundary layer in the second group, that of varying curvature accompanied with non-zero pressure gradient, and specifically on a turbine profile. These include KEMP(1977), HAN(1979), and the present study. (The preceding references do not include all publications of those authors surrounding their particular experiments).

In reported cases of experiments in ducts of constant radius, secondary longitudinal vorticity was made to persist over the entire surface. In cases of varying radius of curvature the flow was seen to break down into a less organized, more turbulent-like structure but with boundary

layer characteristics of a laminar-transitional layer. The experiments involved with constant radius have reported success in measuring and visualizing longitudinal vortices for models of different, but constant, radius of curvature and changes in freestream velocity. In experiments on models of varying radius of curvature this has not occurred. One can conclude that studying the phenomenon of Goertler vorticity on a particular turbine blade of fixed distribution of radius of curvature may not be the best approach to gaining an understanding of the physics of the phenomenon. The results of the study contained in this thesis emphasize the need for experimental data which deal with a systematic variation of the relevant parameters such as curvature, velocity, pressure gradient, freestream turbulence, etc., aimed at determining their interaction and effects on the transition process and the character of the resulting flow.

As shown by the results of chapter five the curvature of the pressure surface coupled with the large acceleration parameter make it likely that Goertler vorticity influences transition and the subsequent boundary layer characteristics. Pressure probe measurements tended to confirm this but did not clarify the physics of the flow phenomenon. In the trailing edge region it was not possible to detect a coherent flow structure yet the velocity profiles measured there are clearly less full than the predicted values indicating a near-surface boundary layer in a state of suspended transition. The flow upstream nearer the high curvature region of the blade indicated more clearly the possibility of vortex structure. Thus, this author suggests that the experiments herein have ended any questions concerning the existence of this secondary flow phenomenon.

Also, until more is known about the mechanism of transition it does not seem productive to attempt to show, as many others have, that the flow behaves according to some stability analysis like that of SMITH(1955) or

TOBAK(1971). Future experiments should include studies on how the experimental apparatus, the wind tunnel or the engine, affects the initiation of instabilities and their subsequent magnification downstream.

The early work of KLEBANOFF(1955) and LIEPMANN(1945) indicates the possibility of a unified theory of transition which would allow a spectrum of behavior. At one end of the spectrum the theory would asymptote to the prediction of flat plate, zero pressure gradient results while at the other end the results of curved, radially unstable flow would be predicted. The theory would patch together usual transition parameters such as momentum thickness Reynolds number, pressure gradient, and freestream turbulence (see SEYB(1972)) with curved surface parameters (FOREST(1977)).

6.5 LARGE CHORD SUCTION SURFACE

Transient measurements of boundary layer characteristics in the O.U.E.L. blowdown tunnel using a flattened pitot probe successfully demonstrated how to attack the problem of probe error and position error. In addressing the former it was found that the emptying and filling rate of a flattened pitot tube differs according to the rate and direction of pressure variation experienced during the boundary layer traverse. One cause of this difference is due to the probe end geometry. Flow entering the narrow slot in the end of the tube experiences a rather sudden area expansion accompanied by adverse pressure gradient and possible separation. Added to this is a contraction loss similar to that of flow entering a duct from a large plenum. These effects occur when the probe is traversed away from the wall toward the freestream. When moving in the opposite direction, toward the wall, air residing in the tube will flow outward. In this case the narrow end of the probe acts like a nozzle, providing a favourable pressure gradient. These effects are most severe for extremely narrow slots. The problem is considered solved when traverses moving either toward

or away from the wall produce similar profiles. To achieve this symmetry one must enlarge the probe and/or allow a longer settling time. The probe used in the boundary layer traverses was 0.3mm in height, and it is estimated that by adding approximately one second to the run times (which usually amount to about a two second data window) a 20% to 30% reduction in probe size, down to a height of approximately 0.2mm, could result.

The data accumulated in the B22 profile boundary layer measurements indicated that in transonic flow the boundary layer flow field over the suction surface should possibly be considered a compressible flow field. (Many sources suggest that boundary layer flow is basically incompressible up to freestream Mach numbers of about two). This aspect was investigated using the program STAN5 by comparing the results for friction coefficient with the compressible and incompressible forms of the Von Karman momentum integral equation (c.f., SCHLICHTING(1979)). In general the M^2 term appearing in the compressible form of the equation accounts for approximately 10% of the calculated value of skin friction coefficient at Mach one (i.e., the incompressible value is 10% larger). (However, skin friction loss obviously increases).

Provisional skin friction coefficients were calculated for the boundary layer data seen in chapter five using a friction velocity obtained from a least squares fit to the inner law given by equation 5.18. The results were generally about 15% higher than calculated by STAN5. This cannot be explained until further testing is done on this blade.

The data only roughly obeyed an inner law and wake law, as shown in chapter five. Although this can be ascribed to early stages in the development of testing techniques, it also points to a general requirement for a better understanding of the basic physical mechanisms in turbulent, compressible flows with pressure gradients. At the moment there is a need for more reliable correlations for such parameters as turbulent kinetic

energy, dissipation rates, shape factors, etc., for these flows.

Comparisons with STAN5 must be judged in light of the physics utilized in the program. The use of a mixing length model, for example, assumes that turbulent kinetic energy is unaffected by upstream flow history and that the turbulent length scale is calculable from local parameters as in an equilibrium flow. This can be a poor approximation in an accelerating flow if one accepts the notion of frozen turbulence suggested by TAYLOR(1937). In this scheme the amplitude of the turbulent fluctuations retain their magnitude as the freestream velocity increases and thus entrainment of mass into the boundary layer domain is streamwise variable. Turbulent dissipation, and thus the turbulent length scale, becomes a stream variable which can only be accounted for by the input of a new empirical correlation. The as-written version of STAN5 allows for but does not include this type of correlation. However, even more sophisticated theories which include transport and stream history effects become less well-fitted to a flow in which the mixing layer is highly curved or in which a strong acceleration occurs. (For example, see RODI(1982)). Thus the use of STAN5 for flows which are strongly influenced by acceleration and other effects, such as curvature and pressure gradient, must be regarded as a severe extrapolation of the applicability of the program.

The study of flows on a model such as the large chord B22 profile is subject to competing flow effects (curvature, pressure gradient, transition, freestream turbulence, etc.) and thus one is hesitant to make sweeping conclusions from one series of tests which do not involve a systematic variation of each of these parameters. However, the data obtained from these initial large chord tests have been useful in identifying future tests and in identifying a useful role for the linear cascade.

This concludes the discussion of results reported in chapter five. Not included in this chapter are discussions surrounding experiments done with hot wires, which are included in chapter four.

CHAPTER VII

CONCLUSIONS

A new blowdown wind tunnel at the Oxford University Engineering Laboratory was commissioned during the term of the experimental work discussed in this thesis. One objective of this work was to certify the tunnel through comparison testing of cascades having previously been tested in other tunnels. These tunnels included the Isentropic Light Piston Tunnel at O.U.E.L. and the high speed cascade tunnel in Braunschweig, West Germany.

The commissioning exercise also included inlet studies, design of a new downstream ejector and experimental calibration of the new tandem ejector system.

In addition to the tunnel commissioning programme a new phase of experimental work was begun on a large chord version of the B22 profile tested by NICHOLSON(1981). As these studies were to have included hot wire boundary layer surveys a considerable amount of investigative work was done on hot wire calibration, and the results contained herein.

Each phase of work on the tunnel commissioning and other experimental studies yielded new information. The primary conclusions to be drawn from the commissioning programme and subsequent experimental work are presented here in abbreviated form. A more complete discussion of the main points can be found in chapters four, five, and six which deal with experimental results and a discussion of each phase of the work.

1. Inlet Flow Conditioning

a. The new blowdown tunnel requires a flow conditioning system upstream of the model in the inlet duct. The severe turning of the flow in

the blowdown plenum causes problems that will occur in any tunnel which utilizes turning of the flow upstream of the test section, be it a closed-loop tunnel with corners or simply an indraft tunnel with an open plenum, i.e., vorticity and shear will be introduced into the main flow. The methods of removing these flow characteristics and managing turbulence levels are time tested and include the installation of entrance turning vanes (cusp), elliptical bellmouth , honeycomb flow straighteners, screens, and turbulence grids. The honeycomb flow straightener was the single best improvement, reducing lateral fluctuations by a factor of 18.

2. Periodicity

a. Growth of inlet sidewall boundary layers and asymmetrical end passage flow can distort the inlet incidence even for an eight-passage cascade. This is corrected by suction through sidewall gaps just upstream of the end passages.

b. The blowdown tunnel at O.U.E.L. utilizes sharp-edged shutter plates to remove Reynolds dependency and provide for a sudden expansion into the end passages. Adjustment of the shutter gap changes the suction. This process is called tuning and correct tuning is achieved only when the incidence and Mach number level is correct.

c. Inlet periodicity must be rechecked in transonic cascade flow when the exit Mach number is changed because an unwanted change in incidence may occur. This is due to the downstream shock and expansion system altering the subsonic flow in the end passages.

d. The total inlet Mach number average for a mistuned inlet with subsonic exit flow may be higher than the value for a tuned inlet with choked downstream flow.

e. Off-design incidence can be created by changing shutter openings, but this should not be the method used to obtain changes in incidence.

Incorrect end passage flow may cause distorted shock and expansion reflections in the exit region and disrupt exit periodicity.

f. Outlet periodicity is tied to shock and expansion reflections off the end passage shear layers and off any surfaces (exit chamber walls, probes, traverse hardware, etc.) in proximity to the cascade exit plane.

3. The Large Chord Two-Passage Cascade

a. The large chord cascade was easily tuned for inlet periodicity and successfully duplicated Mach number distributions obtained from other cascades.

b. Repeatability is a problem if downstream measurement hardware is reconfigured after a run. The proximity of this hardware (made necessary by limited upstream and downstream space) creates changes in upstream flow if, e.g., a pitot rake is installed, or creates downstream pressure blockage if traversing gear is used.

c. Schlieren visualization is a necessary adjunct to pressure testing. On no other cascade at O.U.E.L. is the flow in the instrumented passage in such close proximity to the end passage shear layers and so likely to be affected by spurious shock reflections.

d. Future large chord builds should be pressure tapped in both passages (four surfaces). On the current B22 build the suction surface of the centre, instrumented blade is affected by the shock system emanating from the atypical trailing edge wake off the upstream, far passage blade. At the same time, the suction surface on the downstream blade (near the catcher) is experiencing the assumed proper expansion fan from the centre blade. Assuming the the flow field surrounding the centre blade is correct then one is interested in first, the shock patterns on the suction surface on the near-catcher blade and, second, in how the Mach number distribution on the pressure surface in the far passage relates to the flow on the

centre blade suction surface.

4. B22 Mach Number Results From Two Facilities

a. Blade Mach number distributions on the B22 profile were obtained on two blowdown builds, the 100mm cascade and the large chord cascade, and compared with data obtained from the ILPT (NICHOLSON(1981)).

b. At transonic conditions a comparison of exit Mach numbers does not ensure identical conditions in the two facilities. Schlieren flow visualization comparisons must be the deciding factor.

c. The only consistent differences in data from the two facilities occurred on the suction surface downstream of the throat. In this region it is believed that differences in tunnel geometry and method of exhaust will exert the most influence.

d. Incidence differences account for disagreement on the suction surface upstream of the throat for the Md and M+ conditions. The location of the sonic line, which establishes the throat in the passage, is sensitive to incidence. Off incidence data from the blowdown substantiate this finding. In the future agreement (or disagreement) of early suction surface data can serve as an indicator of comparable inlet conditions for two different cascades.

e. An upshot of part d. is that the lift on this profile appears enhanced by a slightly higher incidence. It appears, for example, that upstream Mach numbers are increased while the rear of the suction surface maintains a flat pressure profile with no apparent separation at the trailing edge. More studies are needed in off-incidence performance, however, since other factors such as losses may be adversely affected.

f. New detail around the leading edge of the large chord blade indicates the presence of sharp deceleration near the blend point on the suction surface. Preliminary schlieren photography suggests a

separation-reattachment bubble at this location. Also, it was not possible to pinpoint the exact location of the stagnation point through pressure measurements.

5. VKI-1 Comparisons In Two Facilities

a. Only a portion of the total data collection was presented but in all flow regimes data from the Braunschweig and Oxford tunnels were in good agreement. In the especially difficult region on the rear portion of the suction surface diffusion was similar even at the critical condition. Lack of schlieren visualization made it impossible, however, to be certain that identical back pressures were being compared.

b. The VKI-1 cascade was tested at a higher Reynolds number in the Oxford blowdown. It was found that at transonic exit conditions the shock on the suction surface appeared to move upstream of that encountered in the lower Reynolds number flow.

c. The smeared shock system on the suction surface may be caused by unsteady fluctuations of the shock emanating from the pressure surface trailing edge wake.

6. Tunnel Influences on Cascade Results

a. Results of cascade data from three facilities (ILPT, O.U.E.L. blowdown and Braunschweig high speed cascade tunnel) indicate that data replication depends on exit flow conditions. For subsonic flow identical Mach number distributions will occur. In transonic flow the best agreement will occur on the upstream portions of both the pressure and suction surfaces. Downstream of the throat, especially on the suction surface, diffusion and/or expansion will depend on the exhaust pressure field. For the tests conducted in the three tunnels the exhaust pressure field suffered various effects of hardware configuration.

b. Downstream shock and expansion waves and their reflections lead to conflicting results on the suction surfaces. These differences, which cannot be resolved soley on the basis of pressure data, can be clarified only by flow visualization.

c. VKI-1 data was qualitatively in better agreement than was the B22 profile data acquired prior to installing the traverse hardware in the Oxford blowdown tunnel. Subsequent to that installation B22 data was in good agreement at all exit conditions. A new change to the ILPT, the addition of a downstream throat, may cause a slight change to B22 data by allowing an expansion on the suction surface near the trailing edge which was observed in both B22 builds in the blowdown tunnel prior to the installation of the traverse hardware.

d. There is no apparent way to account for tunnel-caused differences in exit flows. Standardizing exit conditions by perhaps installing perforated tailboards would introduce more questions about the validity of the data than would be answered by the resultant similarity in exit flows. Also this would be a time consuming process in the operation of a transient tunnel. Accurate numerical modelling of downstream conditions offers a better alternative. This would allow prediction codes to be tailored to tunnel geometry.

7. Large Chord B22 Pressure Surface

a. The flow environment over the pressure surface includes all the necessary ingredients for longitudinal vortex interaction in the boundary layer. The flow is initially laminar over the leading edge, enters into a region of high curvature and destabilized flow, and becomes turbulent-like evidencing characteristics of a laminar-transitional state.

b. The boundary layer 99% thickness is on the order of 2mm. In order to perform measurements in a boundary layer of such small dimensions

the measurement system must not be affected by probe vibration or probe blockage.

c. The flow shows cell-like structure just downstream of the transition region but loses its coherence progressively downstream. At the trailing edge no definite flow structure can be observed.

d. A more systematic investigation is called for in order to understand flow on curved surfaces where the surface curvature varies in the streamwise direction. The work in this thesis, like others before, indicates that while experiments in ducts of constant radius of curvature allow Goertler vortices to persist under some circumstances, under no circumstances have they been reported to persist in ducts of changing radius of curvature.

8. Large Chord Suction Surface

a. It is possible to obtain boundary layer profile data in the new O.U.E.L. blowdown facility using a flattened pitot tube. The method could be improved by extending the the run window to approximately three seconds.

b. Boundary layer traverses in a transient facility using pressure probes can suffer errors in position and time response. The latter can be precluded by insuring repeatability of runs traversed in opposite directions through the boundary layer.

c. Boundary layer data should be backed up by surface skin friction measurements. There is no reliable inner law or velocity defect law for compressible, turbulent flow. Thus it is difficult to infer the friction velocity from velocity profile measurements in the mid region to outer wake region. The use of a least square method to obtain friction velocity from an assumed wall-wake law will yield only approximations to those laws.

d. The velocity profile shape in the wake region of the turbulent boundary layer is, more than in other areas, affected by freestream

pressure gradient.

e. The boundary layer region of a transonic freestream flow field should be considered a compressible flow field to account for compressibility contributions of as much as 10% in skin friction coefficient.

9. STAN5

a. This 2-D viscous flow program authored by Crawford and Kays produces reasonable correlations only if transition is correctly modelled and curvature is not extreme. If a region of separation-reattachment occurs the program must be supplied with a modified surface velocity profile in that region.

b. Results of STAN5 agree substantially with results obtained using the compressible form of the Von Karman momentum integral to calculate skin friction coefficient.

c. STAN5 continues to demonstrate regions of significant disagreement with data produced in transient facilities.

10. The Use of Hot Wires in Transient Tunnels

a. The use of a three-term correlation ($A + BRe^{1/2} + CRe$) in calculating the Nusselt number used in the hot-wire response equation yields better results over extended velocity ranges than does the two-term correlation usually found in King's law.

b. The output (bridge) voltage of a constant temperature anemometer can be corrected for gas temperature effects if the calculated wire temperature takes into account the change in end-support (prong) temperature. The correction term must also include the bridge resistance values in series with the hot-wire probe and include the thermal conductivity evaluated at the mean (film) temperature.

c. Effects of pressure and compressibility on the response of a hot-wire require further study, but some early results indicate that these effects can be accounted for in the Reynolds number terms in the three-term correlation mentioned in part a. above by correcting density and temperature using compressible flow relationships and estimations of temperature recovery effects (i.e., dissipation effects) in the boundary layer.

d. Further investigations of frequency spectra in the boundary layer can be utilized to identify the nature of the convection of freestream turbulence and transfer of turbulent energy into the boundary layer.

11. The Future of 2-D Cascade Testing

It is not economical to build new designs for 2-D linear cascades and then infer rotational and other effects for the full radial design--the testing of new designs seems now in the domain of the annular, rotating test facility. However, engine manufacturers need more information concerning the basic physics of the flow phenomena in turbine passages. The need for information of a fundamental nature can and should be satisfied by the 2-D cascade.

One often hears that data from 2-D facilities is not relevant since 2-D prediction codes are now very reliable. This author suggests that the stated reliability is due to refinements of the empiricisms built into the codes and not necessarily to a better understanding of the underlying physics.

The use of linear 2-D cascades for obtaining design data can most profitably be directed toward understanding such phenomena as transition in accelerated flows, transpiration cooling effects on passage gas dynamics, roughness effects, secondary flows (such as end wall boundary layer induced

losses), flows over profiled endwalls, overtip leakage effects, etc. That is, there will continue to be a need for understanding certain physical phenomena in a generic two-dimensional environment without the additional complication of finite geometry and rotational effects. What is suggested here is that in future linear cascade testing it will be less important to study particular profiles than to study particular effects. It will be important to continue to utilise the 2-D, linear cascade for background support of design testing and vitally important to continue investigating fundamental concepts.

REFERENCES

AL'OMAR, A.F. and BAKHTAR, F., Effect of Pressure on the Calibration Characteristcs of Hot Film Anemometers, J. Mech. Eng. Sci., 12, No.6, (1970).

ANDERSON, J.D.Jr., Computational Fluid Dynamics-An Engineering Tool?, from 'A Collection of Papers in the Aerospace Sciences,' Nagaraja ed., AFAPL-TR-79-2126, June (1982).

ANNAND, W.J.D., The Resistance to Airflow of Wire Gauzes, J. Roy. Aeronaut. Soc., 57, 141, (1953).

BAILLE, A., These Dr. Ing., Univ. Aix Marseille,(1971).

BAINES, N.C., OLDFIELD, M.L.G., JONES, T.V., SCHULTZ, D.L., KING, P.I., and DANIELS, L.C., A Short-Duration Blowdown Tunnel for Aerodynamic Studies on Gas Turbine Blading, ASME paper 82-GT-312, (1982).

BAINES, N.C., Topsy Guide: Transient Tunnel Operating Data Acquisition and Processing System, O.U.E.L. Rept. 1462/83, (1983).

BAINES, N.C., OLDFIELD, M.L.G., KING, P.I., and DANIELS, L.C., The Use of Tandem Ejector Pumps in an Intermittent Blowdown Tunnel, ASME paper 84-GT-226, (1984).

BAINES, N.C., KING, P.I., OLDFIELD, M.L.G., KIOCK, R., HOHEISEL, H., RAMM, G., LEHTHAUS, F., KOST, F., and SIEVERDING, C.H., A Comparison of Aerodynamic Measurements of the Transonic Flow Through a Plane Turbine Cascade in Four European Wind Tunnels, Proceedings of a Symposium on Measuring Techniques in Transonic Flows in Cascades and Turbomachines, Genoa, Italy, M. Troilo ed., Oct., (1985).

BAINES, N.C., Private communication, Imperial College, London, (1986).

BAINES, W.D. and PETERSON, E.G., An Investigation of Flow Through Screens, Trans. ASME, 73, (1951).

BEARMAN, P.W., Corrections for the Effect of Ambient Temperature Drift on Hot Wires in Incompressible Flow, DISA Inf. Series No.11, May (1971).

BHATIA, J.C., DURST, F., and JOVANOVIC, J., Corrections of Hot-Wire Anemometer Measurements Near Walls, JFM, 122, Sept. (1982).

BLAIR, M.F., BAILEY, D.A., and SCHLINKER, R.H., Development of a Large-Scale Wind Tunnel for the Simulatiuon of Turbomachinery Airfoil Boundary Layers, J.Eng.Power, 103, Oct. (1981).

BLAIR, M.F., Influence of Free-Stream Turbulence on Boundary Layer Transition in Favorable Pressure Gradients, J. Engr. for Pow., 104, Oct. (1982).

BRADSHAW, P., An Introduction to Turbulence and its Measurement, Pergamon Press, (1971).

BRADSHAW, P., Effects of Streamline Curvature on Turbulent Flow, AGARDograph AG-169, (1973).

BRIGHAM, E.O., The Fast Fourier Transform, Prentice-Hall Inc., (1974).

BRYER, D.W. and PANKHURST, R.C., Pressure Probe Methods for Determining Wind Speed and Flow Direction, NPL (1971).

BROWN, A. and MARTIN, B.W., A Review of the Bases of Predicting Heat Transfer to Gas Turbine Rotor Blades, ASME paper 74-GT-27, (1974).

BROWN, A. and MARTIN, B.W., Flow Transition Phenomena and Heat Transfer Over the Pressure Surfaces of Gas Turbine Blades, ASME paper 81-GT-107, (1981).

BRUUN, H.H., The Interpretation of a Hot Wire Signal Using a Universal Calibration Law, J.Phys.E: Sci. Instr., 4, (1970).

BRUUN, H.H., Linearization and Hot Wire Anemometry, J.Phys.E: Sci. Instr., 4, (1971).

BRUUN, H.H., On the Temperature Dependence of Constant Temperature Hot Wire Probes with Small Aspect Ratio, J.Phys.E: Sci. Instr., 8, (1975).

BRUUN, H.H., A Digital Comparison of Linear and Nonlinear Hot Wire Data Evaluation, J.Phys.E: Sci. Instr., 9, (1976).

BRUUN, H.H., Interpretation of Hot-Wire Probe Signals in Subsonic Airflows, J.Phys.E: Sci. Instr., 12, (1979).

CARUTHERS, J.E. and MCKAIN, T.F., Through-Flow Calculations: Theory and Practice in Turbomachinery Design, AGARD Conf. Proc. No.195, on Through-flow Calculations in Axial Turbomachinery, Oct. (1976).

CASPAR, J.R., Unconditionally Stable Calculation of Transonic Potential Flow Through Cascades Using an Adaptive Mesh for Shock Capture, ASME paper 82-GT-238, (1982).

CEBECI, T. and SMITH, A.M.O., Analysis of Turbulent Boundary Layers, Academic Press, (1974).

CHAMPAGNE, F.H., SCLEICHER, C.A., and WEHRMANN, O.H., Turbulence Measurements with Inclined Hot Wires. Part 1. Heat Transfer Experiments with Inclined Hot Wires, JFM, 28, pt.1, (1967).

CHURCHILL, S.W. and CHU, H.H.S., Correlating Equations for Laminar and Turbulent Free Convection From a Horizontal Cylinder, Int.J.H.and Mass Tr., 18, 1049, (1975).

COLES, D., The Law of the Wake in the Turbulent Boundary Layer, JFM, 1,

pt.2, (1956).

COLLADAY, R.S. and STEPKA, F.S., Similarity Constraints in Testing of Cooled Engine Parts, NASA TN D-7707, June (1974).

COLLIS, D.C. and WILLIAMS, M.J., Two-Dimensional Convection From Heated Wires at Low Reynolds Numbers, JFM, 6, (1959).

COMTE-BELLOT, G., Measurement of Unsteady Fluid Dynamic Phenomena; The Hot-Wire and the Hot-Film Anemometers, VKI LS 73, Jan. (1975).

CONSIGNY, H. and RICHARDS, B.E., Short Duration Measurements of Heat-Transfer Rate to a Gas Turbine Rotor Blade, J. Engr. Pow., 104, No. 2, July (1982).

CRANE, R.I. and WINOTO, S.H., Longitudinal Vortices in a Concave Surface Boundary Layer, AGARD Symposium, The Hague (1979).

CRAWFORD, M.E. and KAYS, W.M., STAN5-A Program for Numerical Computation of Two-Dimensional Internal and External Boundary Layer Flows, NASA CR-2742, (1976).

DANIELS, L.C., Film Cooling Of Gas Turbine Blades, D. Phil. Thesis, Oxford University, (1979).

DAVIS, R.W. and MILLAR, D.A.J., Through Flow Calculations Based on Matrix Inversion: Loss Prediction, AGARD Conf. Proc. No. 195 on Through Flow Cal;culations in Axial Turbomachinery, Oct., (1976).

DENTON, J.D., A Time Marching Method for Two- and Three-Dimensional Blade to Blade Flows, ARC R&M 3775, (1975).

DENTON, J.D., An Improved Time Marching Method for Turbomachinery Flow Calculation, ASME paper 82-GT-239 (1982).

DRING, R.P. and HEISER, W.H., Turbine Aerodynamics, AFAPL-TR-78-52, The Aerothermodynamics of Aircraft Gas Turbine Engines, G. Oates, ed., July, (1978).

DRING, R.P., BLAIR, M.F., and JOSLYN, H.D., An Experimental Investigation of Film Cooling on a Turbine Rotor Blade, J. Engr. Pow., 102, (1980).

EPSTEIN, A.H., GUENETTE, G.R., and NORTON, R.J.G., The MIT Blowdown Turbine Facility, unpublished, (1984).

ERWIN, J.R. and EMERY, J.C., Effect of Tunnel Configuration and Testing Technique on Cascade Performance, NACA TN 2028, (1950).

FARN, C.L. and WHIRLOW, D.K., Application of Time-Dependent Finite Volume Method to Transonic Flows in Large Turbines, Transonic Flow Problems in Turbomachinery, edited by Adamson and Platzer, Hemisphere Pub. Corp., (1977).

FLORYAN, J.M. and SARIC, W.S., Stability of Goertler Vortices in Boundary Layers, AIAA J, 20, No. 3, March, (1982).

FLUGGE, W., Handbook of Engineering Mechanics, McGraw-Hill, (1962).

FOREST, A.E., Engineering Predictions of Transitional Boundary Layers, AGARD CP 224, 22, (1977).

GAUGLER, R.E., Some Modifications to, and Operational Experiences with, the Two-Dimensional Finite Difference, Boundary Layer Code, STAN5, ASME paper 81-GT-89 (1981).

GAUGLER, R.E., A Review and Analysis of Boundary Layer Transition Data for Turbine Application, ASME paper 85-GT-83 (1985) (a).

GAUGLER, R.E., Private communication, Nasa Lewis, (1985) (b).

GOETHERT, B.H., Transonic Wind Tunnel Testing, Pergammon Press, (1961).

GOODMAN, A.W., Modern Calculus with Analytical Geometry, Vol.1, McMillan, (1967).

GOPALAKRISHNAN, S. and BOZZOLA, R., Computation of Shocked Flows in Compressor Cascades, ASME paper 72-GT-31 (1972).

GOSTELOW, J.P., Cascade Aerodynamics, Pergamon Press, (1984).

GRANT, H.P., Measuring Time-averaged Stagnation Pressure in Pulsatile Air Flow, I.S.A. 23rd Int. Instrumentation Sym., ISBN 87664-362-4, (1977).

GRAZIANI, R.A., BLAIR, M.F., TAYLOR, J.R., and MAYLE, R.E., An Experimental Study of Endwall and Airfoil Surface Heat Transfer in a Large Scale Turbine Blade Cascade, J. Engr. Pow., 102, No. 2, April, (1980).

HALL, P., The Linear Development of Goertler Vortices in Growing Boundary Layers, JFM, 130, (1983).

HAN, L.S., COX, W.R., and CHAIT, A., Investigation of the Boundary Layer Behavior on Turbine Airfoils, AFAPL-TR-79-2011 (1979).

HAN, L.S. and COX, W.R., A Visual Study of Turbine Blade Pressure-Side Boundary Layers, ASME paper 82-GT-47 (1982).

HEBBAR, K.S., Wall Proximity Corrections for Hot-Wire Readings in Turbulent Flows, DISA Inf. Series No.25, Feb (1980).

van der HEGGE ZIJNEN, B.G., Modified Correlation Formulae for Heat Transfers by Natural and by Forced Convection from Horizontal Cylinders, Appl. Sci. Res., 6, Sec. A, No.s 2-3, (1956).

HILPERT, R., Warmeabgage von Geheizten Drahten und Rohren im Luftstrom, ForshArb. IngWes., 4, (1933).

HINZE, J.O., Turbulence, McGraw-Hill, (1975).

HOHEISEL, H., The Cascade Wind Tunnels of the Institut fur Aerodynamik-Short Description, DFVLR Braunschweig, IB 151-74/13, (1974).

HOHEISEL, H. and KIOCK, R., Zwanzig Jahre Hochgeschwindigkeits - Gitterwindkanal des Institut fur Aerodynamik der DFVLR in

Braunschweig, Z.F.W. 1, No. 1, (1977).

HORLOCK, J.H., Axial Flow Turbines, Butterworth and Co. Ltd., (1966).

HUFFMAN, G.D., ZIMMERMAN, D.R., and BENNET, W.A., The Effect of Free-Stream Turbulence Level on Turbulent Boundary Layer Behavior, Boundary Layer Effects in Turbomachines, J. Surugue, ed., AGARD-AG-164, (1972).

INCROPERA, F.P. and DEWITT, D.P., Fundementals of Heat Transfer, John Wiley&Sons, (1981).

JEANS, A.H. and JOHNSTON, J.P., The Effects of Streamwise Curvature on Turbulent Boundary Layer Structure, AFOSR-TR-82-1015, (1982).

JOHN, J.E.A., Gas Dynamics, Allyn and Bacon Inc., (1969).

JONES, T.V., Heat Transfer, Skin Friction, Total Temperature and Concentration Measurements, Measurement of Unsteady Fluid Dynamic Phenomena, B.E. Richards, ed., McGraw-Hill, (1971).

JONES, W.P. and LAUNDER, B.E., The Prediction of Laminarization with a Two-Equation Model of Turbulence, Int. J. Heat Tr., 15, (1972).

KANEVCE, G. and OKA, S., Correcting Hot-Wire Readings for Influence of Fluid Temperature Variations, DISA Inf. Series No.15, Oct., (1973).

KATSANIS, T., Computer Program for Calculating Velocities and Streamlines on a Blade-to-Blade Streamsurface of a Turbomachine, NASA TN D-4525, (1968).

KATSANIS, T., Fortran Program for Calculating Transonic Velocities on a Blade-to-Blade Stream Surface of a Turbomachine, NASA TN D-5427, (1969).

KEMP, A.S., The Boundary Layer of the Pressure Surface of a Turbine Blade in Cascade, Euromech 72, Univ. of Salford, (1976).

KEMP, A.S., The Boundary Layer on the Pressure Surface of Turbine Blades in Cascade, Ph. D. Thesis, Cambridge Univ., (1977).

KING, L.V., On the Convection of Heat From Small Cylinders in a Stream of Fluid, Phil. Trans. A, 214, (1914).

KING, P.I. and OLDFIELD, M.L.G., An Examination of Curve Smoothing Using Digital Filter Theory, U.S. Air Force Academy Aeronautics Digest, USAFA-TR-85-2, April, (1985).

KIOCK, R., Experimentelle Untersuchungen am Turbinengitter VKI-1 biem Schaufelhonenverhaltnis h/l=3,0 , DFVLR Braunschweig Report No. 151-HGB-80/2, (1980).

KIOCK, R., LEHTHAUS, F., BAINES, N.C., and SIEVERDING, C.H., The Transonic Flow Through a Plane Turbine Cascade as Measured in Four European Wind Tunnels, ASME Intl Gas Turbine Symp., Bejing, Sept., (1985).

KIOCK, R., Private communication, DFVLR, Braunschweig, (1982).

KIRBY, S., Private communication, Rolls-Royce Ltd., Derby, (1983).

KLEBANOFF, P.S. and TIDSTROM, K.D., Evolution of Amplfied Waves Leading to Transition in a Boundary Layer with Zero Pressure Gradient, NASA TN D-195, (1959).

KLEBANOFF, P.S., TIDSTROM, K.P., and SARGENT, L.M., The Three-dimensional Nature of Boundary Layer Instability, JFM, 12, (1962).

KLEIN, A., Aerodynamics of Cascades, AGARDograph No. 220, (1977).

KOCH, F.A. and GARTSHORE, I.S., Temperature Effects on Hot Wire Anemometer Calibrations, J.Phys.E: Sci. Instr., 5, (1972).

KOVASZNAY, L.S.G., The Hot-Wire Anemometer in Supersonic Flow, J. Aero. Sci., Sept., (1950).

KRAMERS, H., Heat Transfer from Spheres to Flowing Media, Physics, 12, (1946).

KRISHNAMOORTHY, V., Effect of Turbulence on the Heat Transfer in a Laminar and Turbulent Boundary Layer Over a Gas Turbine Blade, ASME paper 82-GT-146, (1982).

KUETHE, A.M. and CHOW, C.Y., Foundations of Aerodynamics: Bases of Aerodynamic Design, John Wiley and Sons, (1976).

LANGSTON, L.S., NICE, M.L., and HOOPER, R.M., Three-dimensional Flow Within a Turbine Cascade Passage, J. Engr. Pow., 99, No. 1, Jan., (1977).

LARSEN, S.E. and BUSCH, N.E., Hot Wire Measurements in the Atmosphere, DISA Inf. Series No. 16, July, (1974).

LEHTHAUS, F., Experimentelle Untersuchungen an einem Gasturbinen Laufrad-Gitter mit dem Schaufelprofil VKI-1, DFVLR-AVA Report No. 251 75 A 07, (1975).

LEHTHAUS, F., Computation of Transonic Flow Through Turbine Cascades Using the Time Increment Method (translation), Dissertation TU Braunschweig, (1977).

LIEPMANN, H.W., Investigations on Laminar Boundary Layer Stability and Transition on Curved Boundaries, ARC R&M 7802, (1943).

LIEPMANN, H.W., Investigation of Boundary Layer Transition on Concave Walls, NACA Wartime Report, ACR No. 4J28, (1945).

MAISE, G. and McDONALD, H., Mixing Length and Kinematic Eddy Viscosity in a Compressible Boundary Layer, AIAA J., 6, No. 1, Jan., (1968).

MARTIN, B.W. and BROWN, A., Factors Influencing Heat Transfer to the Pressure Surfaces of Gas Turbine Blades, Int. J. of Heat and Fluid Flow, No. 3, (1979).

MARTINEZ-VAL, R., JIMENEZ, J., and REBOLLO, M., Sensor Contamination Effects in Hot-Wire Anemometry in Air, DISA Inf. Series No.27, Jan. (1982).

MATHEWS, D.C., CHILDS, M.E., and PAYNTER, G.C., Use of Cole's Universal Wake Function for Compressible Turbulent Boundary Layers, J. Acft., 7, No. 7, March-April, (1970).

McCORMACK, P.D., WELKER, H., and KELLEHER, M., Taylor-Goertler Vortices and Their Effect on Heat Transfer, J. Heat Trans., (1970).

McDONALD, P.W., The Computation of Transonic Flow Through Two-Dimensional Gas Turbine Cascades, ASME paper 71-GT-89, (1971).

MEHTA, R.D., Turbulent Flow Through Screens, AIAA paper 84-0538, Reno, Jan., (1984).

METZGER, D.E. and MAYLE, R.E., Gas Turbine Engines, Mech. Engr., 44, June, (1983).

MORETTI, G. and ABBETT, M., A Time-Dependent Computational Method for Blunt Body Flows, AIAA J., 4, No. 12, Dec., (1966).

MOTALLEBI, F. and NORBURY, J.F., The Effect of Base Bleed on Vortex Shedding and Base Pressure in Compressible Flow, JFM, 110, (1981).

NALLASAMY, M., A Critical Evaluation of Various Turbulence Models as Applied to Internal Fluid Flows, NASA Tech Paper 2474, May, (1985).

NARAYANAN, M.A.B., On the Large Scale Structure of Turbulence In Boundary Layer and Shear Flows, AFAPL-TR-79-2126, June, (1982).

NAUDASCHER E. and FARELL, C., Unified Analysis of Grid Turbulence, Proceedings of the ASCE, EM Div. EM2, Apr., (1970).

NICHOLSON, J.H., Experimental and Theoretical Studies of the Aerodynamic and Thermal Performance of Modern Gas Turbine Blades, D. Phil. Thesis, Univ. of Oxford, (1981).

OATES, G.C., Elementary Theory of Blade Aerodynamics, The Aerothermodynamics of Aircraft Gas Turbine Engines, AFAPL-TR-78-52, G.C. Oates, ed., (1978).

OATES. G.C., Aerothermodynamics of Gas Turbine and Rocket Propulsion, AIAA Inc., (1984).

OKA, S. and KOSTIC, Z., Influence of Wall Proximity on Hot-Wire Velocity Measurements, DISA Inf. Series No.13, May, (1972).

OLDFIELD, M.L.G., Users Handbook for GT6 (MKI and MKII) Galvanometer Drive Amplifier System, O.U.E.L. Rept. 1130/75, (1975).

OLDFIELD, M.L.G., JONES, T.V., and SCHULTZ, D.L., On-Line Computer for Transient Turbine Cascade Instrumentation, IEEE Trans. on Aerosp. and Elec. Sys., Vol. AES-14, No.5, Sept. (1978).

OLDFIELD, M.L.G., KIOCK, R., HOLMES, A.T., and GRAHAM, C.G., Boundary Layer Studies on Highly Loaded Cascades using Heated Thin Films and a Traversing Probe, ASME paper 80-GT-137, (1980).

OM, D., VIEGAS, J.R., and CHILDS, M.E., Transonic Shock-wave/Turbulent Boundary Layer Interactions in a Circular Duct, AIAA J., 23, No. 5, May, (1985).

PANTANKAR, S.V. and SPALDING, D.B., Heat and Mass Transfer in Boundary Layers, Morgan-Grampian, London, (1967).

PANTANKAR, S.V. and SPALDING, D.B., Heat and Mass Transfer in Boundary Layers, 2nd ed., Intertext Books, London, (1970).

PERRY, A.E., Hot-Wire Anemometry, Clarendon Press, Oxford, (1962).

PERRY, A.E. and MORRISON, G.L., Static and Dynamic Calibrations of Constant Temperature Hot-Wire Systems, JFM, 47, pt.4, (1972).

PIANKO, M., ed., Modern Methods of Testing Rotating Components of Turbomachines, AGARD-AG-167, (1972).

PIANKO, M., ed., Modern Methods of Testing Rotating Components of Turbomachines (Instrumentation), AGARD-AG-207, (1975).

RAE, W.H. and POPE, A., Low Speed Wind Tunnel Testing, John Wiley and Sons, (1984).

RAGAB, S.A. and NAYFEH, A.H., Goertler Instability, Phys. Fluids, 24/8, (1981).

RODI, W., Examples of Turbulence Models for Incompressible Flows, AIAA J., 20, No. 7, July, (1982).

RODI, W. and SCHEUERER, G., Calculation of Curved Shear Layers with Two-equation Turbulence Models, Phys. Fluids, 26, No. 6, (1983).

ROUSE, H. and HASSAN, M.M., Cavitation-Free Inlets and Contractions, Mech. Eng., March, (1949).

SCHLICHTING, H., Boundary Layer Theory, McGraw-Hill, 7th ed., (1979).

SCHULTZ, D.L. and JONES, T.V., Heat Transfer Measurements in Short-Duration Hypersonic Facilities, AGARDograph AG-165, (1973).

SCHULTZ, D.L., JONES, T.V., OLDFIELD, M.L.G., and DANIELS, L.C., A New Transient Cascade Facility for the Measurement of Heat Transfer Rates, AGARD Conf. Proc. 229, High Temperature Problems in Gas Turbine Engines, (1977).

SCRIVENER, C.T.J., Private communication, Rolls-Royce, Derby, (1980).

SEYB, N.J., The Role of Boundary Layers in Axial Flow Turbomachines and the Prediction of Their Effects, AGARD CP 164, (1972).

SHARMA, O.P. and GRAZIANI, R.A., Influence of Endwall Flow on Airfoil Suction Surface Mid-Height Boundary Layer Development in a Turbine Cascade, ASME paper 82-GT-127, (1982).

SIDDALL, R.G. and DAVIES, T.W., An Improved Response Equation for Hot-Wire Anemometry, Int.J.H.and Mass Tr., 15, (1972).

SIEVERDING, C.H., Experimental Data on Two Transonic Turbine Blade Test Sections and Comparison with Various Theoretical Methods, VKI Lecture Series 59, (1973).

SIEVERDING, C.H., Recent Progress in the Understanding of Basic Aspects of Secondary Flows in Turbine Blade Passages, ASME paper 84-GT-78, June, (1984).

SINGH, U.K., Computation of Transonic Flow in Cascade with Shock and Boundary Layer Interaction, Proc. 1st Int. Conf. Num. Meth. in Laminar and Turbulent Flow, Swansea, July, (1978).

SMITH, A.M.O., On the Growth of Taylor-Goertler Vortices Along Highly Concave Walls, Q. Appl. Math., 13, (1955).

SMITH, L.H.Jr., The Radial Equilibrium Equation of Turbomachinery, J. Eng. Pow., 88, (1966).

SUN, C. and CHILDS, M.E., A Modified Wall Wake Velocity Profile for Turbulent Compressible Boundary Layers, J. Acft., 10, No. 6, June, (1973).

SUO, M., Turbine Cooling, AFAPL-TR-78-52, The Aerothermodynamics of Aircraft Gas Turbine Engines, G.C. Oates, ed., (1978).

TANI, I. and YASHUHIKO, A., Goertler Vortices and Boundary Layer Transition, ZAMP, 20/39, (1969).

TAYLOR, G.I., The Spectrum of Turbulence, Proc. Roy. Soc., Series A, Vol 164, (1937).

THOMANN, H., Effect of Streamline Curvature on Heat Transfer in a Turbulent Boundary Layer, JFM, 33, pt. 2, (1968).

THWAITES, B., Approximate Calculation of the Laminar Boundary Layer, Aero. Quart., 1, Nov., (1949).

TOBAK, M., On Local Goertler Instability, ZAMP, 22, (1971).

TRAUPEL, W., New General Theory of Multistage Axial Flow Turbomachines, Navships 250-445-1, translated by C.W. Smith, General Electric Co., (1942).

VAN DRIEST, E.R., Turbulent Boundary Layer in Compressible Fluids, J. Aero. Sci., 18, (1951).

WHITE, F.M., Viscous Fluid Flow, McGraw-Hill, (1974).

WINOTO, S.H., DURAO, D.F.G., and CRANE, R.I., Measurements with Goertler Vortices, J. Fluids Eng., 101, (1979) (a).

WINOTO, S.H. and CRANE, R.I., Vortex Structure in Laminar Boundary Layers on a Concave Wall, Rpt. TP/C/7903, Dept. Mech. Eng., Imp. College, London, (1979) (b).

WOOD, N.B. and MOORE, M.J., Measuring Techniques in Transonic and Supersonic Cascade Flow, CERL Lab Note No. RD/L/N 166/79, Job No. VE374, Feb., (1980).

WILKINSON, D.H., Calculation of Blade-to-Blade Flow in a Turbomachine by Streamline Curvature, ARC R&M 3704, (1970).

WU., C. and WOLFENSTEIN, L., Application of Radial-Equilibrium Condition to Axial Flow Compressor and Turbine Design, NACA Report 955 (1950).

A P P E N D I X A

BLOWDOWN RUN SETUP

What follows are the considerations involved in calculating valve openings and ejector settings for a particular run. The example used will be for the large chord B22 cascade, run 1190, where both ejectors were needed in order to lower the cascade exhaust pressure.

For the large chord cascade (or any model) certain conditions are known. These include Reynolds number, Mach number, and cascade geometry. From these values one calculates upstream and downstream pressures using equations 5.6, 5.11 and 5.12. For the large chord B22 cascade the required run conditions are listed below.

300mm Large Chord B22 Cascade: M Design

Cascade Throat Area (est. A^*_{cas})	$0.068m^2$
Reynolds Number (isentropic, based on true chord)	$2x10^6$
Exit Mach Number (isentropic)	0.96
Total Temperature	285K
Inlet Total Pressure	0.434bar
Exit Total Pressure (isentropic)	0.24bar

The cascade A^*_{cas} value was found by adding the throat area (per unit span) for two passages, 190mm, to the A^* value for the two end passages. To find the latter value one can assume an average Mach number of 0.4 in the end passages, and, with shutter openings of 6mm and 56mm (a first try at tuning), A^* for the end passages is equal to $0.62x(0.006+0.056)m$. Multiplying the A^* sums by the span dimension of 0.3m yields $0.068m^2$.

From commissioning tests valve calibrations (A^* vs mm setting) are known. Openings for the supply valve and tank valve (figure 2.1) are set using graduated indicators attached to their respective valve stems. If the

second ejector is used it is run with the four discrete nozzles fully open. Thus the pressure ratio and choked flow area for ejector two, fully open, are known. Also known is the choked flow area of the variable orifice regulator in the fully open position. Ejector one driving pressure is also known from equation B.1 below. These and other information are summarized in the following table.

Known Calibration Quantities

A^*_{supply}	vs mm opening
A^*_{tank}	vs mm opening
A^*_{ej2}	$0.017m^2$, 4 nozzles fully open
A^*_{reg}	$0.0035m^2$, fully open
A_4	$0.1486m^2$
A_7	$0.3761m^2$
P_{ej1}/P_{reg}	eqn. B.1
P_{ej2}/P_{reg}	0.75

The quantities to be found now are regulator pressure, P_{reg}, ejector one setting, A^*_{ej1}, and valve areas A^*_s and A^*_t, the supply valve and tank valve areas respectively.

a) Selection of one ejector or two

If one ejector can be used the annular ejector (ejector one) is chosen because of the ease of adjustment. However, from BAINES et al.(1984) the limit on pressure ratio for ejector one in operation singly is approximately 0.3atm, not low enough for the required cascade condition, 0.24bar. Thus, tandem ejector operation is required.

b) Find P_{reg} and A^*_{ej1}

The key to finding P_{reg} is in finding ejector pressure P_{ej2}. One obtains this quantity by finding P_6/P_{o7} and using figure 11 from BAINES et al.(1984). The primary-flow pressure ratio is found using the cascade exit pressure and 2nd diffuser exit pressure (with empirical factor 1.02),

$$P_2/P_{o7} = 0.24\text{bar}/(1.01\text{barx}1.02) = 0.233$$

With P_{o4} approximately equal to P_6 and using equations 2.3 and 2.4 one finds

$$P_6/P_{o7} = 0.56$$

From Baines op cit., figure 11, the above ratio leads to ejector two pressure,

$$P_{ej2} = 10.2\text{bar}$$

The regulator pressure is thus determined,

$$P_{reg} = 10.2/0.75 = 13.6\text{bar}$$

With $P_{o4}=0.56P_{o7}$ and using figure 9 of Baines op cit.,

$$(PA^*)_{ej1} = 0.044\text{m}^2\text{bar}$$

One iterates the above for the pressure and area by starting with P_{ej1} equal to P_{reg} and correcting P_{ej1} after each calculation using:

$$P_{ej1} \;/\; P_{reg} = \sum_{n=0}^{n=5} a_n y^n \qquad \ldots\text{B.1}$$

The coefficients for use in equation B.1 were determined during the initial blowdown calibration from a 5th order curve fit through calaibration data on the regulator:

$$\begin{aligned} a_5 &= -0.47209\text{x}10^{-7} \\ a_4 &= \;\;0.12134\text{x}10^{-5} \\ a_3 &= -0.23156\text{x}10^{-4} \\ a_2 &= -0.16445\text{x}10^{-4} \\ a_1 &= -0.64649\text{x}10^{-2} \\ a_o &= 1.00632 \end{aligned}$$

The values y in equation B.1 are scaled ejector one areas,

$$y = 1000A^*_{ej1} \quad (\text{m}^2) \qquad \ldots\text{B.2}$$

One then finds after iteration,

$$A^*_{ej1} = 0.0033m^2$$

$$P_{ej1} = 13.38bar$$

Once the ejector choked area is calculated the setting l_m in mm is calculated from equation B.3,

$$A^*_{ej1} = 237.637861_m - 0.0932914391_m^2 \qquad ...B.3$$

Ejector one has a zero offset equal to 65mm so the actual measured setting, l_{set}, is

$$l_{set} = l_m + 65 \qquad ...B.4$$

c) Gate Valve Settings

The tank valve choked area is found by equating mass flow through the valve to the mass flow through the cascade.

$$P_{reg}A^*_t = P_oA^*_{cas} \qquad ...B.5$$

All values in equation B.5 are known except A^*_t. The setting in mm is obtained from existing calibration data.

The supply valve area is determined from the known pre-run resevoir pressure, P_s, by equating mass flow through the system assuming constant total temperature,

$$P_sA^*_s = P_oA^*_{cas} + (PA^*)_{ej1} + (PA^*)_{ej2} \qquad ...B.6$$

All values in equation B.6 are known except A^*_s. Note that the regulator flow, $(PA^*)_{reg}$, was not included in the calculation. This insures that the calculated value of supply valve opening will be sufficiently small that regulator flow will begin soon after tunnel start. This method of calculation has been found to produce satisfactory regulation for about two seconds.

A P P E N D I X B

AN EXAMINATION OF CURVE FITTING USING DIGITAL FILTER THEORY

The paper appearing on the following pages was published in the U.S.Air Force Academy Aeronautics Digest, USAFA-TR-85-2, April, 1985. In the paper are discussed various numerical smoothing techniques. One of these, the windowed moving average, was instrumental in reducing boundary layer data for this thesis.

Dr. M.L.G. Olfield reviewed the paper and suggested some changes which were incorporated in the final draft. In view of his assistance he was asked and kindly agreed to be co-author.

P.I.K.

AN EXAMINATION OF CURVE SMOOTHING USING DIGITAL FILTER THEORY

Paul I. King,* and Martin L.G. Oldfield**

Abstract

The theory of digital filters is used to explain the effect of applying a smoothing function to data which contains unwanted frequency components. The smoothing of a curve is viewed as the convolution of the raw data with the impulse response values of a finite impulse response, non-recursive filter. By the convolution theorem the frequency response of the smoothed curve is then the product of the response of the raw data and the frequency response of the filter. Two filter impulse responses are examined, the windowed moving average and the moving least square polynomial. The windowed moving average is easy to use and for the same number of smoothing coefficients produces a qualitatively smoother curve. For studying transient peak data the least square polynomial is the best choice.

I. Introduction

In recent years the development of high speed analog-to-digital (A/D) recording devices has solved the problem of sampling and storing certain measurements of physical phenomena at appropriate rates for detailed postmortem analysis. At the same time the evolution of fast Fourier transform algorithms along with the development of digital filter theory has given engineers and scientists powerful mathematical and computational tools for the analysis of complex waveforms inherent in the recorded data.

It is not uncommon nowadays to acquire a large amount of data in a short period of time such as is shown in Figure 1. This figure shows the results of pressure measurements made in a turbulent boundary layer. The turbulent fluctuations represent a numerically noisy signal and it is difficult to extract meaningful information from this raw

---

*Major, USAF, Assistant Professor of Aeronautics, DFAN

**Lecturer, Oxford University, England

data. A common technique is to numerically smooth the data so that qualitative analysis is facilitated and numerical differentiation is made possible. What follows is an examination of smoothing viewed as a process of filtering raw data -- that is, a process in which one retains (passes) relevant data and discards (attenuates) spurious or irrelevant data.

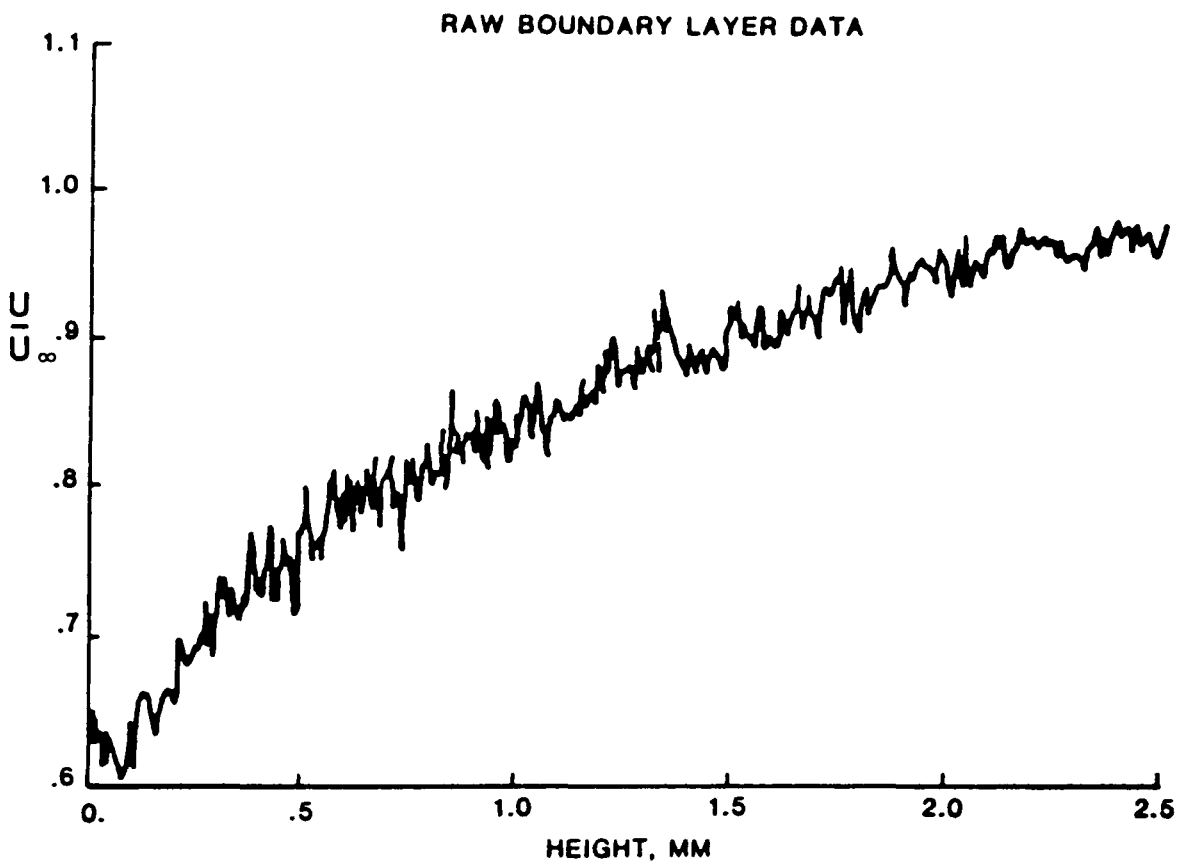

Figure 1. Raw Data from High Speed Data Acquisition

The filtering (smoothing) of data after the experiment holds many advantages including affording one the time to examine data away from the hectic environment of the experiment itself. More importantly one can structure the filter network (smoothing function) so as to avoid the problems intrinsic to real-time analog filtering. The ability to look ahead in time allows the digital filter to avoid the time delay and phase shift common to analog filters.

This paper discusses the considerations important to the selection of a smoothing function for a particular application. In doing so the

frequency response of the function must be considered and thus some familiarization with transform analysis and convolution must be gained. In particular two filter functions are examined: the simple running average and the running least square polynimial fit.

II. The Smoothing Function Viewed as a Filter

In the following analyses, the data are assumed to be a function of a single variable, such as amplitude vs time or amplitude vs distance. For discussion purposes it is assumed that amplitude is the ordinate value, and time or distance is the value on the abscissa axis. The discussion on frequency analysis is applicable to any function of a single variable.

One can view the unsmoothed data as a synthesized signal composed of oscillating waves of varying amplitude and phase, superimposed on a time varying mean signal whose form and magnitude is to be determined. The synthesized signal is sampled in uniform time or spacial increments. The samples form a sequence x(nT) or simply x(n) where

$$x(n) = x(t)_{t=nT} \qquad -\infty<n<\infty \tag{1}$$

and T is the sampling interval (Ref. 1.).

The problem in curve smoothing is finding an appropriate filter to act on the sampled data after the fact and produce a result having the desired frequency characteristics. The features of this problem are shown in block diagram form in Figure 2. Here one assumes linearity as well as a correspondence between the input and output signals. This correspondence is defined by the convolution (smoothing formula),

$$y(n) = \sum_{m=-\infty}^{m=\infty} x(n-m)C_m \tag{2}$$

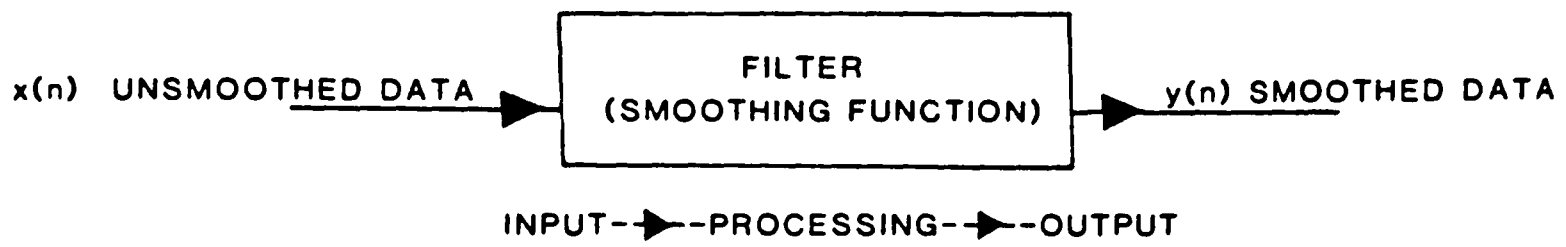

Figure 2. The Smoothing Function Viewed as a Filter

The value y(n) is the smoothed value formed by the convolution of the unsmoothed values, x(n-m), with the convolution variables C_m. These variables, C_m, are explained in the theory of digital filtering as the impulse response of a linear finite impulse response (FIR) filter (Ref. 1).

The convolution summation shown above produces a moving weighted average of the input data. One example of such a moving weighted average is the set of convolution variables C_m = constant = 1/N, where N represents the length of the convolution interval. This is a finite convolution formed by a truncated smoothing formula composed of N terms, N usually being an odd integer. The weighted value y(n) replaces the original data value x(n). The smoothed values are

$$y(n) = 1/N \sum_{m=-\frac{(n-1)}{2}}^{m=\frac{(n-1)}{2}} x(n-m) \qquad (3)$$

This is the simple running average of which more will be said later.

As shown in Equation 3, y(n) depends only on values of the input samples. This type of correspondence defines the coefficients of what is commonly called a non-recursive FIR filter.

As with any filtering process, analog or digital, the characteristics of the filter must be analyzed. All filters will distort and/or remove information from the input signal. It is convenient to think of the filter's action on the data as involving a transfer function in the sense that information is processed in order to produce an output. The filter coefficients, C_m, are the coefficients of the transfer function and are thereby related to the response of the filter.

III. The Fourier Transform and Convolution

To examine the response of the filter, it is necessary to review certain characteristics of discrete data as observed in the time (real)domain and the frequency domain -- the transformed time domain. The two regions are mapped by the Fourier transform. A continuous time based signal, h(t), is transformed to the frequency domain with amplitude H(f) via this Fourier transform,

$$H(f) = \int_{\infty}^{\infty} h(t)e^{-j2\pi ft}\, dt \qquad (4)$$

H(f) is the frequency response of the signal h(t) and is generally a complex value, indicating that both amplitude and phase must be determined for any frequency. If the continuous signal is sampled N times with sampling interval T, the tranform has discrete values computed as (Ref. 3),

$$H(n/NT) = \sum_{K=0}^{N-1} h(kT)e^{-j2\pi nk/N} \qquad (5)$$

A shorthand notation for this mapping process is

$$h(kT) <> H(n/NT) \tag{6}$$

The Fourier transform is used to study the effects of a smoothing function in conjunction with a powerful analytical tool, the convolution theorem.

Convolution of two continous signals, x(t) and h(t), is defined as

$$y(t) = \int_{-\infty}^{\infty} x(\tau)h(t-\tau)d\tau \tag{7}$$

where y(t) is the result of summing the product of signal $x(\tau)$ with the lagged signal $h(t-\tau)$. This is written in notational form

$$y(t) = x(t) * h(t) \tag{8}$$

The convolution integral is best understood in a graphical sense. The signal h(t) is folded, or rotated, about the ordinate axis and displaced an amount t. The overlap region of $x(\tau)$ and $h(t-\tau)$ is then multiplied point for point and the products summed to yield y(t). Recall that this is similar to the process used to obtain the smoothed values y(n) in Equation 2.

If one is processing data acquired in discrete form, the convolution integral (summation) for period N is written

$$y(kt) = \sum_{i=0}^{N-1} x(iT)h((k-i)T) \tag{9}$$

or in notational form,

$$y(kt) = x(kt) * h(kt) \tag{10}$$

A mathematical relationship, the convolution theorem, relates the Fourier transform and the convolution integral. In notational form this is written

$$X(t) * h(t) <> X(f)H(f) \tag{11}$$

IV. The Smoothing Function's Relationship to Frequency Response

As suggested by Equation 11, the Fourier transform of the convolution product is the product of the individual transforms. Thus convolution in the time domain is mathematically equivalent to multiplication in the frequency domain. This can be related to the filtering process.

Filtering is usually represented in the frequency domain as the product of the signal response with the filter response as shown in Figure 3. From the convolution thereom, this is equivalent in the time domain to convolution of the signal with the inverse transform of the filter frequency response. When a filter is subjected to an impulse input, the Fourier transform of its time response to the impulse is the filter's frequency response. Therefore, the inverse transform just referred to is called the filter impulse response. It is evident that the smoothing process can be analyzed by examining either the smoothing function time characteristics, or its frequency response in the transformed domain. Furthermore, if one can specify the desired frequency response of the filter, one can, in theory, invert the response to obtain the time domain values, C_m. These ideas form the basis of digital filtering theory.

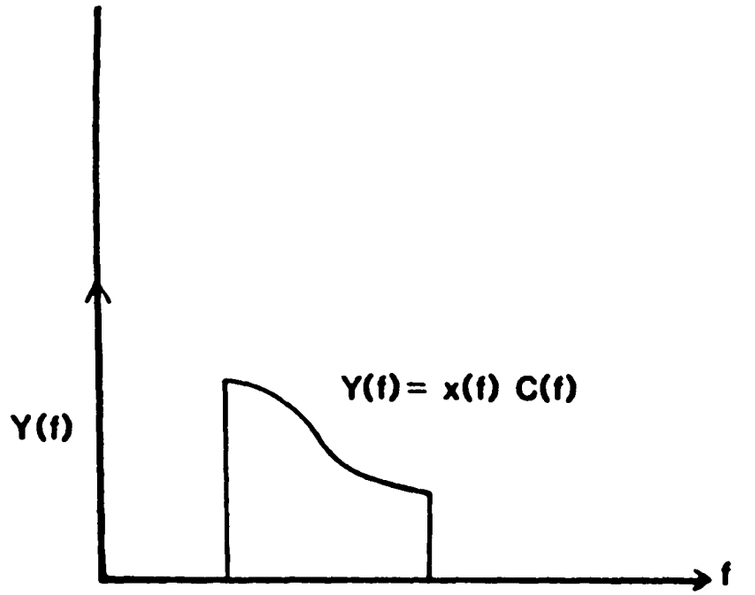

A. FOURIER TRANSFORM OF FILTERED SIGNAL

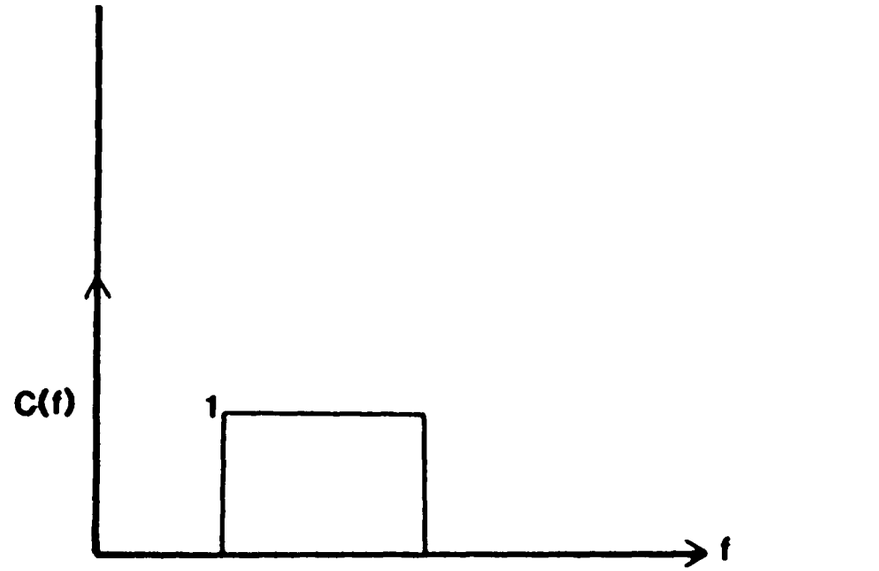

B. FOURIER TRANSFORM OF IDEAL BANDPASS FILTER

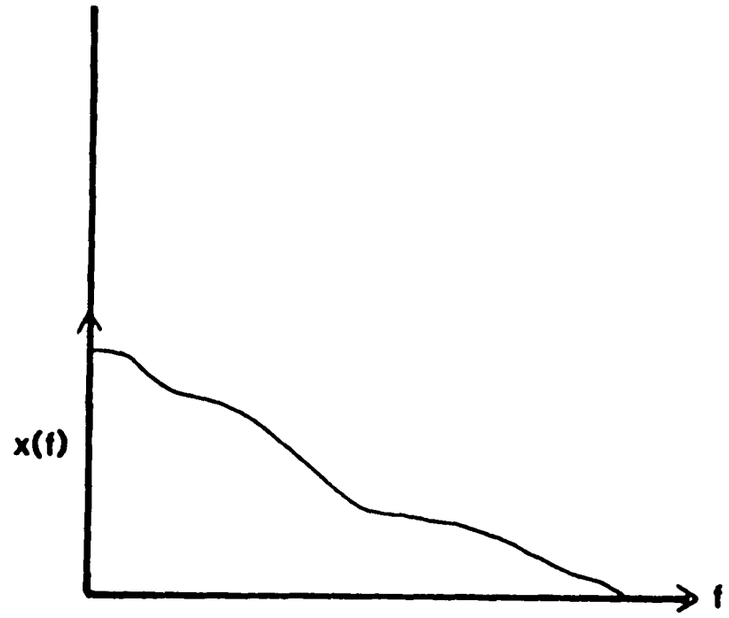

C. FOURIER TRANSFORM OF RAW SIGNAL

Figure 3. Analog Filtering as Viewed in the Frequency Domain

Stearns (Ref. 4) shows that the frequency response of a numerical smoothing function is the discrete Fourier transform of some function C(t) which has been sampled and stored as C(mT) or simply C_m. He demonstrates that the convolution variables, C_m, as shown earlier (Equation 2) do indeed represent the impulse response of the filter. Substituting these values for h(kT) in Equation 5, the discrete frequency response is

$$C(n/NT) = \sum_{m=0}^{N-1} C_m e^{-j2\pi nm/T} \qquad (12)$$

Conversely, if the frequency characteristics, C(n/NT), are known or specified, then one obtains the filter synthesis formula (Ref. 3).

$$C = 1/N \sum_{n=0}^{N-1} C(n/NT) e^{j2\pi nm/T} \qquad (13)$$

V. Choosing an Appropriate Filter Function

At this point, it is instructive to examine the frequency response of some candidate smoothing functions. Figures 4a and 5a represent the impulse responses of two common filters, the moving average, and ideal filter respectively.

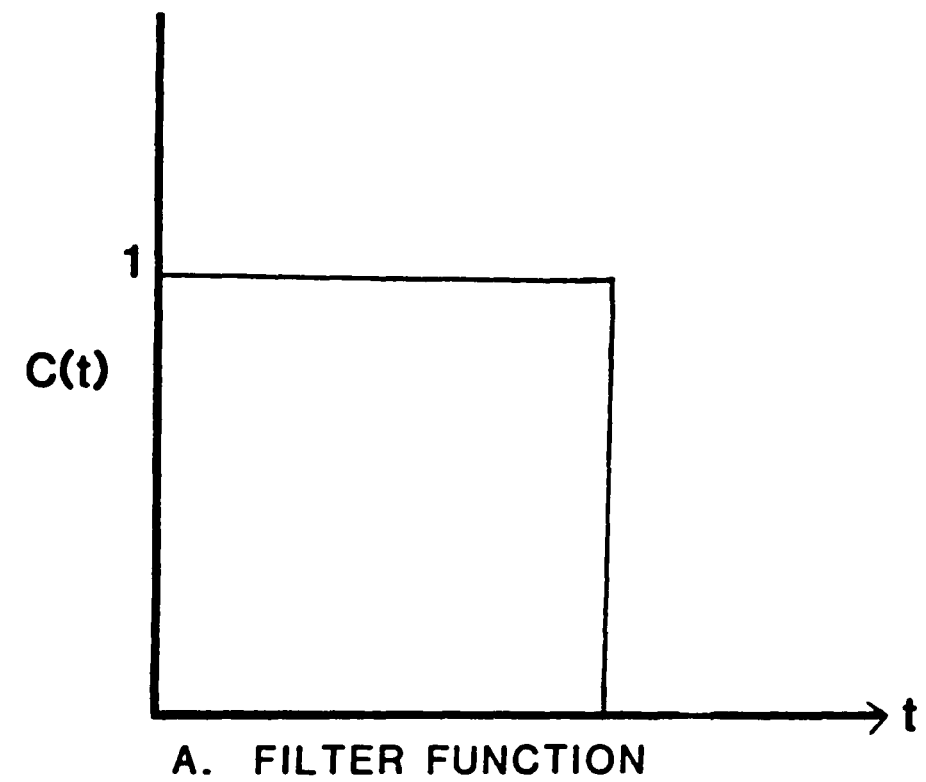

Figure 4. The Simple Moving Average Filter Function

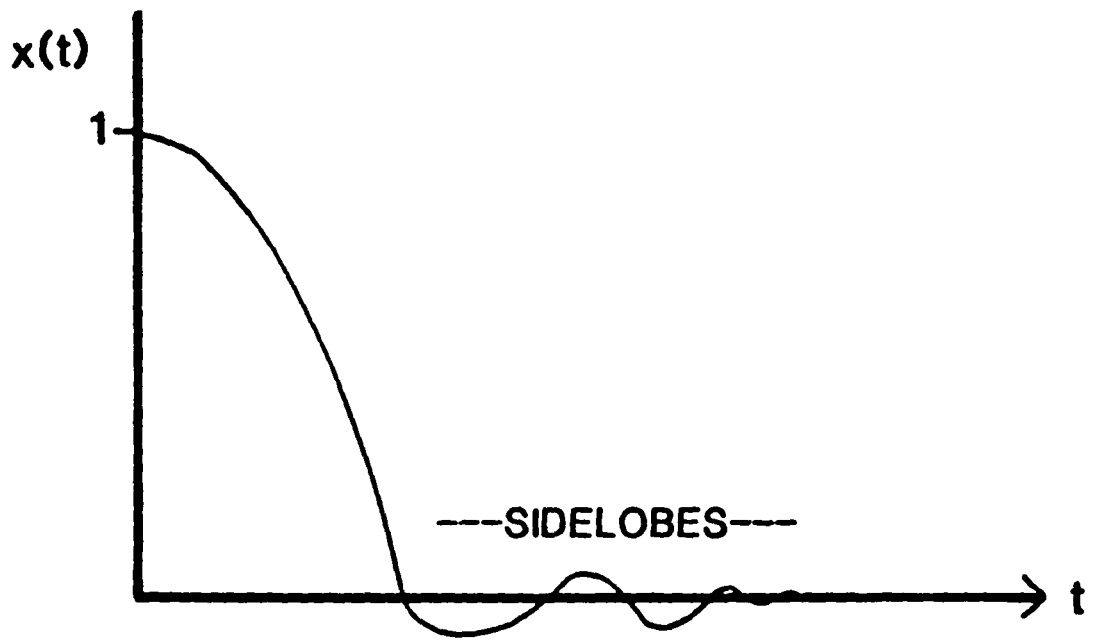

A. INVERSE FOURIER TRANSFORM

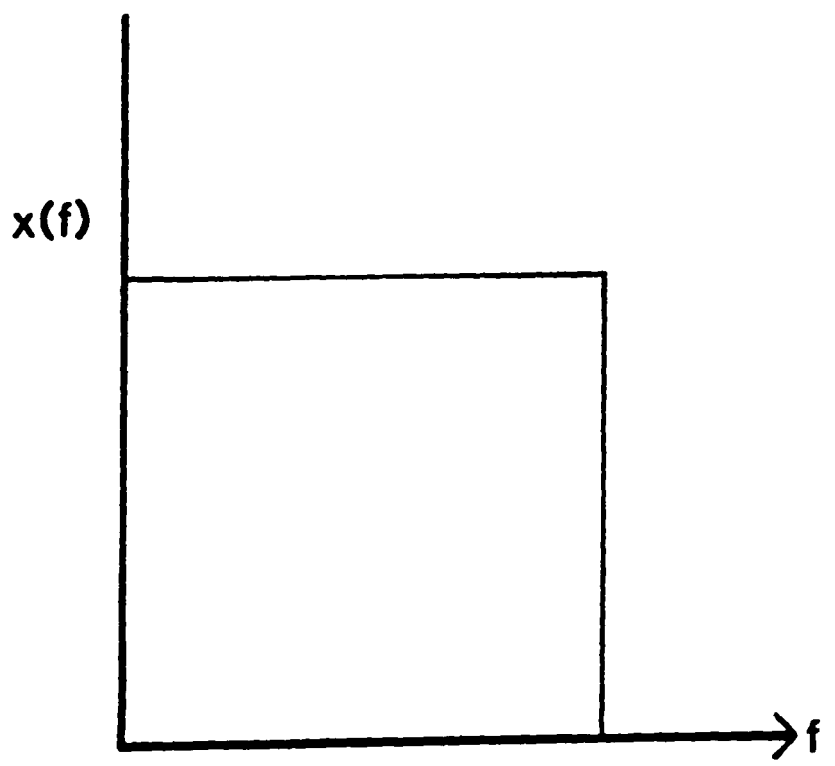

B. IDEAL FILTER

Figure 5. Time Response Required for Ideal Filter

As mentioned earlier, the simplest function is the moving average, which in the time domain is a rectangular truncation function. The function and its transform are shown in Figure 4 (only positive frequencies are shown). The sidelobes in the frequency domain are due to truncation in the time domain and are indicative of what happens when truncation occurs in either the time or frequency domain (see Figure 5). The moving average thus introduces undesirable frequency characteristics, and one is motivated to search for a more suitable function.

An obvious selection would seem to be the so called ideal filter for which frequency response is the rectangular truncation function as shown in Figure 5b. The impulse response of the ideal filter has sidelobes which extend to infinity and which are caused by the truncation (sharp cutoff) in the frequency function. To accurately represent such a function would require a series of infinite length. To obtain a practical convolution series one usually would truncate the infinite series after n terms as an approximation to the full series. However, truncation after the nth term will cause the well known Gibb's phenomenon, an overshoot and oscillatory frequency response (Figure 6 and Ref. 4).

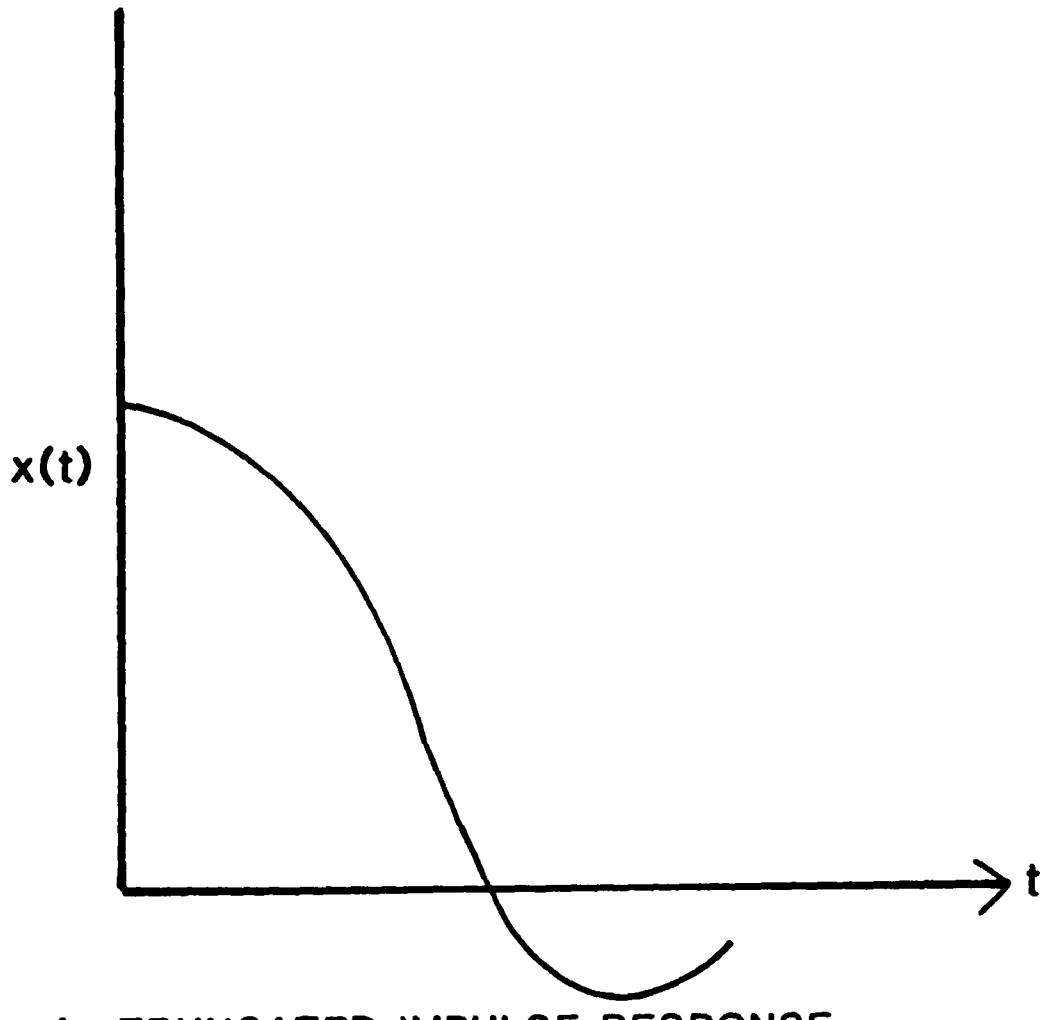

A. TRUNCATED IMPULSE RESPONSE

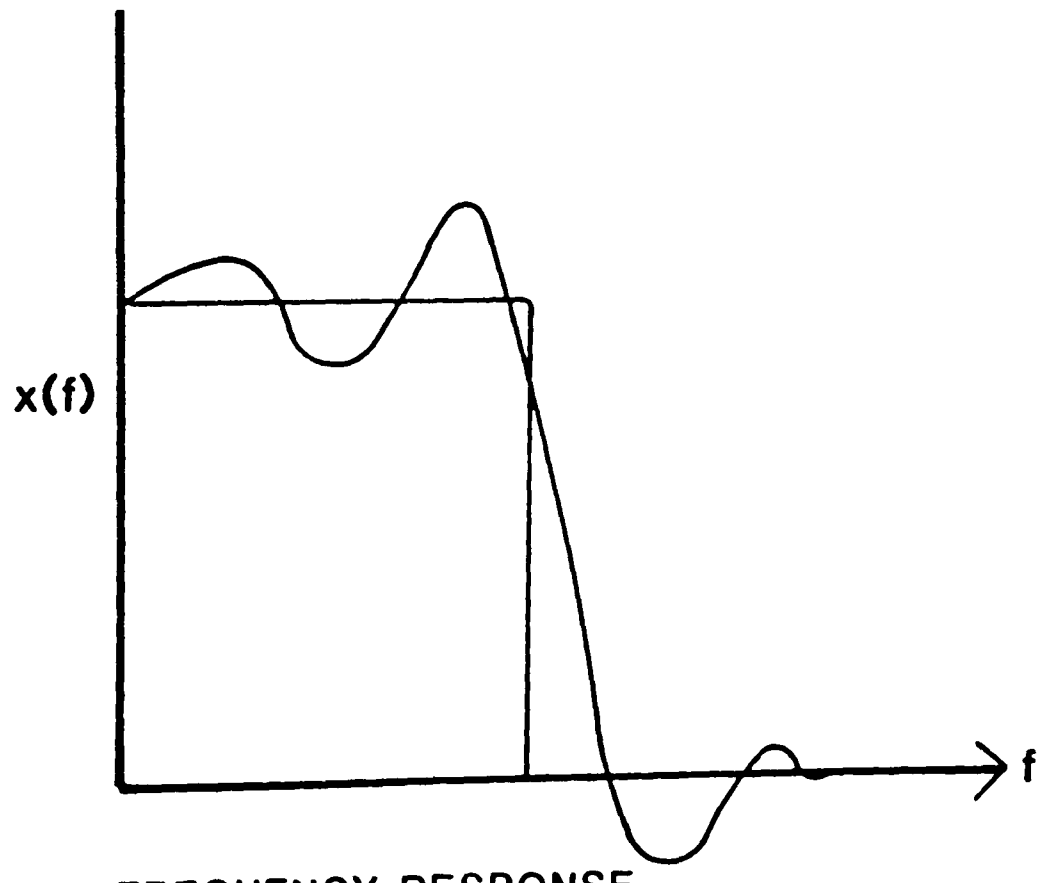

B. FREQUENCY RESPONSE

Figure 6. Gibb's Phenomenon

In summary, there are two problems associated with choosing a filter function which will yield the desired results and which is mathematically realizable. First, it is always necessary for any realizable function to be limited in time. That is, it must be of finite length (a truncated function); the values C_m must equal zero beyond a specified upper limit on m. As shown above, this will lead to oscillatory and undesirable frequency characteristics in the frequency domain. Second, it is necessary for the sidelobes of the impulse response to be as small as possible. This implies that the frequency response cannot have a sharp cutoff. Figure 5 shows that a sharp cutoff necessitates sidelobes of significant magnitude in the impulse response coefficients. These two problems would seem to preclude the use of the ideal filter function or simple running average in their usual form.

VI. Windowing

The solution to these problems is to window the filter function coefficients (Ref. 1). That is, weight the coefficients in some manner to reduce the end effects caused by truncation. Two approaches are recommended. The first (Ref. 4) is to window the truncated impulse response series shown in Figure 6. This series represents the approximate impulse response of the ideal bandpass filter. As shown in Figure 7, by using an appropriate window function (discussed below) it is possible to reduce frequency domain ripple (Gibb's phenomeon). Windowing also diminishes the strength of the sidelobes which results in a loss of sharpness of the frequency cutoff.

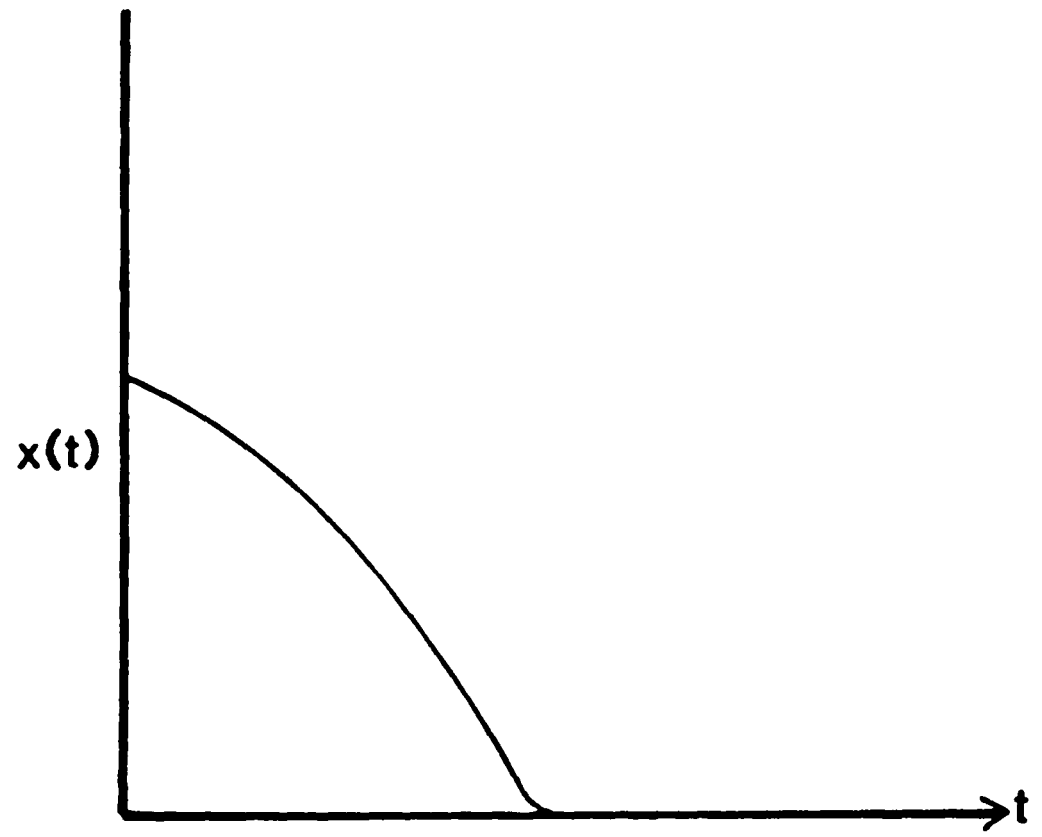

A. WINDOWED IMPULSE RESPONSE

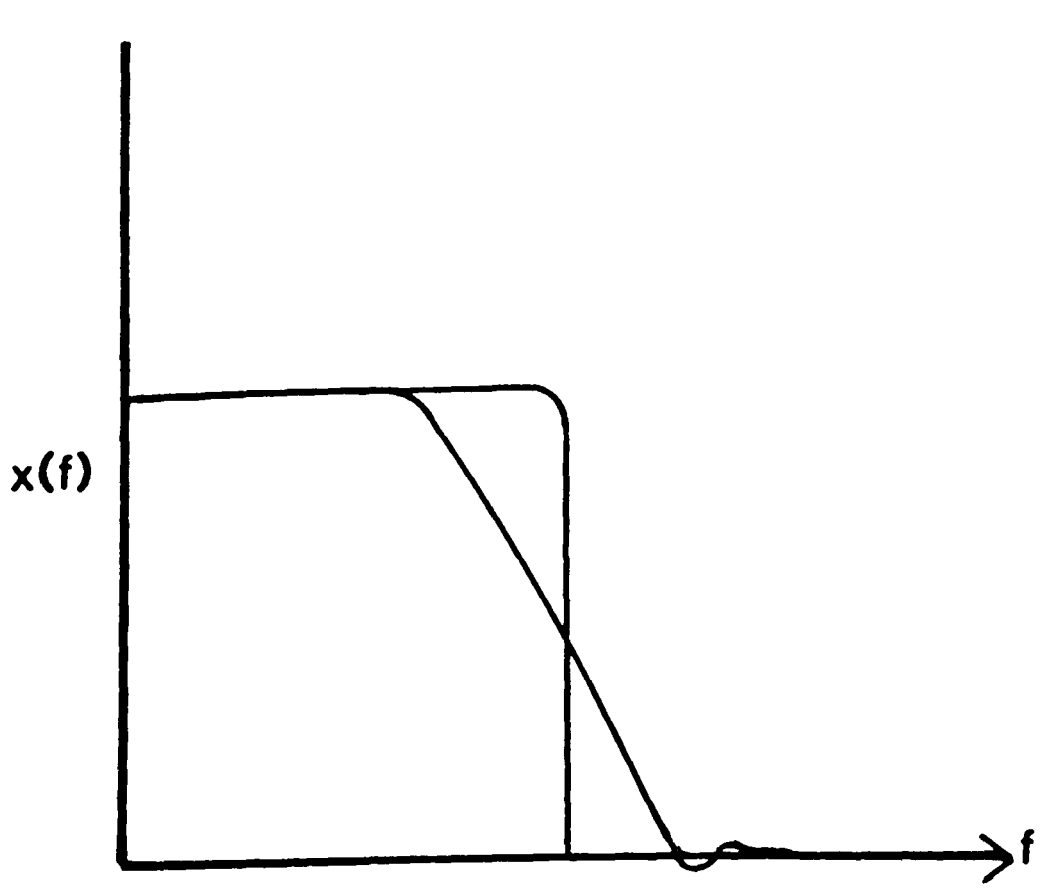

B. FREQUENCY RESPONSE

Figure 7. Effect of Windowing on Approximated Ideal Filter

A second and mathematically simpler method is to window the running average coefficients $C_m=1/N$. The same benefits accrue as in windowing the ideal filter, but a further loss in cutoff sharpness results. However, the ease of the method outweighs this problem, and for the purposes of discussion this method will be the one referred to for the remainder of this paper.

Many window functions exist (Ref. 1), but for discussion purposes only the two most often used for data smoothing will be examined here.

The first is the cosine bell or Hamming window. This function can be expressed in discrete form as

$$h(n) = \alpha + (1-\alpha)\cos 2\pi n/N \qquad (14)$$

where h(n) represents discrete values of the window function. The best α is 0.54 (Ref. 1).

Using this α and multiplying by the coefficients of the running average function, one obtains the coefficients of the windowed running average function as

$$C_m = (1/.54N)(.54 + .46\cos 2\pi m/N) \qquad (15)$$

The value 0.54 has been placed in the denominator for the purpose of scaling the frequency response to the value one at zero frequency.

Another often used window function is the least squares polynomial developed by Savitzky and Golay (Ref. 2). This method involves fitting an mth order polynomial through the data using the least squares criteria for each interval of 2n+1 points in the smoothing convolution. The new central value of the group is the value that lies on the

fitted curve at the corresponding data location.

Savitzky and Golay (Ref. 2) have tabulated the values of the convoluting variables, C_m, for a number of polynomials and their derivatives beginning with a quadratic-cubic polynomial. (The quadratic and cubic polynomials have identical convolution coefficients.) This polynomial is adequate for most work since "any smooth curve will look more or less like a quadratic in the vicinity of a peak or like a cubic in the vicinity of a shoulder" (Ref. 2). The smoothing coefficients for this function are

$$C_m = \frac{3\,(5m(N+1-m)-1/2(N+2)(N+3))}{(N-2)N(N+2)} \qquad (16)$$

where N is an odd number representing the length of the function and m varies from one to N. One advantage of the least squares polynomial method is the relative simplicity of the derivative functions. The smoothing coefficients for the first derivative quadratic function are

$$C_m = m - 1/2(N+1) \qquad (17)$$

The discrete Hamming and quadratic-cubic least square functions are displayed in Figure 8. The two values of N shown, 65 and 129, were chosen for mathematical ease in computing discrete Fourier transforms by computer. These two functions possess the desired impulse characteristics of a mathematically suitable smoothing function -- finite length and reduced sidelobes. The discrete Fourier transform of these functions are shown in Figure 9. As indicated in the figure, the frequency response of these functions are also finite functions with reduced sidelobes. Also indicated in Figure 9, for two functions of

the same length, the Hamming function has a lower cutoff but attenuates the higher frequencies more than the least squares function.

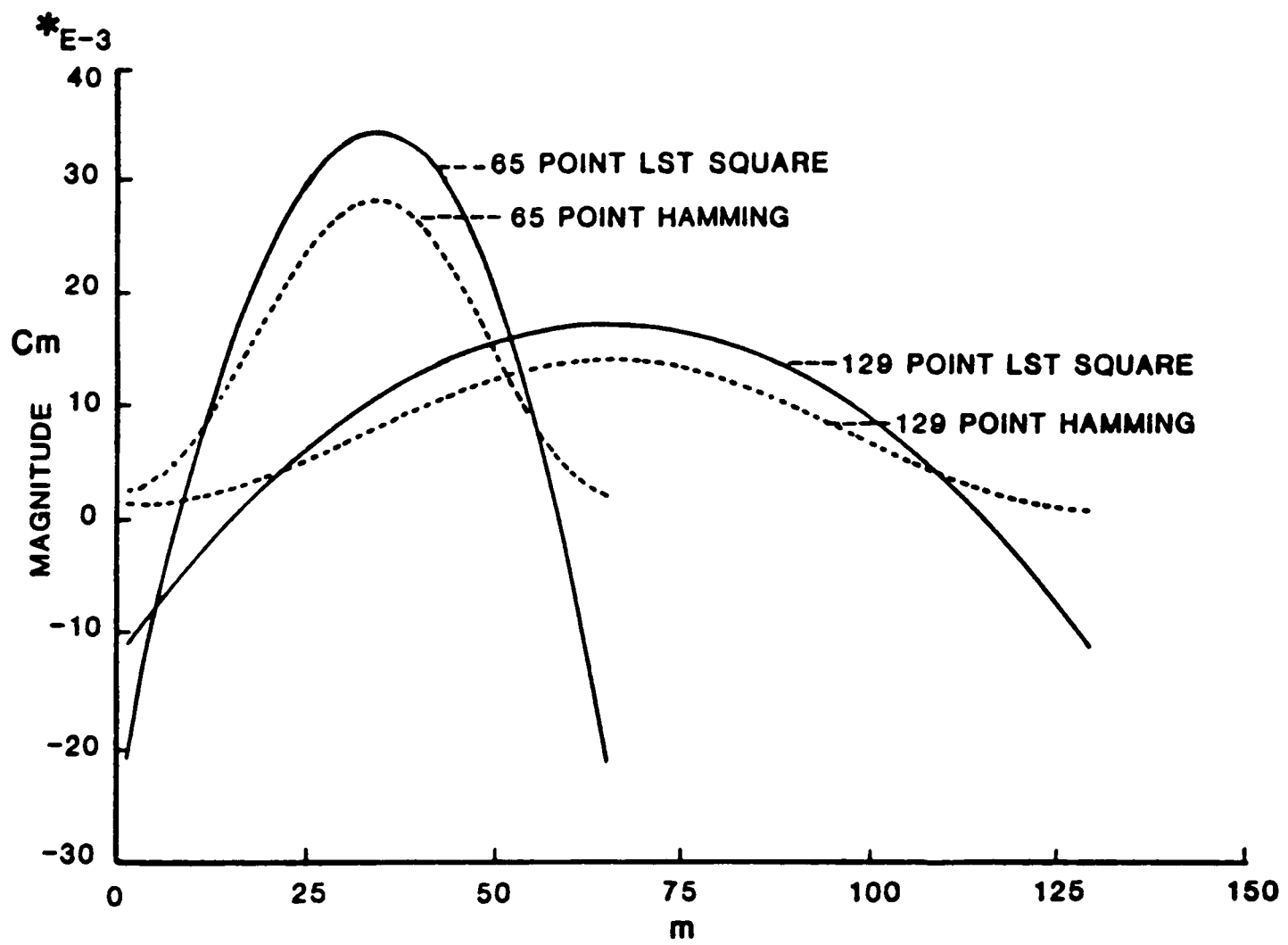

Figure 8. Comparison of Convolution Coefficients for Two Windowed Functions

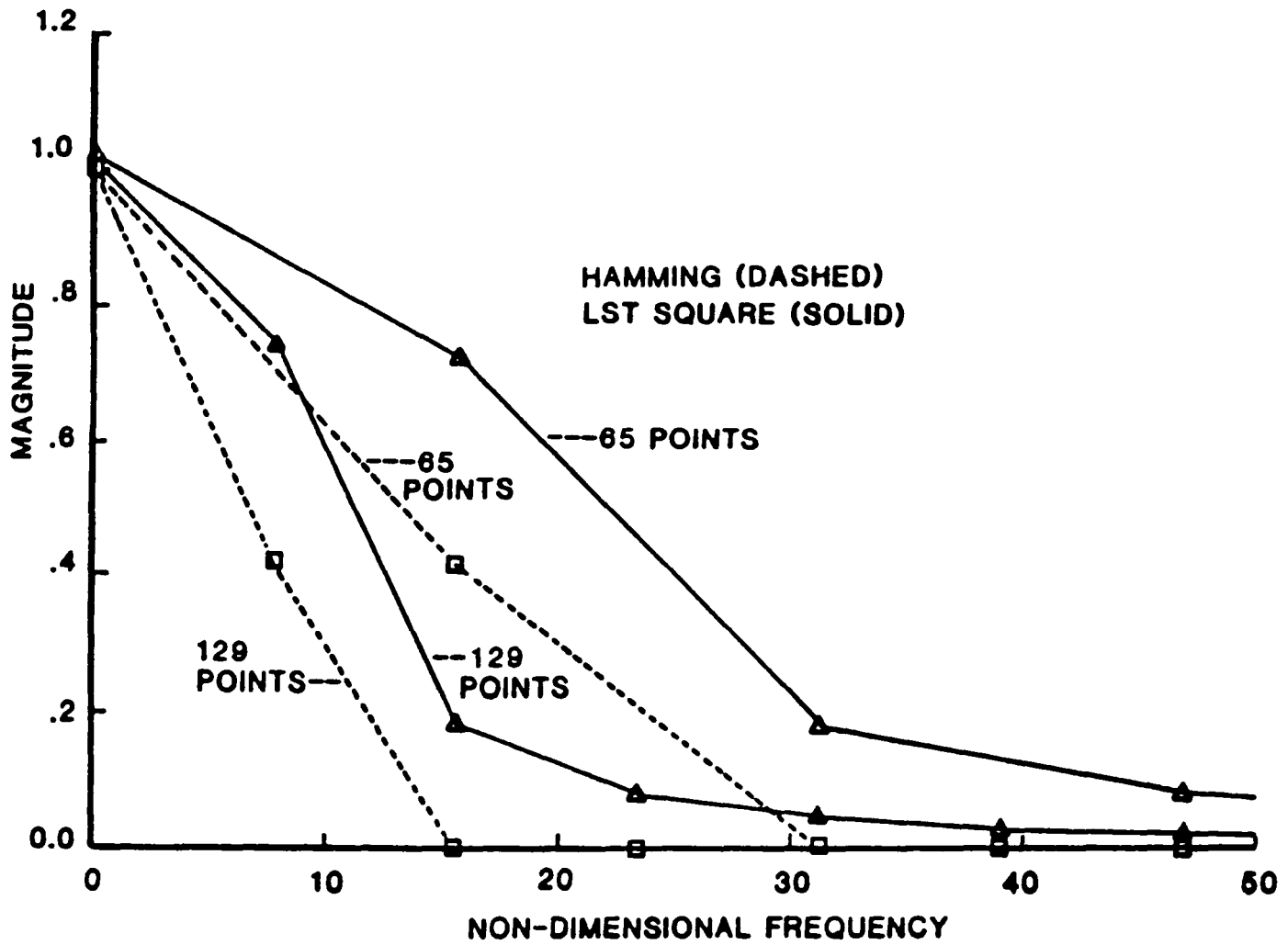

Figure 9. Frequency Response of Two Filter Functions

*E-3

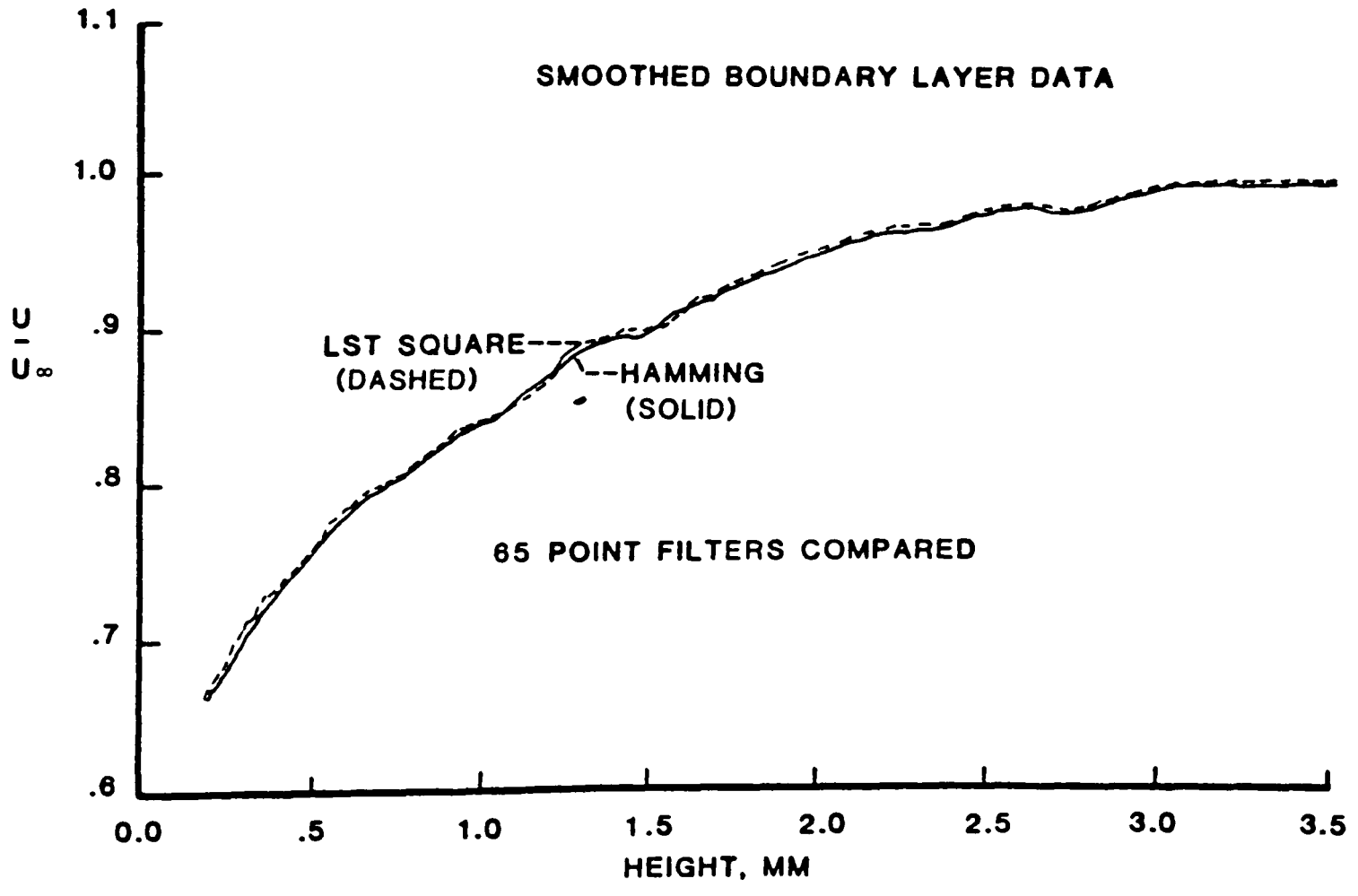

Figure 10. Smoothed Data from Figure 1

The results of using 65-point functions to smooth the data from Figure 1 are shown in Figure 10, in which the raw data has been omitted. One can see that the two functions produce a similar mean curve; however, the least square result contains more ripples while the Hamming window result is attenuated more in the region where the mean is changing rapidly. In Figure 9, one can observe that the 65-point Hamming result is similar to the 129-point least square result. This would seem to indicate that an N-point Hamming smoothing is similar to a 2N-point least square smoothing. If one were truncating unsmoothed end points, the Hamming function would allow for a larger number of retained end points. This is demonstrated in Figure 11, in which smoothing has been carried out on the data of Figure 1. Using the 65-point and 129-point functions for each smoothing operation, N-1 points have been truncated, half at each end. (The data was not smoothed to the full right hand end in order to conserve computer time.) The results of the 65-point Hamming smoothing are qualitatively similar to the 129-point least square smoothing.

Figure 11. Comparison of Data Smoothed by Different Functions

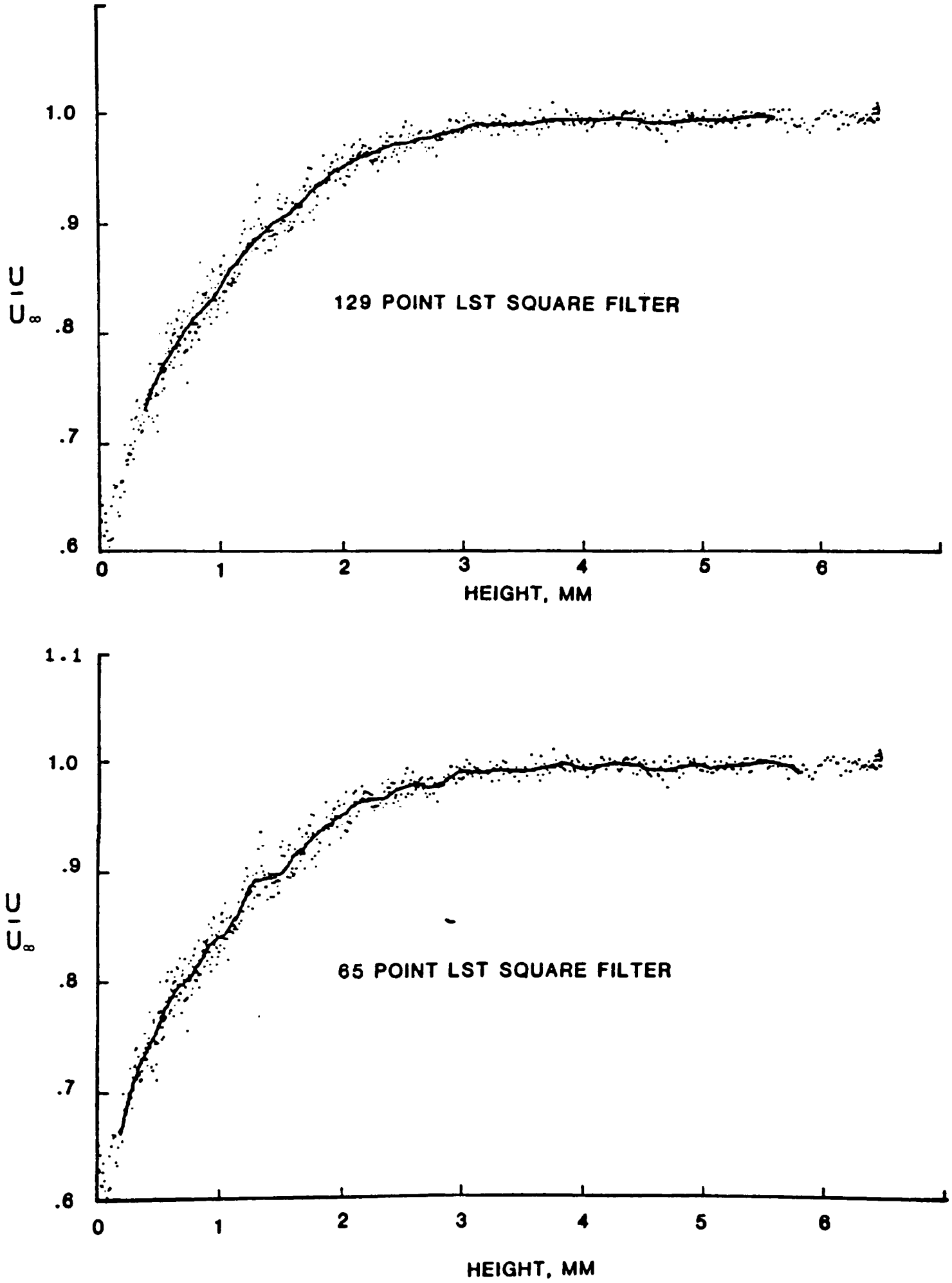

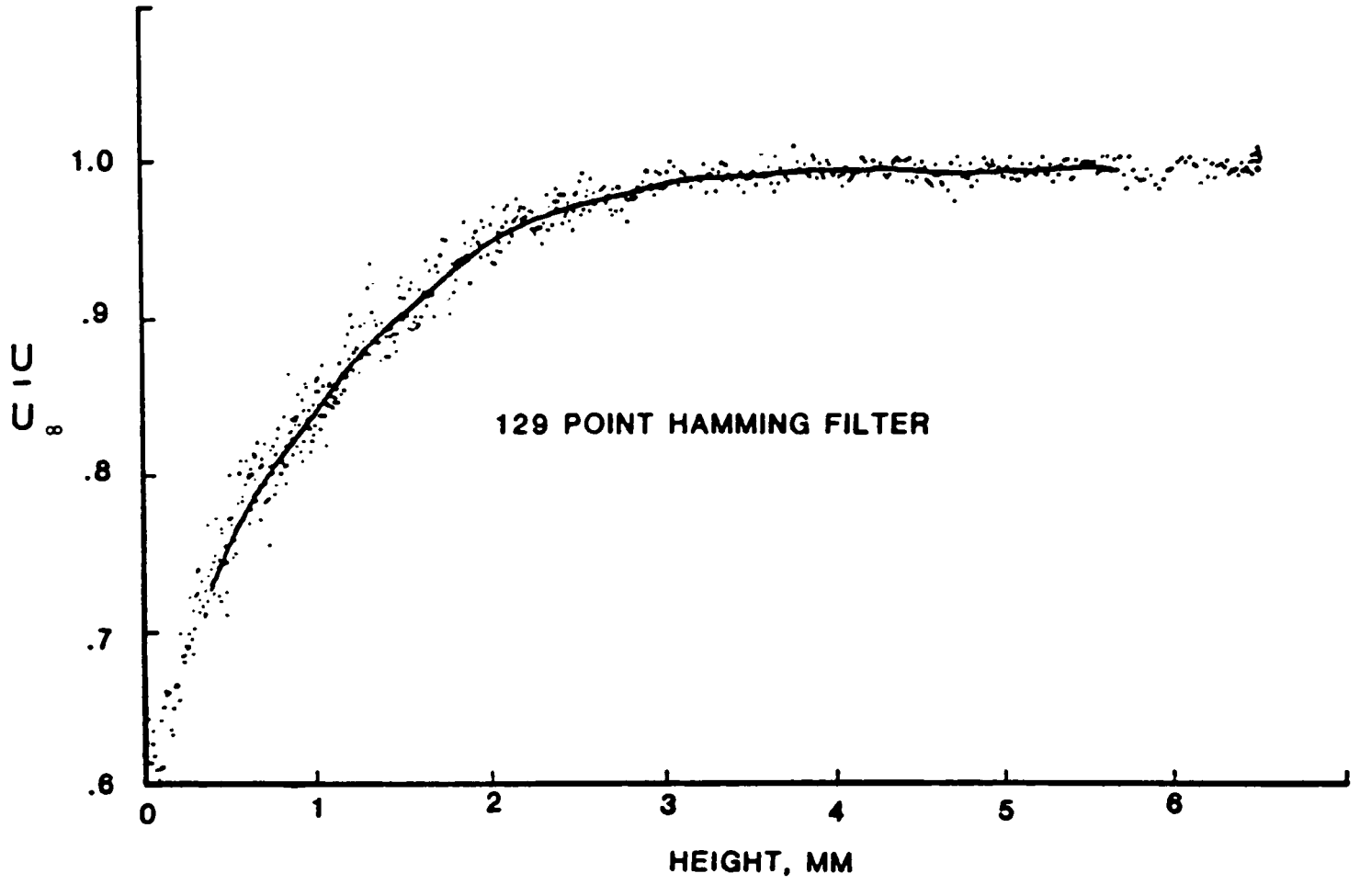
1.0
.9
.8
.7
.6
$\frac{U}{U_\infty}$
129 POINT HAMMING FILTER
0
1
2
3
4
5
6
HEIGHT, MM

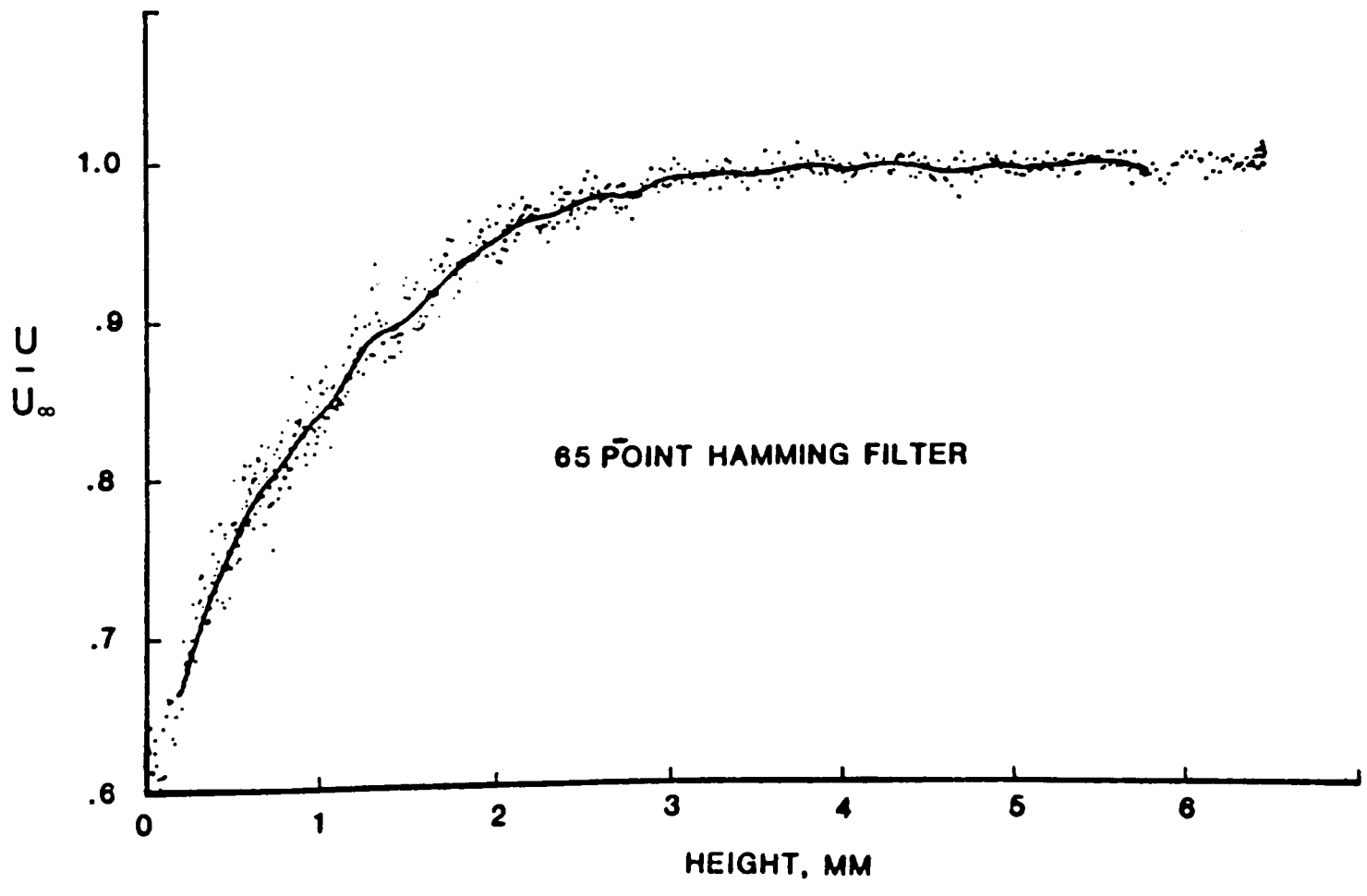
1.0
.9
.8
.7
.6
$\frac{U}{U_\infty}$
65 POINT HAMMING FILTER
0
1
2
3
4
5
6
HEIGHT, MM

VII. Length of Smoothing Function

Once one has decided to use a smoothing function, the length (number of points) must be determined. This will be governed by the type of data one is examining and the amount of data that one can afford to lose at the end points. Addressing the latter point first, it is recognized that for a 2n+1 convolution function the central point (n+1 th point) is replaced by the convolution summation, and at either end of the data set, n points cannot be smoothed. For example, in using a nine point function, eight points are unsmoothed for each pass of the smoothing function, four at each end. Many theories exist on how to treat these end points. One is to use a shorter function on the end points than that used on the central portion of the data. A second solution is simply to truncate the end points after each smoothing convolution. There is no general answer to this question; it must be decided based upon the smoothing effects desired.

The length of the smoothing function will depend on whether one wants to examine the mean of the data, the peak waveforms, or a combination of the two. A filter function used to identify the mean would reduce the standard deviation of the data about the mean. According to a study by Enke and Nieman (Ref. 5) this filter function should be as long as possible but small enough so that not more than one inflection in the observed data is included in any convolution interval of 2n+1 points.

In order to study peaks in the data, the smoothing function should cause as little distortion in waveform shape as possible and at the same time increase the ratio of peak values to signal noise. Enke and Nieman suggest that this type of data is best filtered by a function in which width at half-peak height equals that of the peaks in the data

and in which the function length, 2n+1, is twice that of the afforementioned width. This is closely approximated by a quadratic-cubic function. This criteria will lead to shorter functions than those used to simply identify mean values and will produce a compromise between noise reduction and signal distortion. To choose a function with which to smooth data in which both mean values and peaks are of interest will require a judgement based on the relative importance of the signal mix.

VIII. Conclusions

In summary, the Hamming function would seem to provide for the least end point truncation and be best suited for smoothing data in which the mean is of highest interest. The least squares function on the other hand appears to have a sharper frequency rolloff and thus is well suited to data in which peak values and waveform shape are of interest. The choice made to smooth the boundary layer data shown in Figure 1 was governed by a consideration of the loss of end points in the data. Thus the Hamming function was chosen to provide the best smoothed results for this data.

Regardless of the choice of smoothing functions, it is important that the effects of the smoothing procedure be understood. When one views the procedure as one of filtering the data with a low pass filter, it is evident that not only can data be obscured or even lost but spurious data can be introduced (the Gibb's phenomenon). The use of a windowed function offers the best solution to the smoothing problem. This paper has compared two popular functions: the Hamming (or windowed retangular function) and the moving least square polynomial.

References

1. Rabiner, L.R. and B. Gold, Theory and Application of Digital Processing, Prentice-Hall Inc., 1975.

2. Savitzky, A. and M.J.E. Golay, "Smoothing and Differentation of Data by Simplified Least Squares Procedures," Analytic Chemistry, 36, No. 8, July 1964, pp. 1627-1639.

3. Brigham, E.O., The Fast Fourier Transform, Prentice-Hall Inc., 1974.

4. Sterns, S.D., Digital Signal Analysis, Hayden Book Company Inc., 1975.

5. Enke, C.G., and T.A. Nieman, "Signal-to-Noise Ratio Enhancement by Least Squares Polynomial Smoothing," Analytic Chemistry, 48, No. 8, July 1976, pp. 705A-712A.

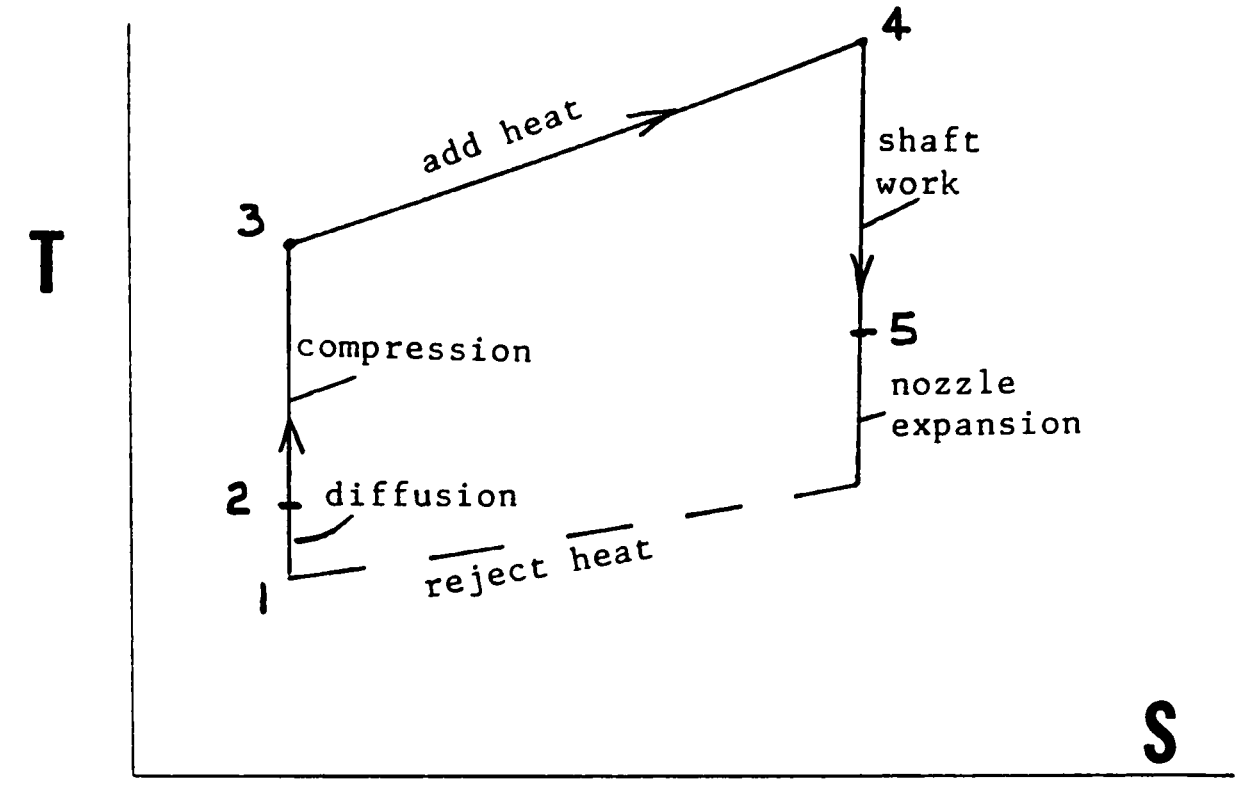

FIG. 1.1 Ideal Brayton Cycle

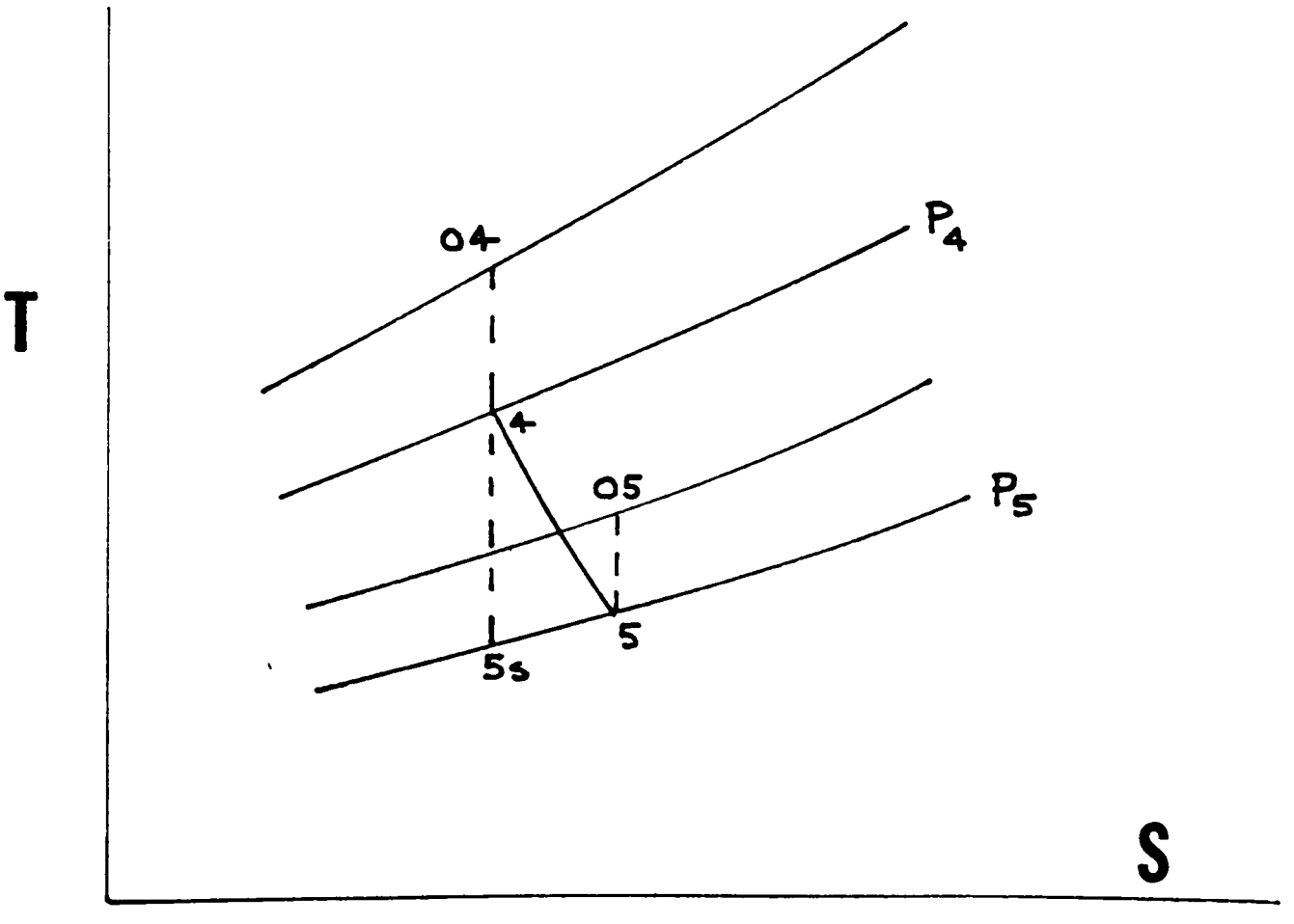

FIG. 1.2 Actual Turbine Process

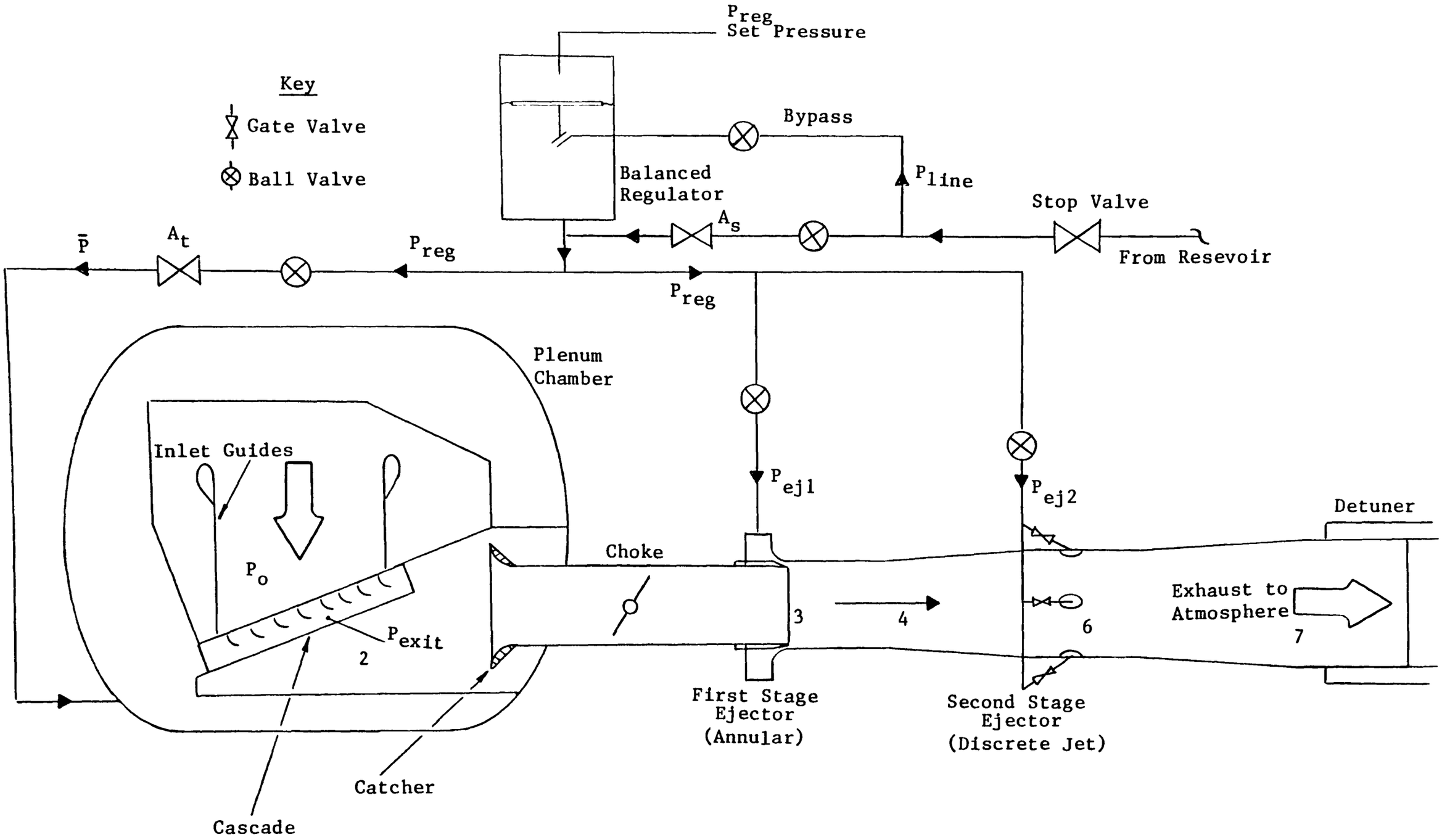

FIG.2.1 SCHEMATIC DIAGRAM OF O.U.E.L. BLOWDOWN TUNNEL

THIRD ANGLE PROJECTION

O.U.E.L. BLOWDOWN TUNNEL.

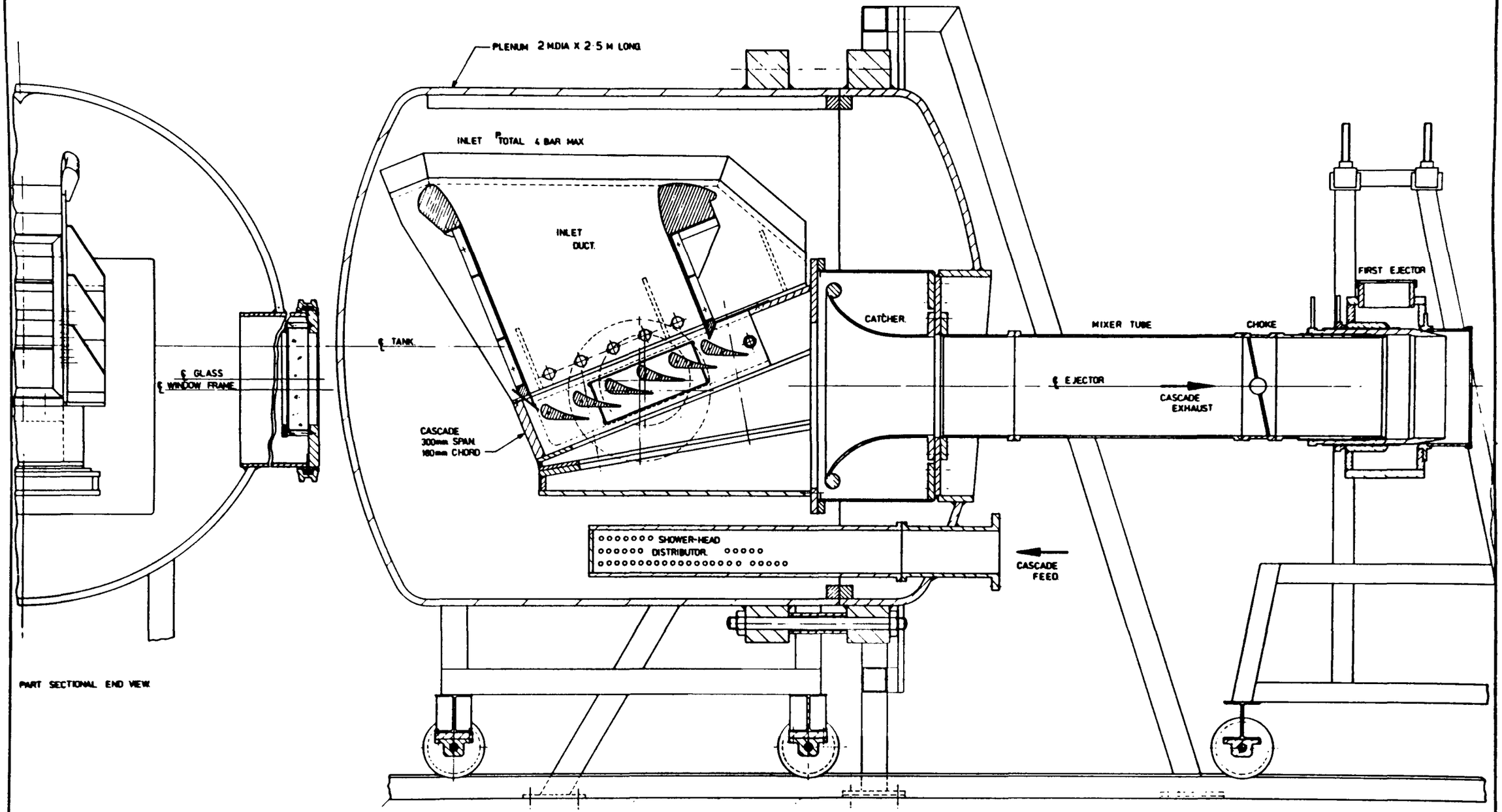

FIG.2.2 BLOWDOWN TUNNEL WORKING SECTION

G A OF BLOWDOWN TUNNEL

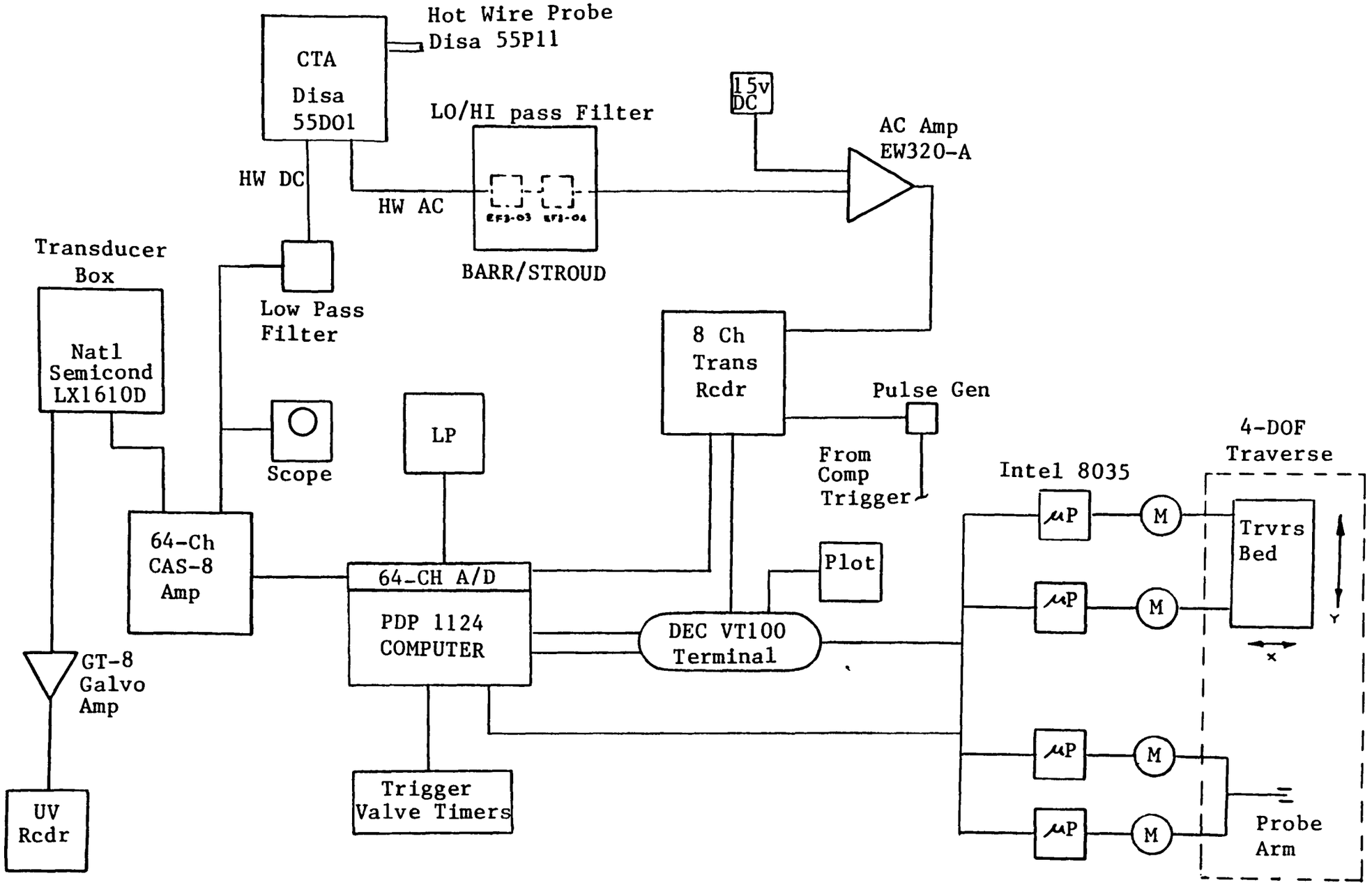

FIG.2.3 DATA ACQUISITION HARDWARE

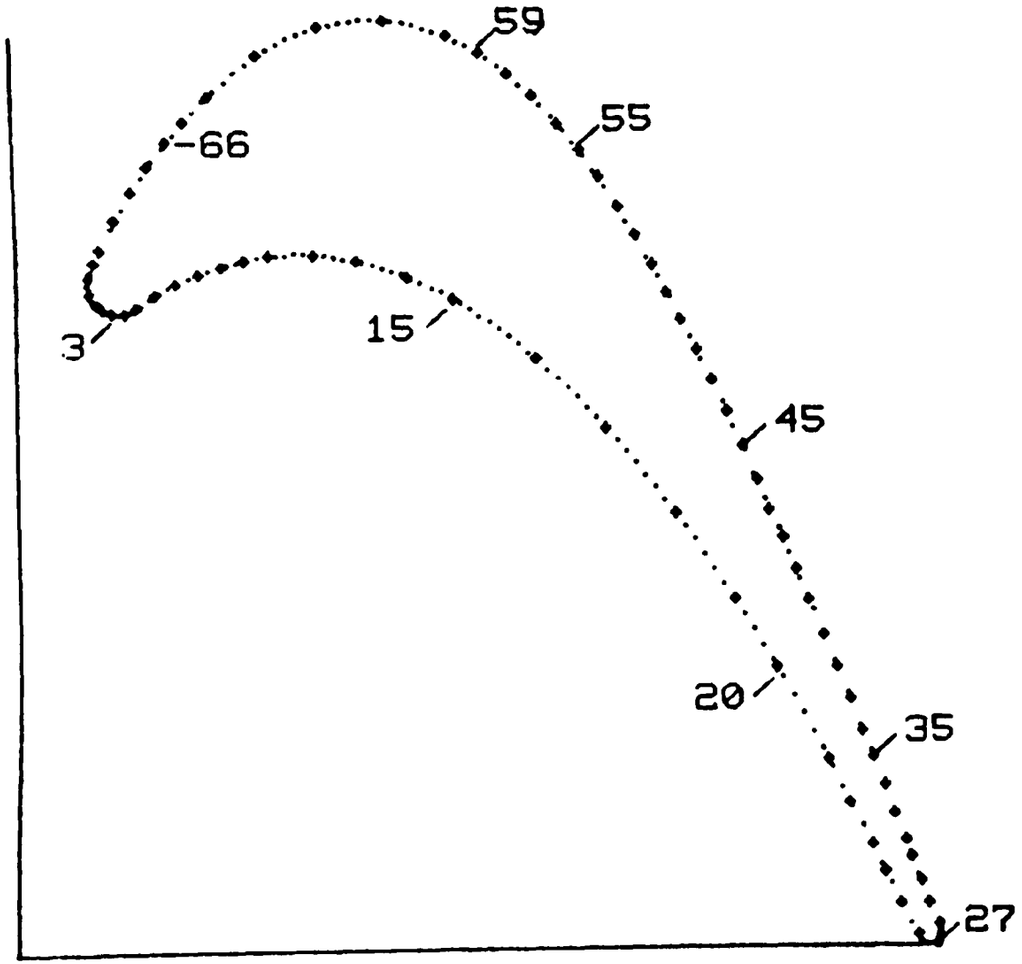

FIG.2.4 B22 PROFILE AND TAP LOCATIONS

TABLE 2.1 300MM CHORD B22 PROFILE PRESSURE TAP LOCATIONS

POINT	X/CAX	X/S	POINT	X/CAX	X/S	POINT	X/CAX	X/S
1	0.0	0.0	26	.987	.977	50	.674	.545
2	.01	.007	27	1.0	1.0	51	.658	.525
3	.022	.016	28	.99	.988	52	.639	.504
4	.036	.026	29	.98	.972	53	.617	.482
5	.05	.036	30	.969	.956	54	.593	.46
6	.078	.056	31	.959	.942	55	.572	.439
7	.106	.076	32	.95	.928	56	.549	.417
8	.134	.096	33	.937	.908	57	.515	.394
9	.162	.116	34	.924	.889	58	.484	.372
10	.189	.135	35	.913	.871	59	.452	.35
11	.216	.155	36	.90	.852	60	.419	.327
12	.266	.192	37	.885	.83	61	.348	.285
13	.324	.23	38	.87	.808	62	.269	.243
14	.379	.273	39	.856	.786	63	.197	.200
15	.436	.314	40	.84	.763	64	.14	.158
16	.536	.401	41	.825	.742	65	.115	.138
17	.618	.482	42	.81	.721	66	.09	.118
18	.698	.571	43	.795	.699	67	.07	.099
19	.768	.658	44	.78	.678	68	.051	.080
20	.819	.727	45	.763	.655	69	.028	.060
21	.879	.815	46	.745	.632	70	.007	.040
22	.905	.855	47	.728	.609	71	.003	.029
23	.929	.893	48	.71	.586	72	0.0	.019
24	.946	.919	49	.693	.566	73	0.0	.009
25	.965	.947						

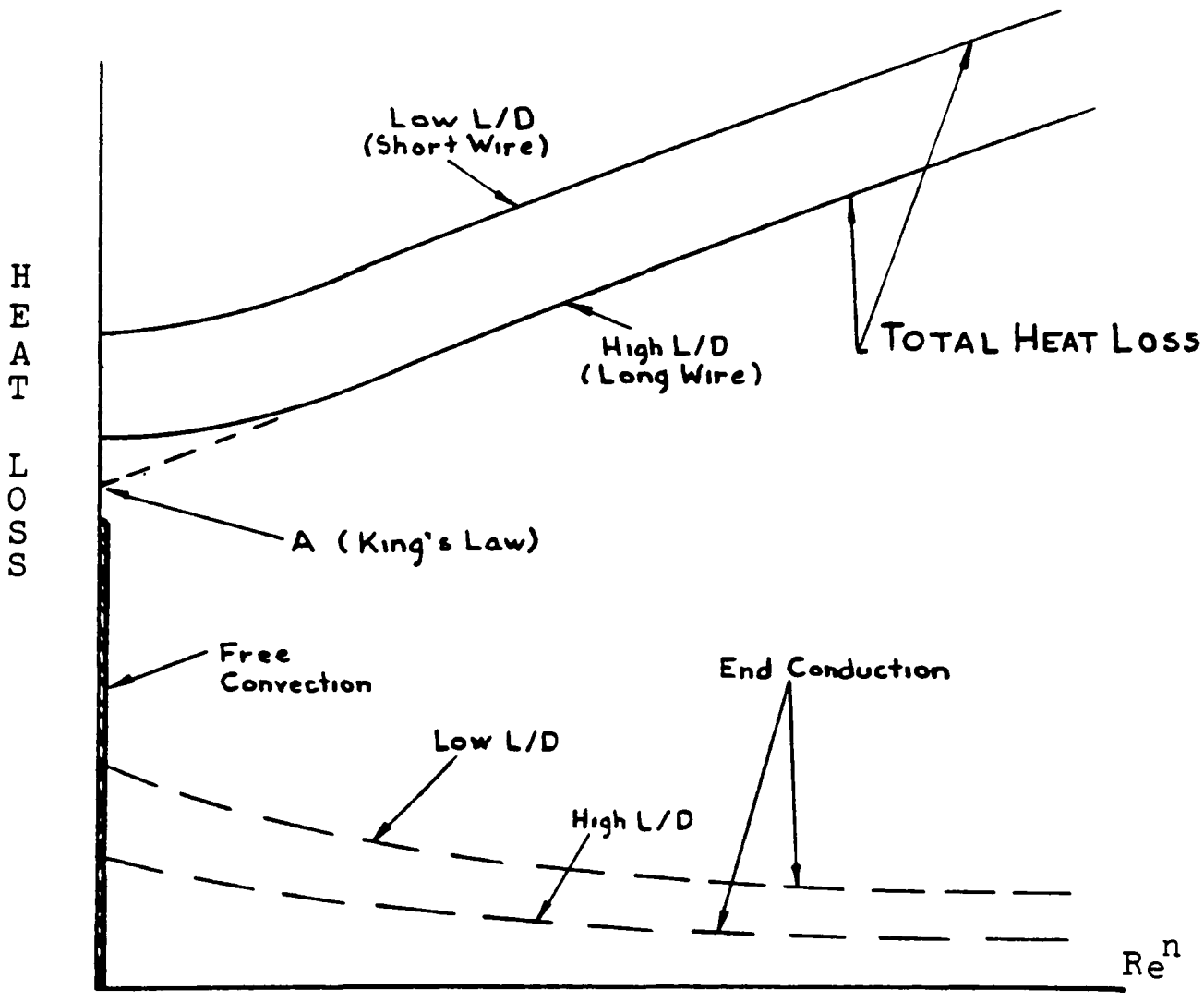

FIG. 4.1 Heat Transfer Model for a Hot Wire

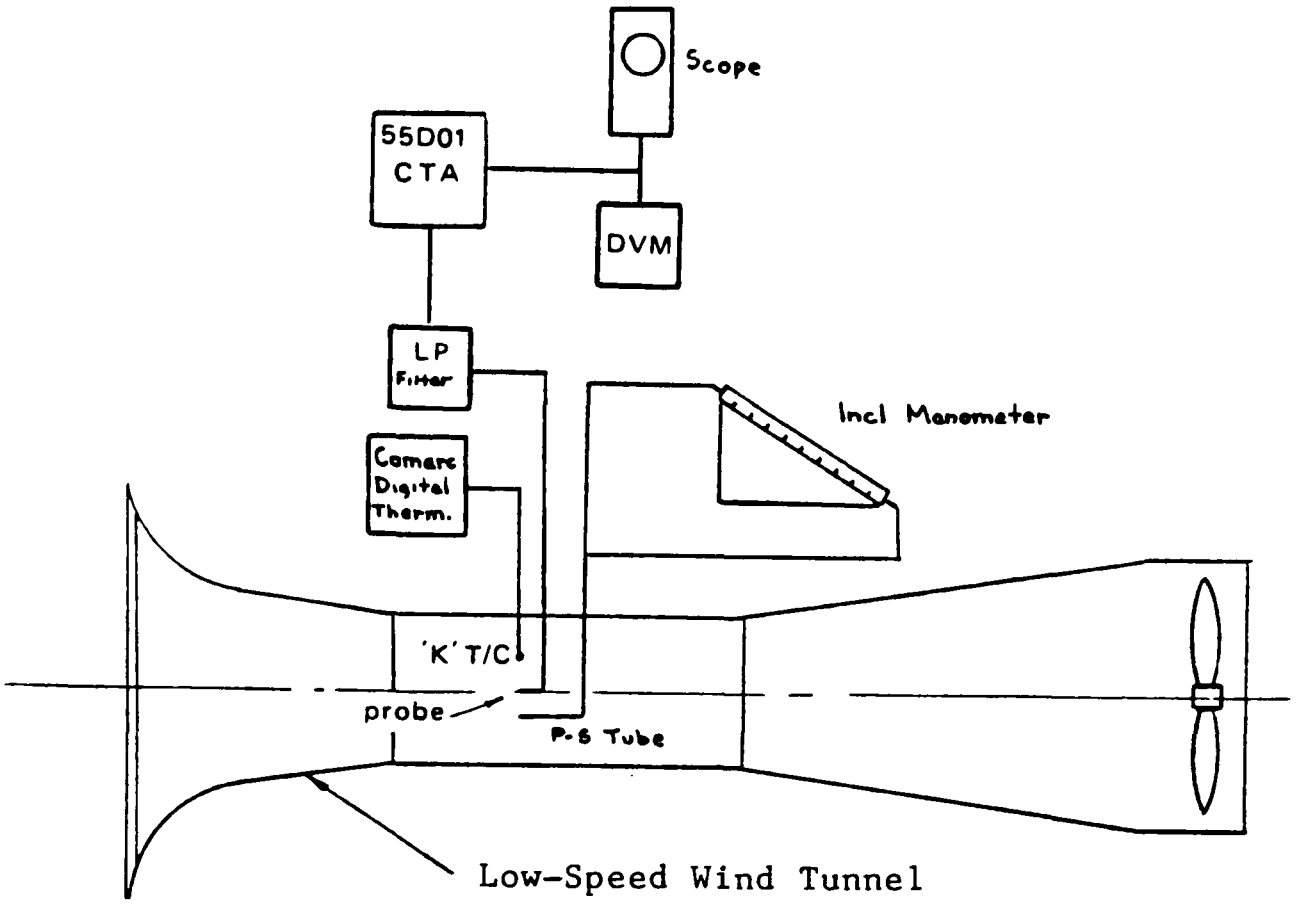

FIG. 4.2 Experimental Arrangement for Calibrating Hot Wires

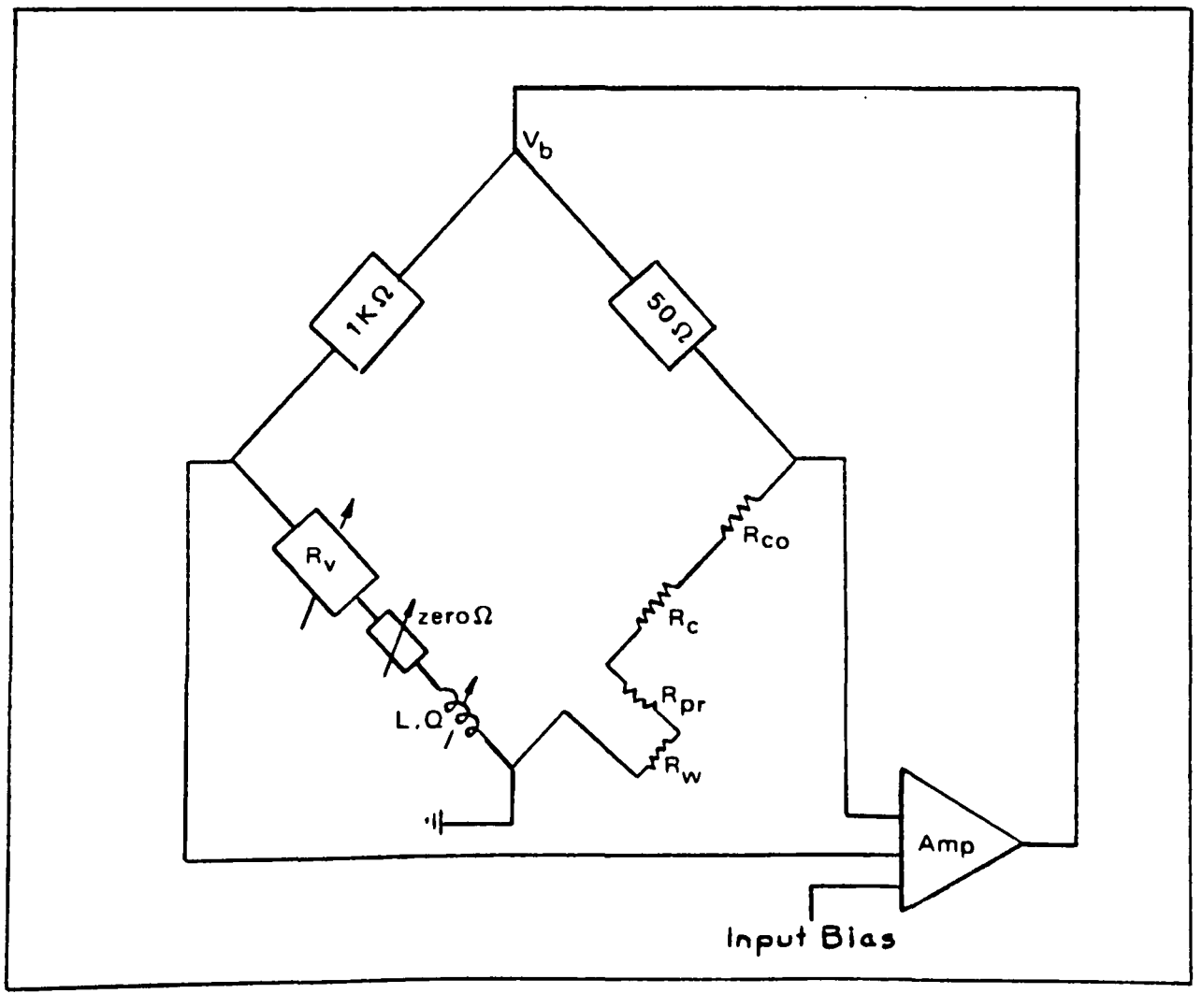

FIG. 4.3 Constant Temperature Anemometer Bridge Schematic

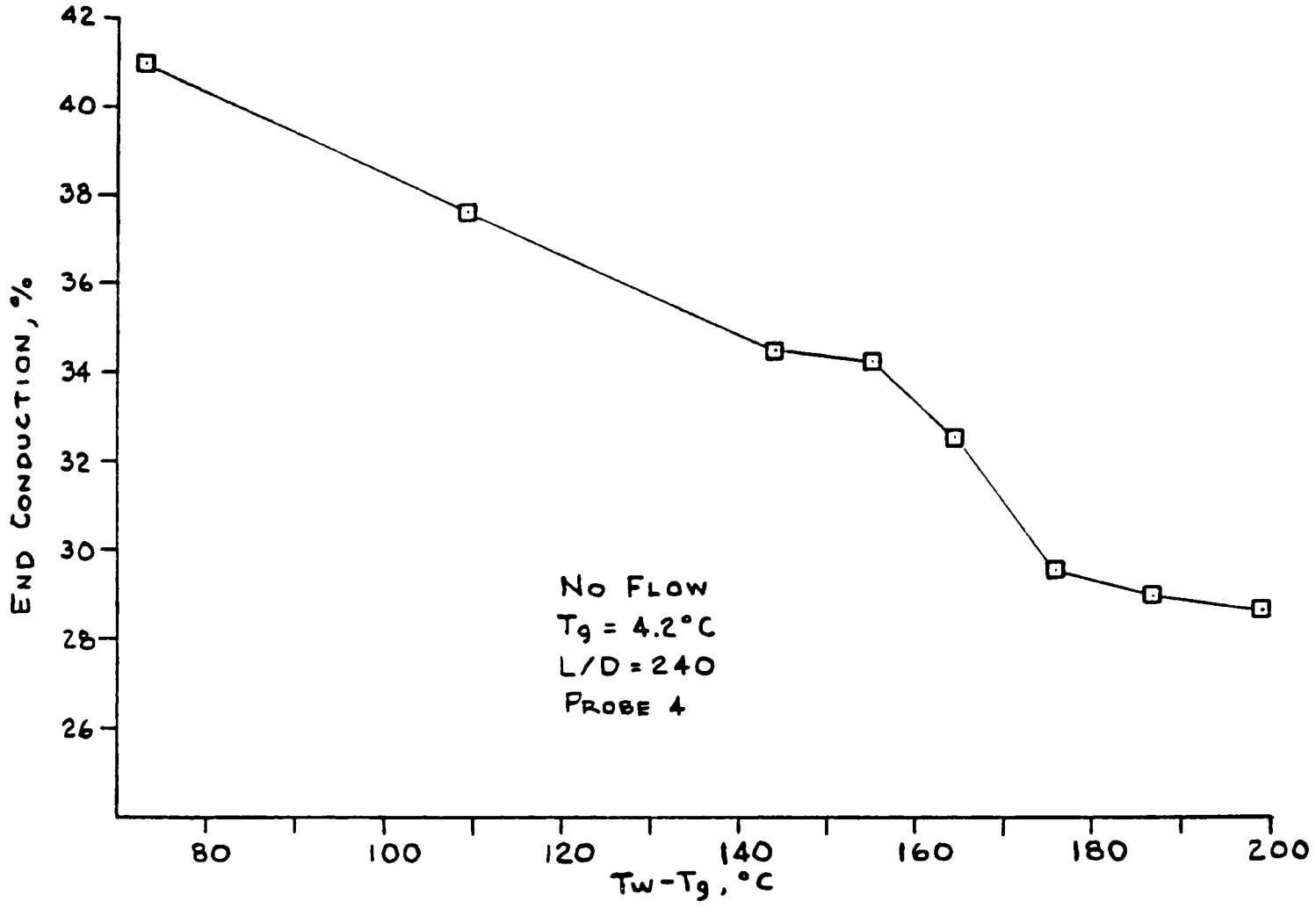

FIG. 4.4 Zero-Flow End Conduction Heat Loss

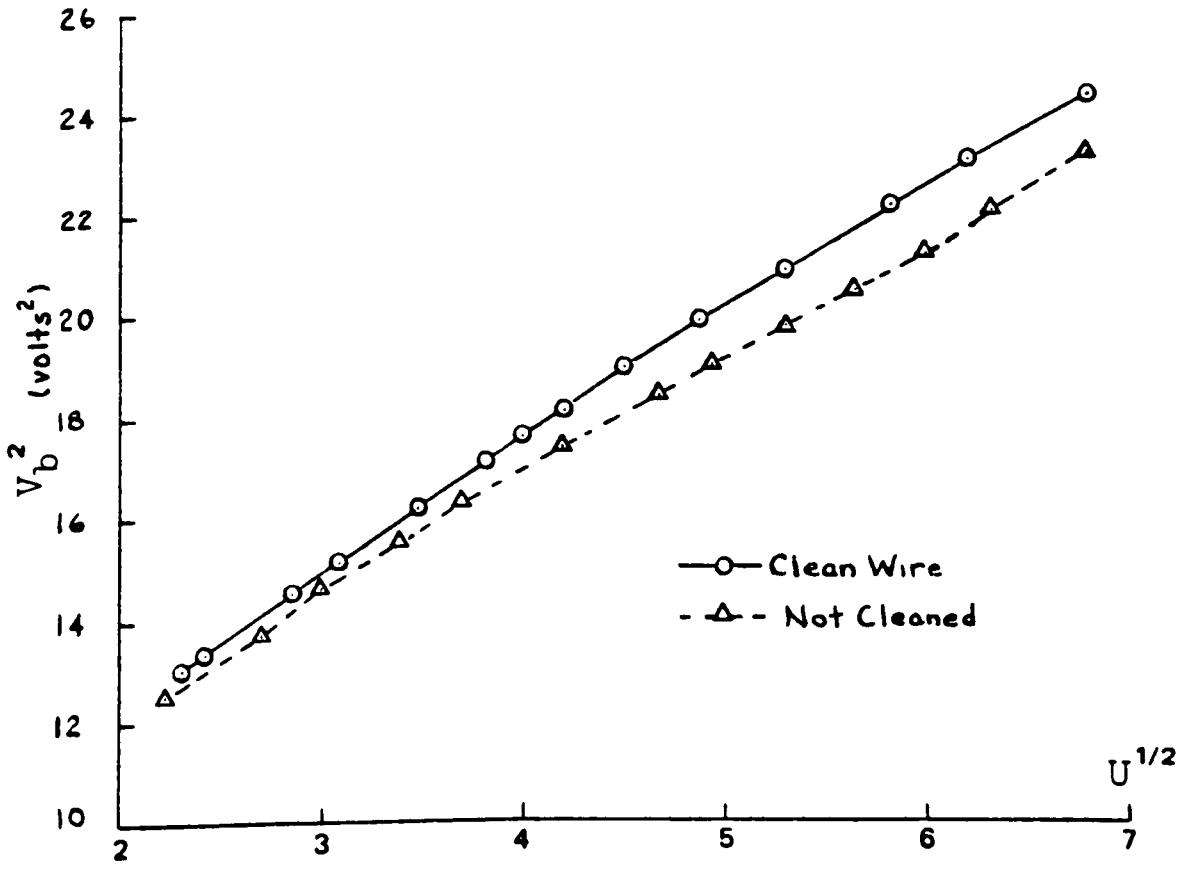

FIG. 4.5 Effect of Wire Contamination

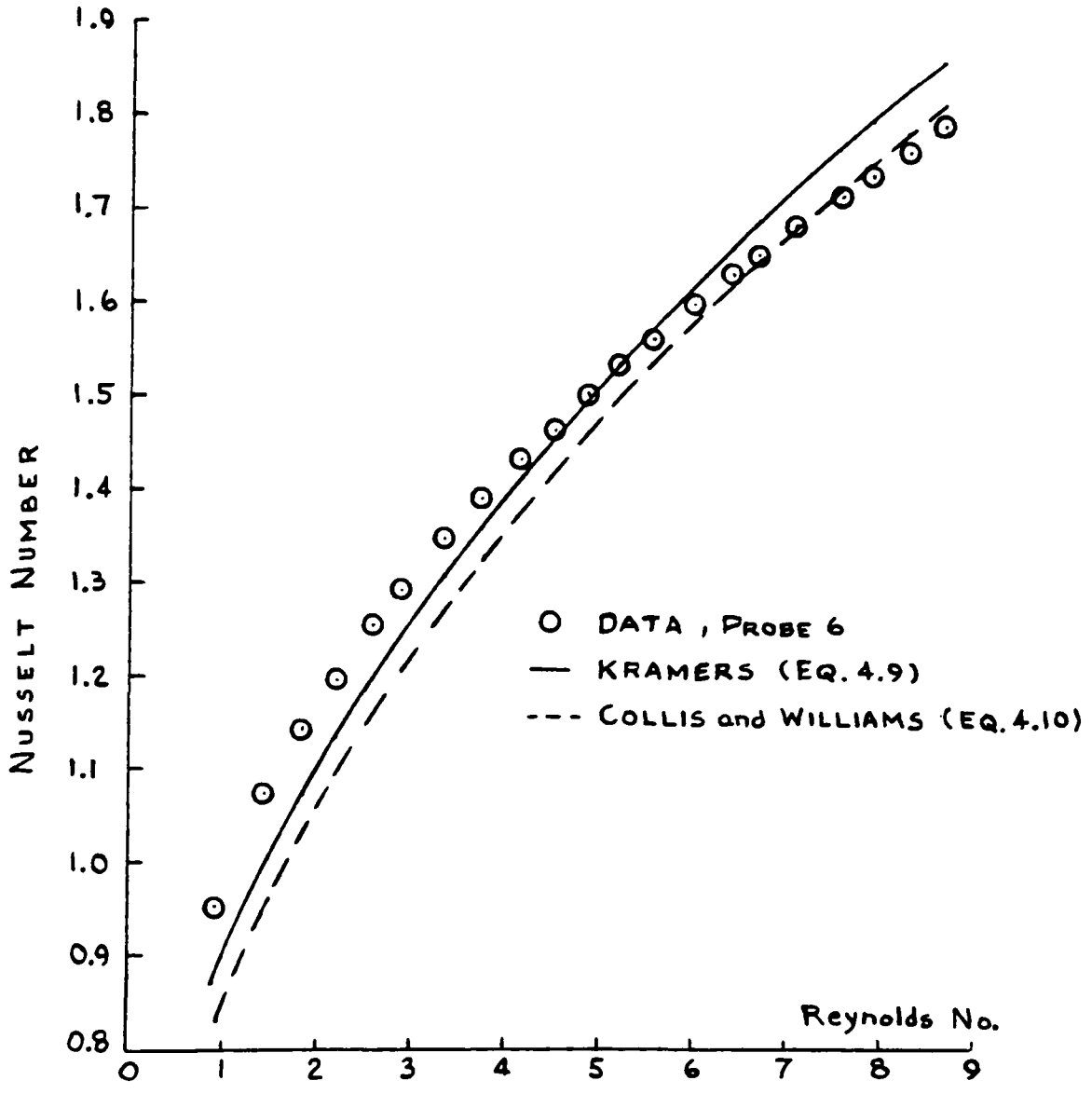

FIG. 4.6 Typical Hot-Wire Data for 55P11 Probe Compared with Correlations for Long Cylinders

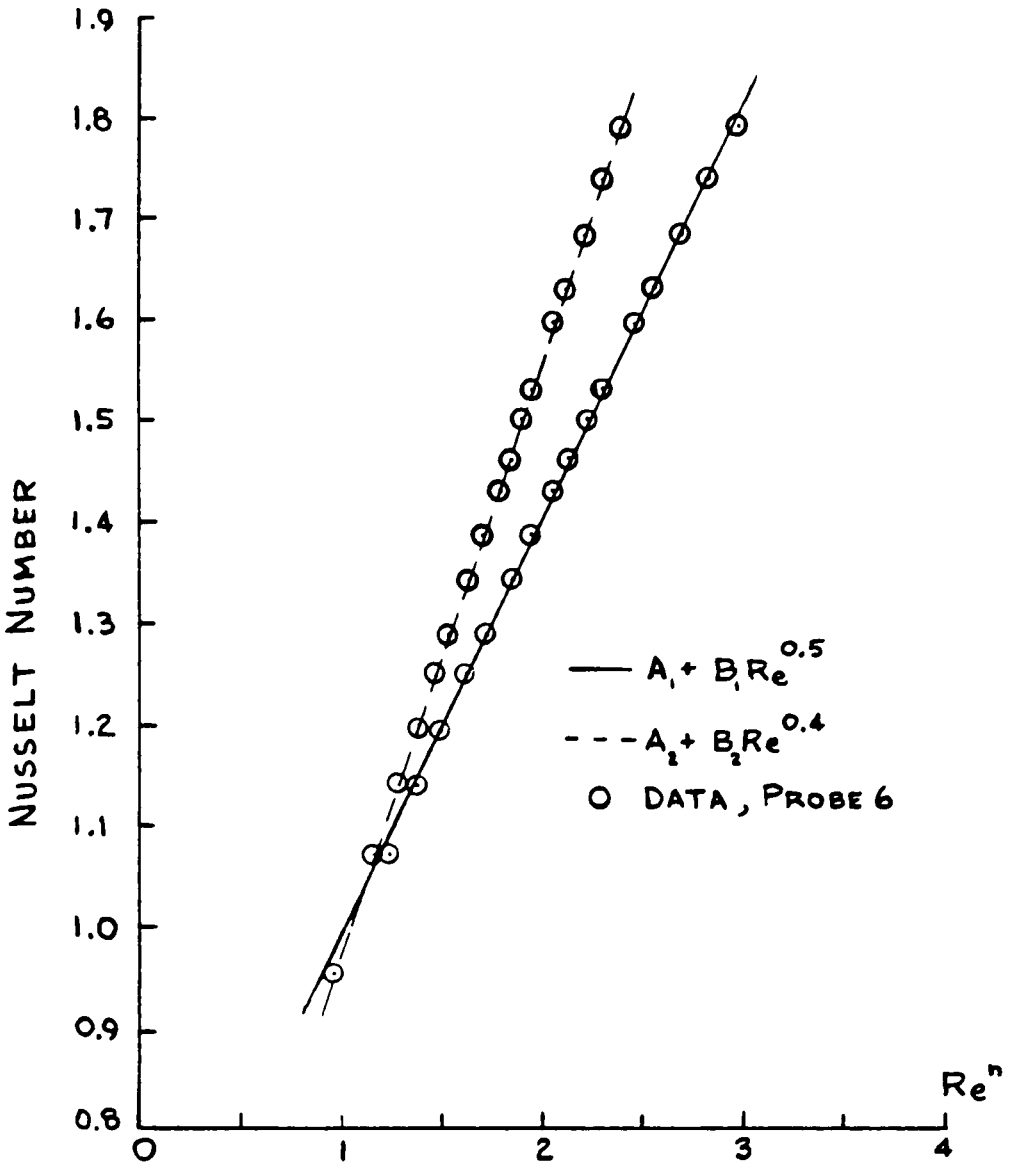

FIG. 4.7 Data of Fig.4.6 Fitted to Two Response Laws

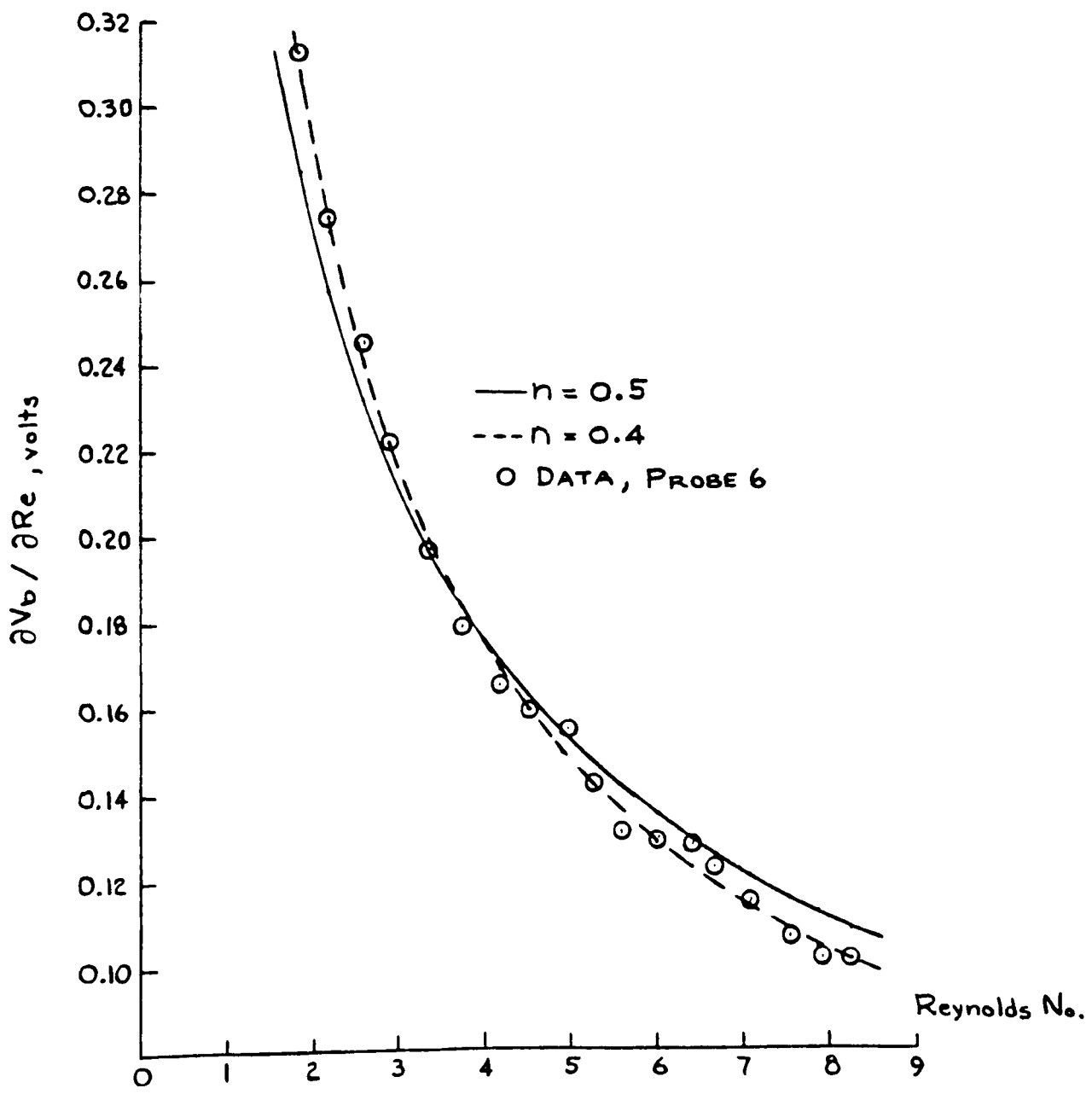

FIG. 4.8 Hot-Wire Sensitivity Data Compared with Two Response Laws

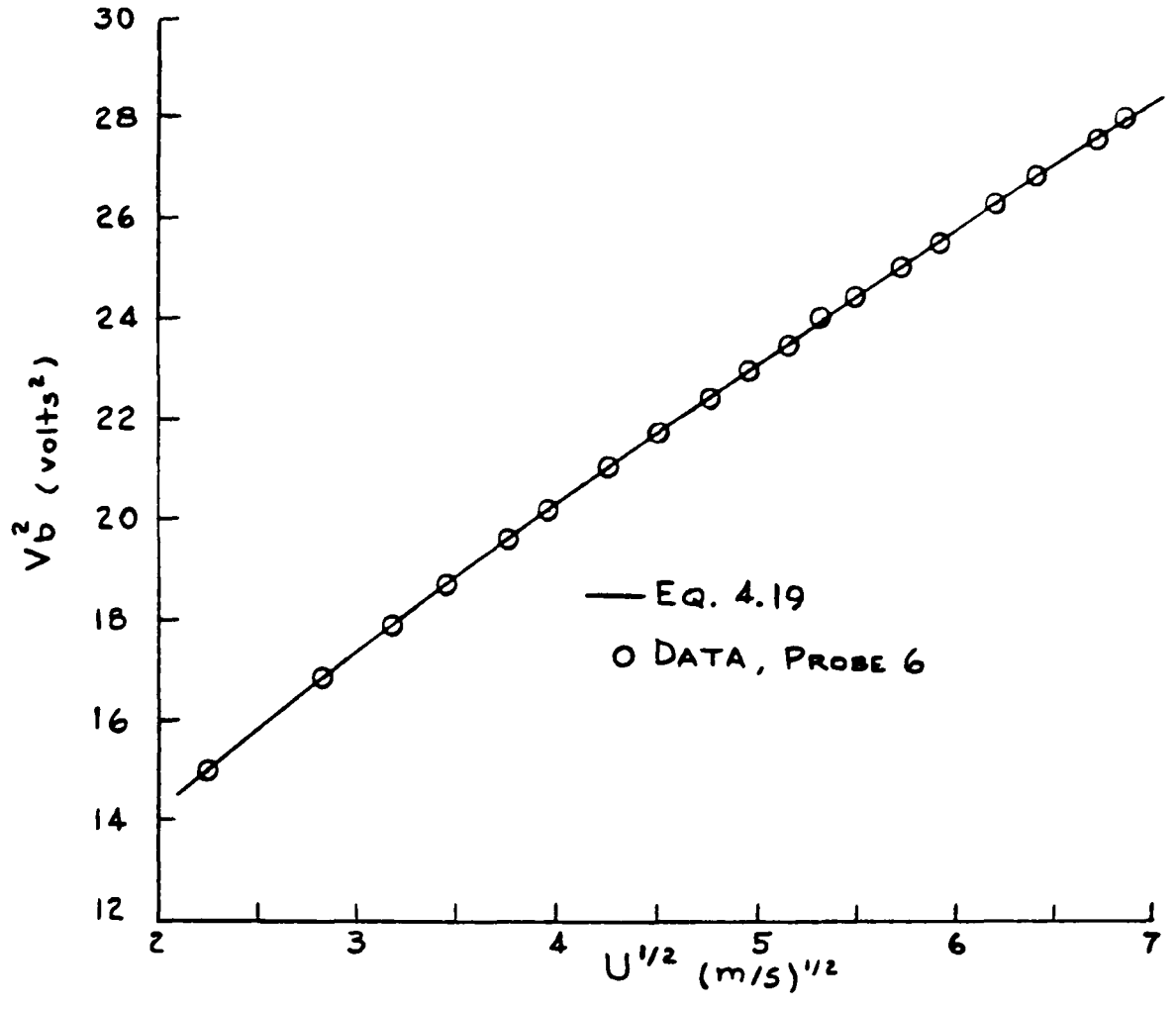

FIG. 4.9 Data Fitted to a Three-Term Response Law

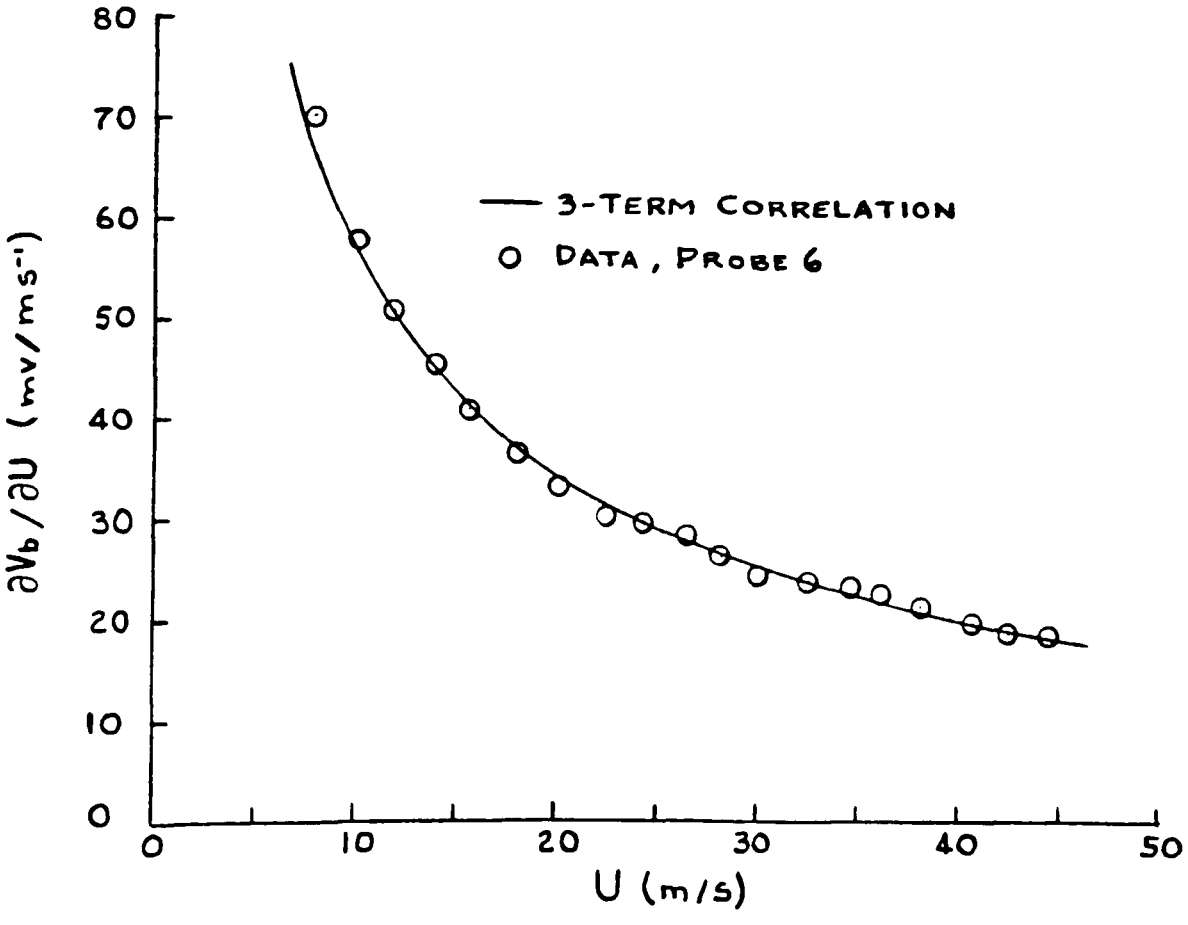

FIG. 4.10 Hot-Wire Sensitivity Data Compared with Three-Term Response Law

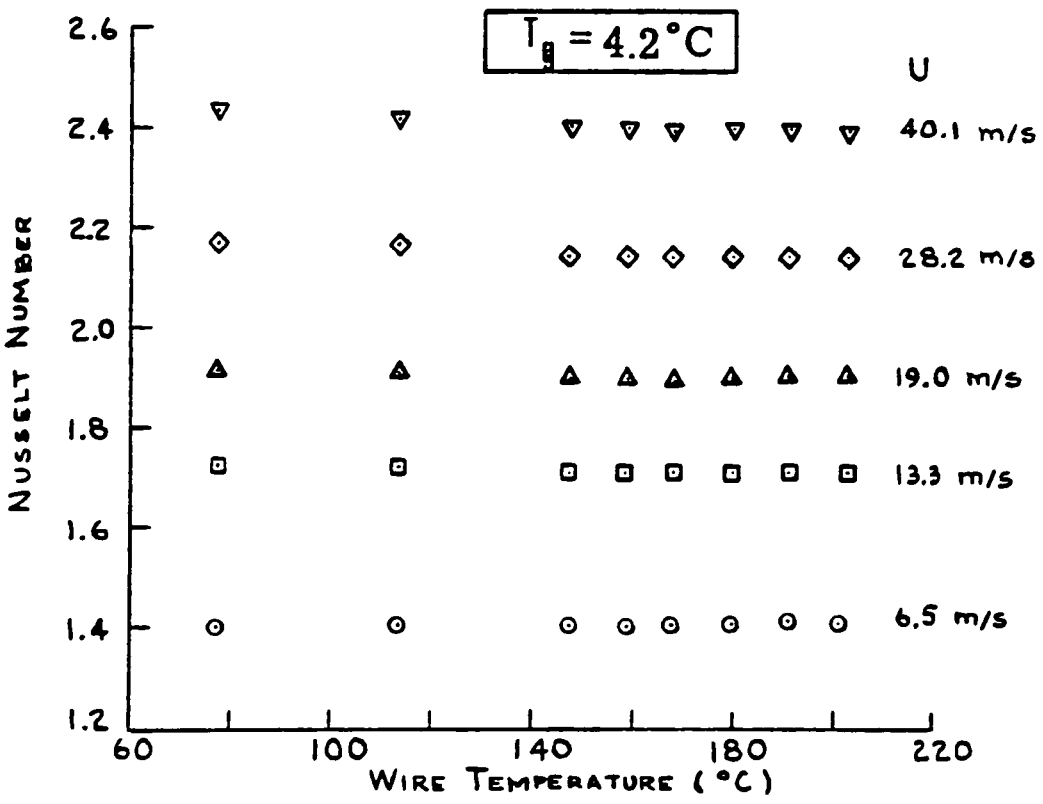

FIG. 4.11 Effect of Wire Temperature at Constant Gas Temperature. All Gas Properties Evaluated at the Gas Temperature

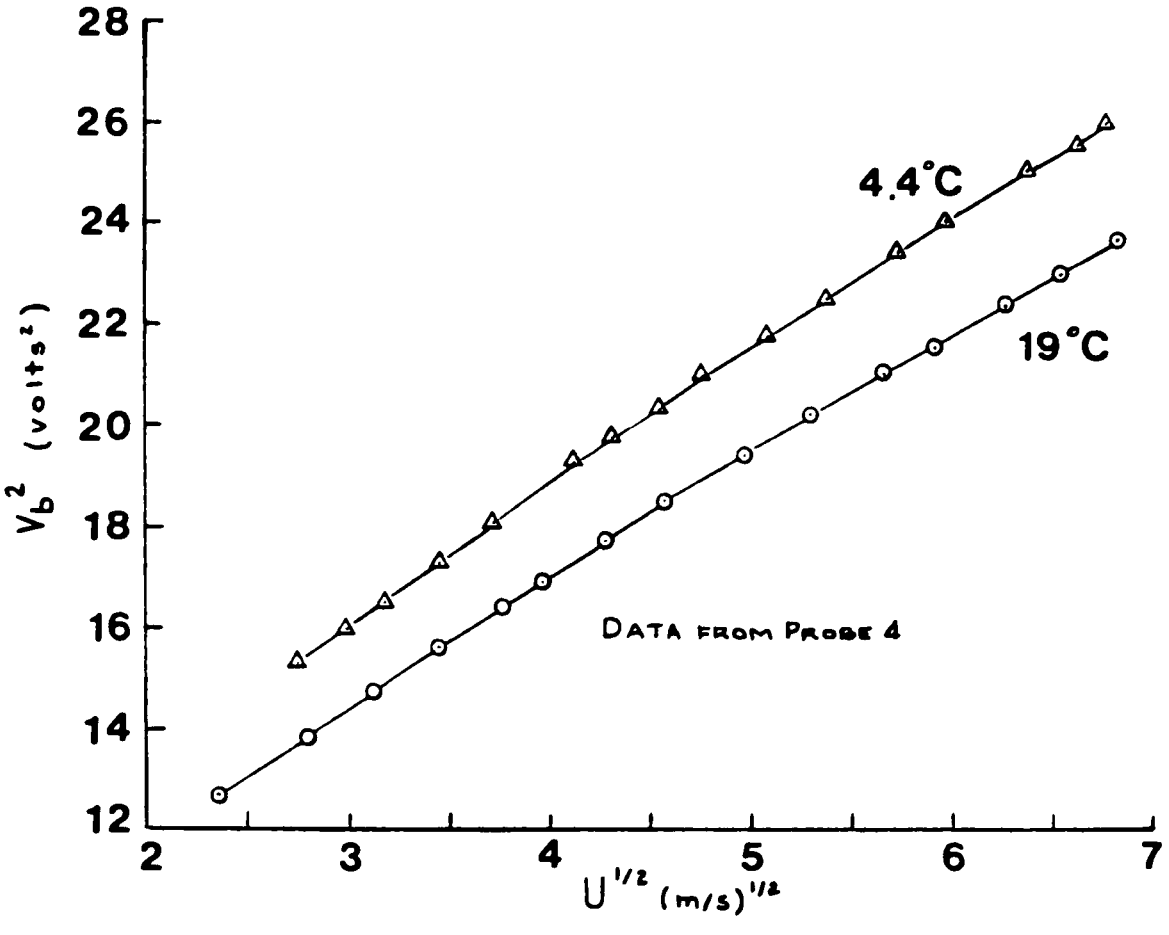

FIG. 4.12 Effect of Freestream Temperature on Hot-Wire Response at Constant Wire Temp.

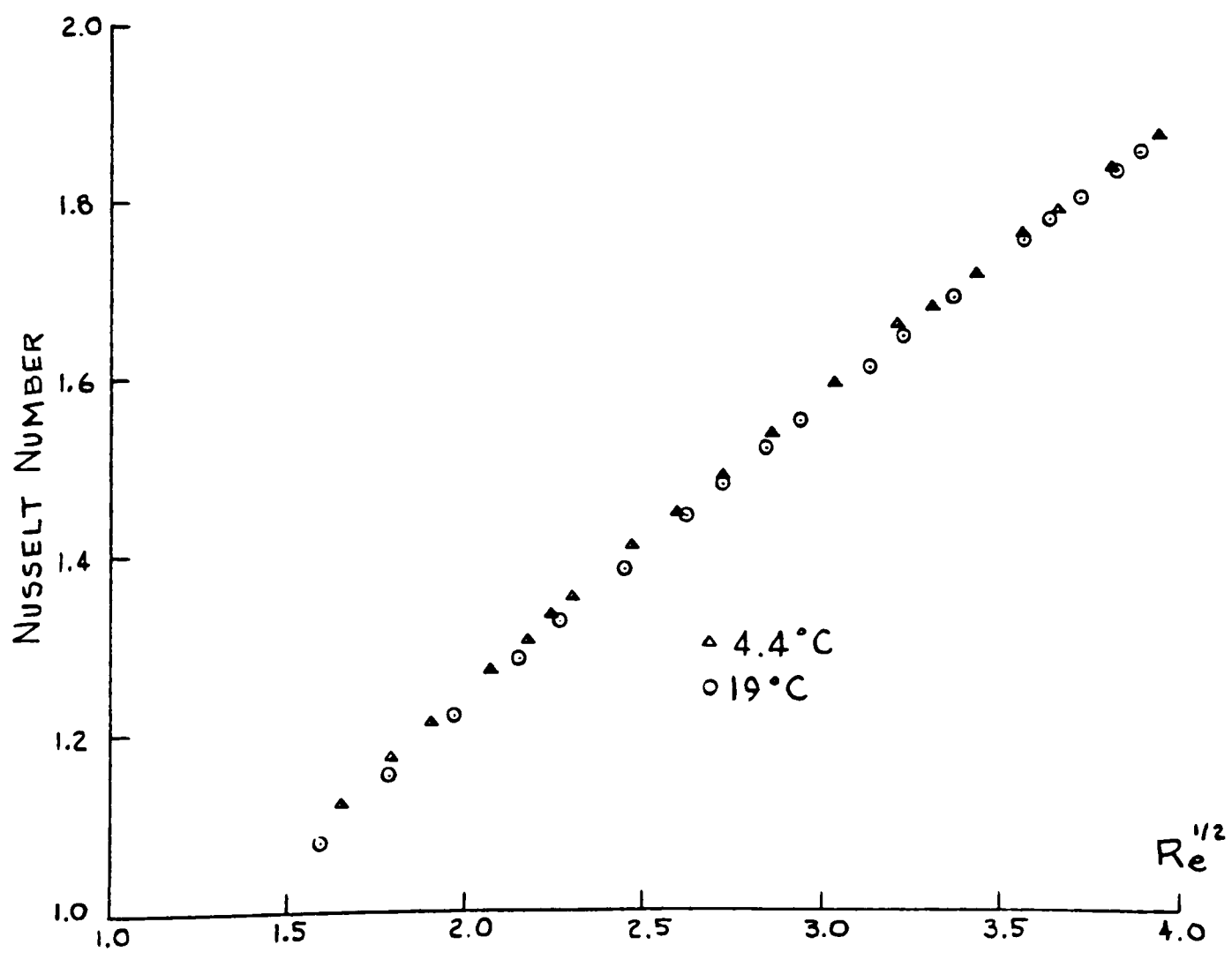

FIG. 4.13 Effect of Freestream Temperature on Nusselt Number at Constant Wire Temperature

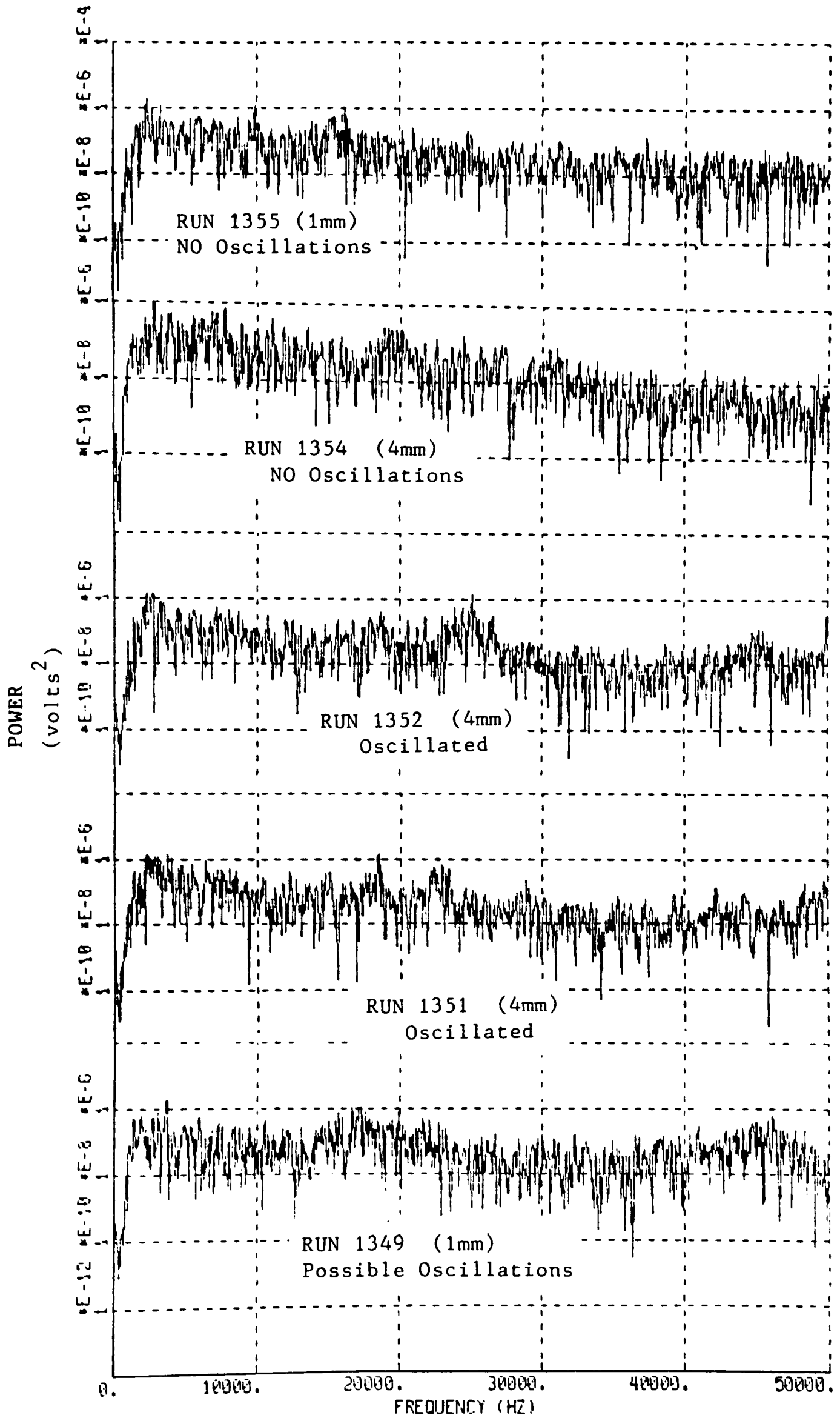

FIG. 4.14 Frequency Spectrum on Large-Chord B22 Suction Surface

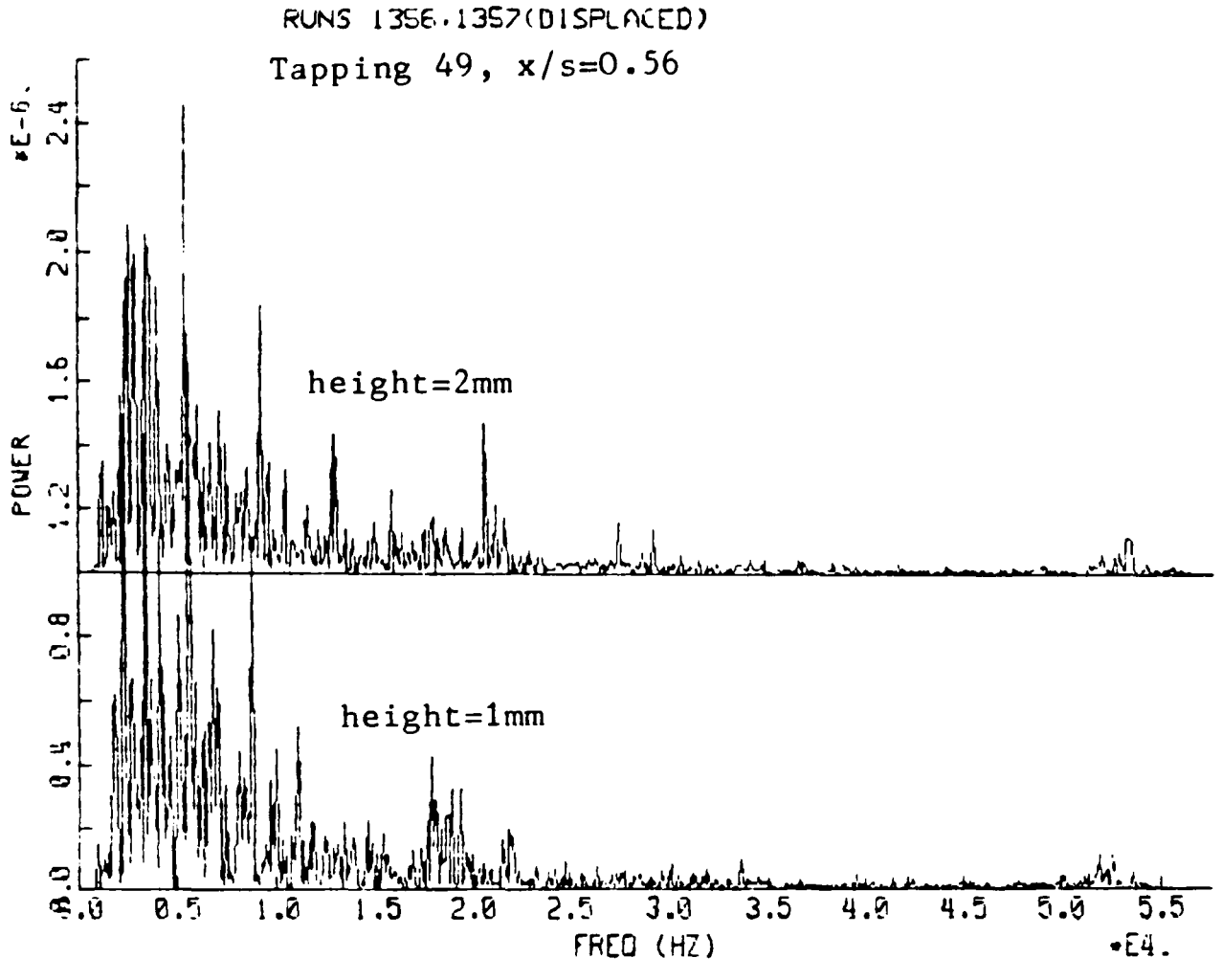

FIG. 4.15a Boundary Layer Frequency Spectrum

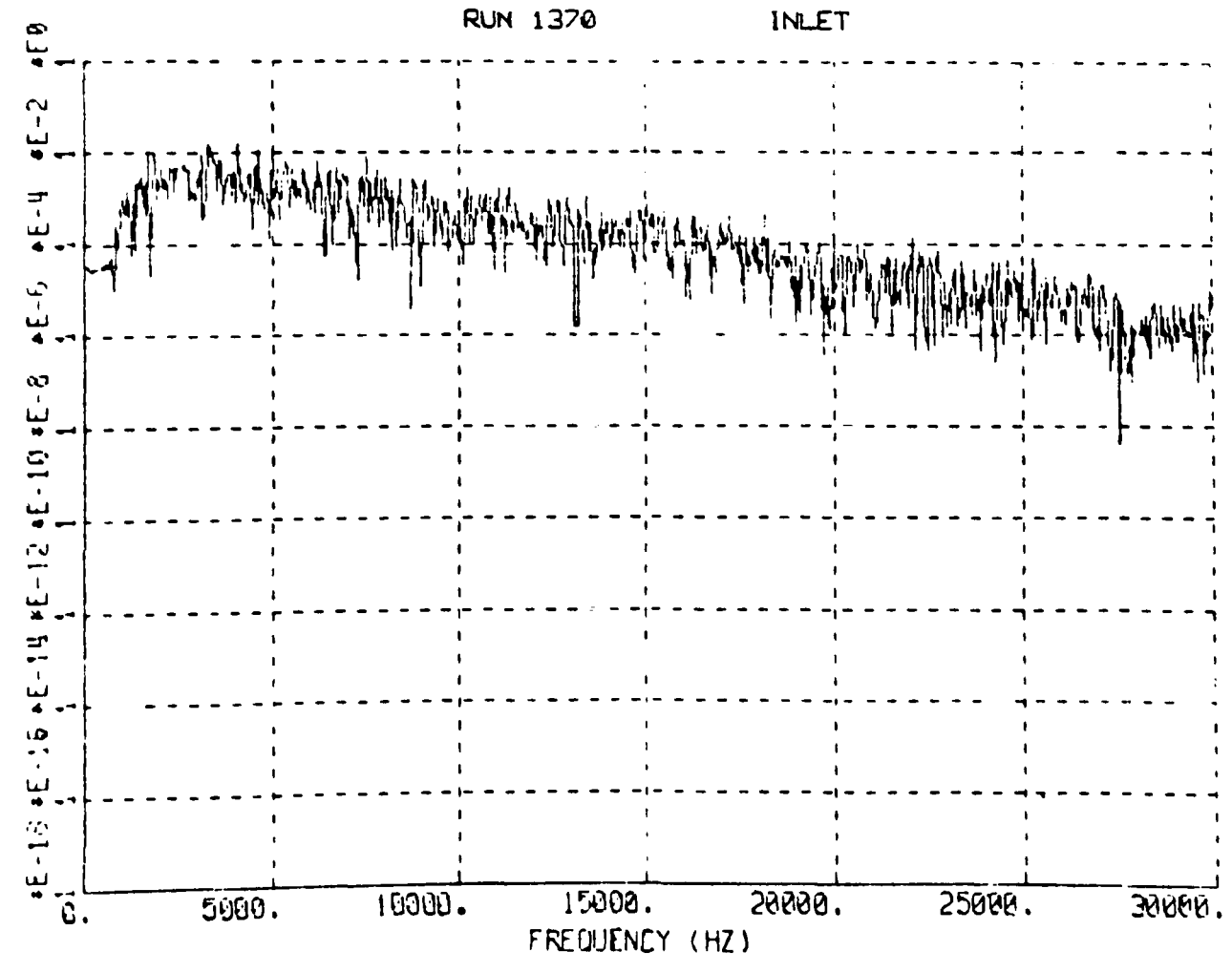

FIG. 4.15b Frequency Spectrum--Large-Chord Cascade Inlet

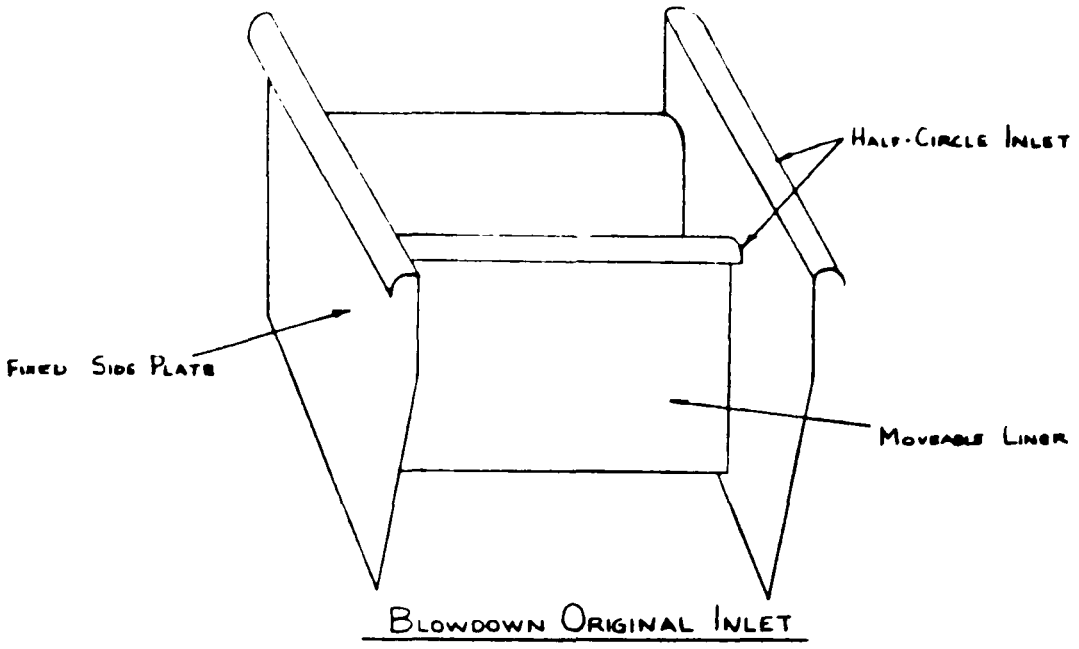

Blowdown Original Inlet

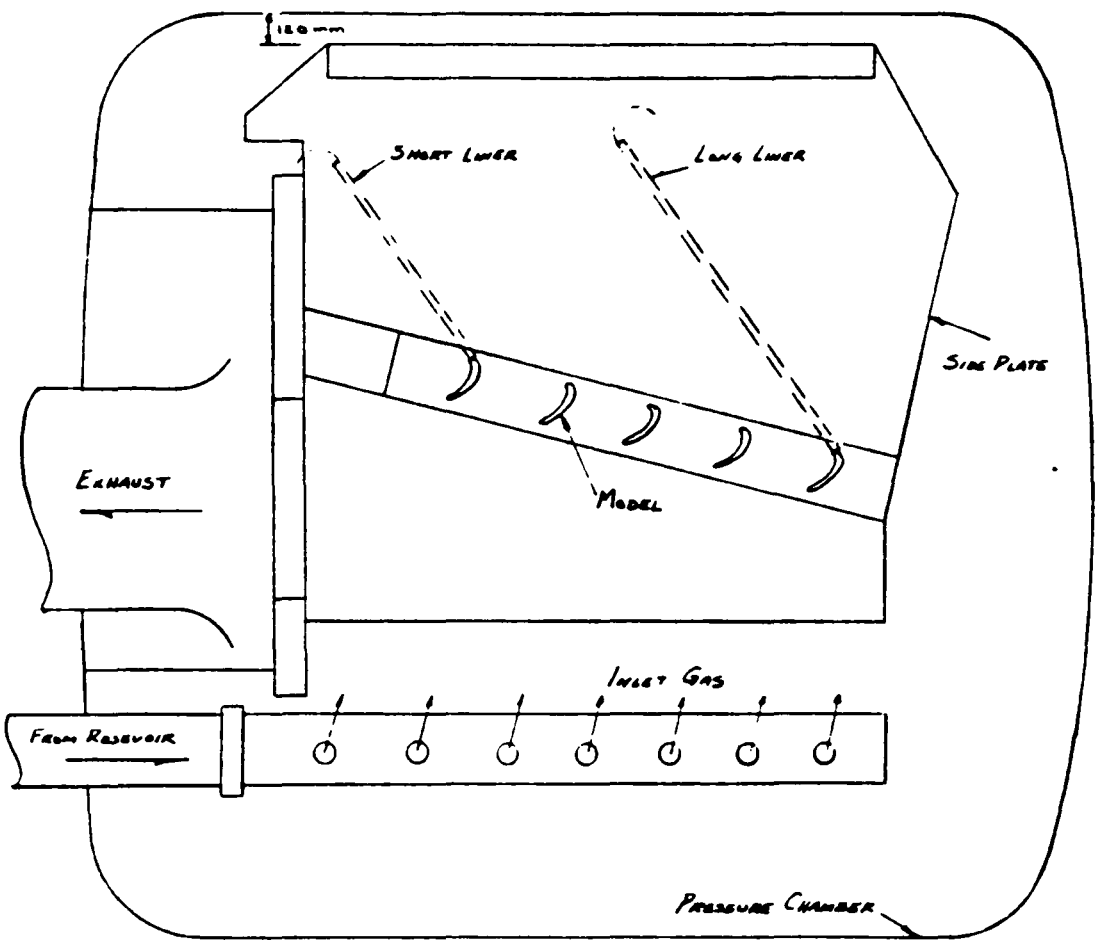

Fig. 5.1.a Original Blowdown Inlet Assembly

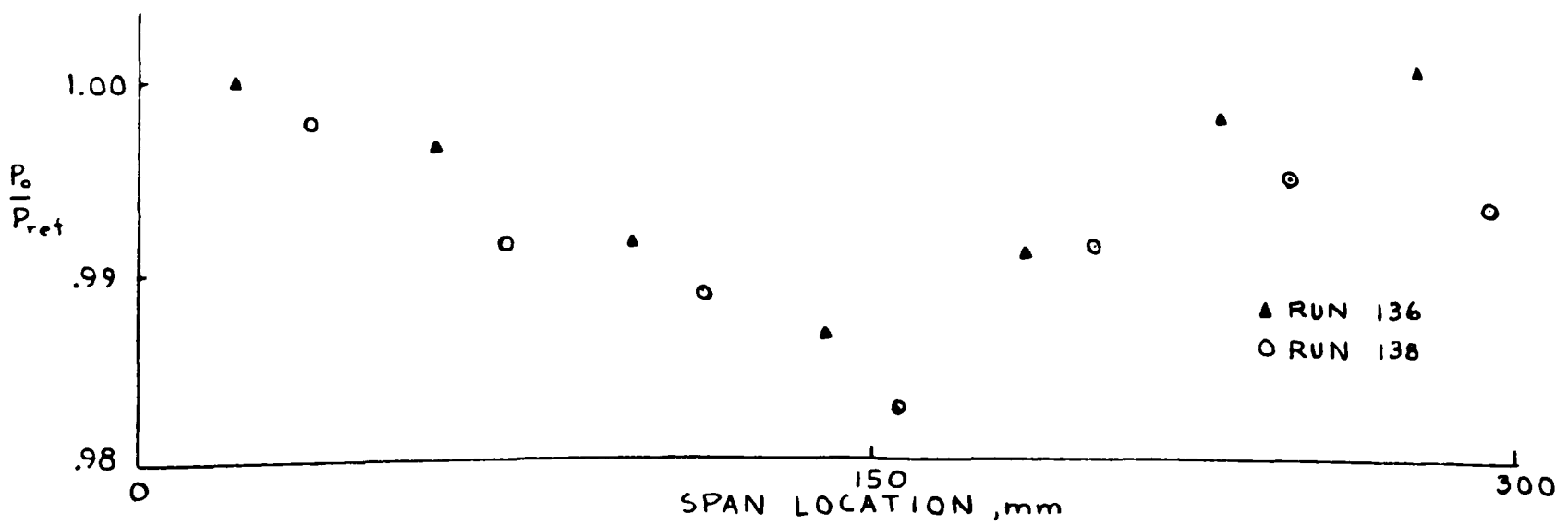

Fig. 5.1.b. Total Pressure Survey - Clean Inlet

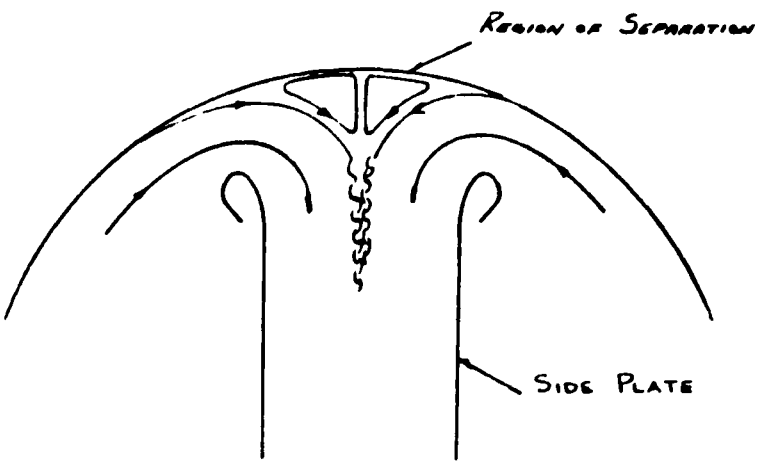

Original Region on Top of Tank

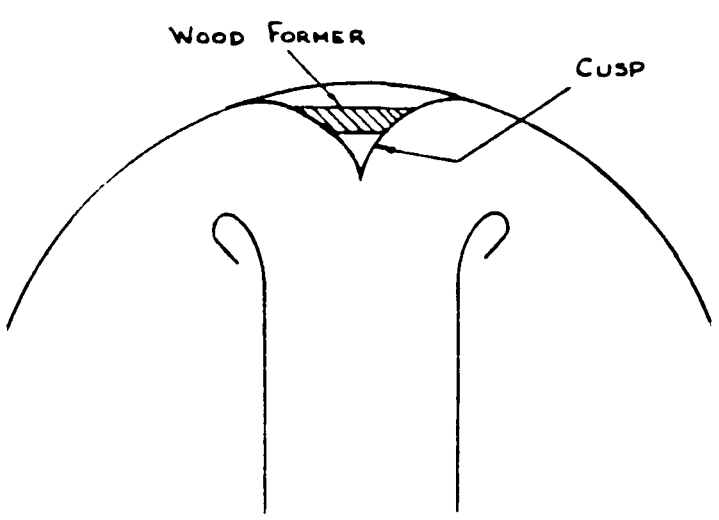

New Cusp Installed in Tank

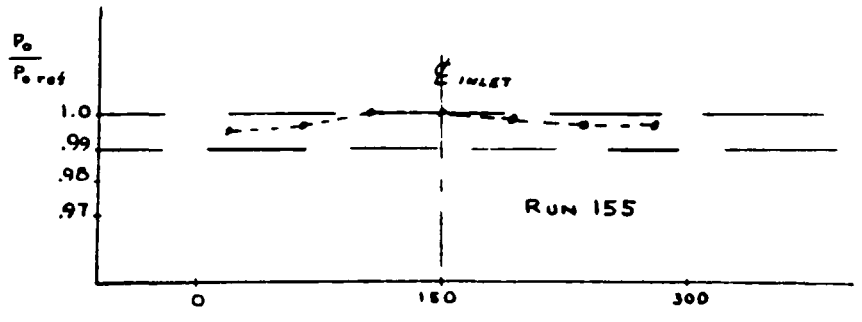

Fig. 5.2 Flow Improvemt with Cusp

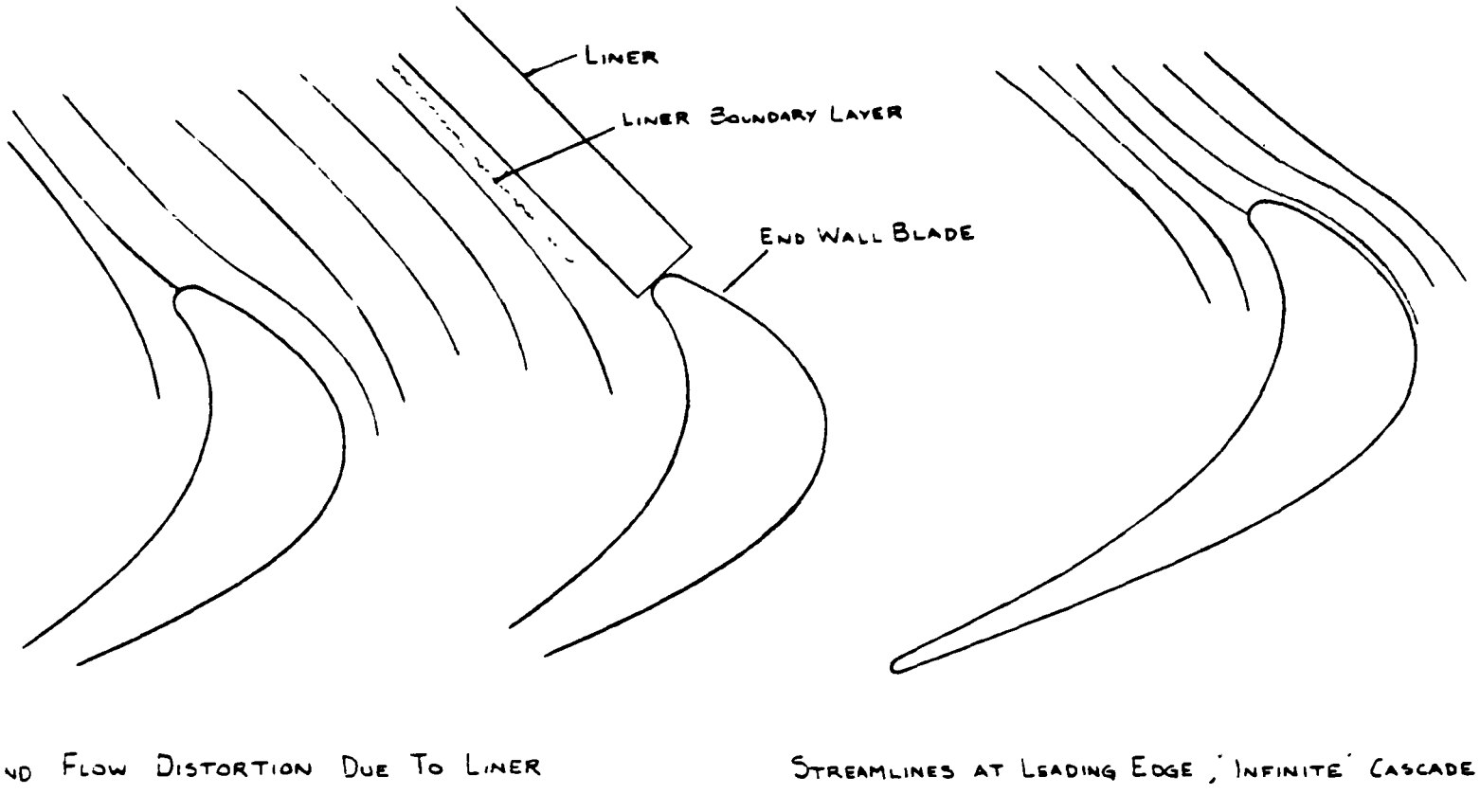

FIG.5.3a Effect of Endwall

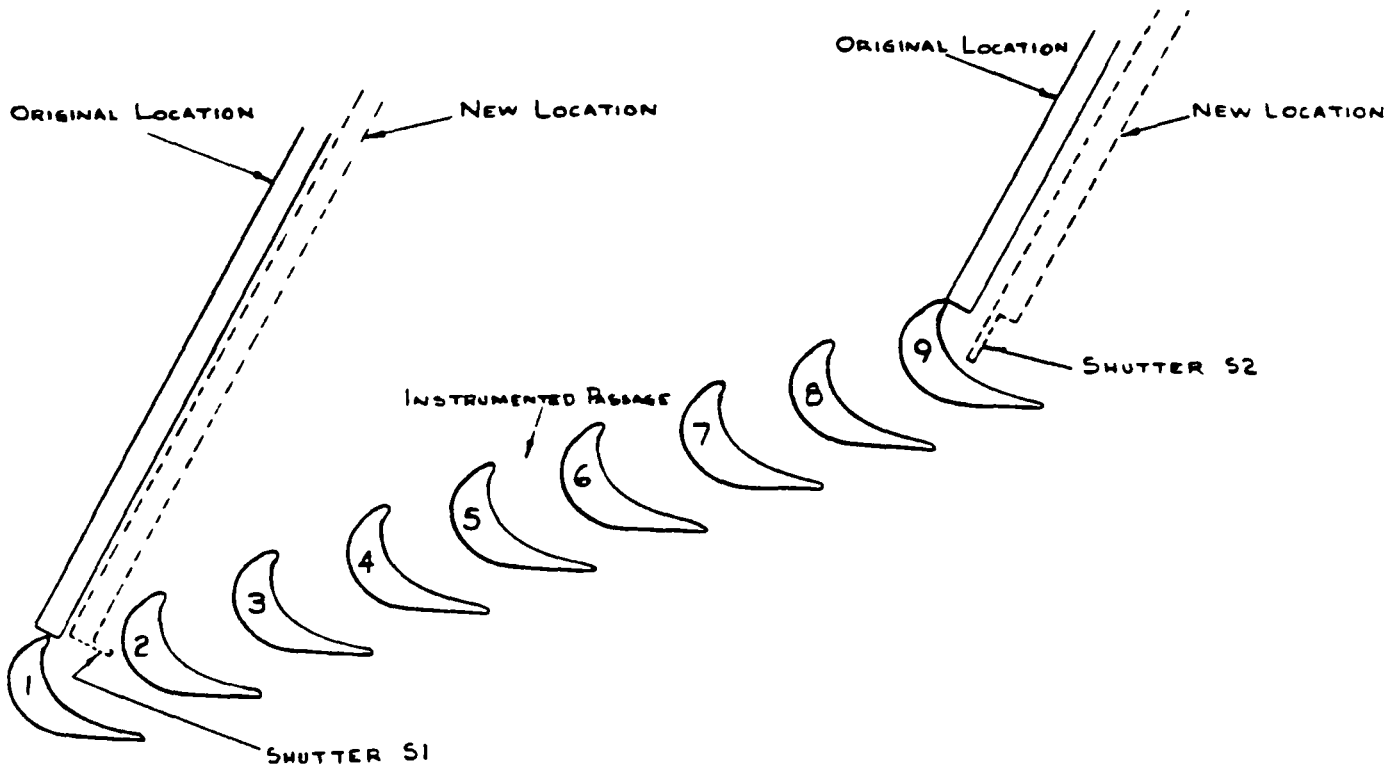

FIG.5.3b Changes to Inlet

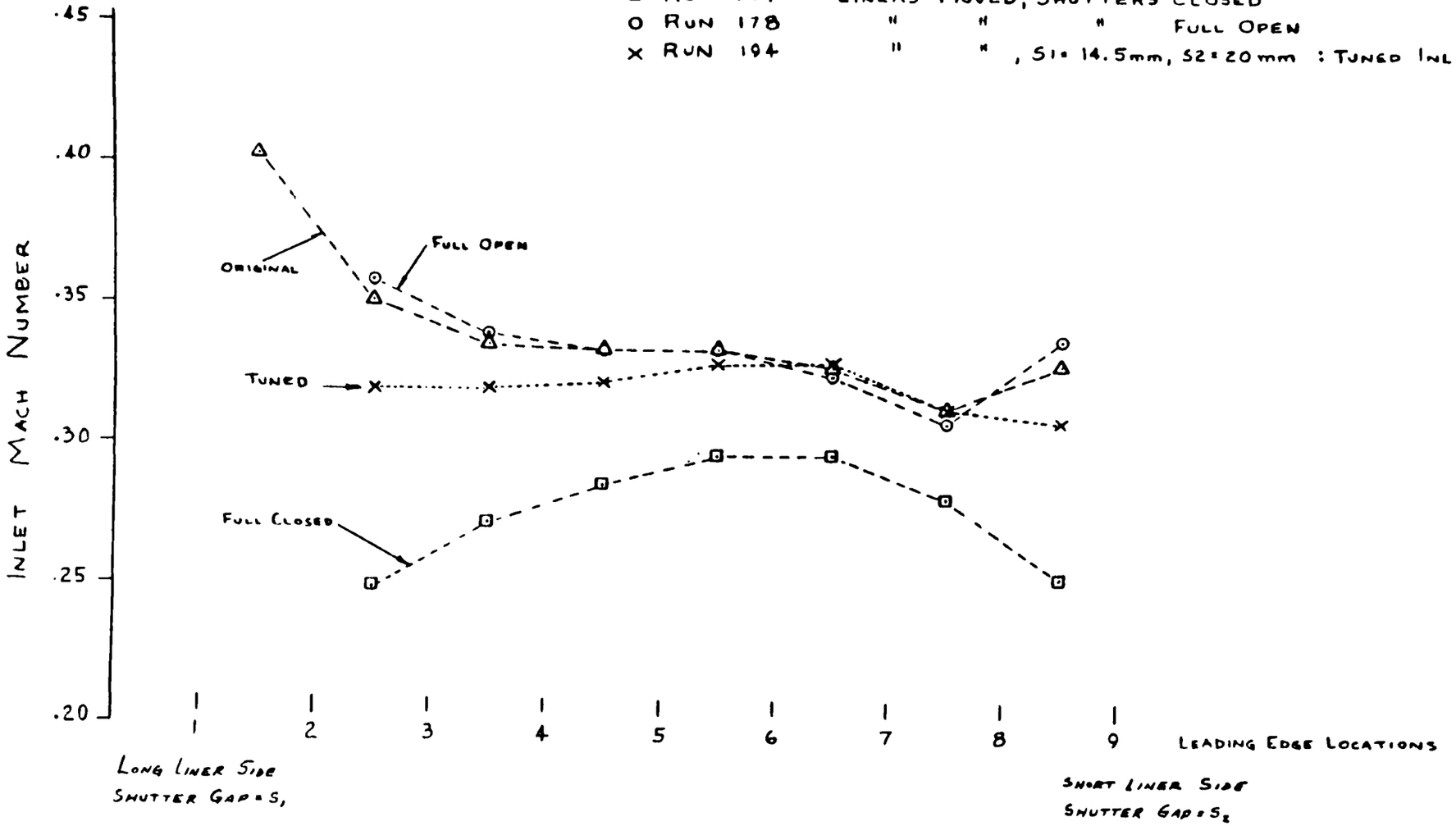

FIG. 5.4 Pitchwise Mach Number Variation with Shutter Changes

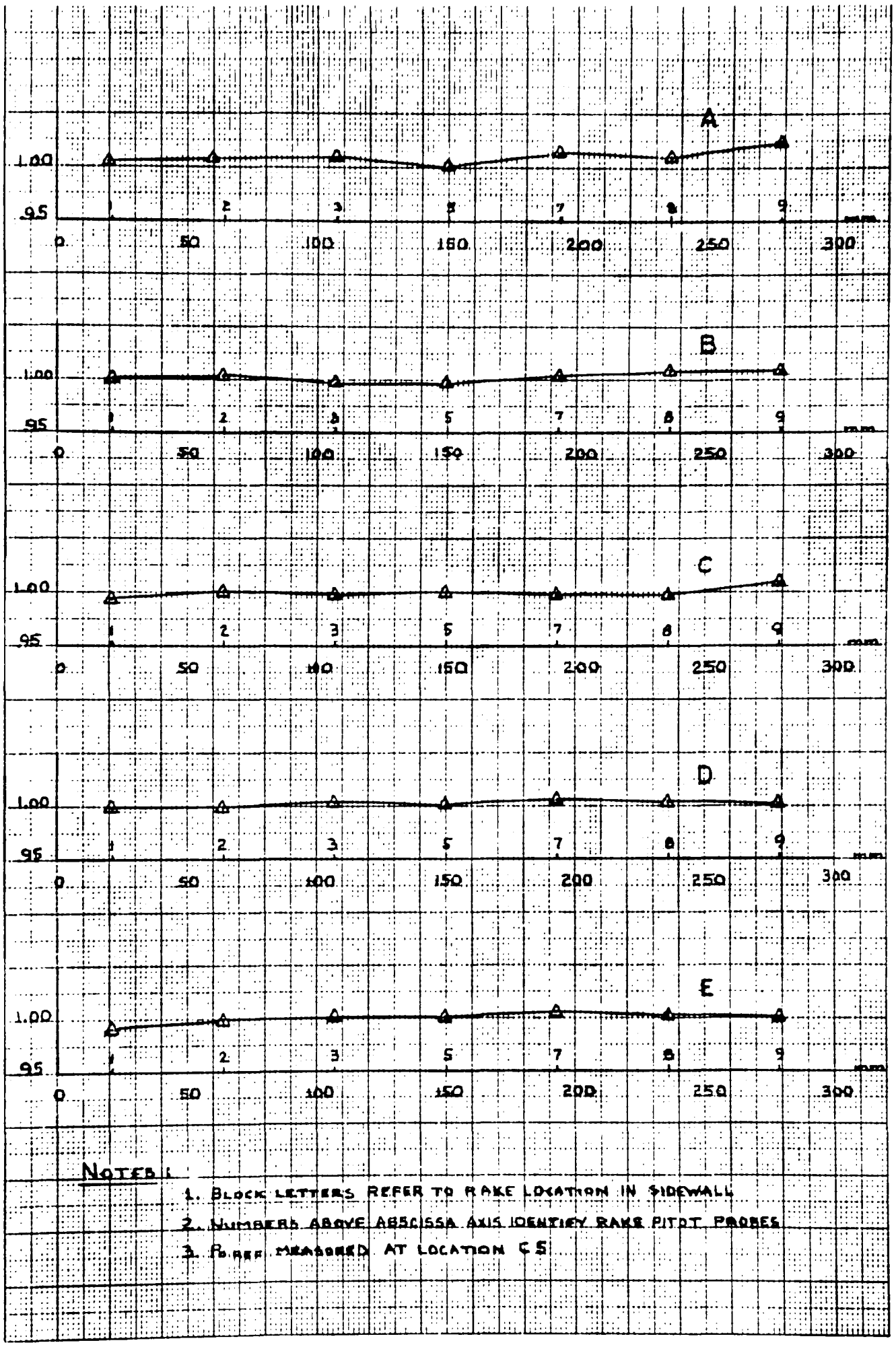

FIG. 5.5 Po_{local}/Po_{ref} vs Duct Location

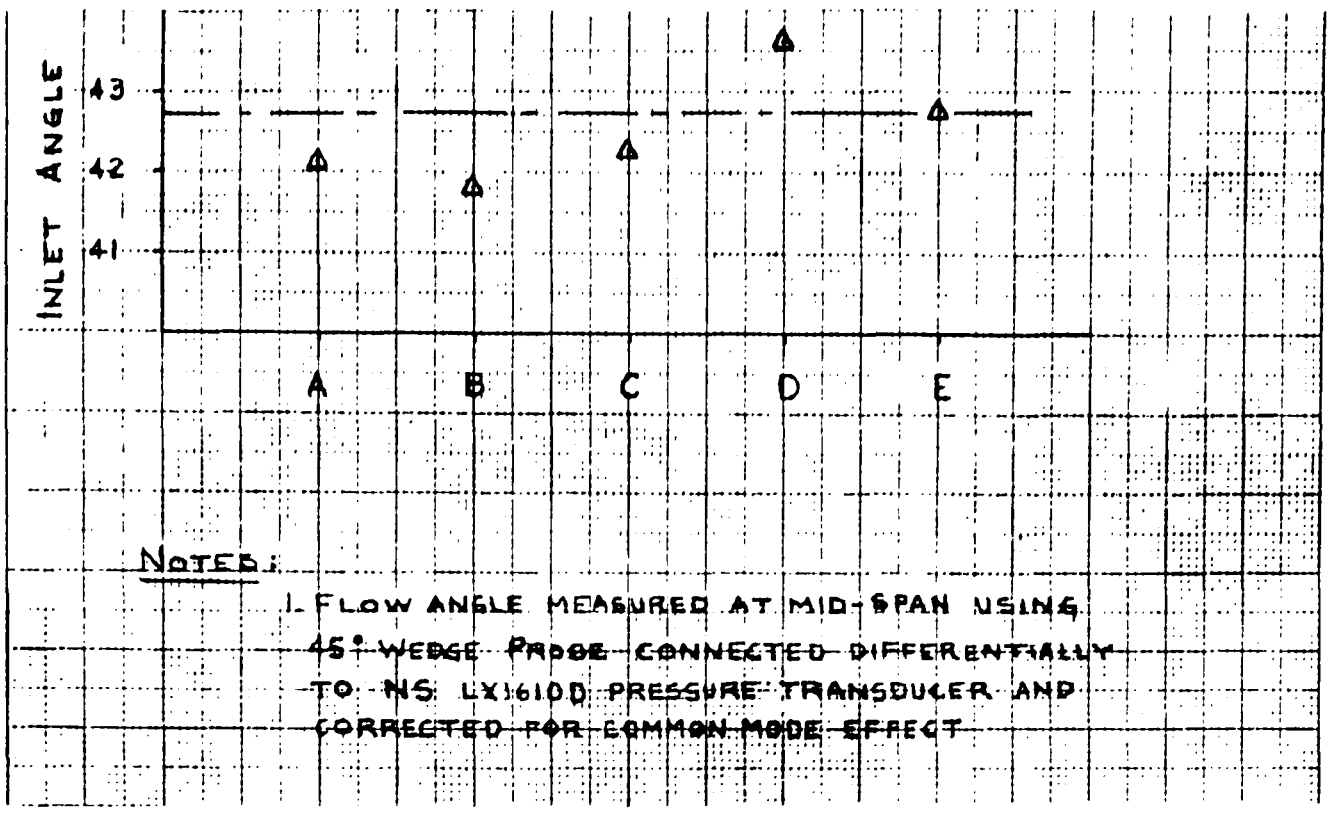

FIG.5.6 Flow Incidence Angle at
Various Inlet Locations

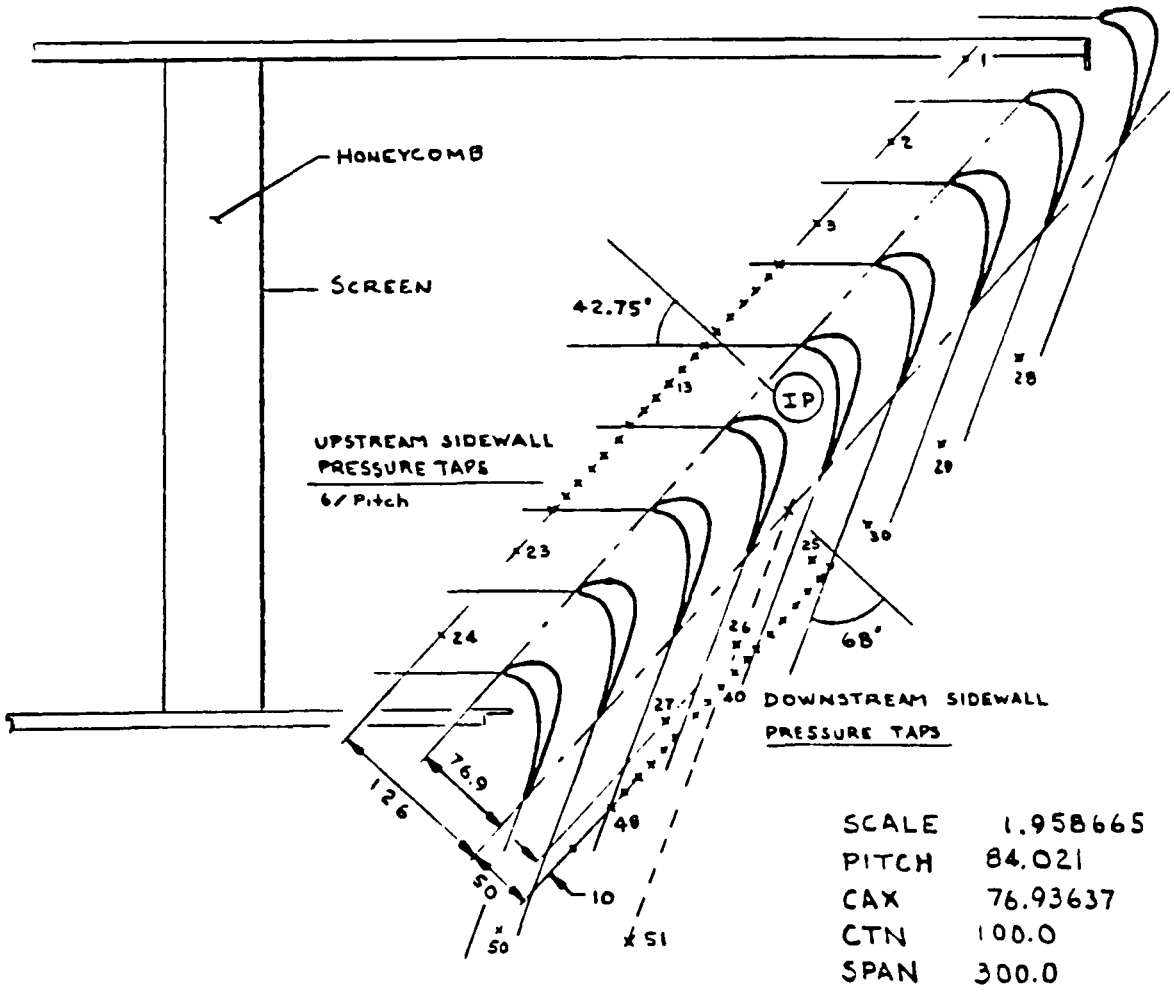

FIG. 5.7 100mm B22 Cascade Dimensions

ROTOR UPSTREAM SIDEWALL STATIC PRESSURE DISTRIBUTION

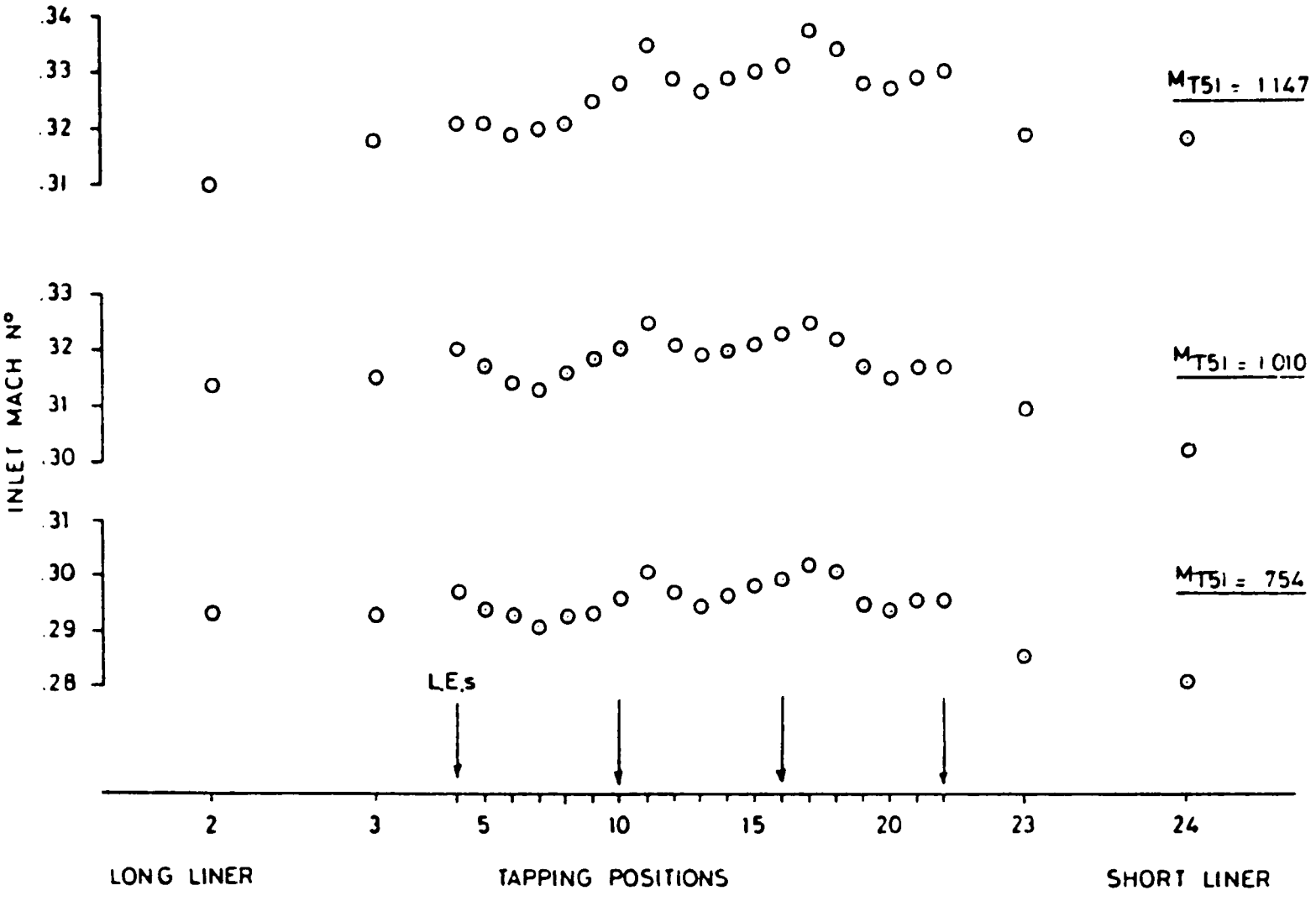

FIG.5.8a

DOWNSTREAM SIDEWALL STATIC PRESSURE DISTRIBUTION

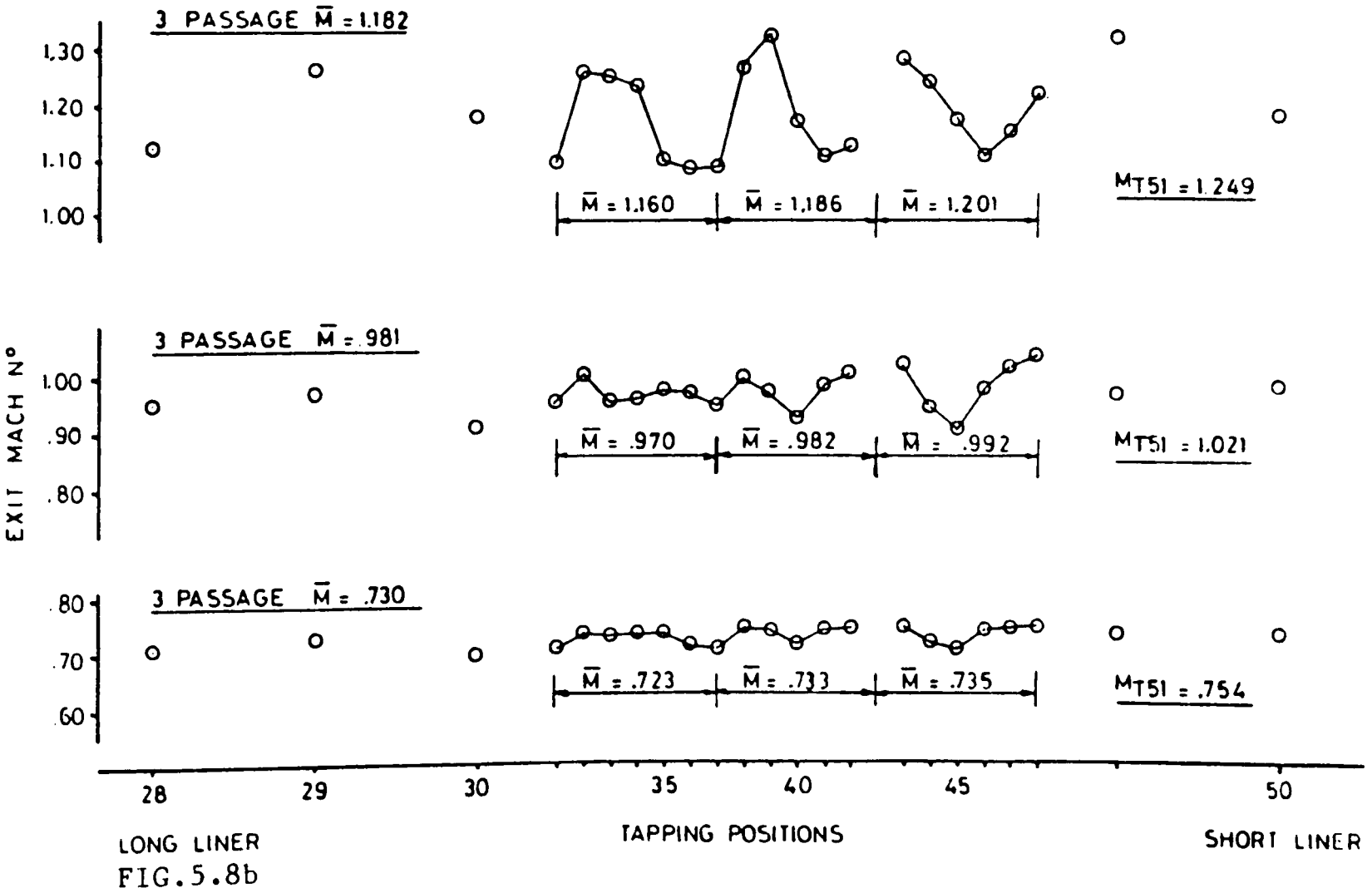

FIG.5.8b

FIG. 5.8 Inlet and Exit Mach Numbers

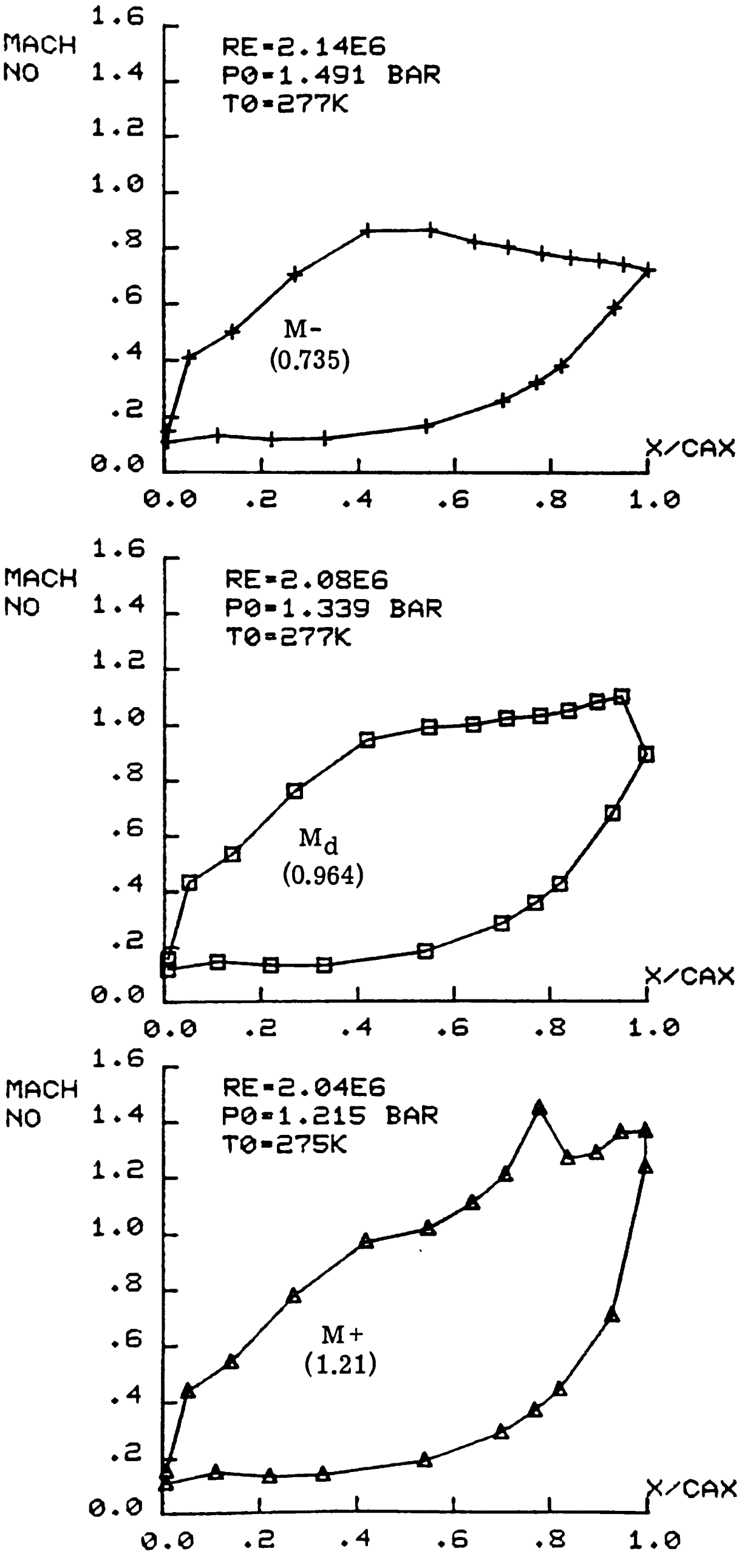

FIG. 5.9 100mm Chord Results

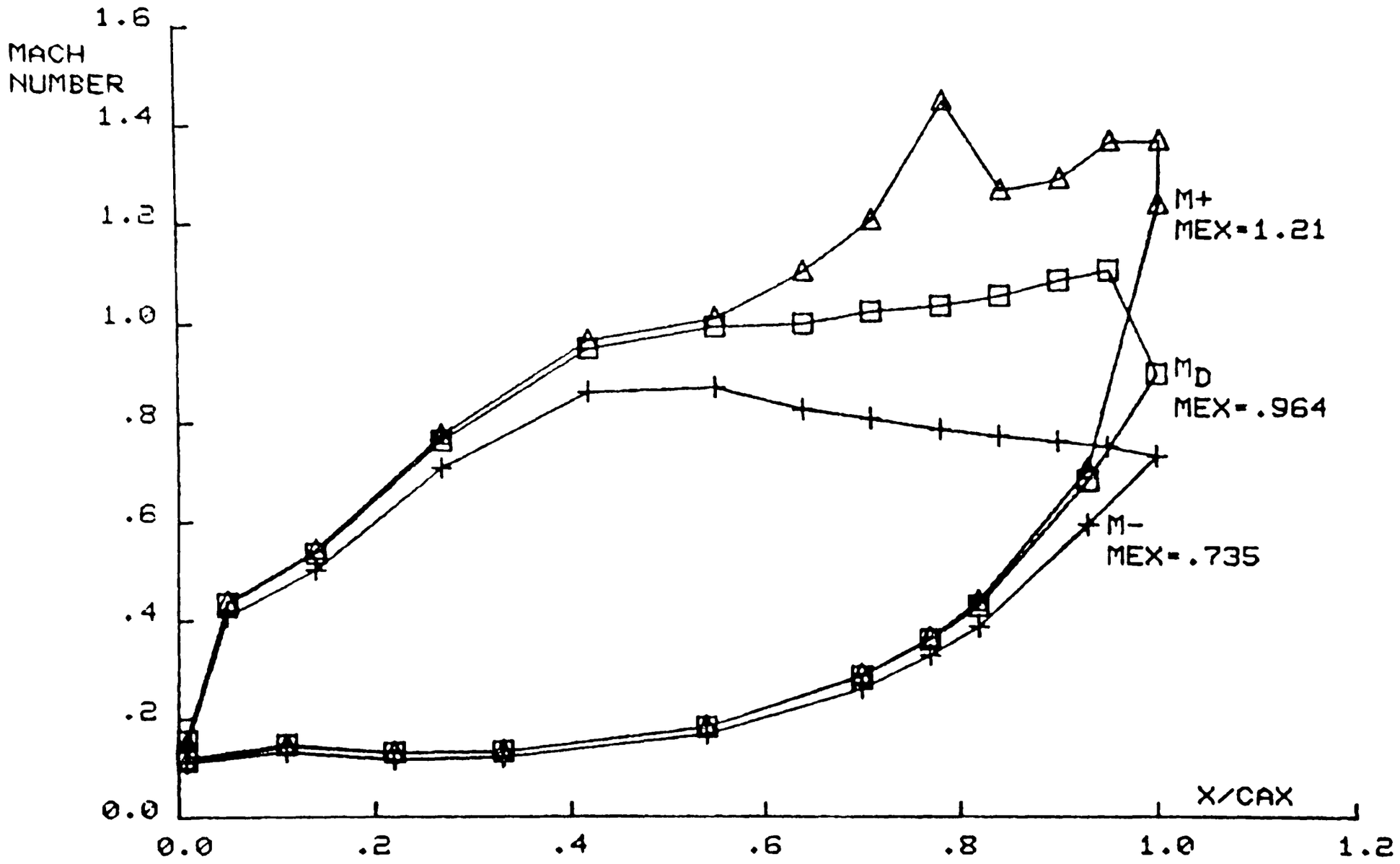

FIG.5.10 BLADE SURVEY COMPARISONS FOR VARIOUS EXIT MACH NO'S

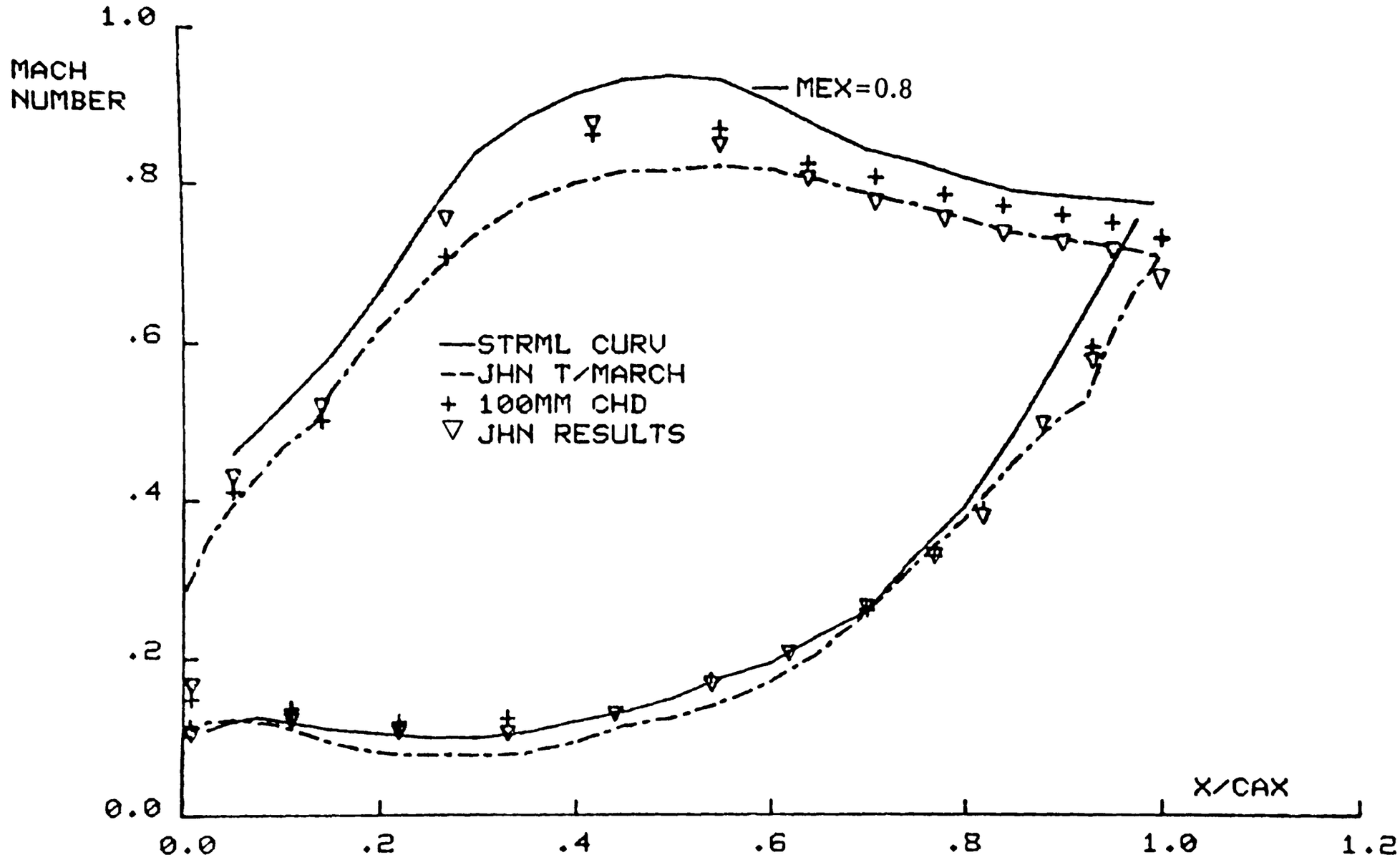

FIG.5.11 B22 DATA COMPARED TO PREDICTIONS FOR M- CONDITION

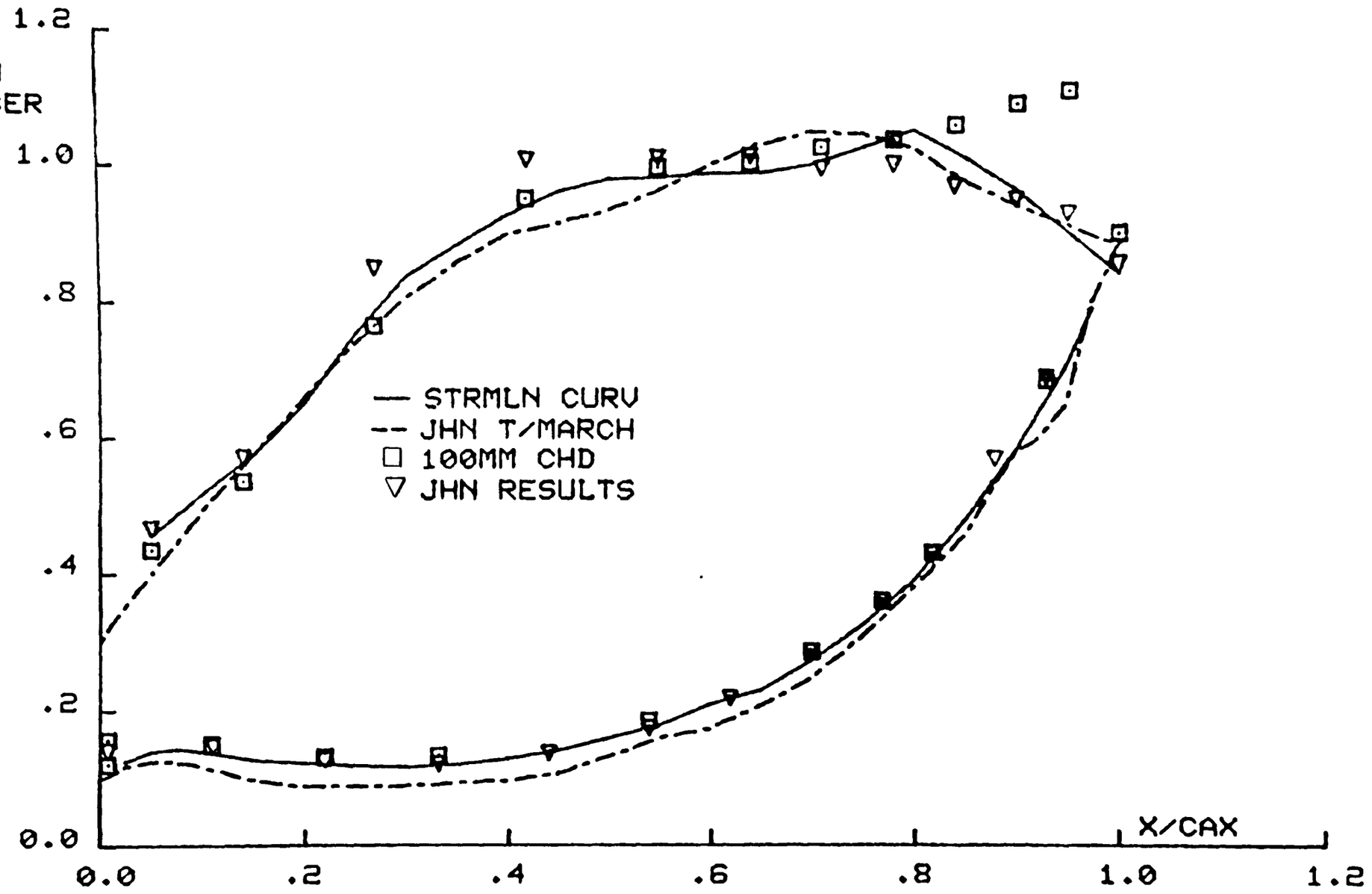

FIG.5.12 B22 DATA COMPARED TO PREDICTIONS FOR MDES CONDITION

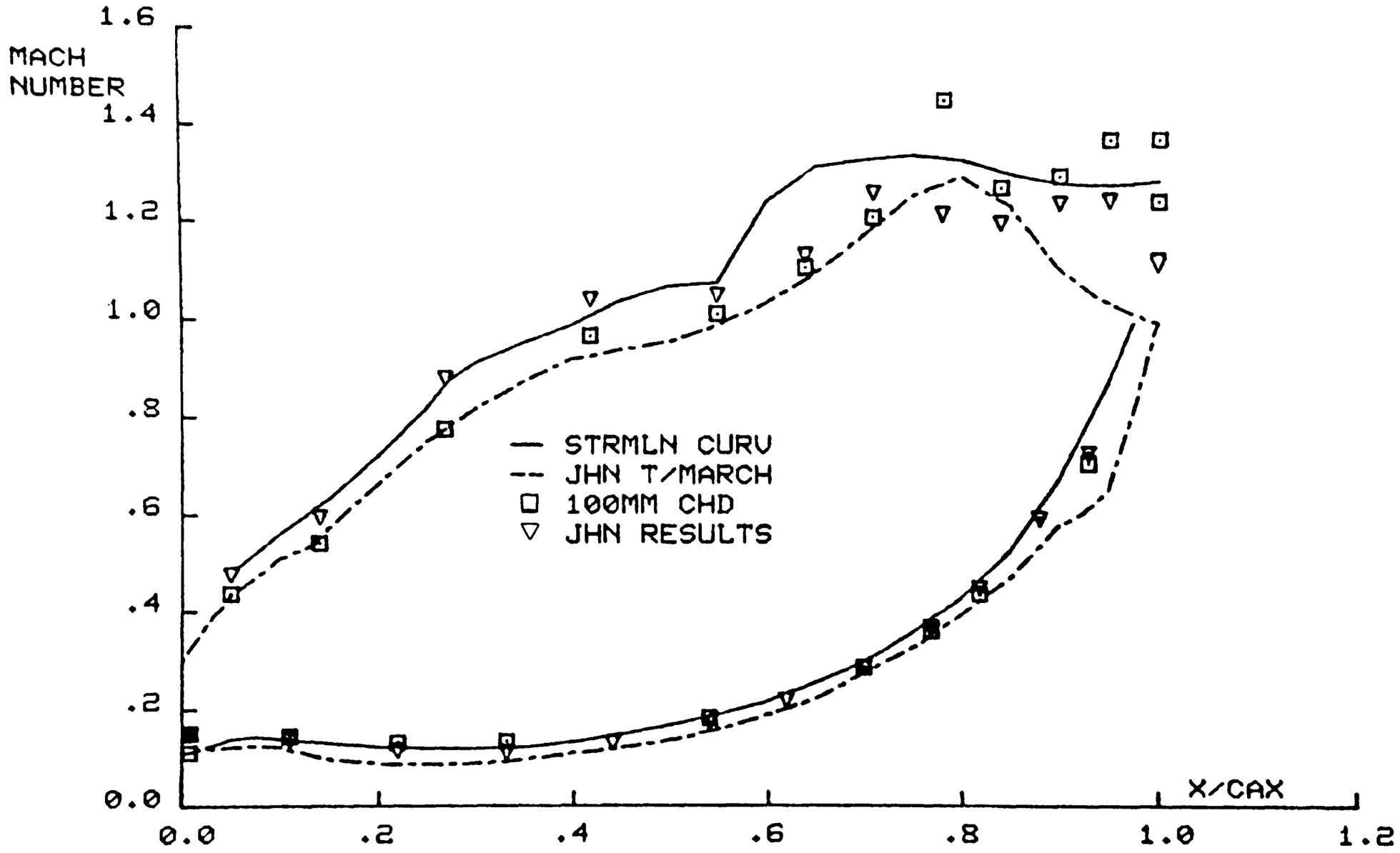

FIG.5.13 B22 DATA COMPARED TO PREDICTIONS FOR M+ CONDITION

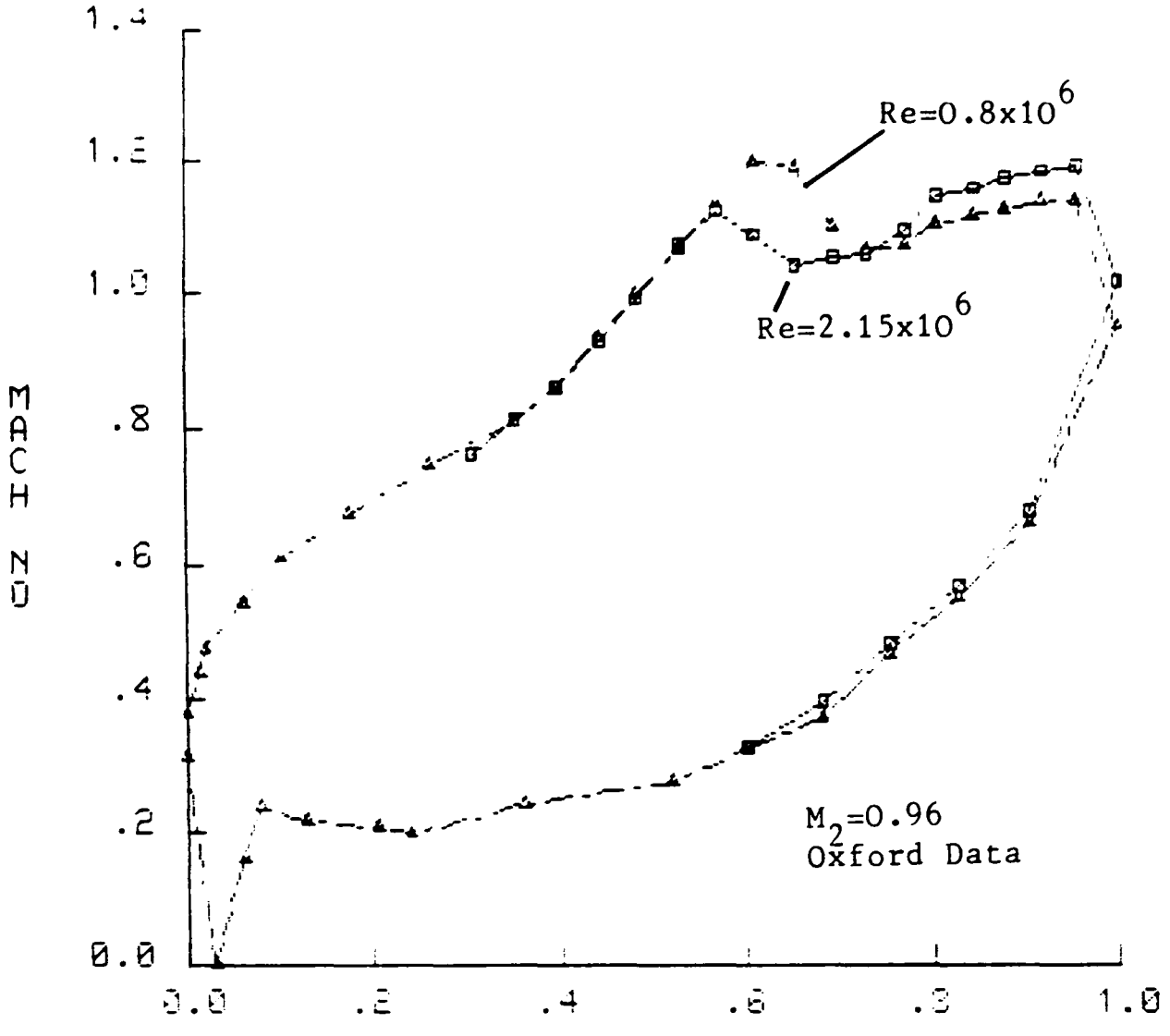

FIG.5.14 Reynolds Number Effect on VKI-1 Data

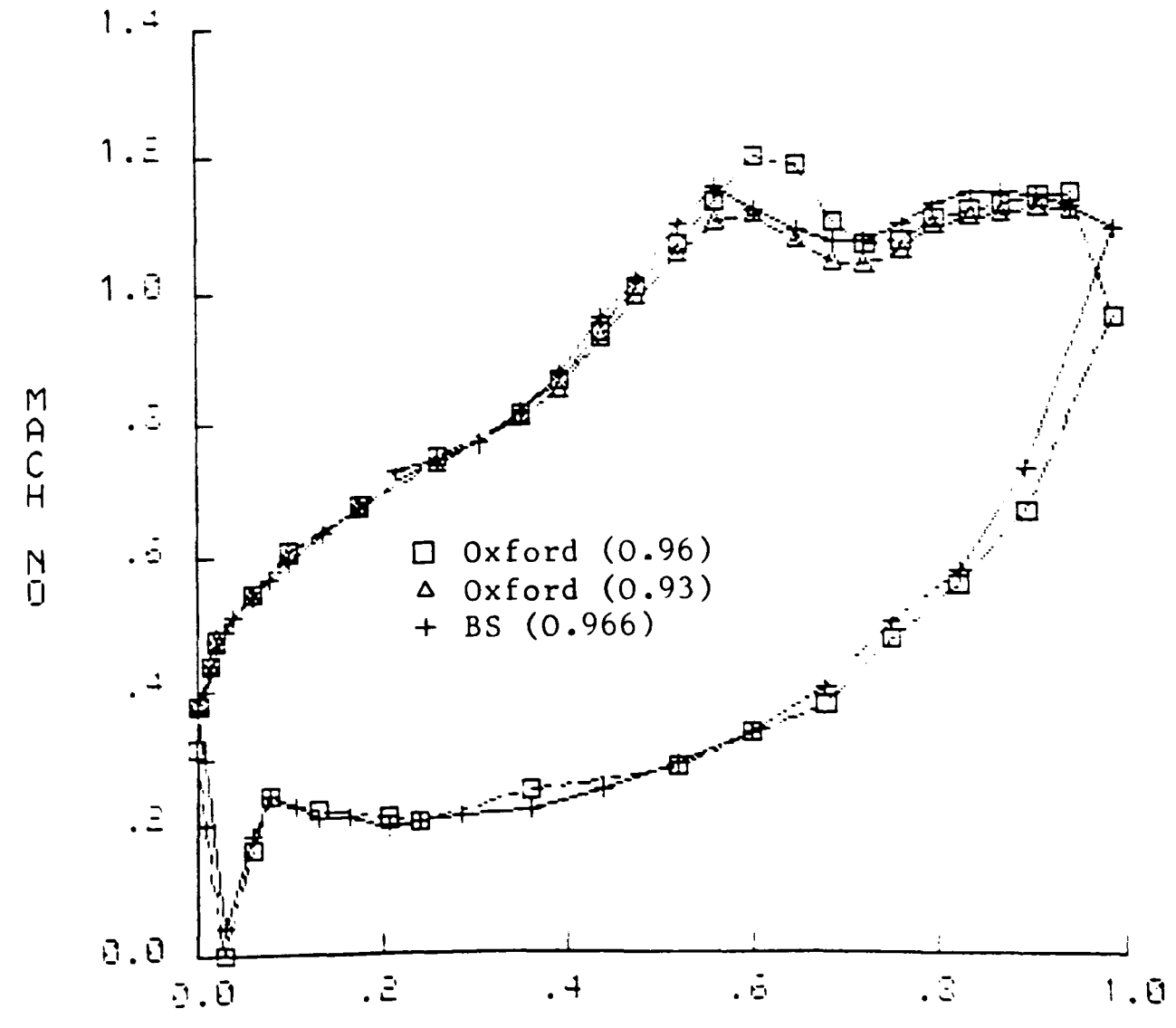

FIG.5.15 VKI-1 Data From Two Tunnels

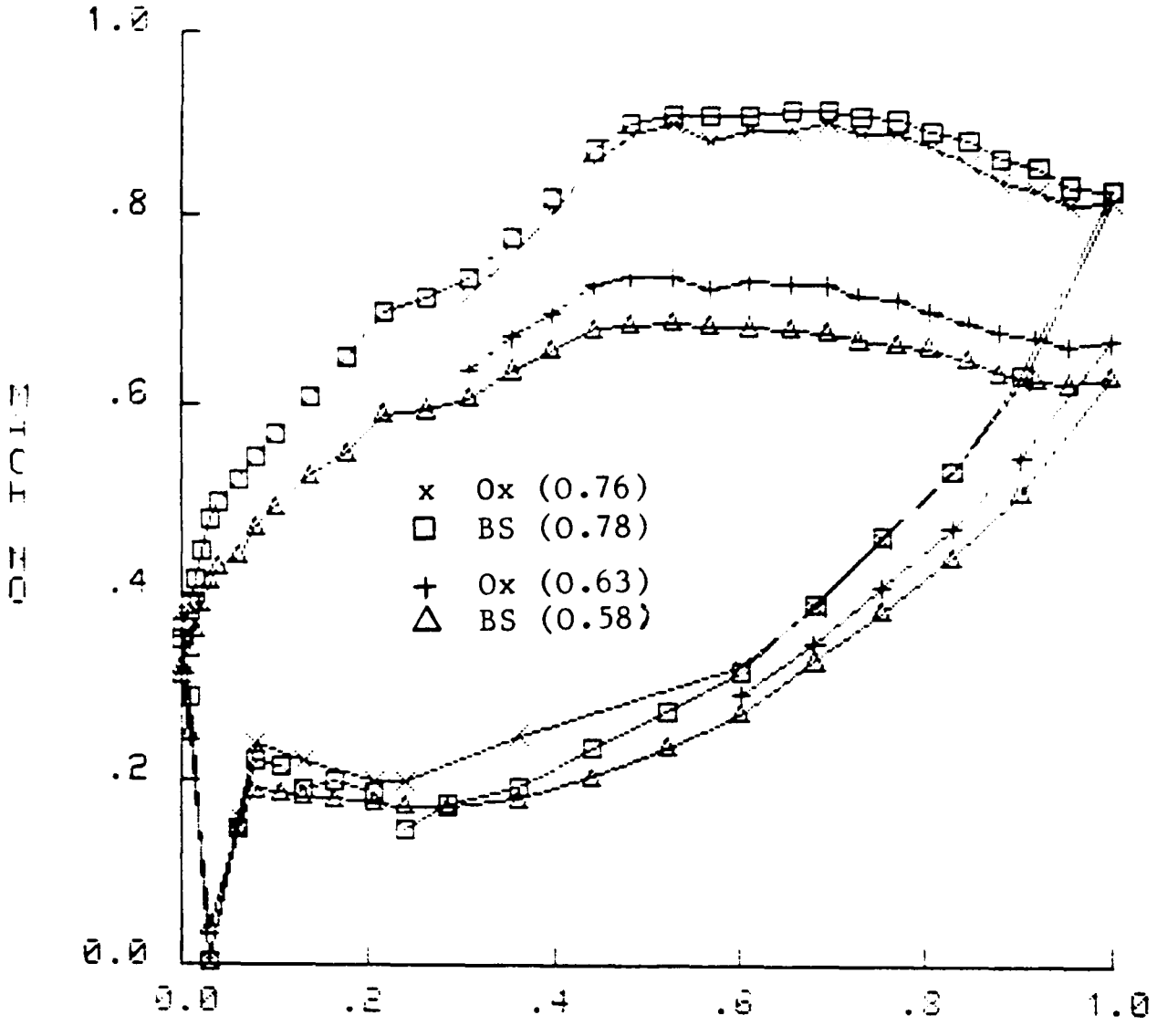

FIG.5.16 VKI-1 Data From Two Tunnels (Subsonic)

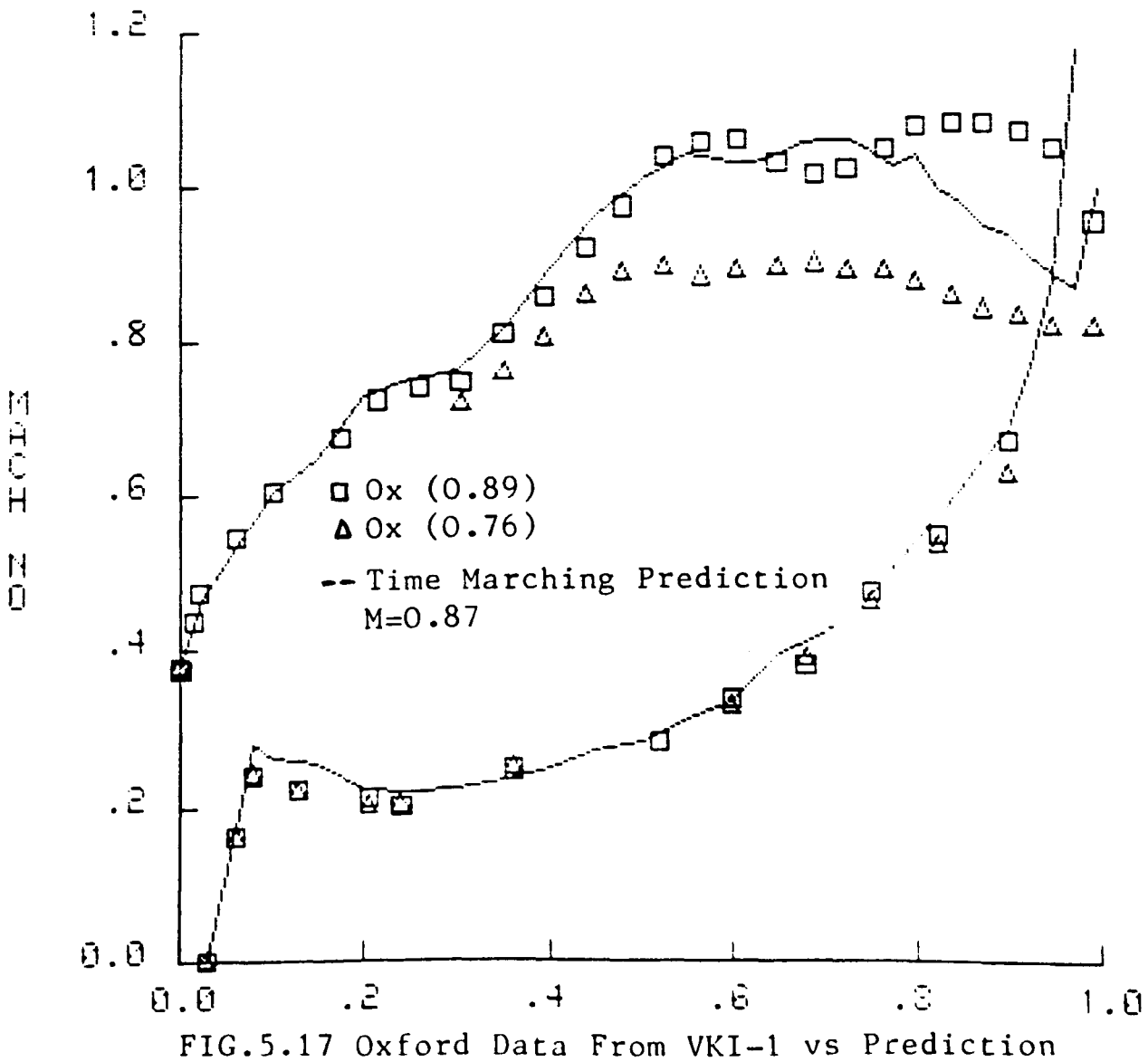

FIG.5.17 Oxford Data From VKI-1 vs Prediction

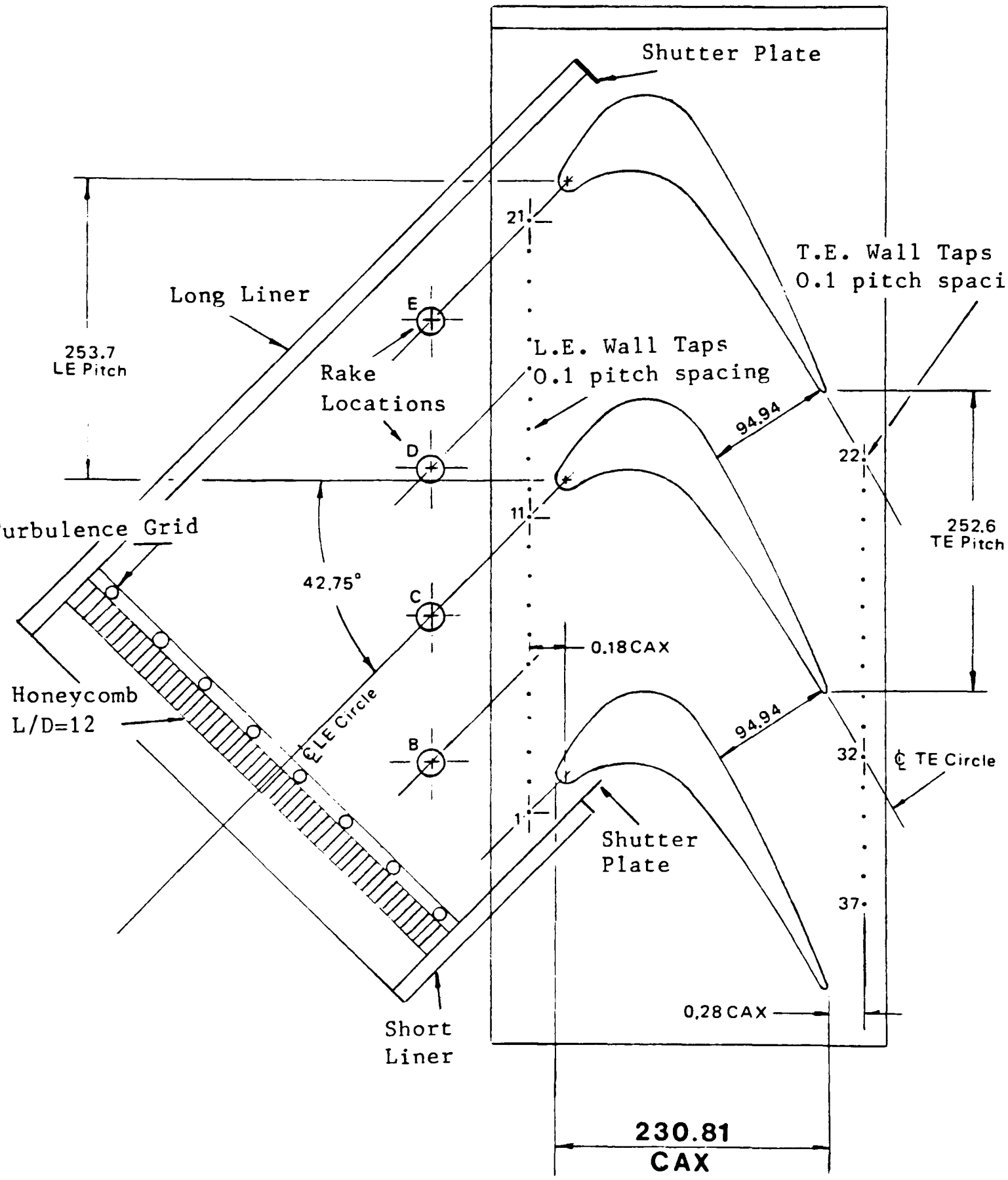

FIG. 5.18 Large Chord B22 Cascade Principal Dimensions

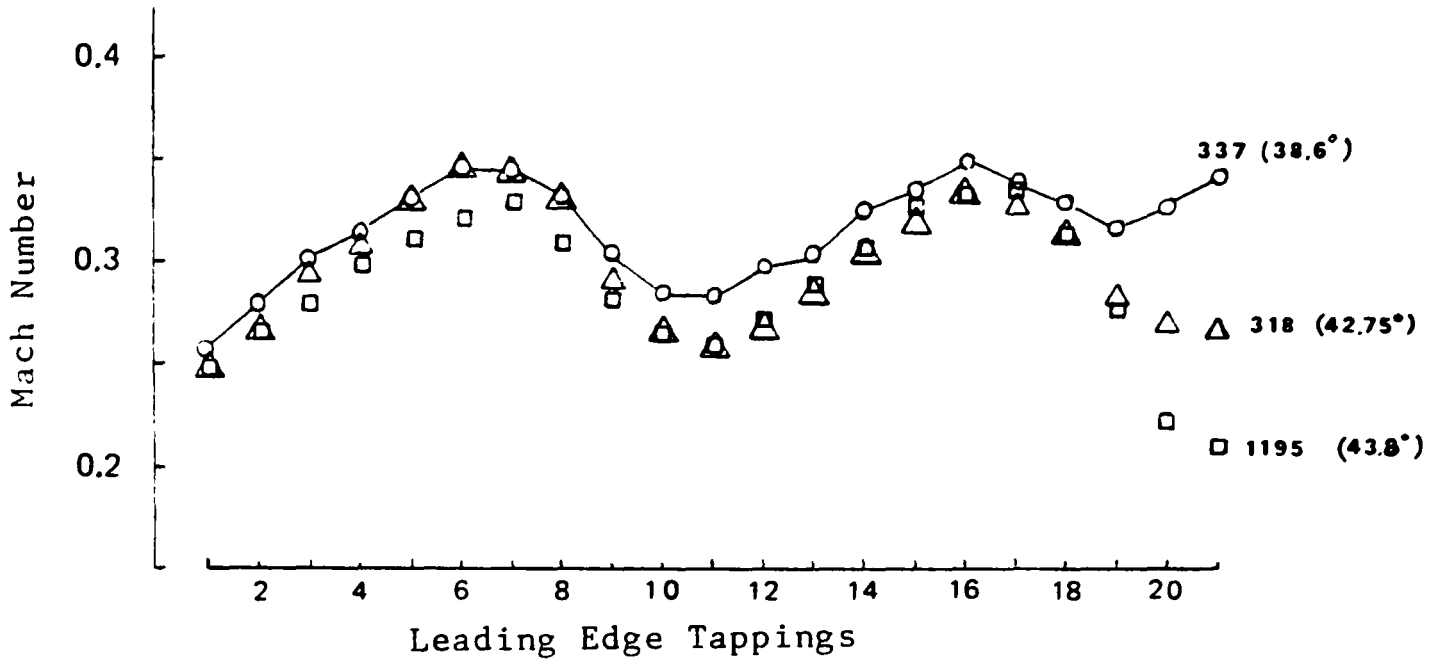

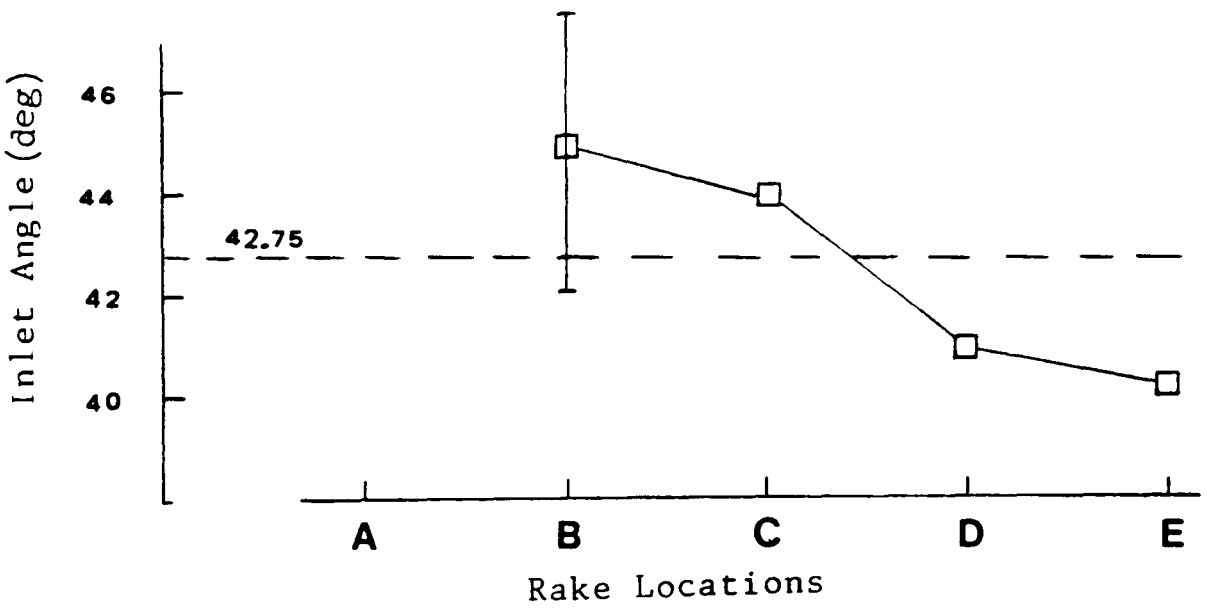

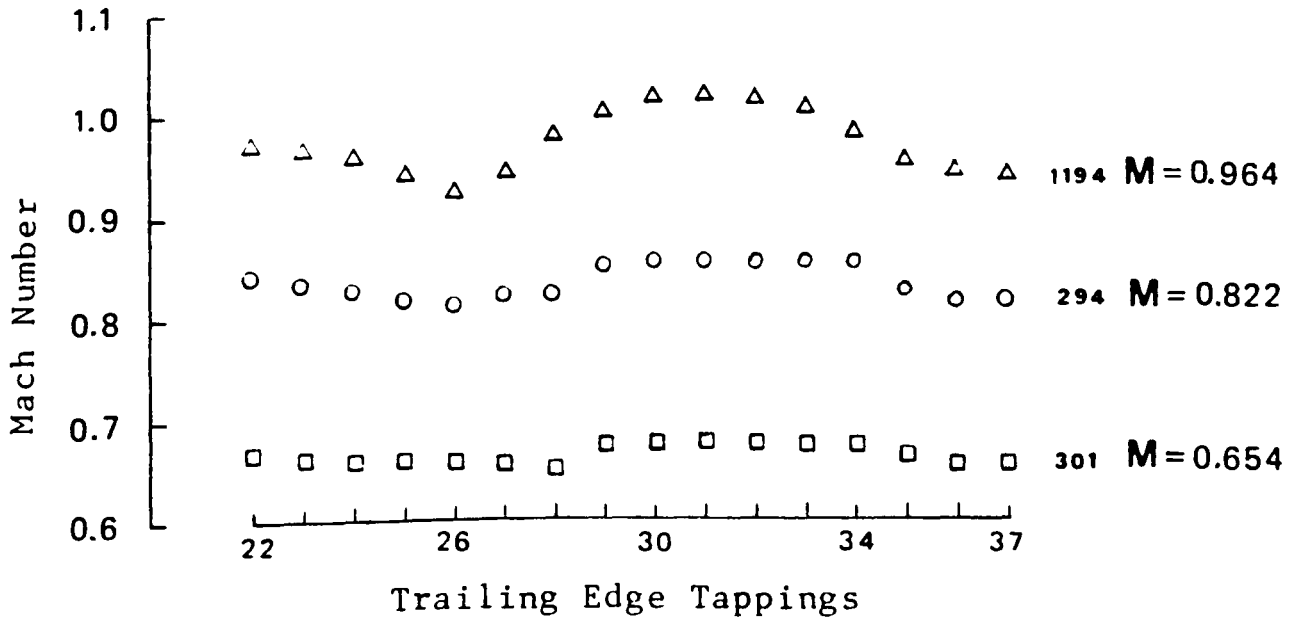

FIG.5.19 Upstream/Downstream Periodicity LCH B22

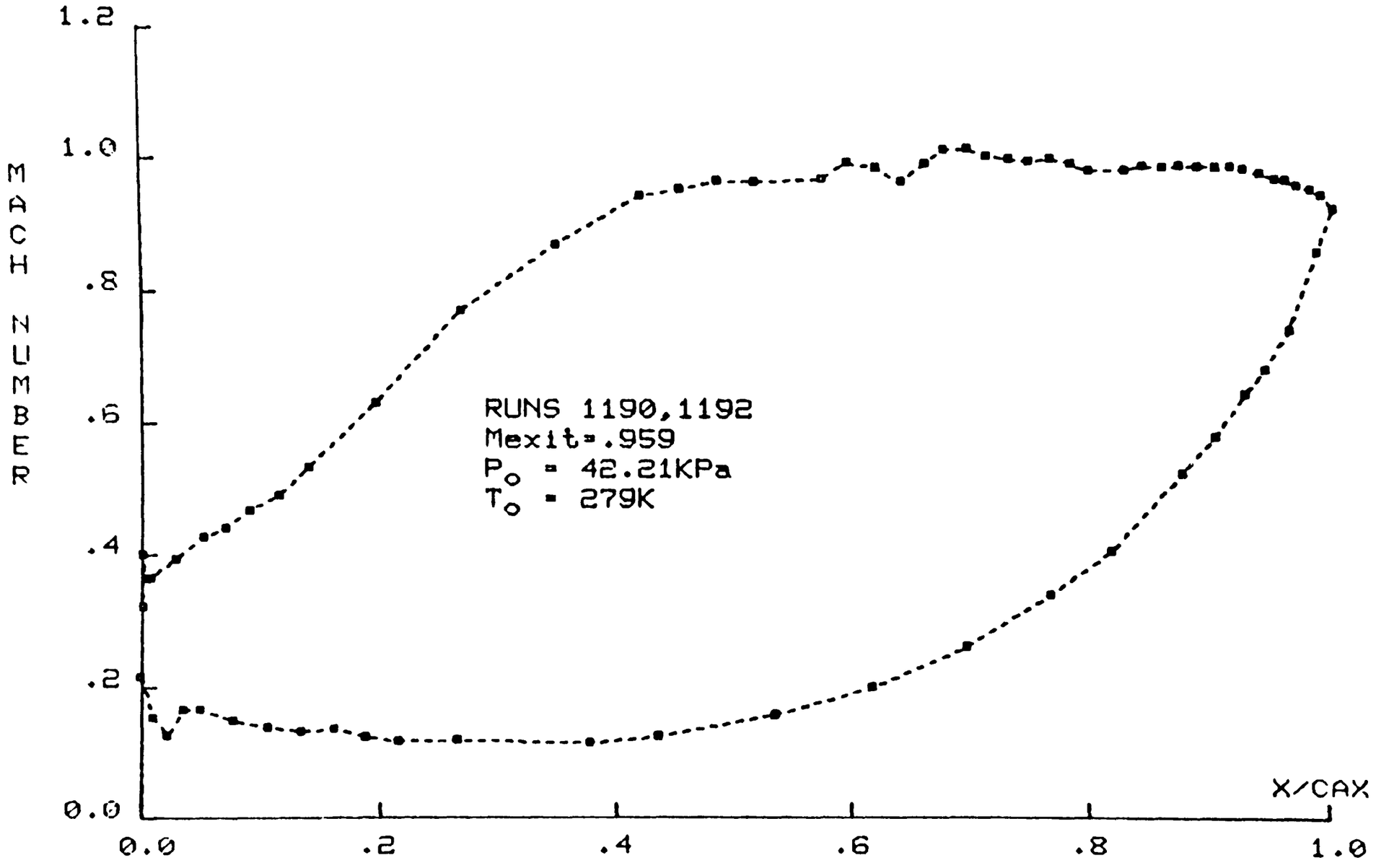

FIG. 5.20a LARGE CHORD B22 RESULTS AT M DES (0.96)

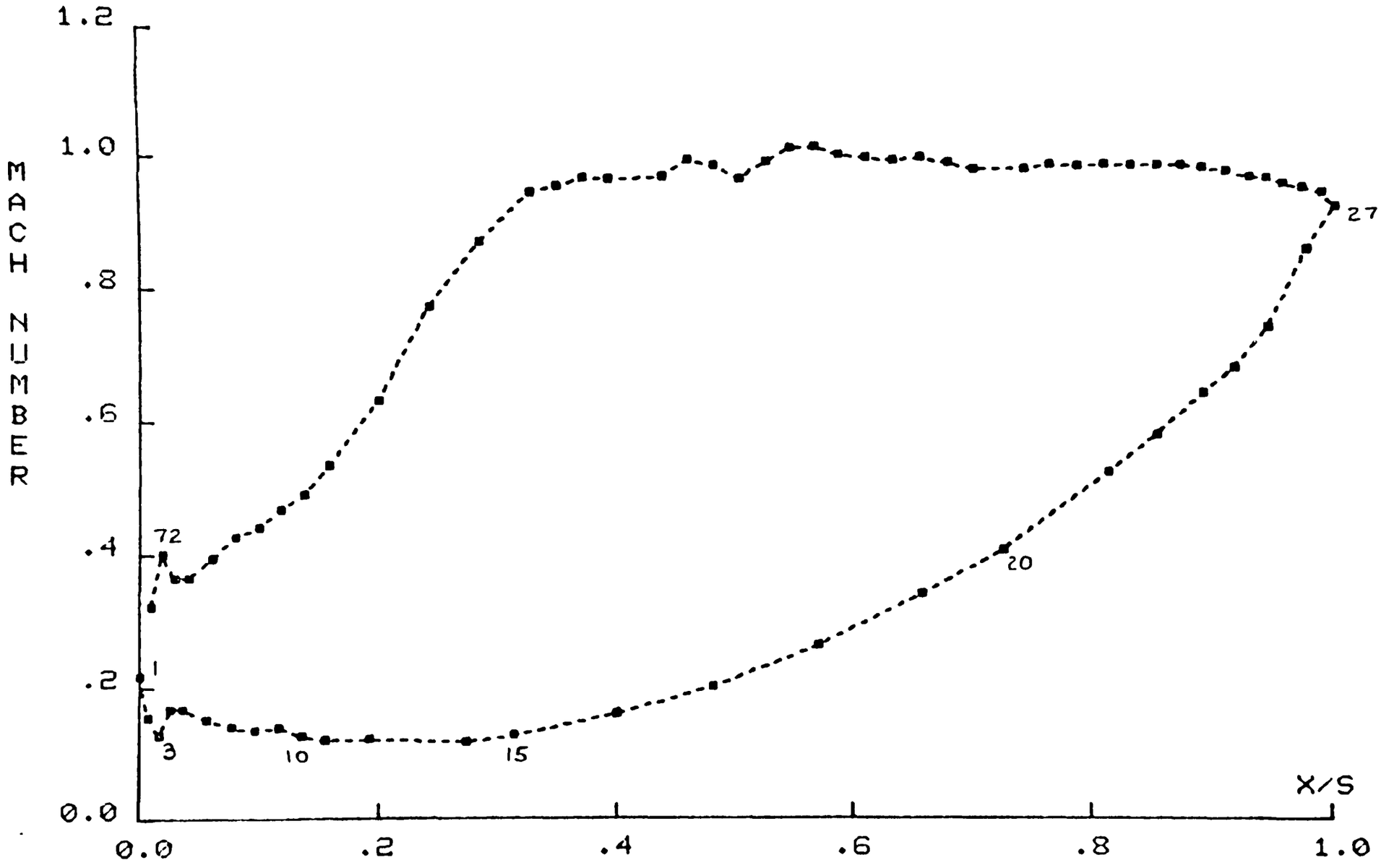

FIG. 5.20b LARGE CHORD B22 RESULTS AT MDES (0.96)

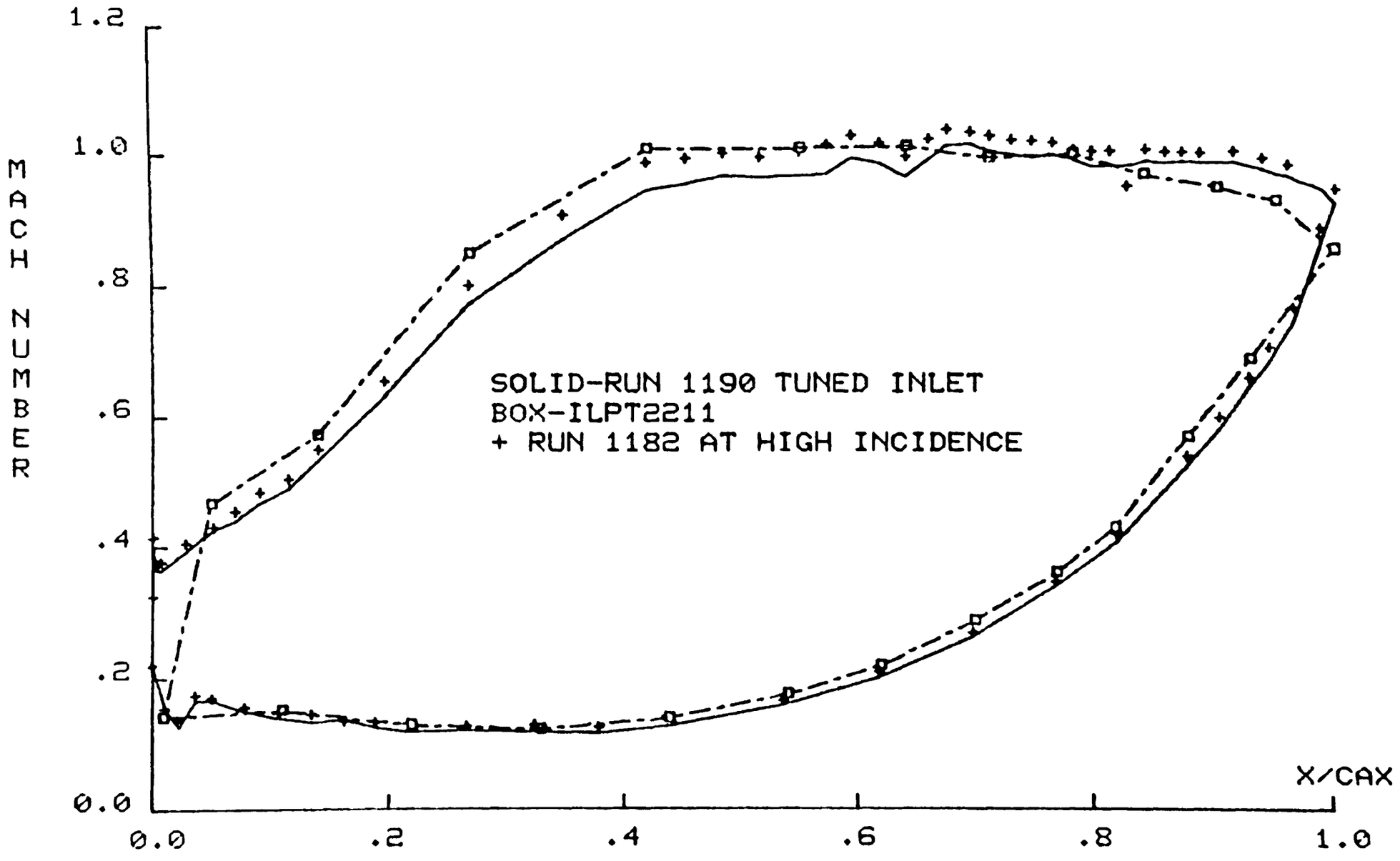

FIG. 5.21 APPARENT CHANGE IN THROAT POSITION DUE TO INCIDENCE

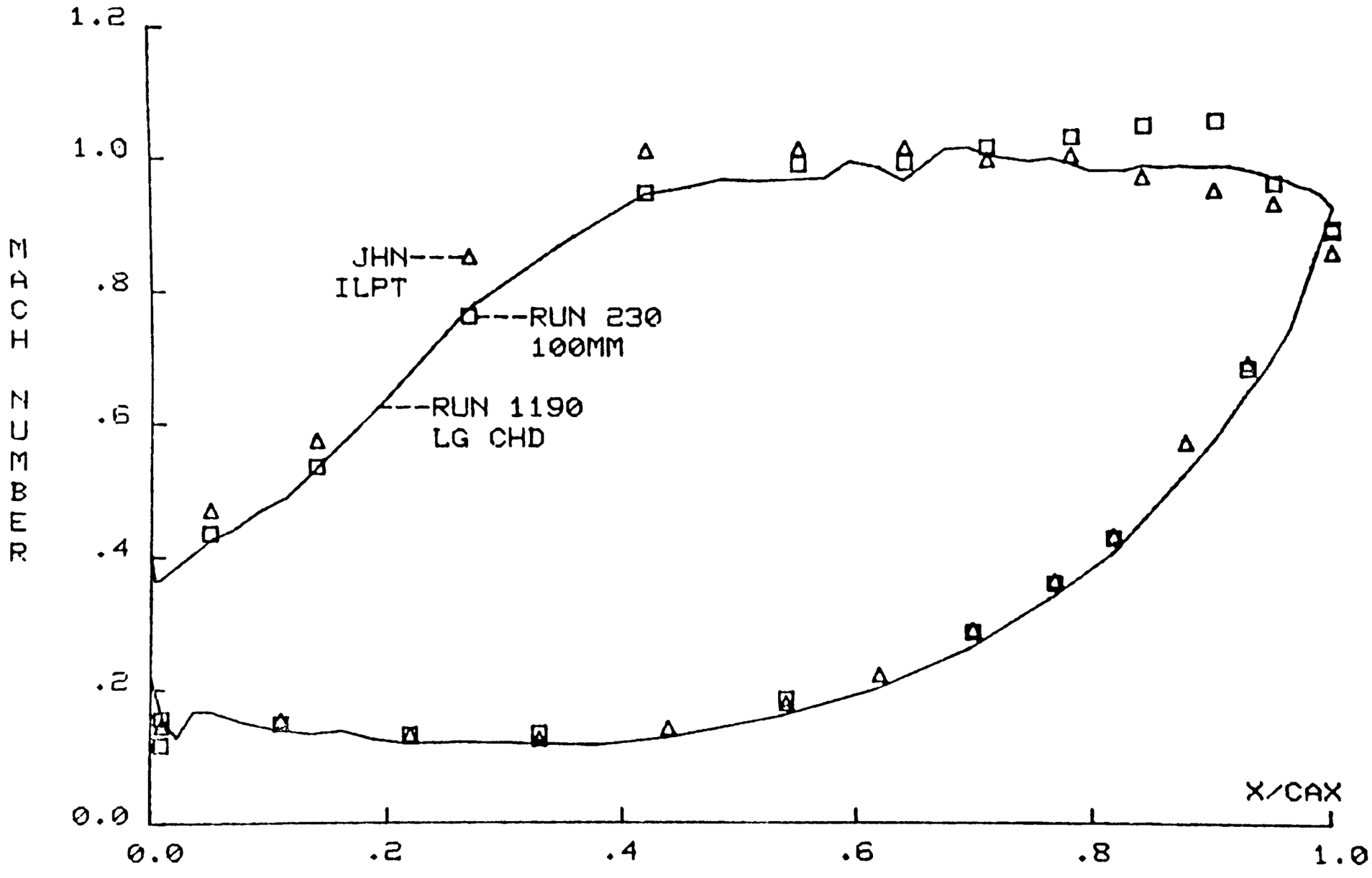

FIG. 5.22 B22 DATA FROM THREE CASCADES

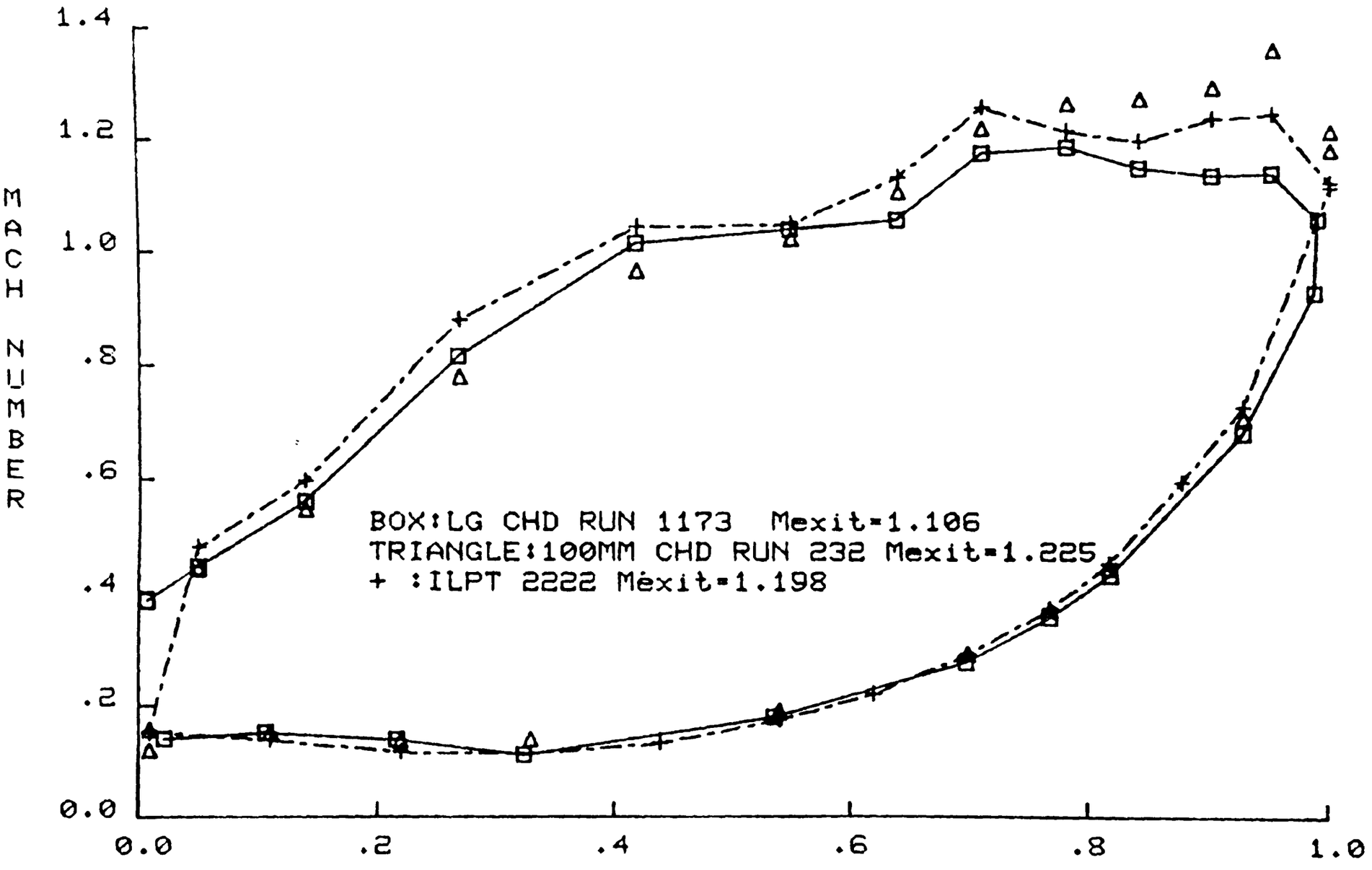

FIG.5.23 THREE CASCADES AT Re DES, HIGH EXIT MACH NUMBER

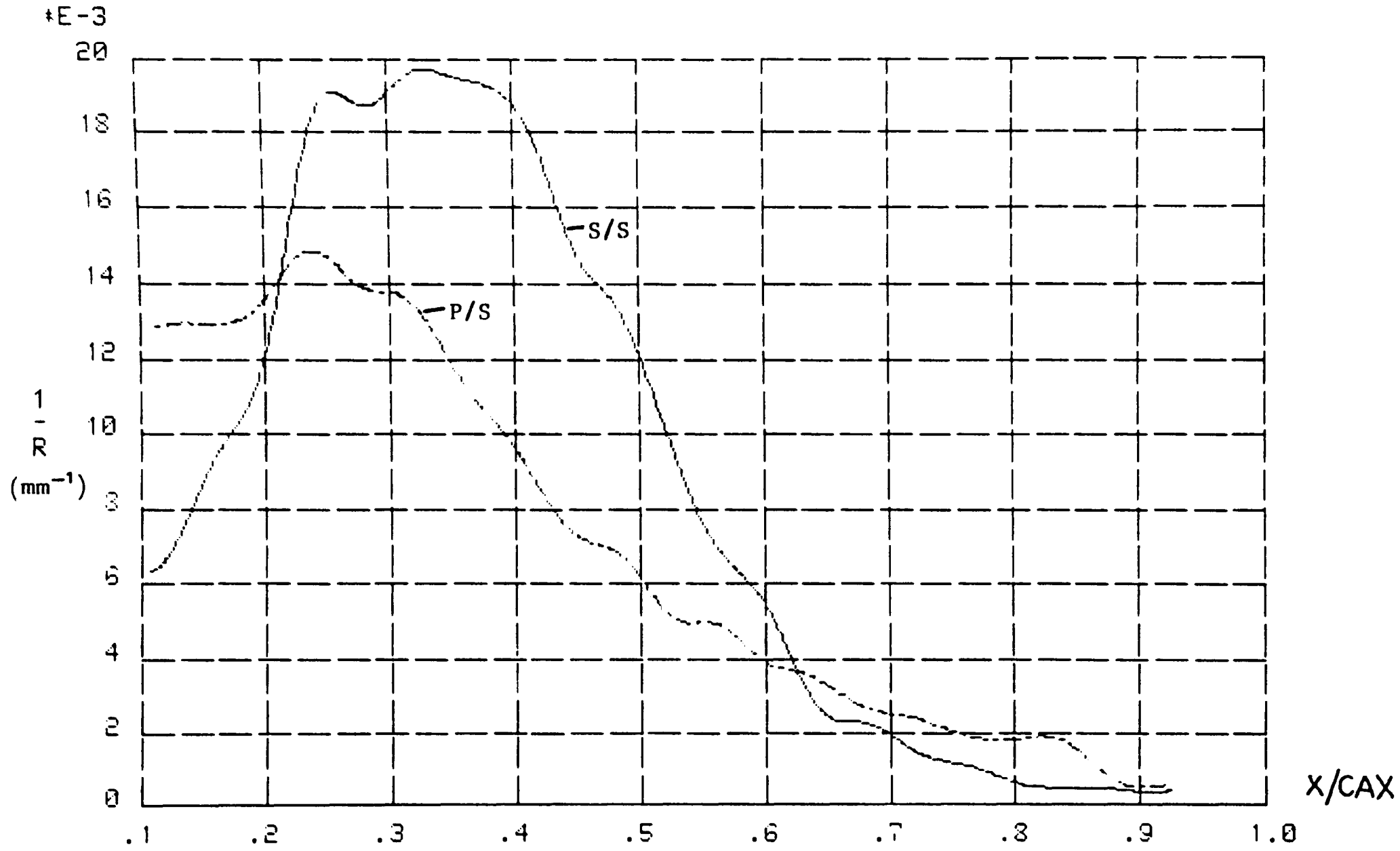

FIG.5.24 B22 Large Chord Curvature

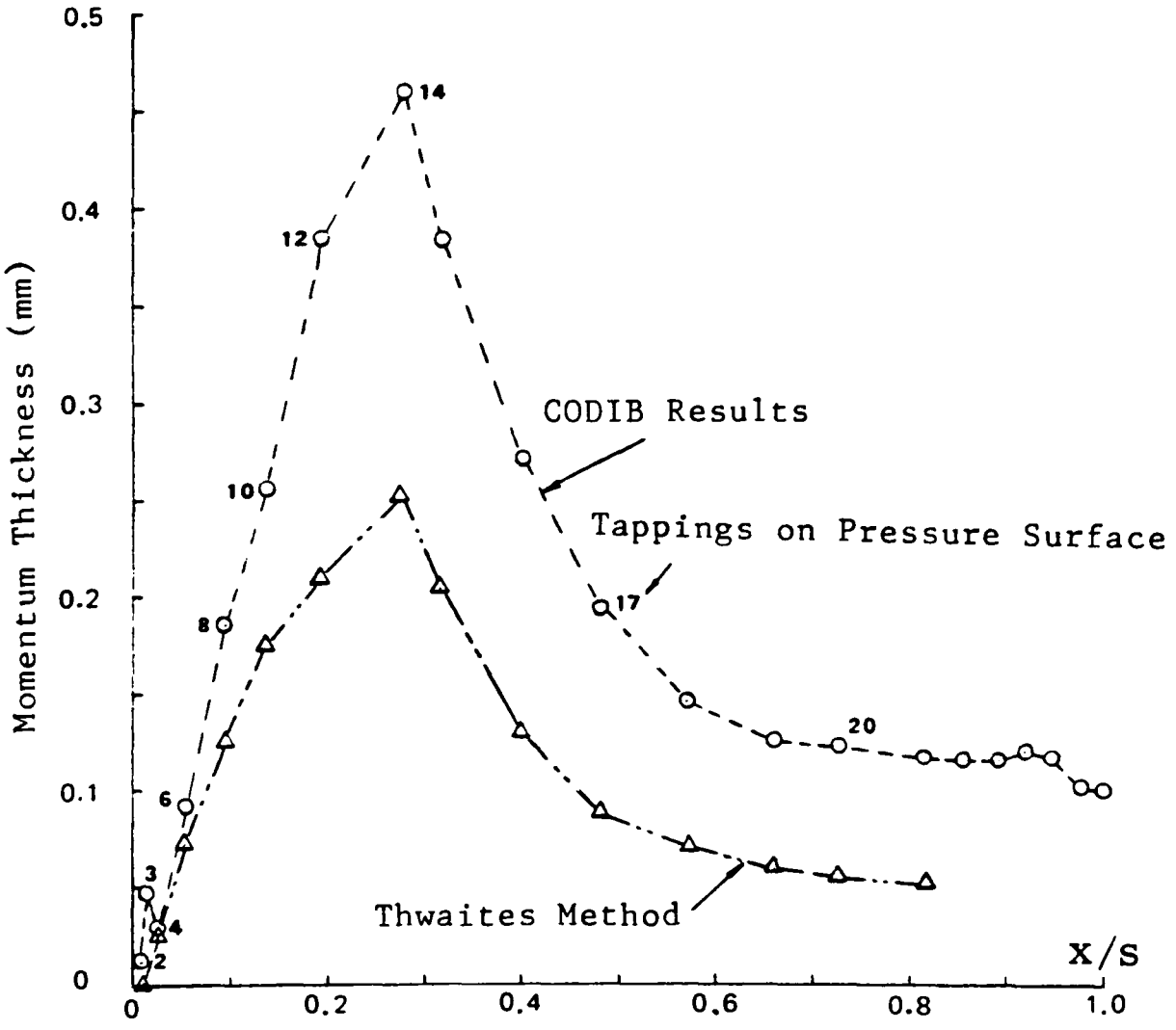

FIG. 5.25 Computed Momentum Thickness on Large-Chord B22 Blade at M_{des} (0.96)

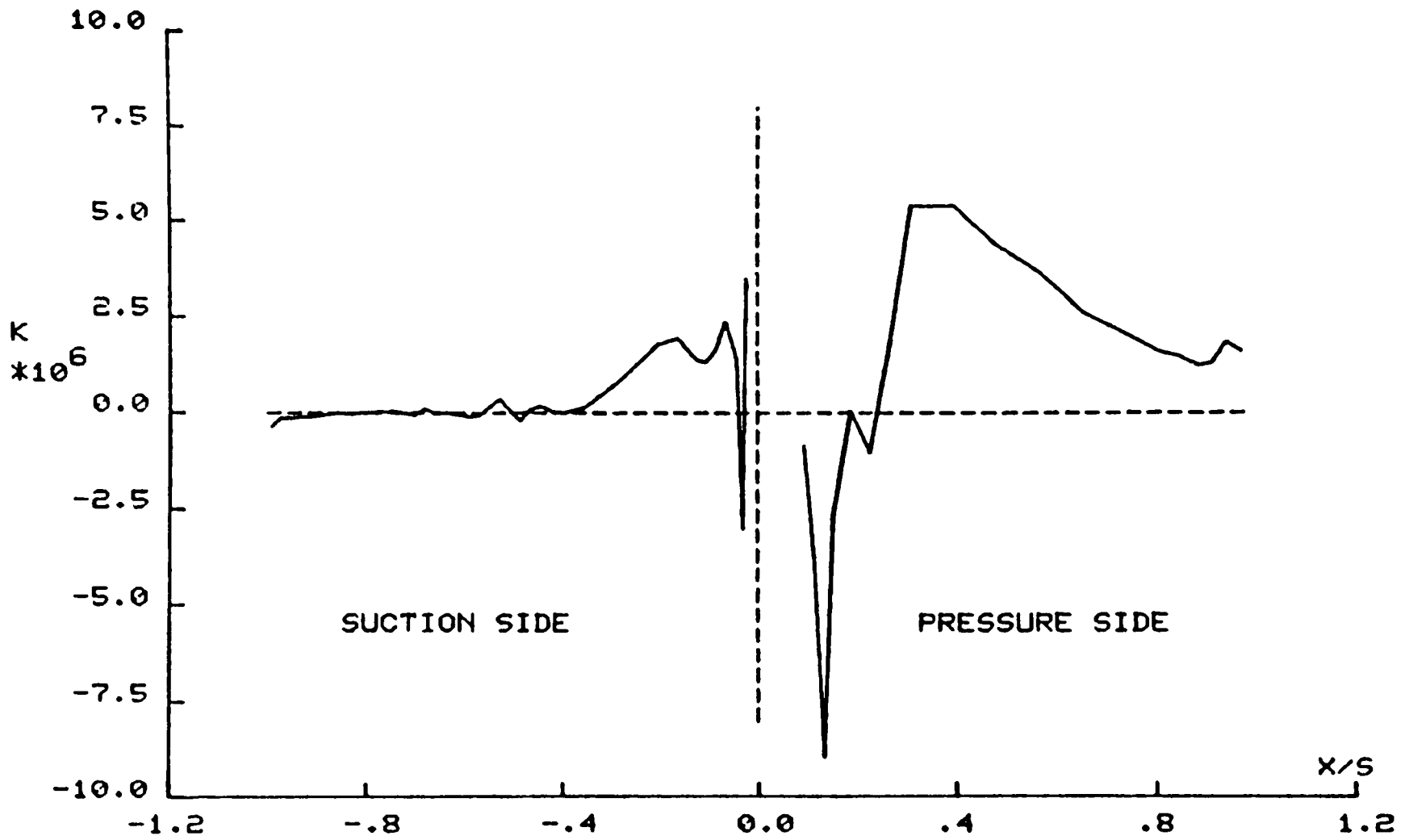

FIG.5.26 B22 ACCELERATION PARAMETER

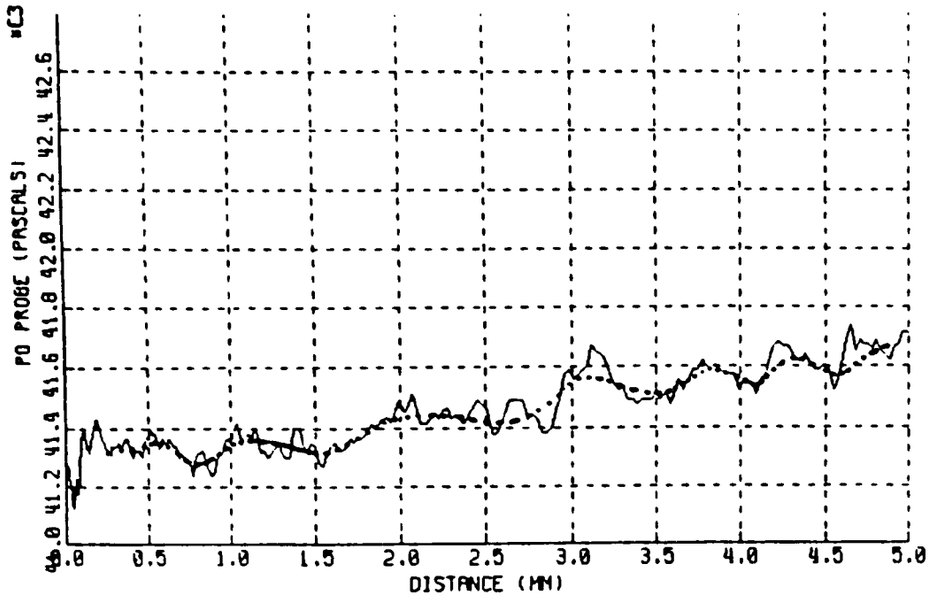

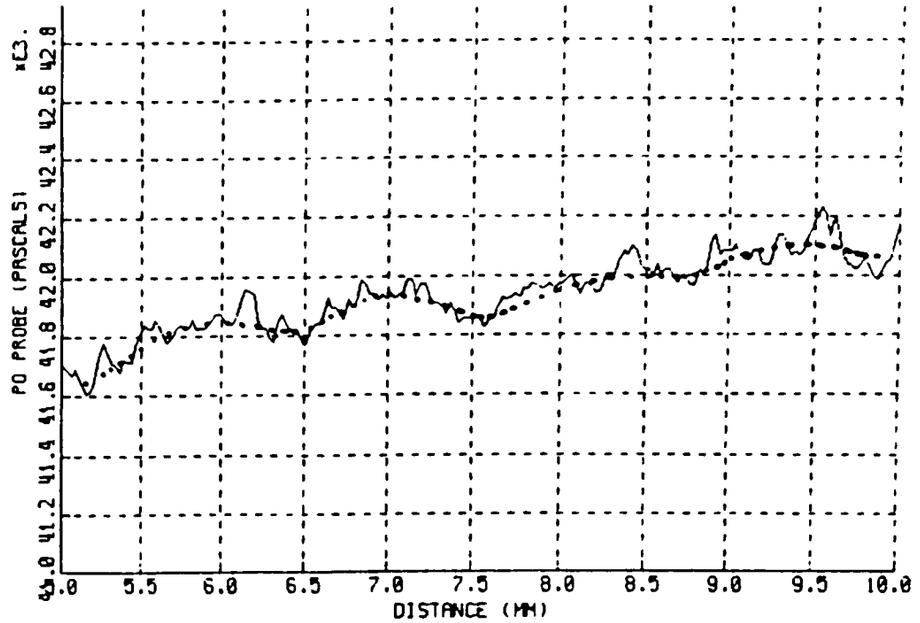

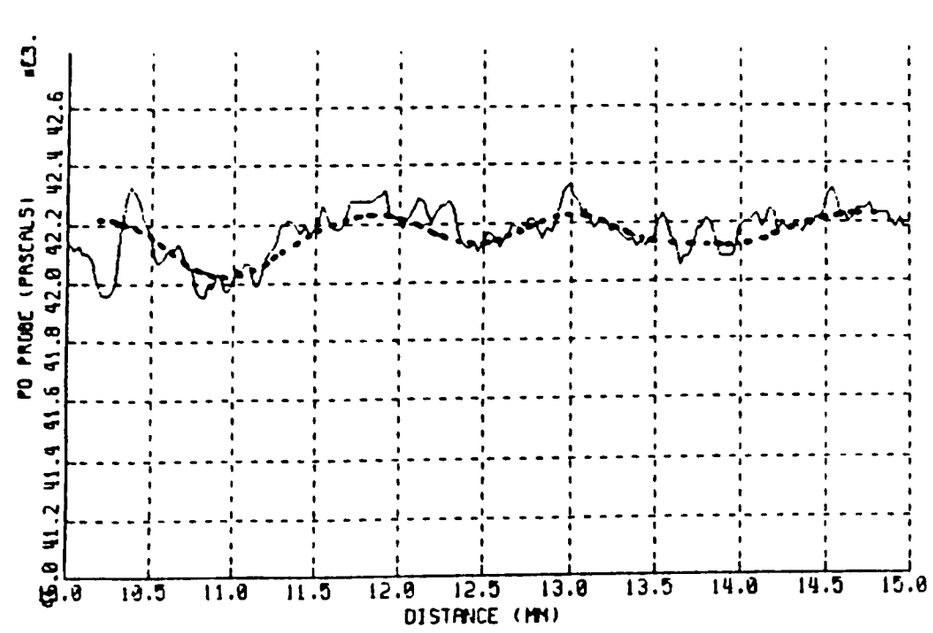

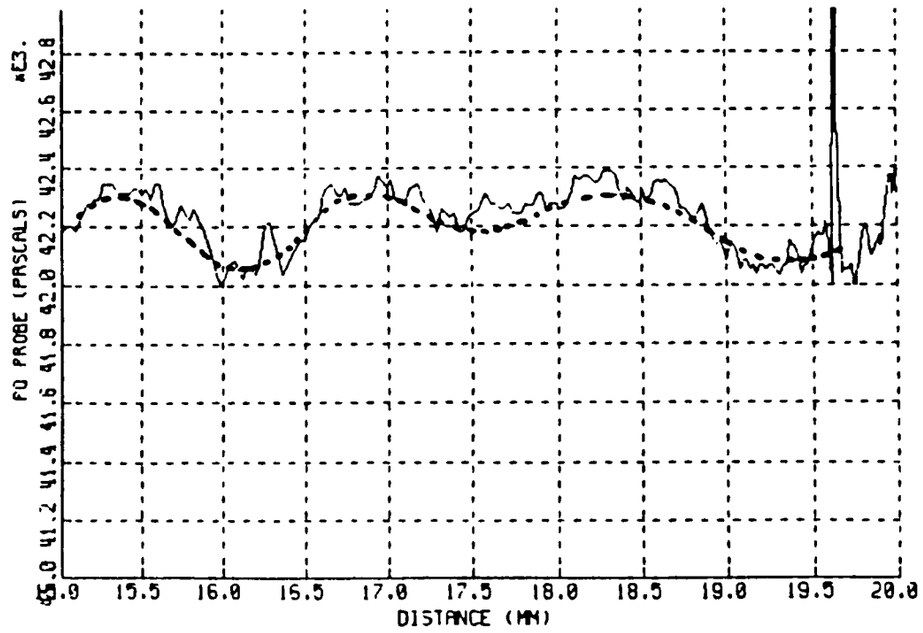

FIG. 5.27 Spanwise Boundary Layer on Pressure Surface of LCH B22 at x/s=0.44

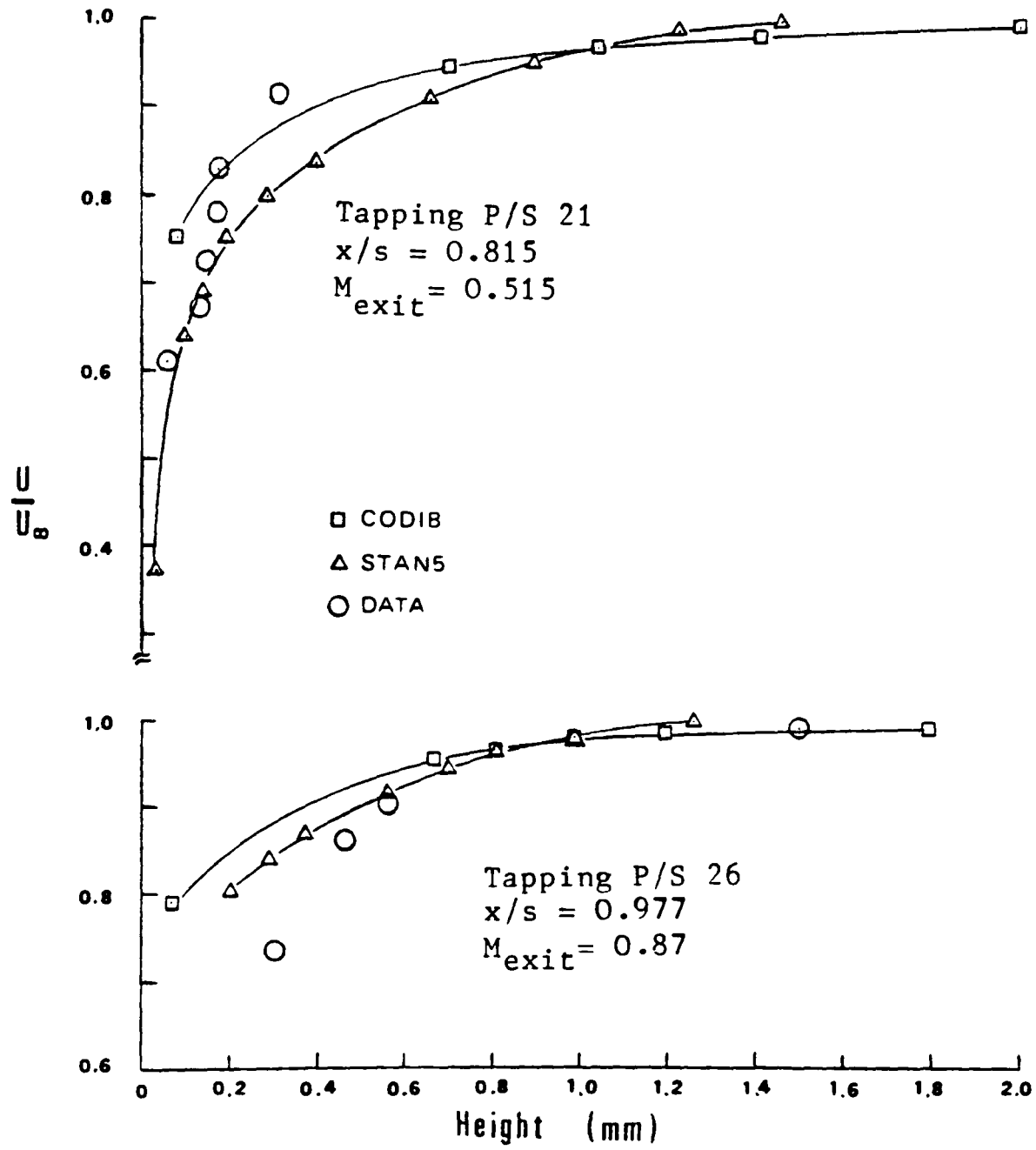

FIG. 5.28 Preliminary B22 Pressure Surface Data Compared with Theoretical Results

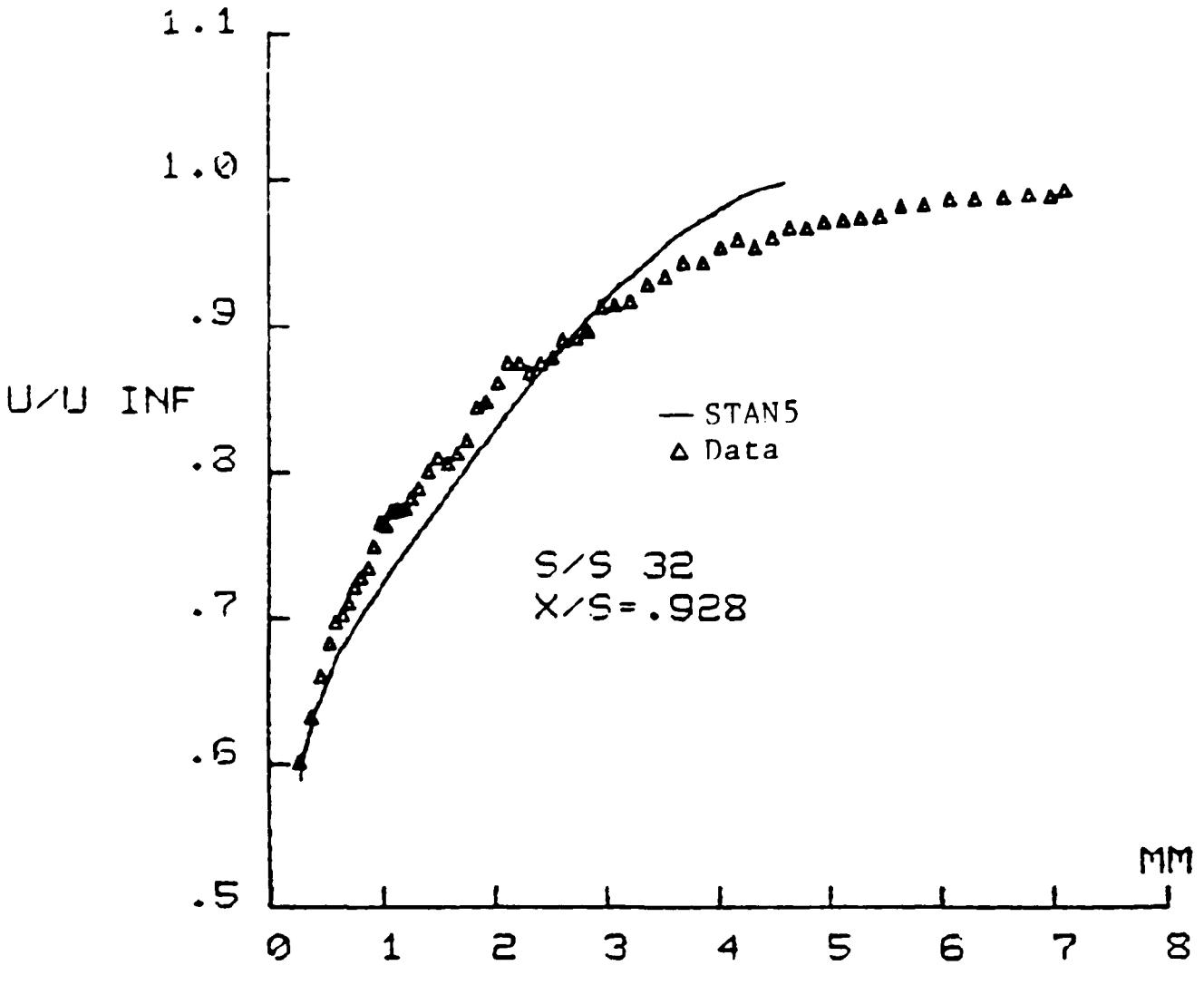

FIG. 5.29 PROFILE DATA VS STAN5

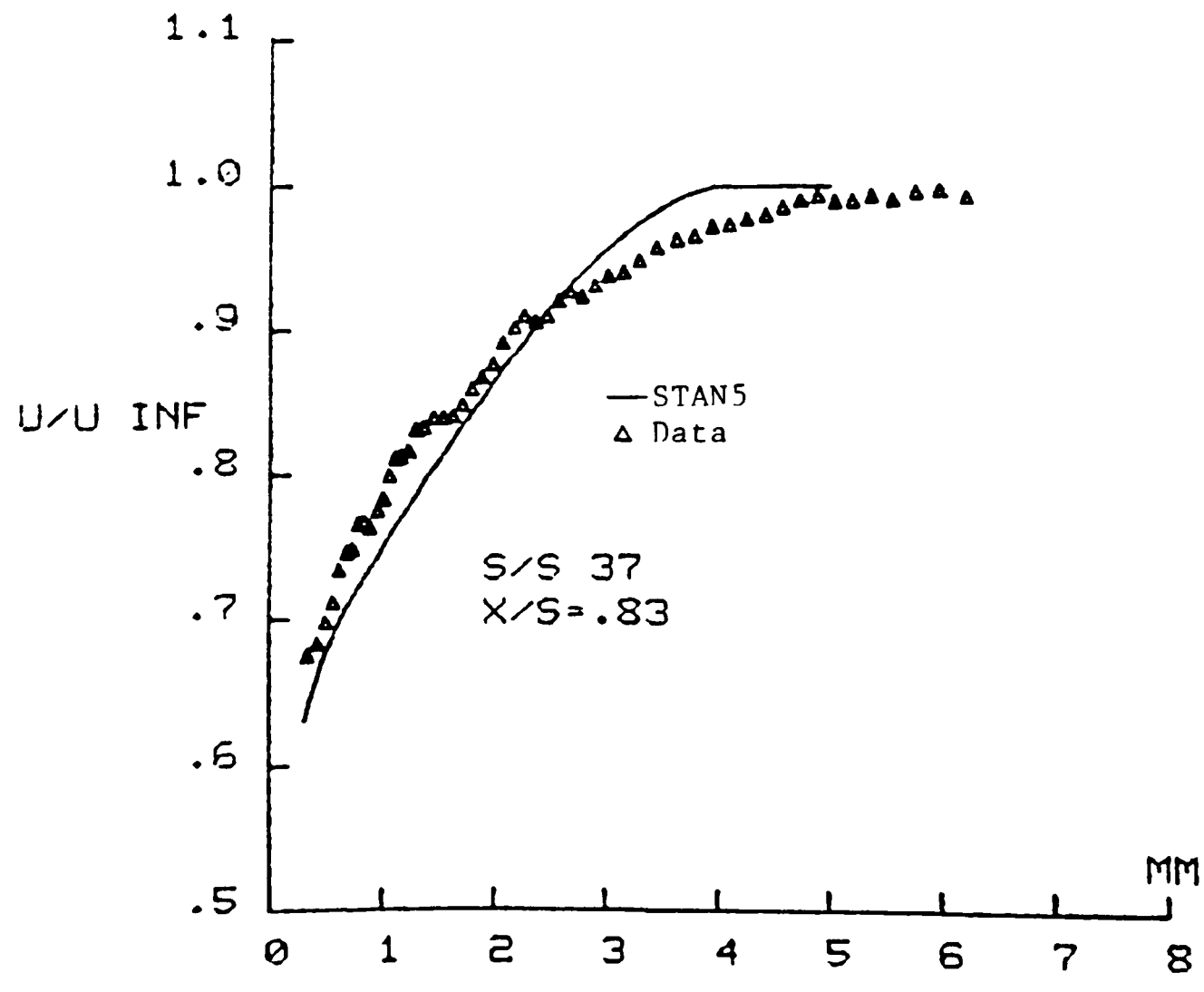

FIG. 5.30 PROFILE DATA VS STAN5

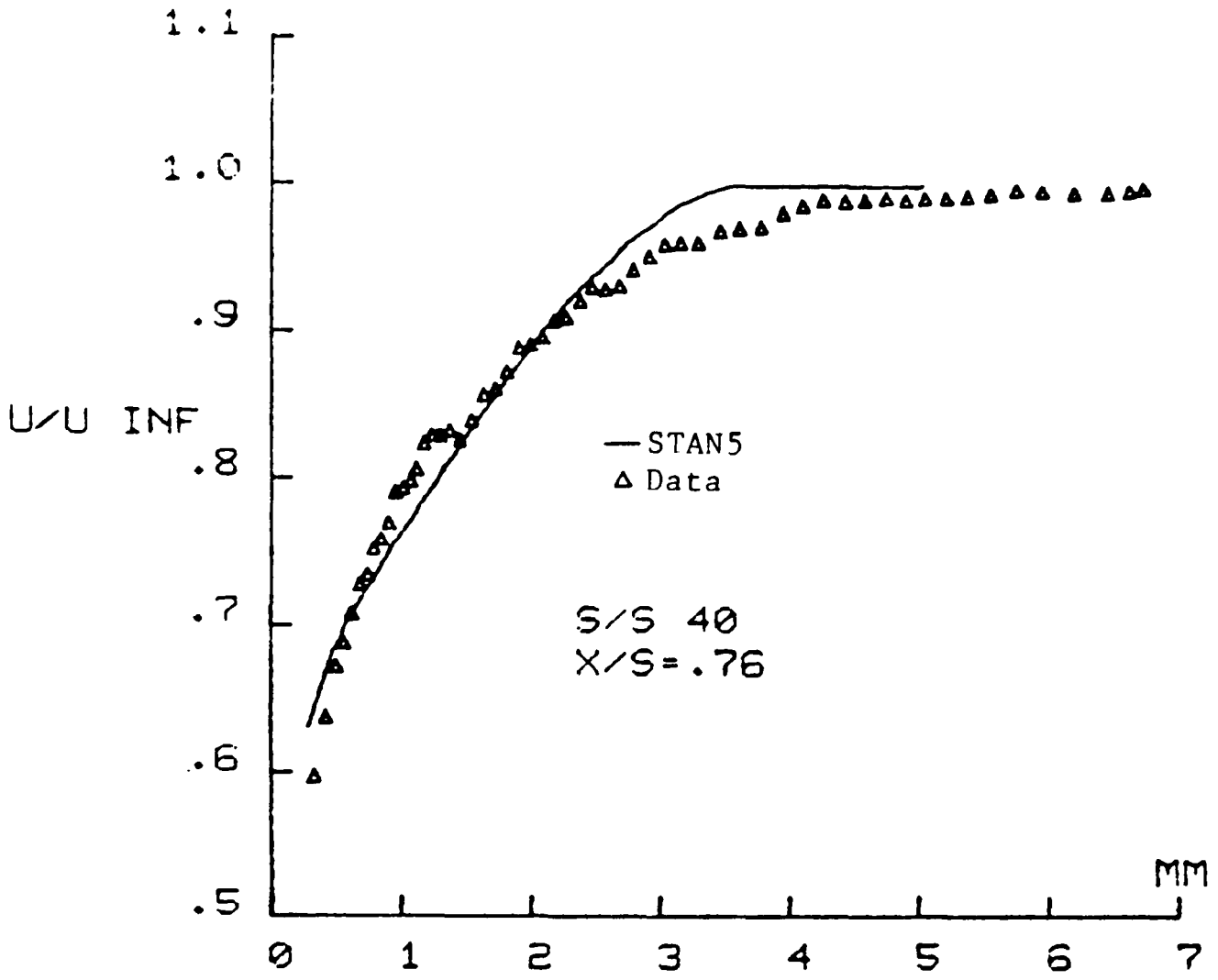

FIG. 5.31 PROFILE DATA VS STAN5

FIG. 5.32 PROFILE DATA VS STAN5

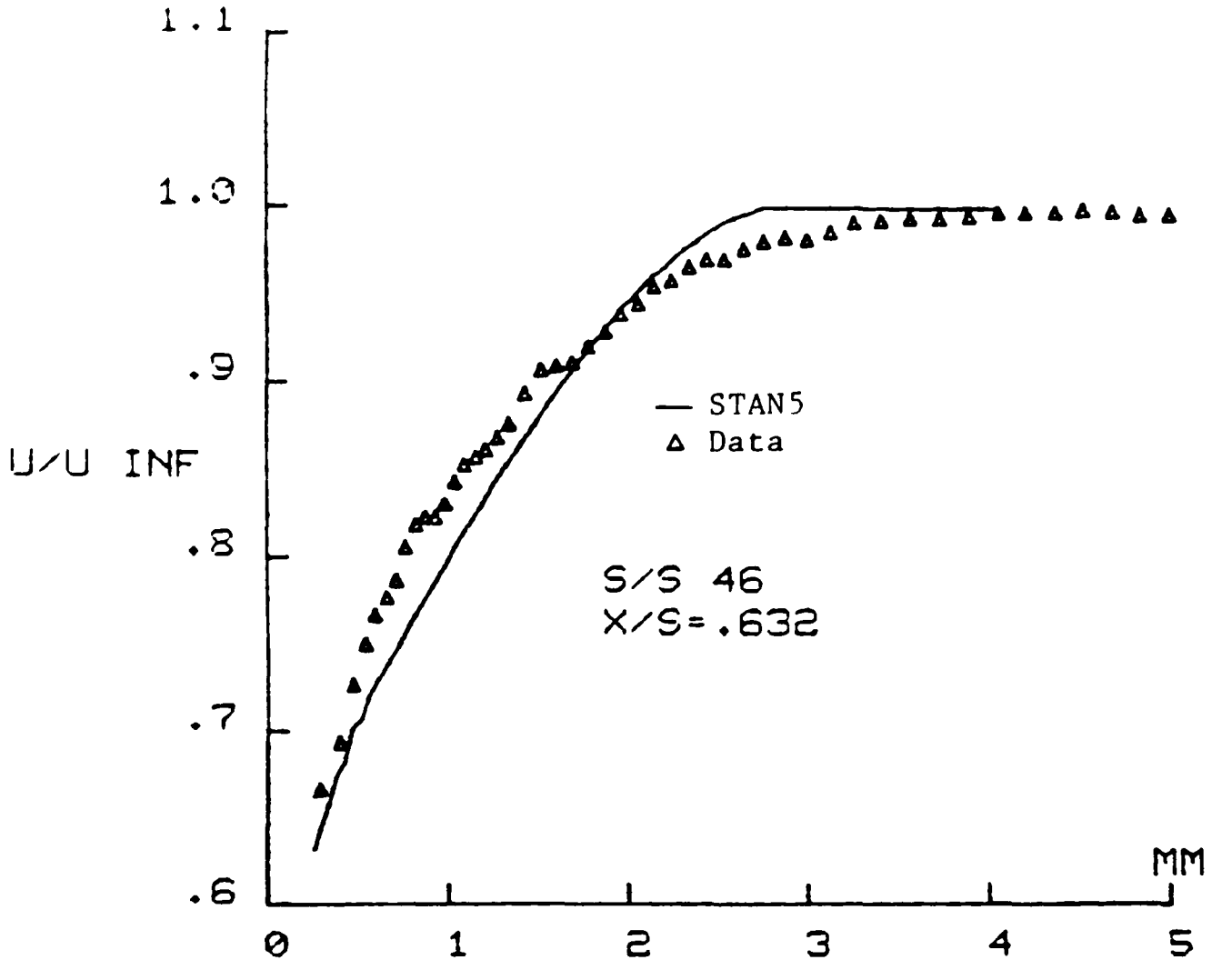

FIG. 5.33 PROFILE DATA VS STAN5

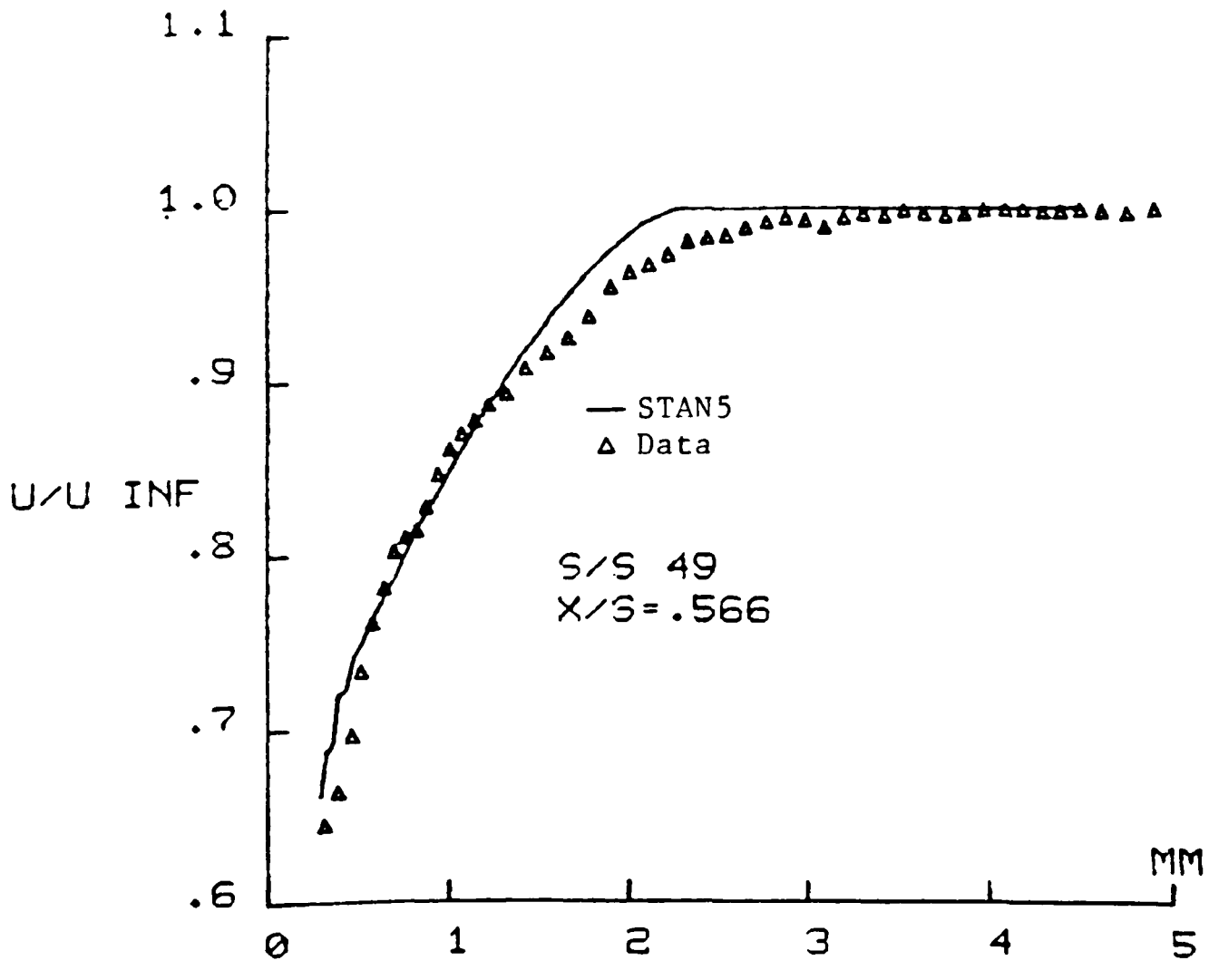

FIG. 5.34 PROFILE DATA VS STAN5

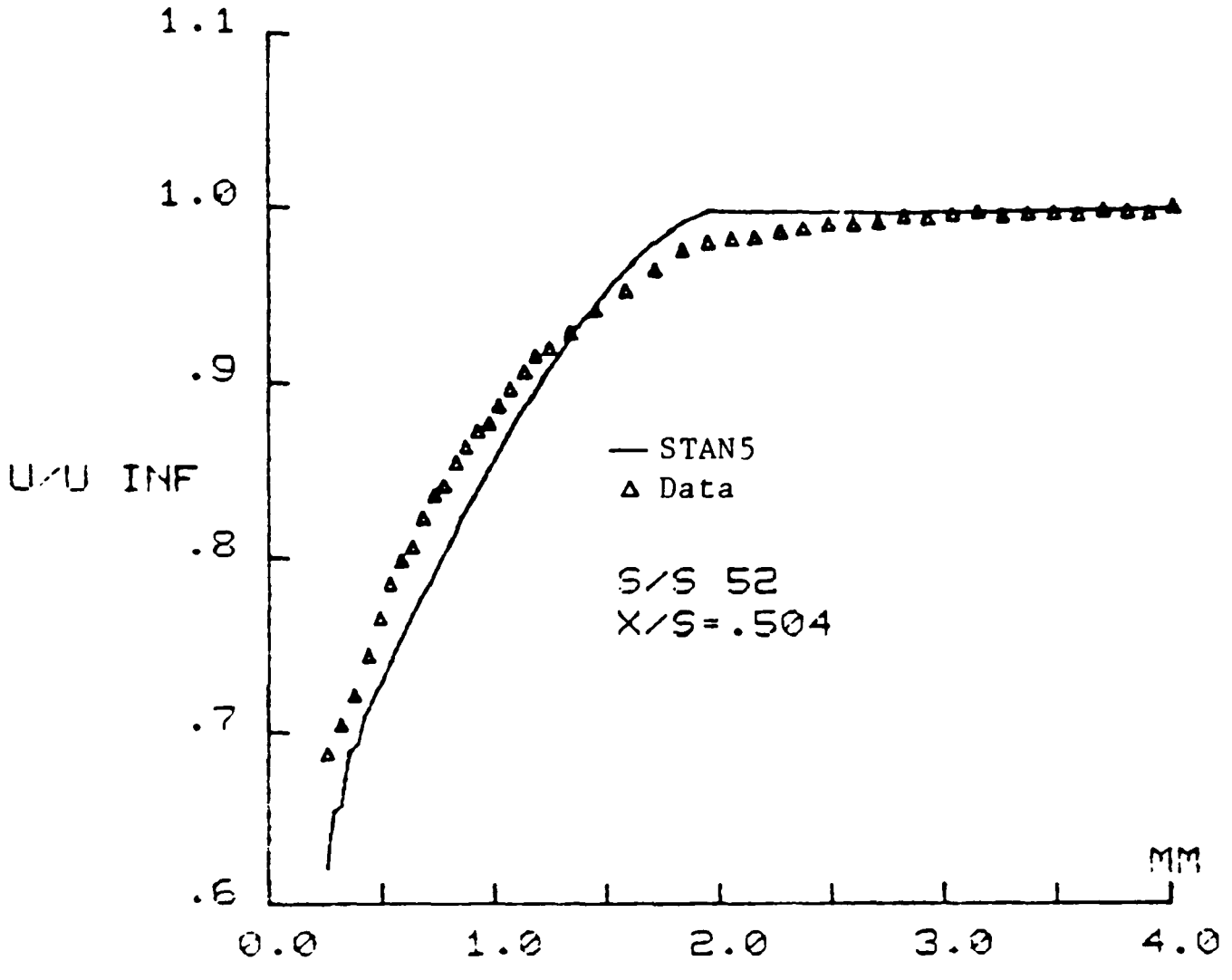

FIG. 5.35 PROFILE DATA VS STAN5

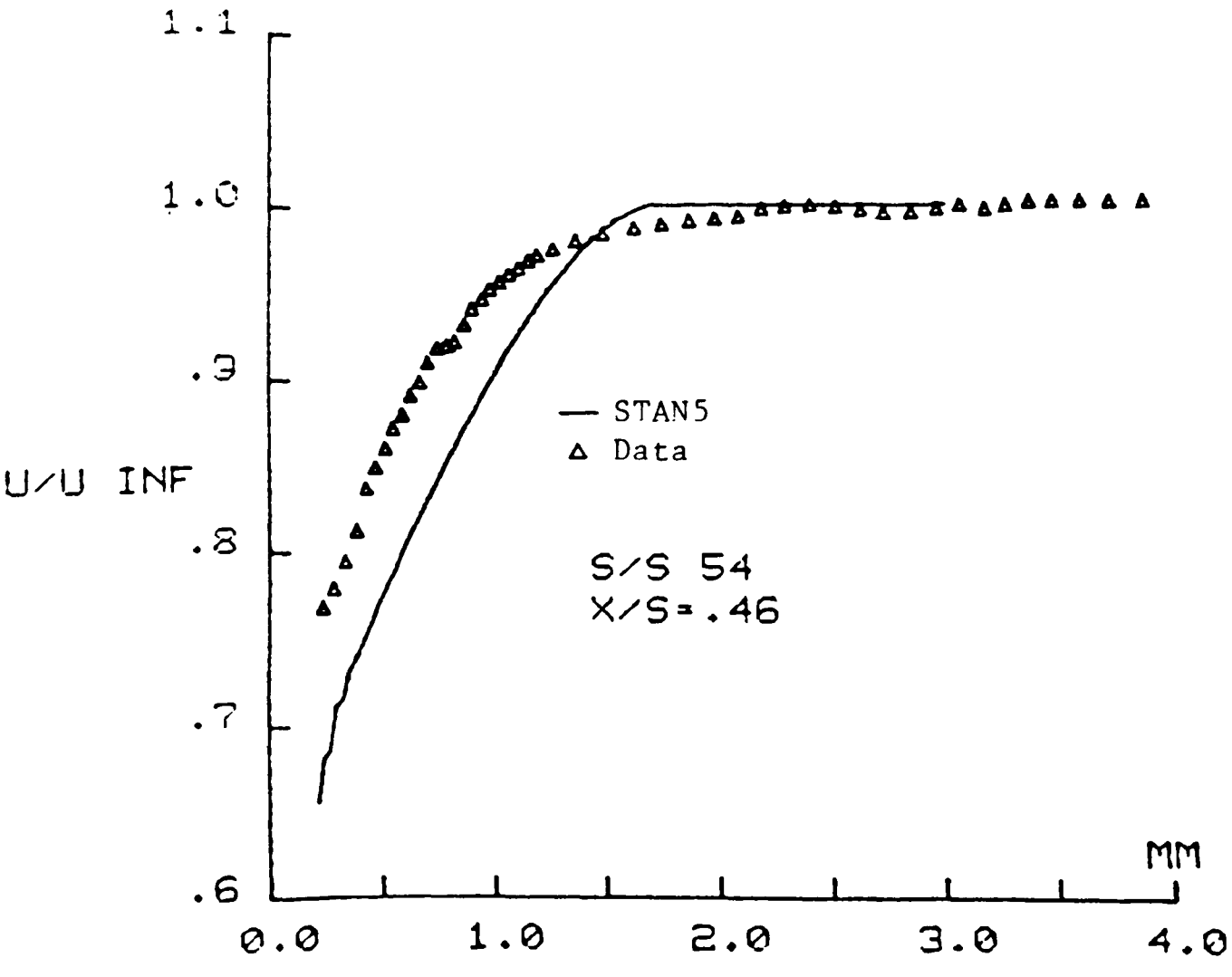

FIG. 5.36 PROFILE DATA VS STAN5

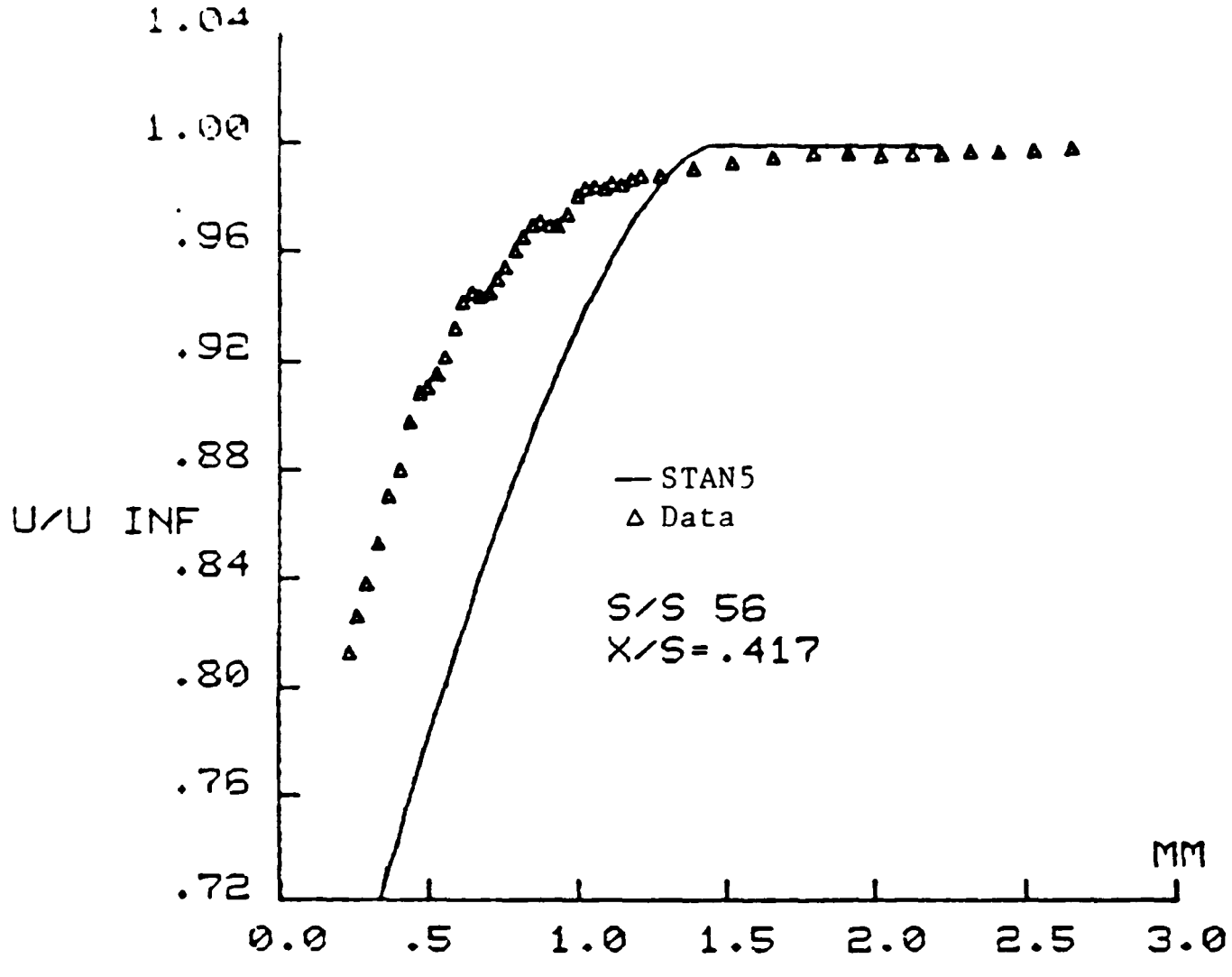

FIG. 5.37 PROFILE DATA VS STAN5

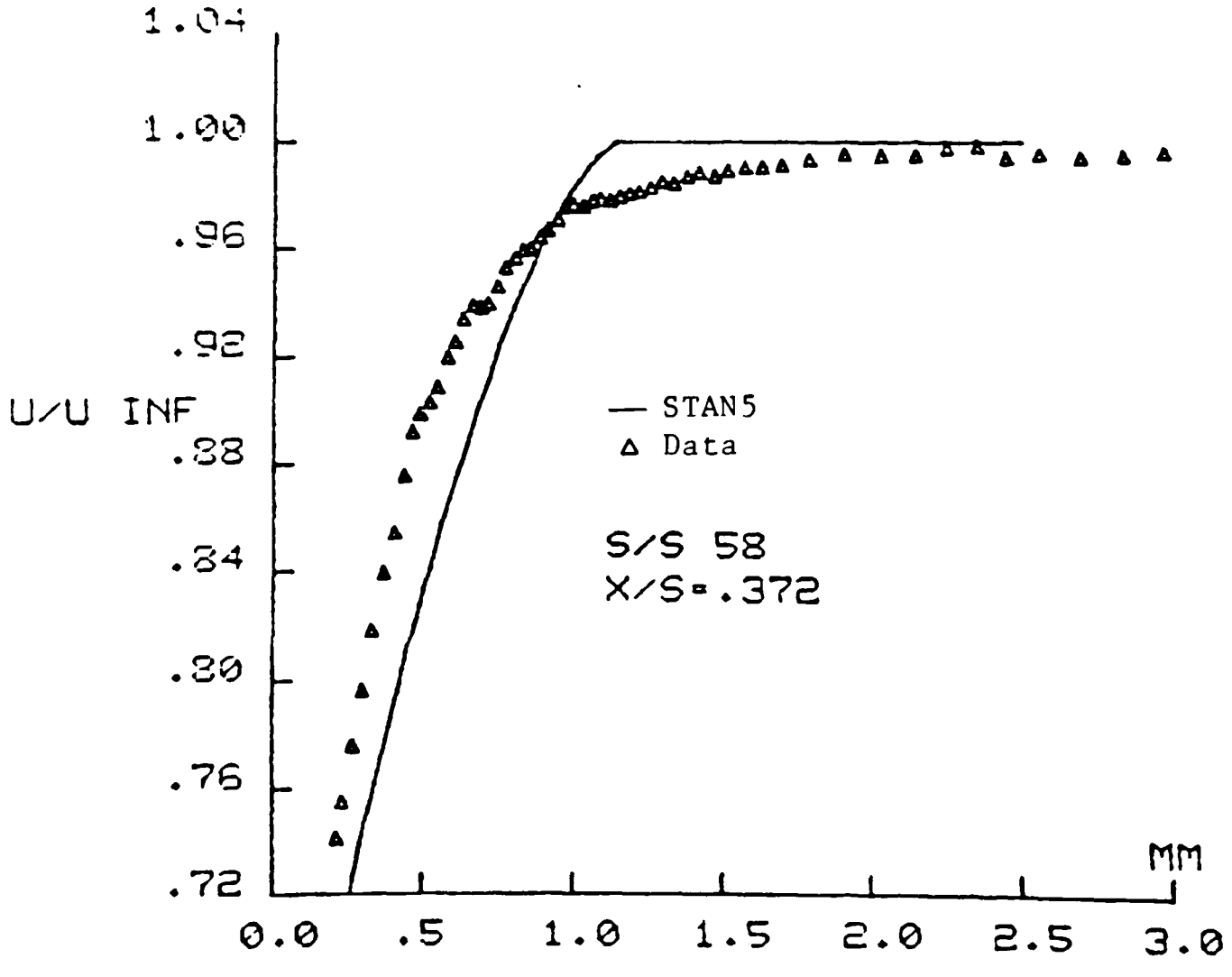

FIG. 5.38 PROFILE DATA VS STAN5

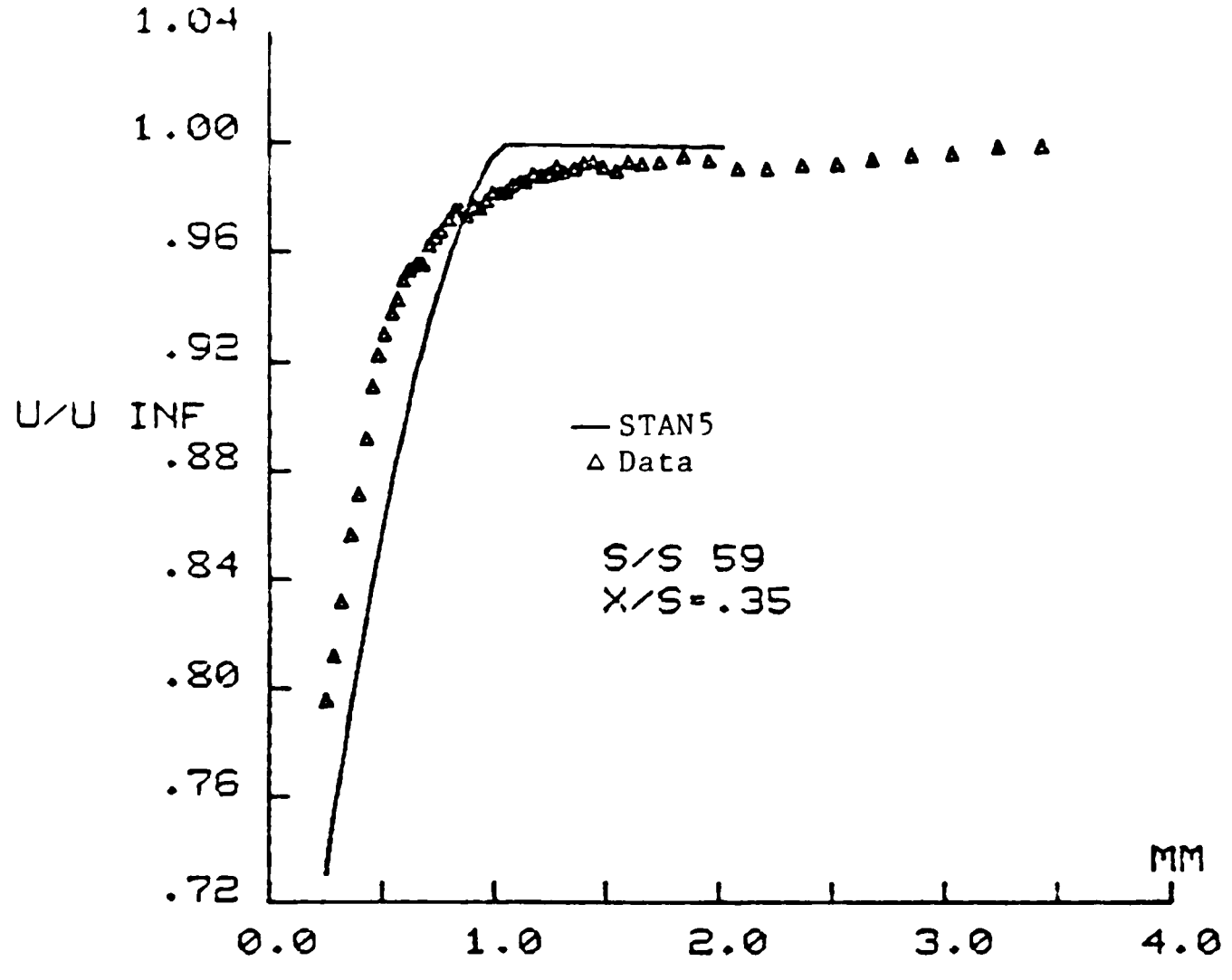

FIG. 5.39 PROFILE DATA VS STAN5

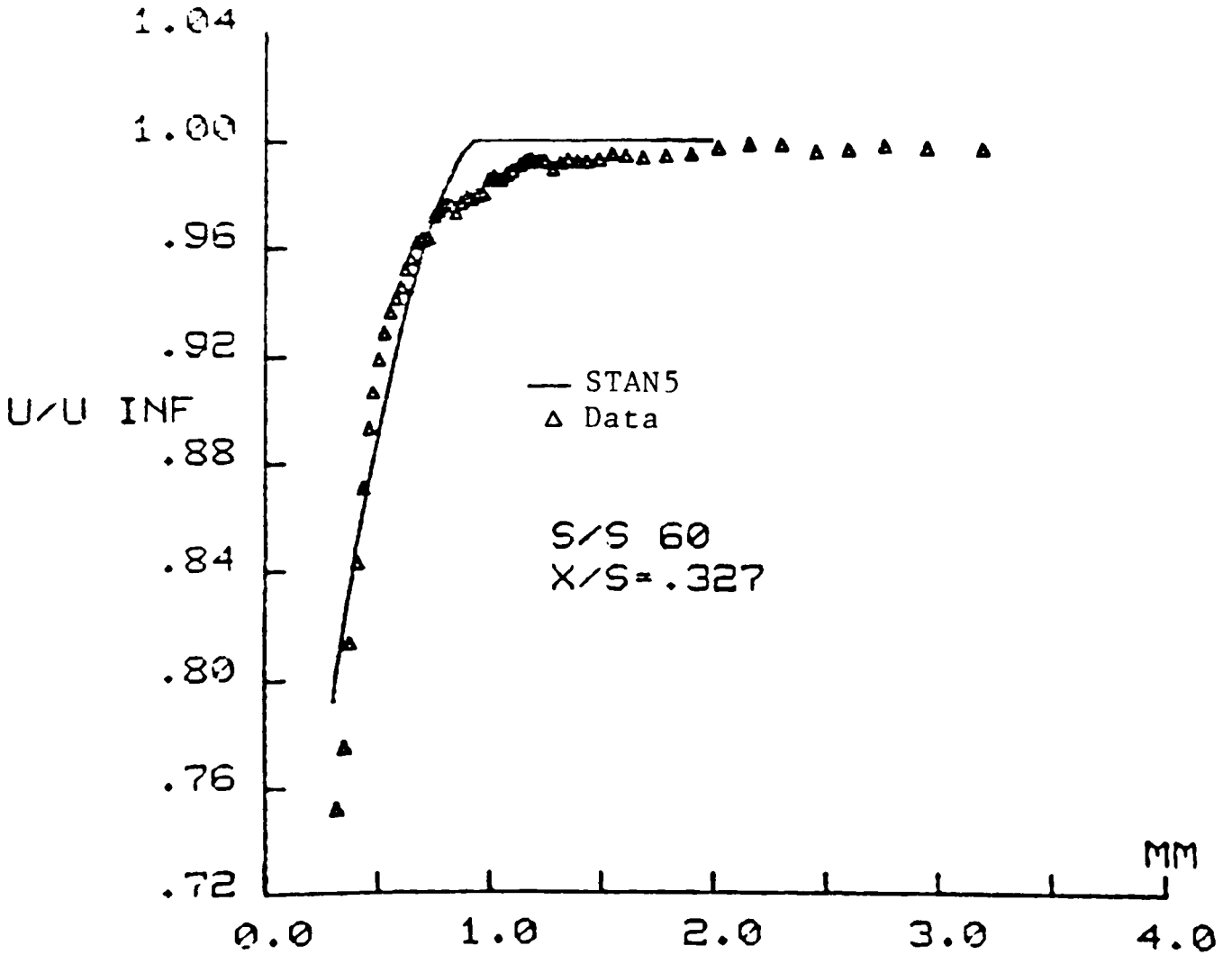

FIG. 5.40 PROFILE DATA VS STAN5

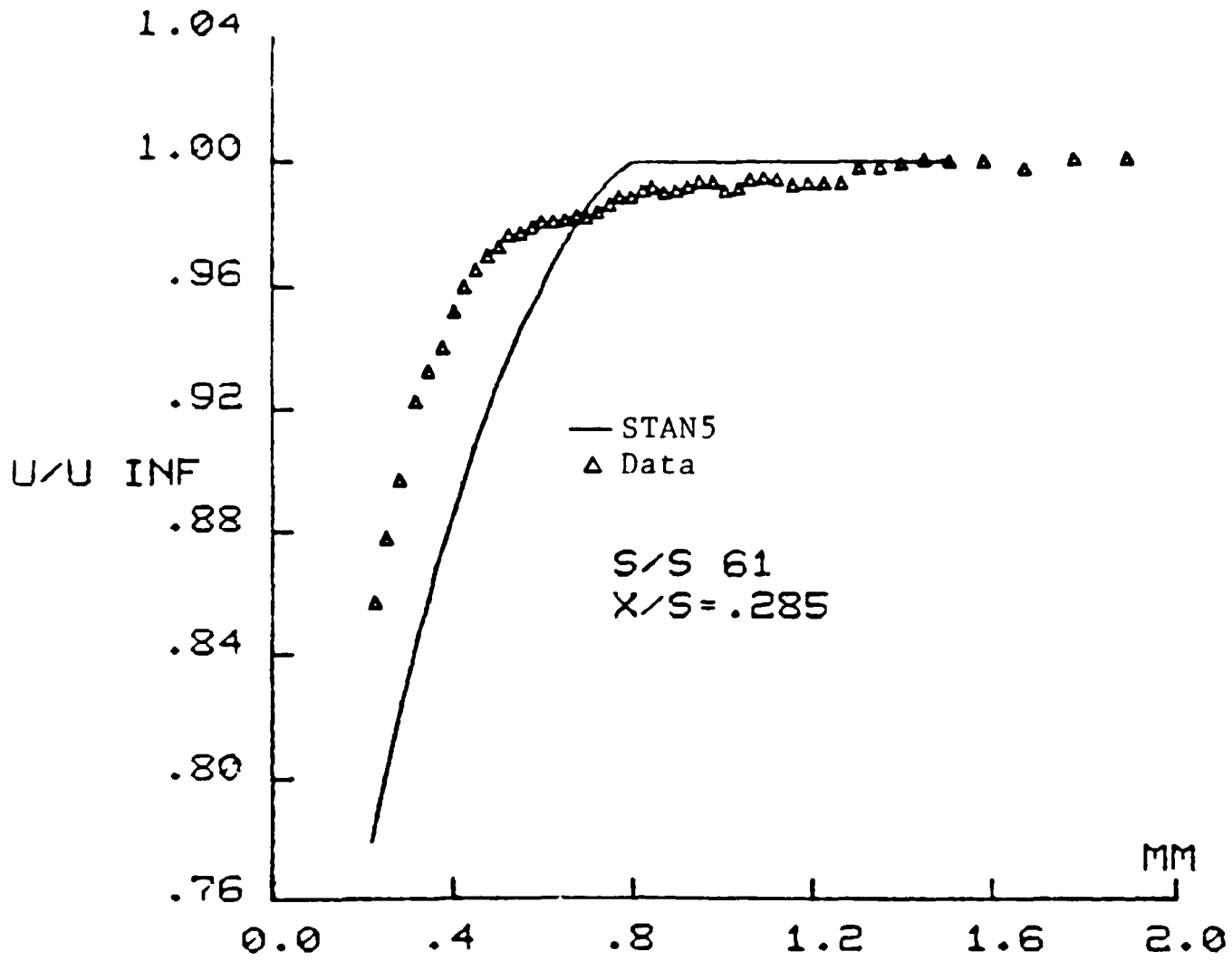

FIG. 5.41 PROFILE DATA VS STAN5

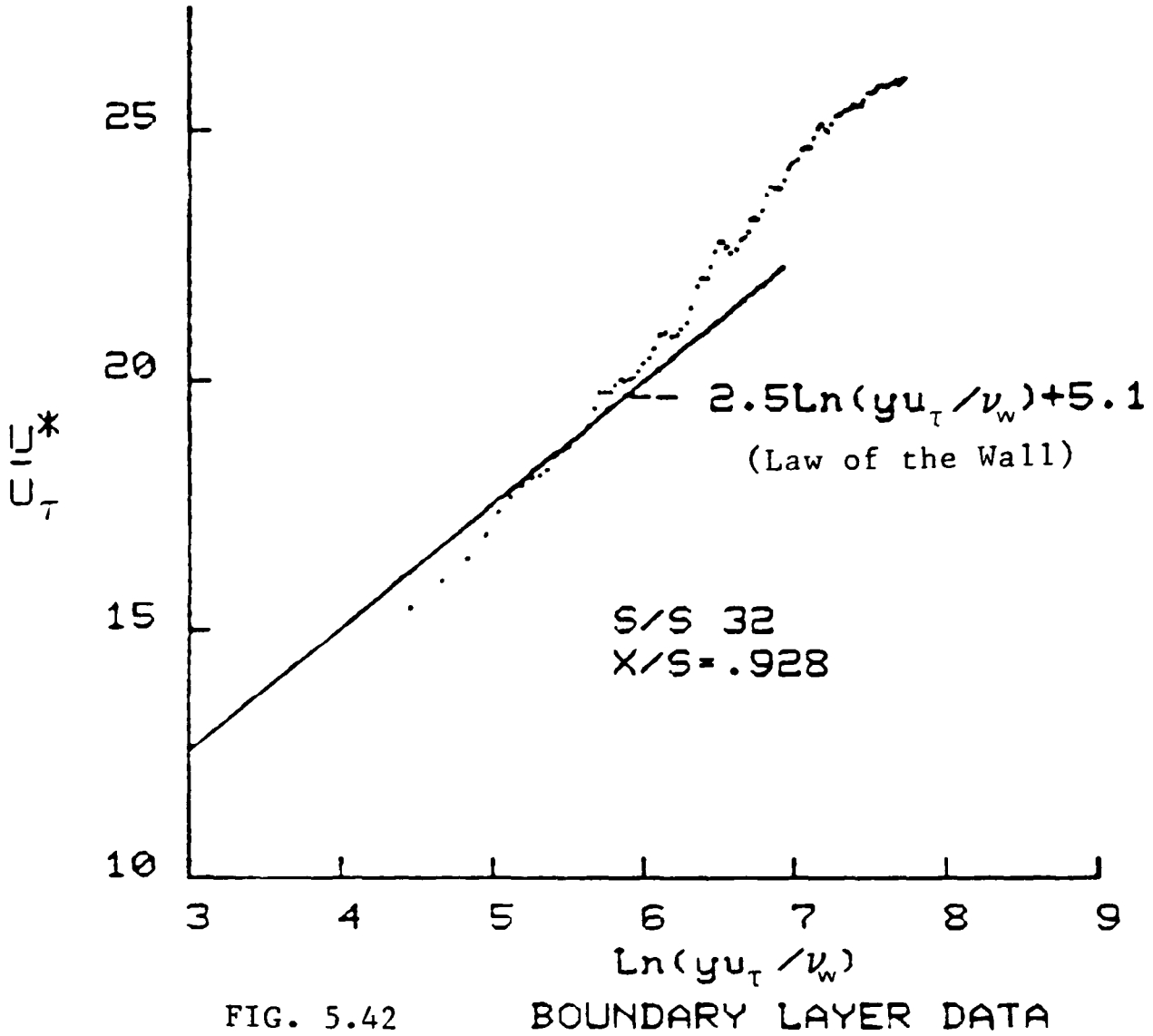

FIG. 5.42 BOUNDARY LAYER DATA

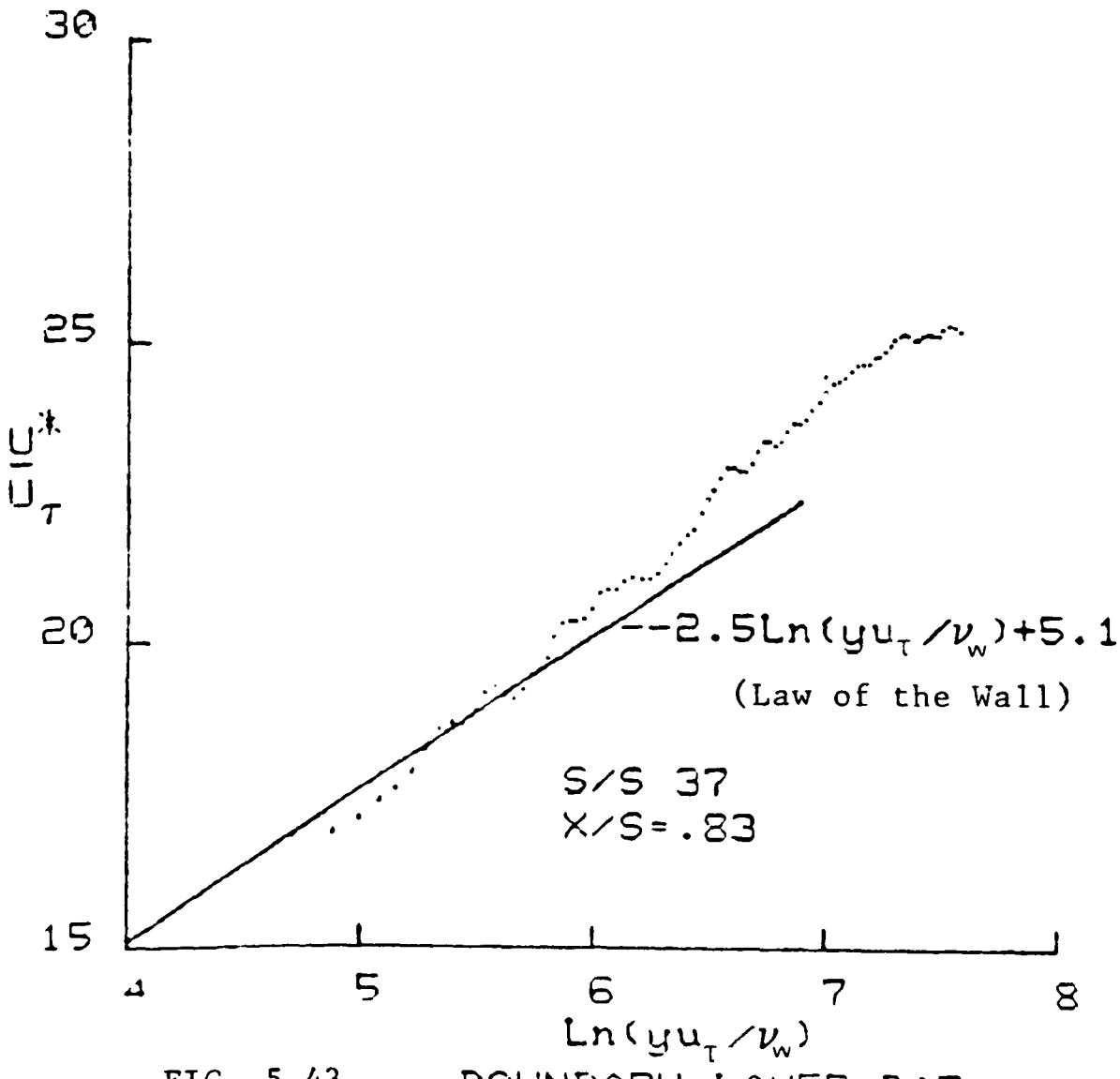

FIG. 5.43 BOUNDARY LAYER DATA

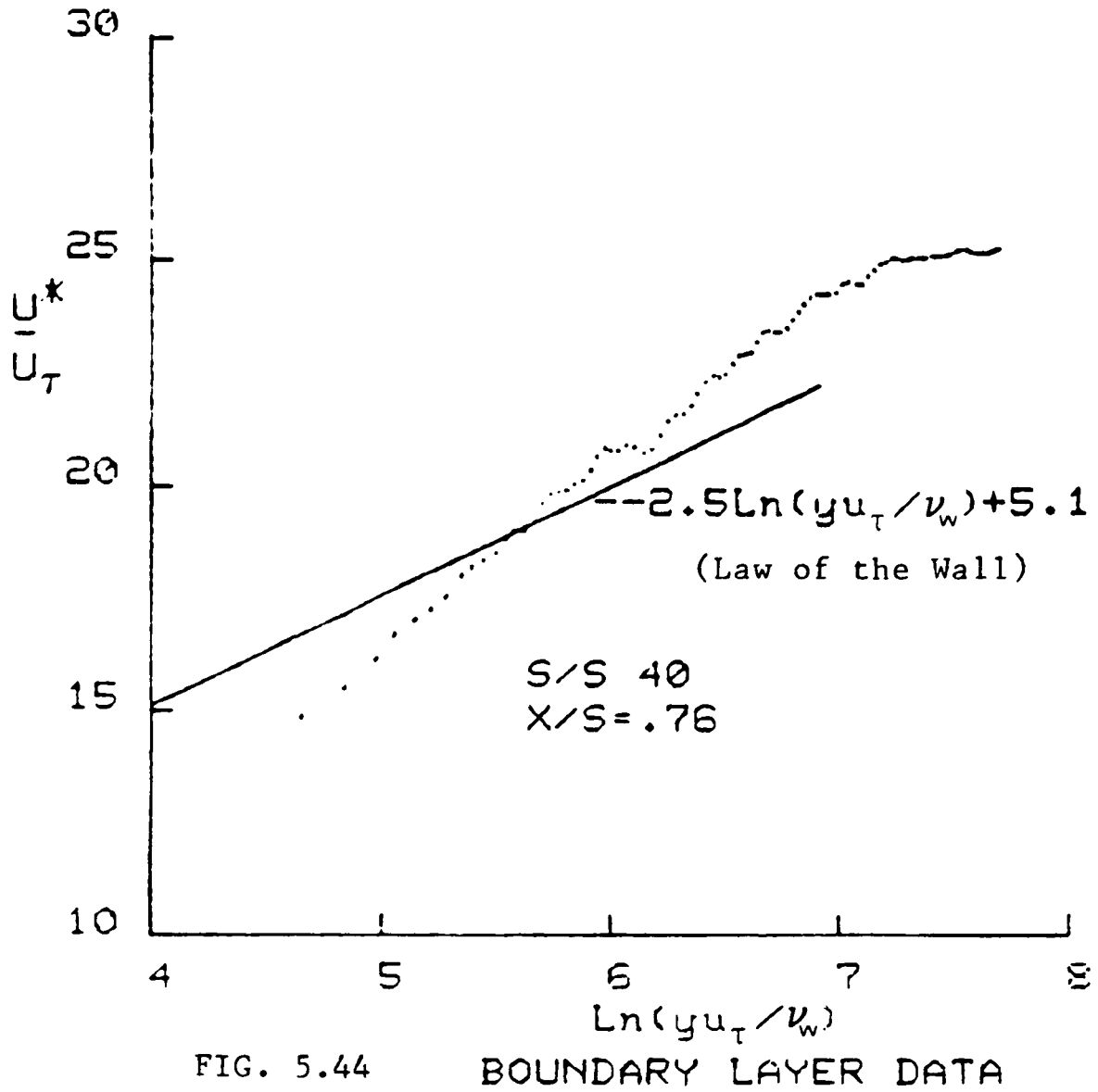

FIG. 5.44 BOUNDARY LAYER DATA

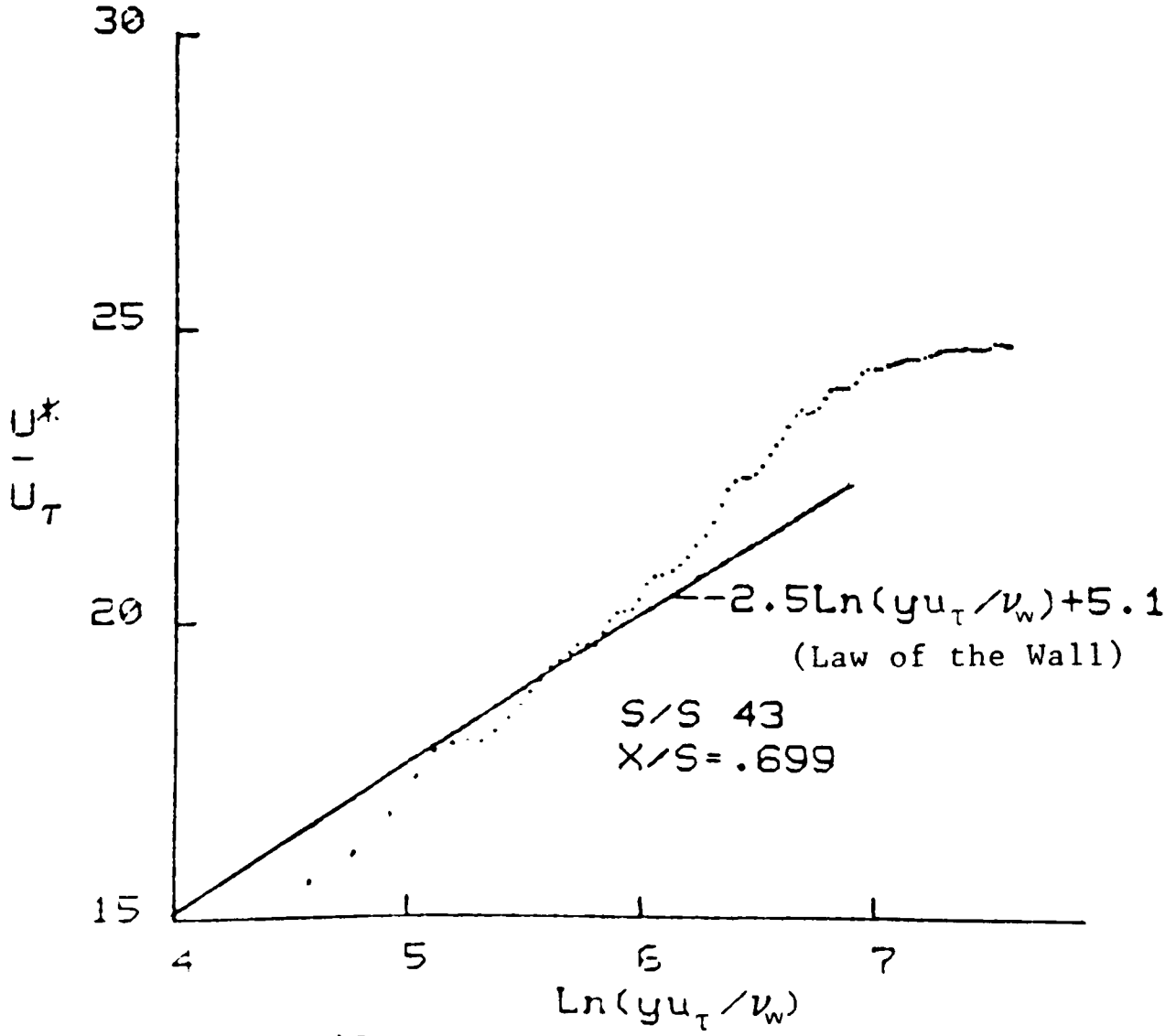

FIG. 5.45 BOUNDARY LAYER DATA

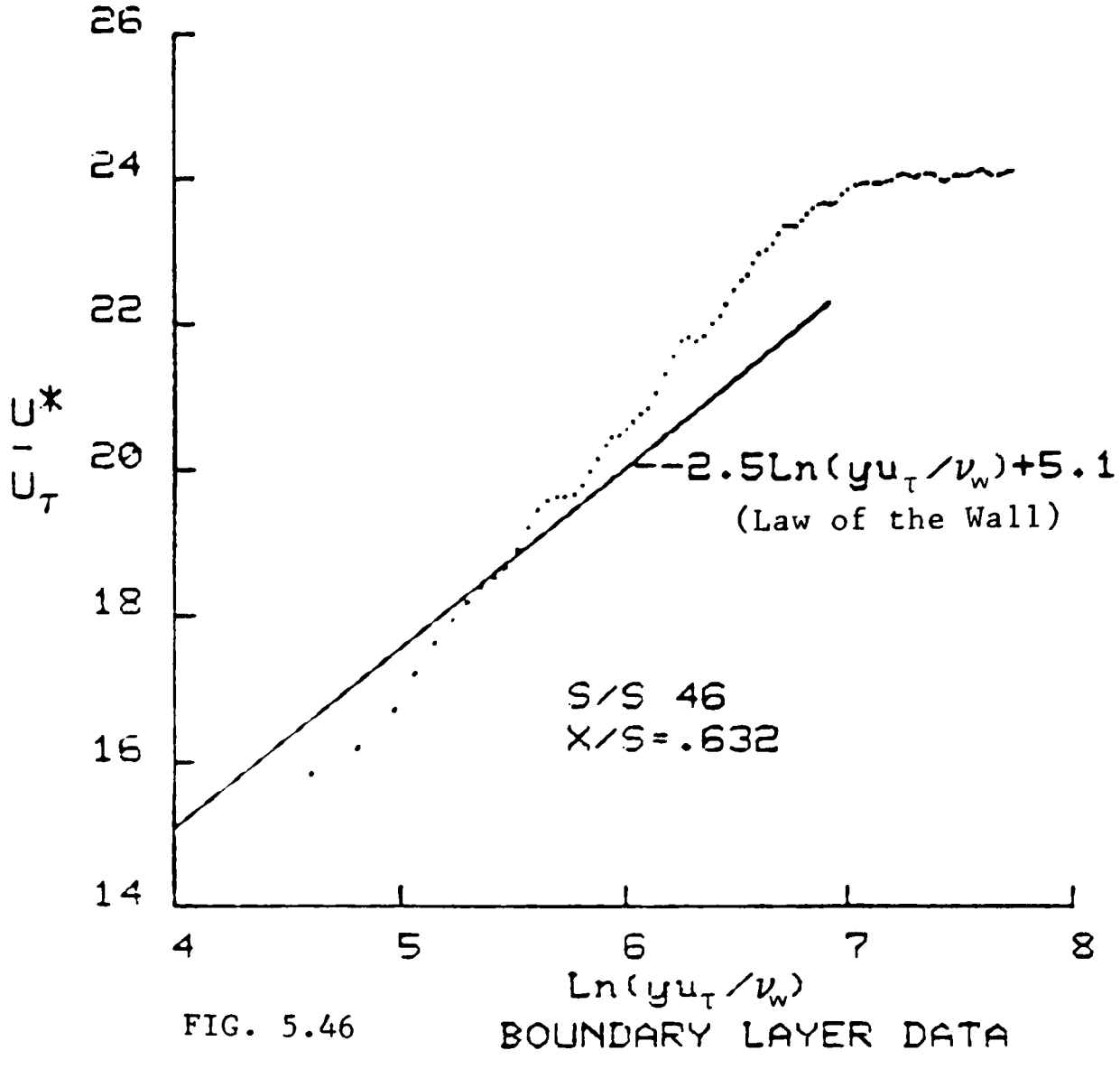

FIG. 5.46

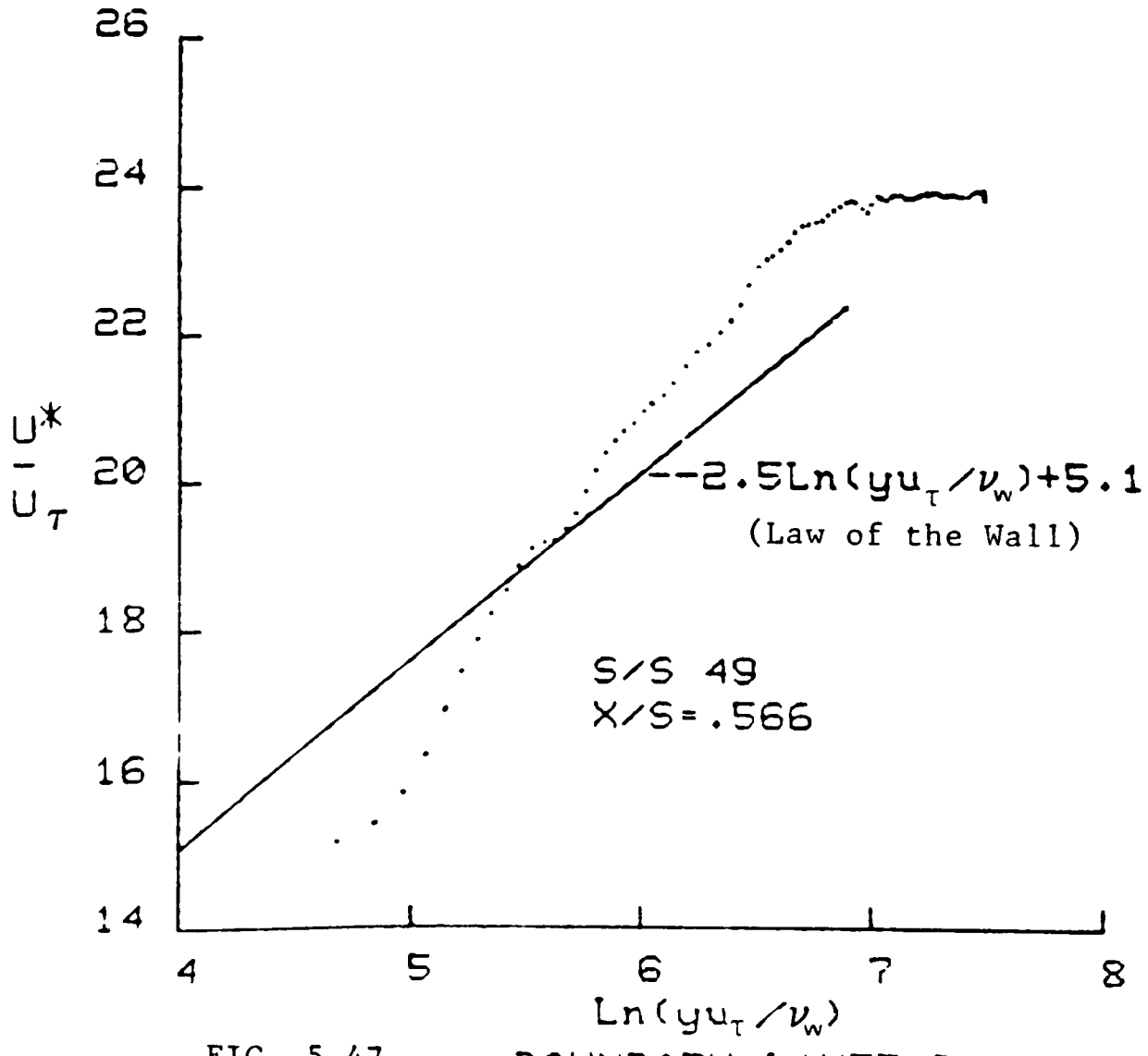

FIG. 5.47

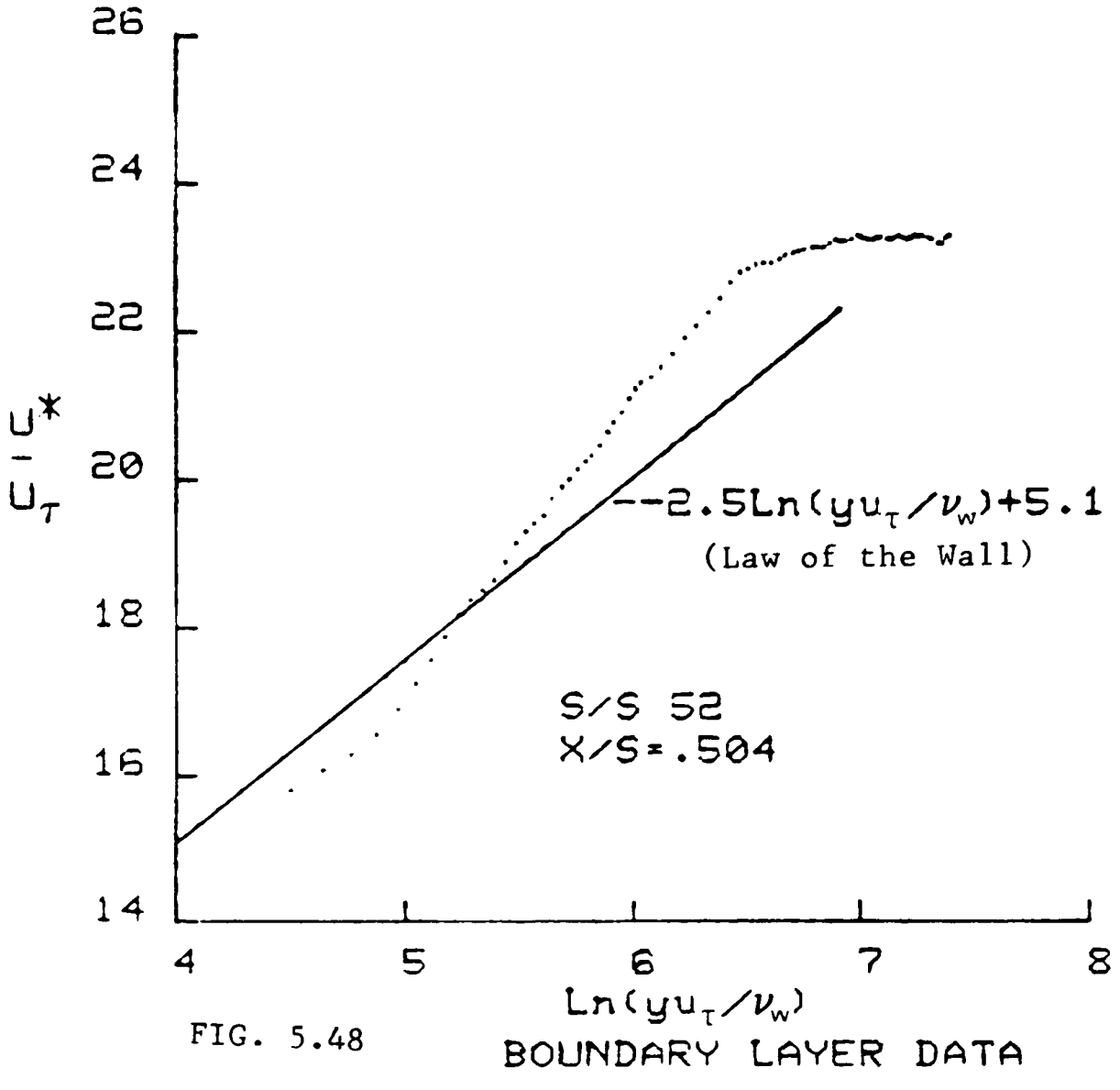

FIG. 5.48

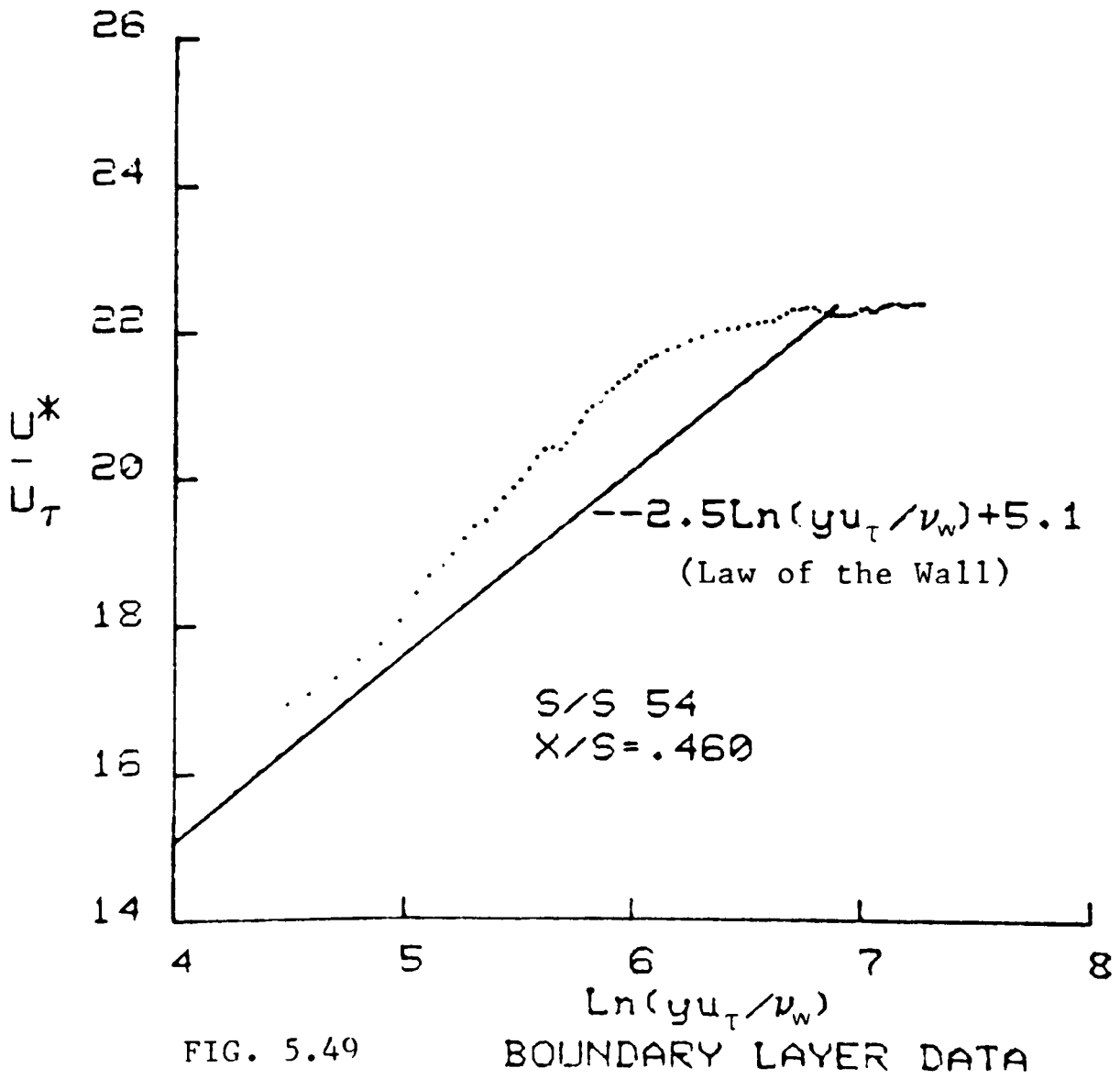

FIG. 5.49

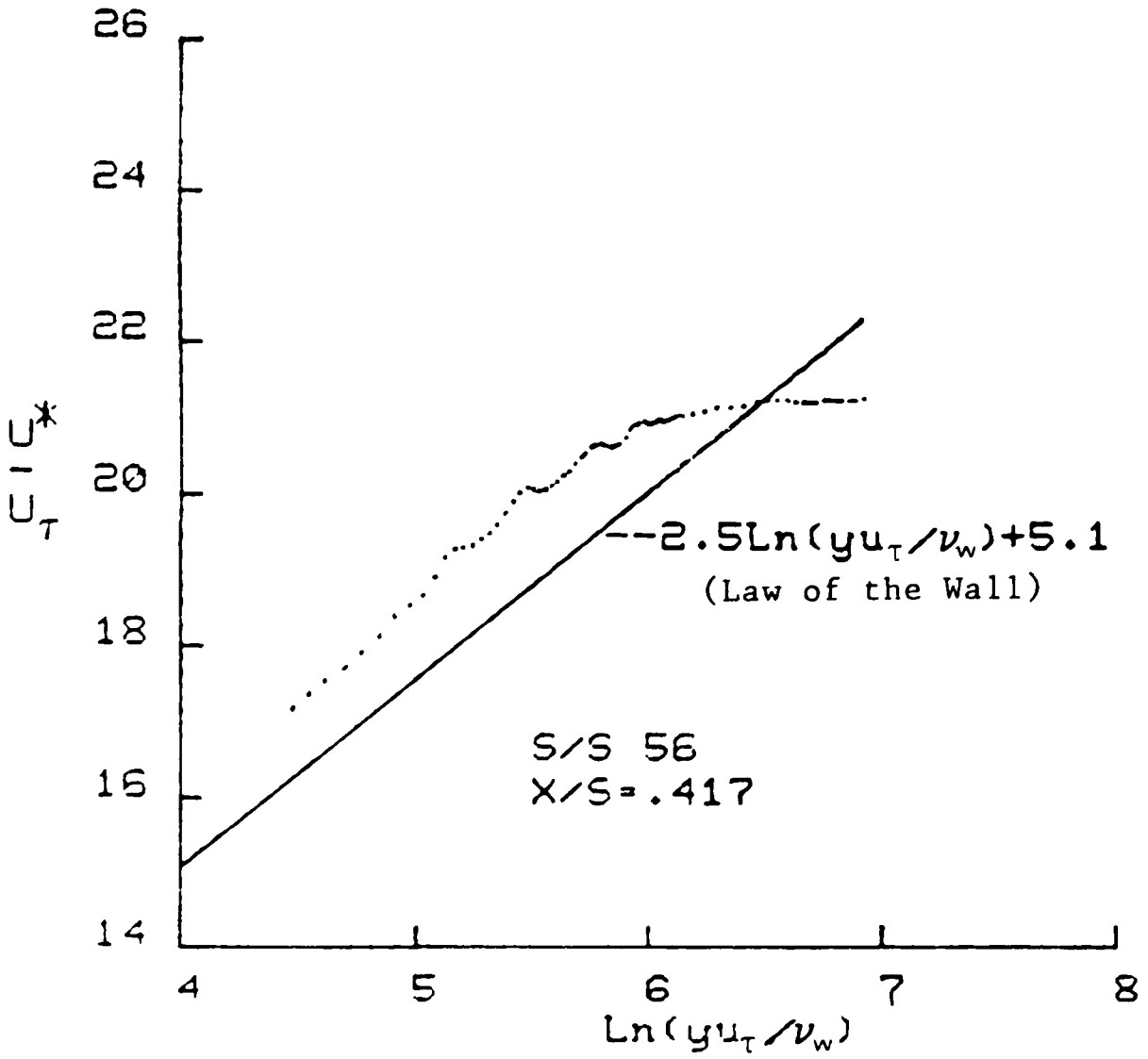

FIG. 5.50 BOUNDARY LAYER DATA

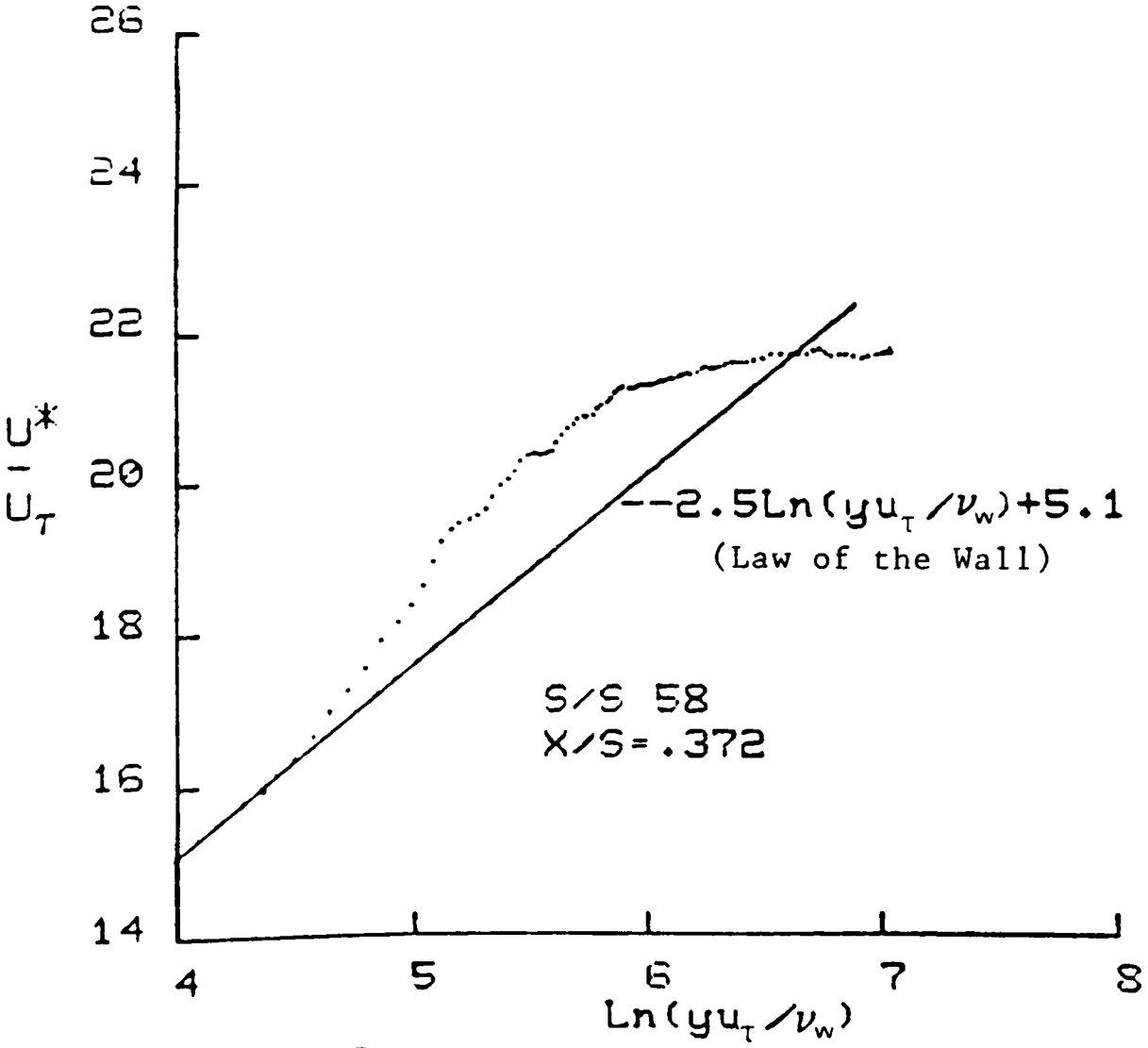

FIG. 5.51 BOUNDARY LAYER DATA

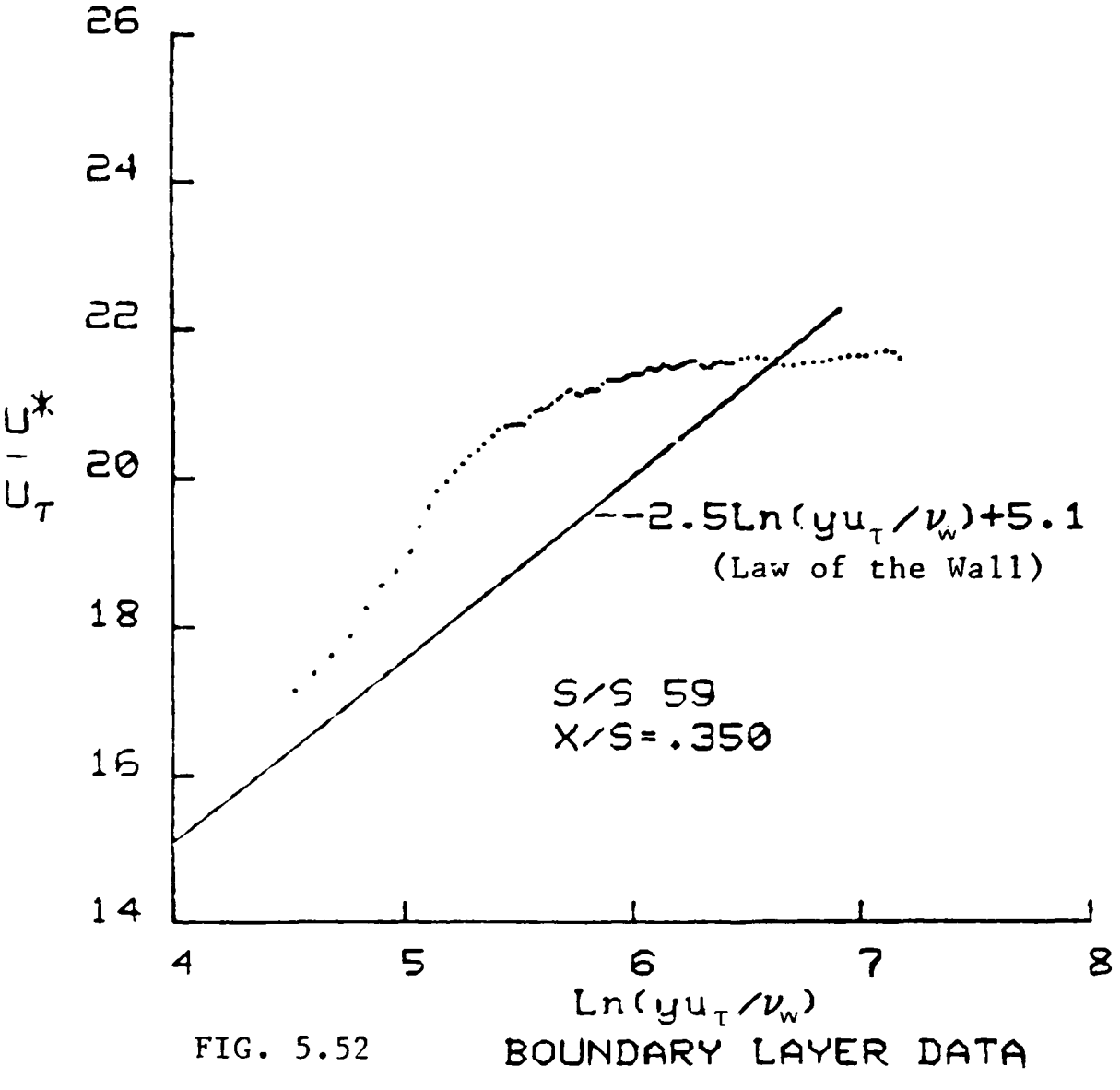

FIG. 5.52 BOUNDARY LAYER DATA

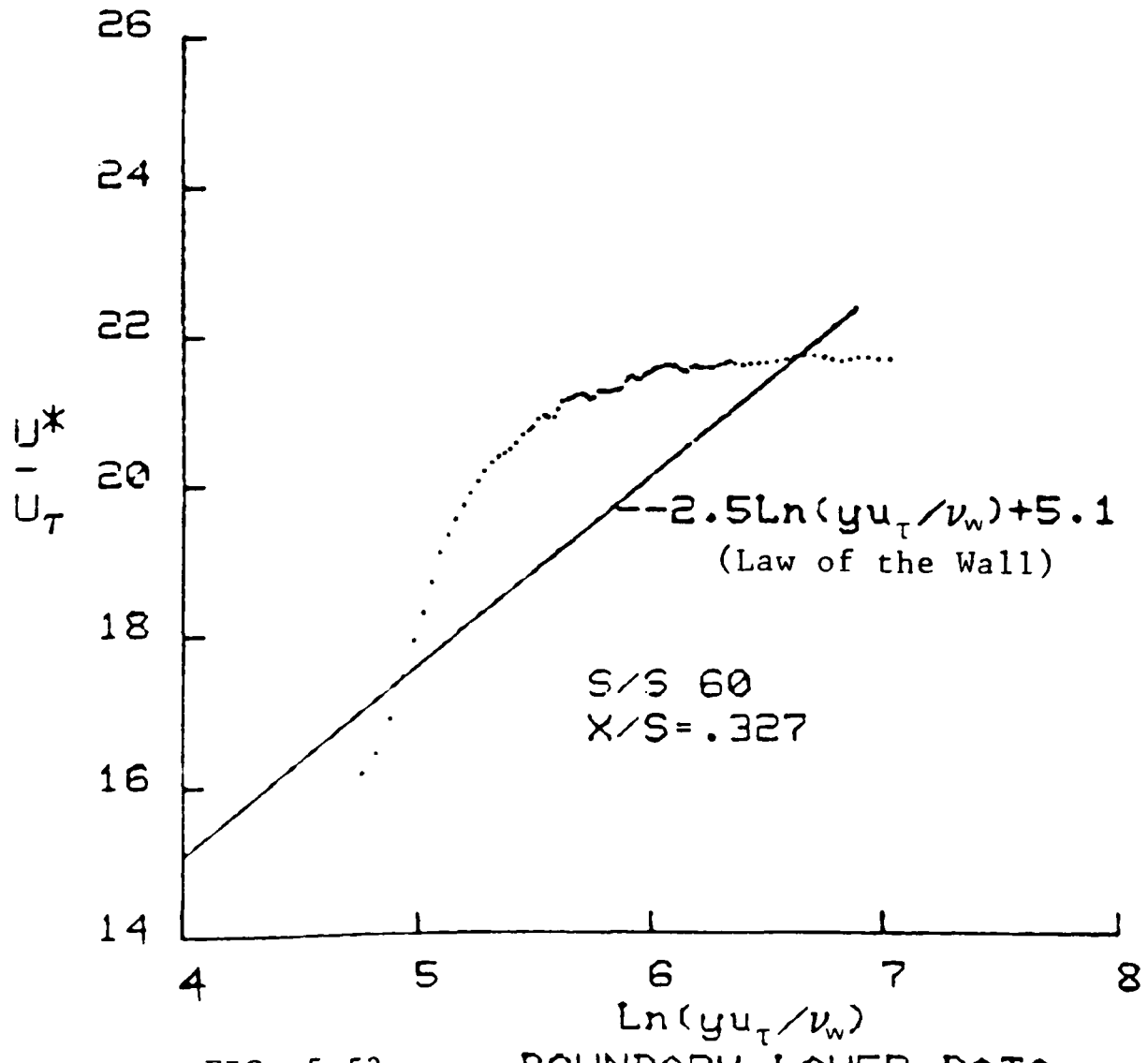

FIG. 5.53 BOUNDARY LAYER DATA

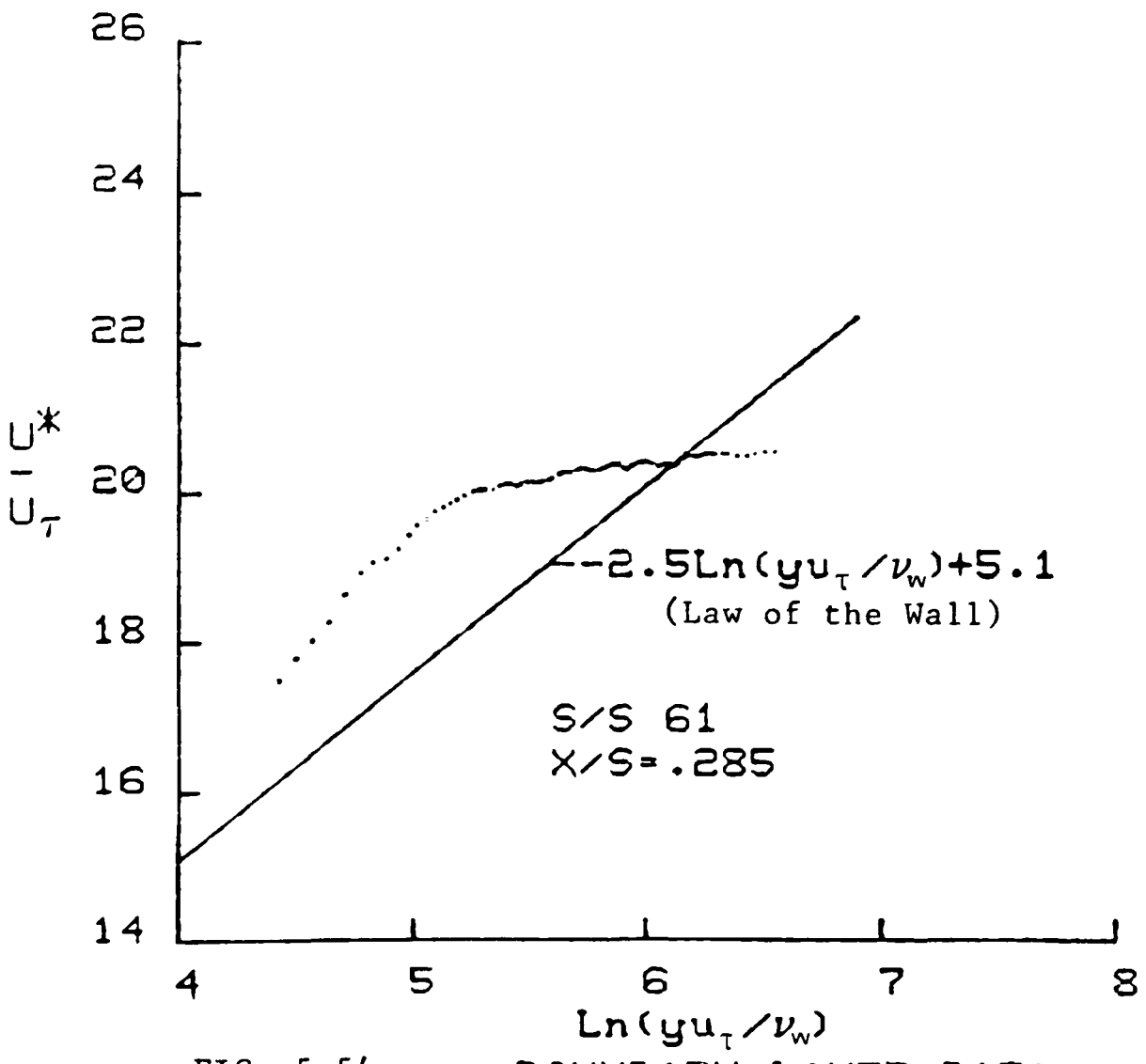

FIG. 5.54 BOUNDARY LAYER DATA

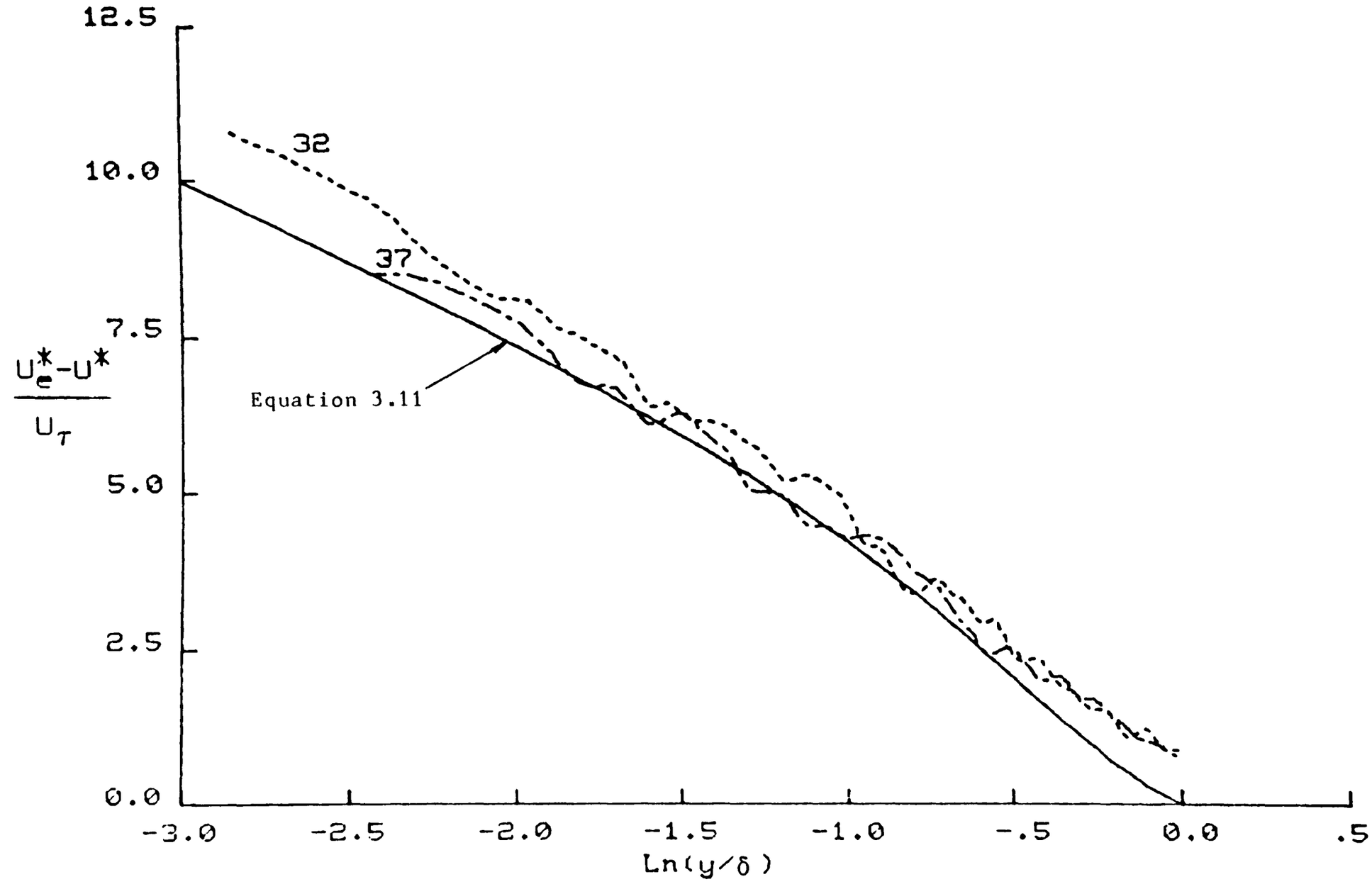

FIG. 5.55 EXP. DATA VS DEFECT LAW

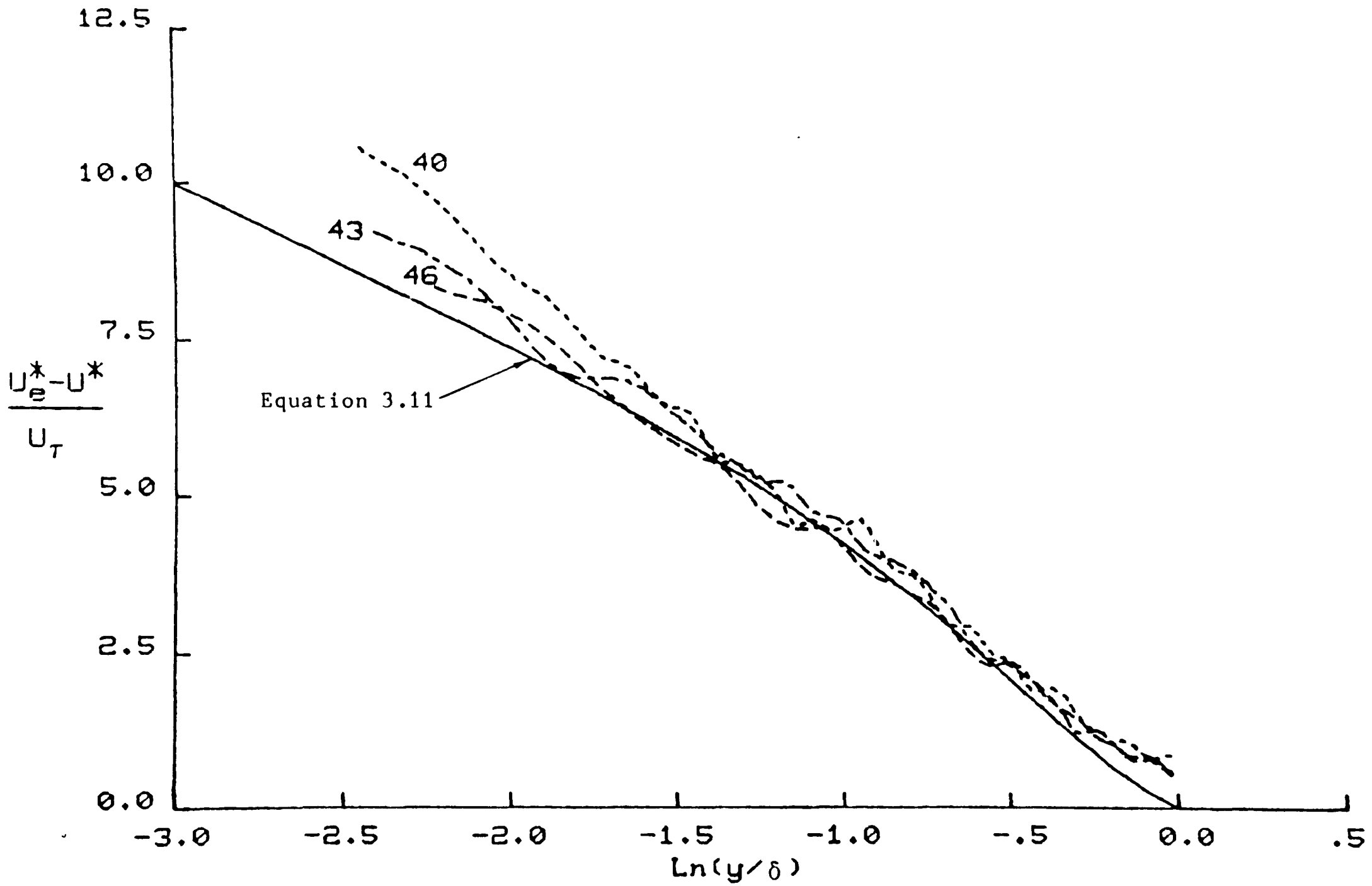

FIG. 5.56 EXP. DATA VS DEFECT LAW

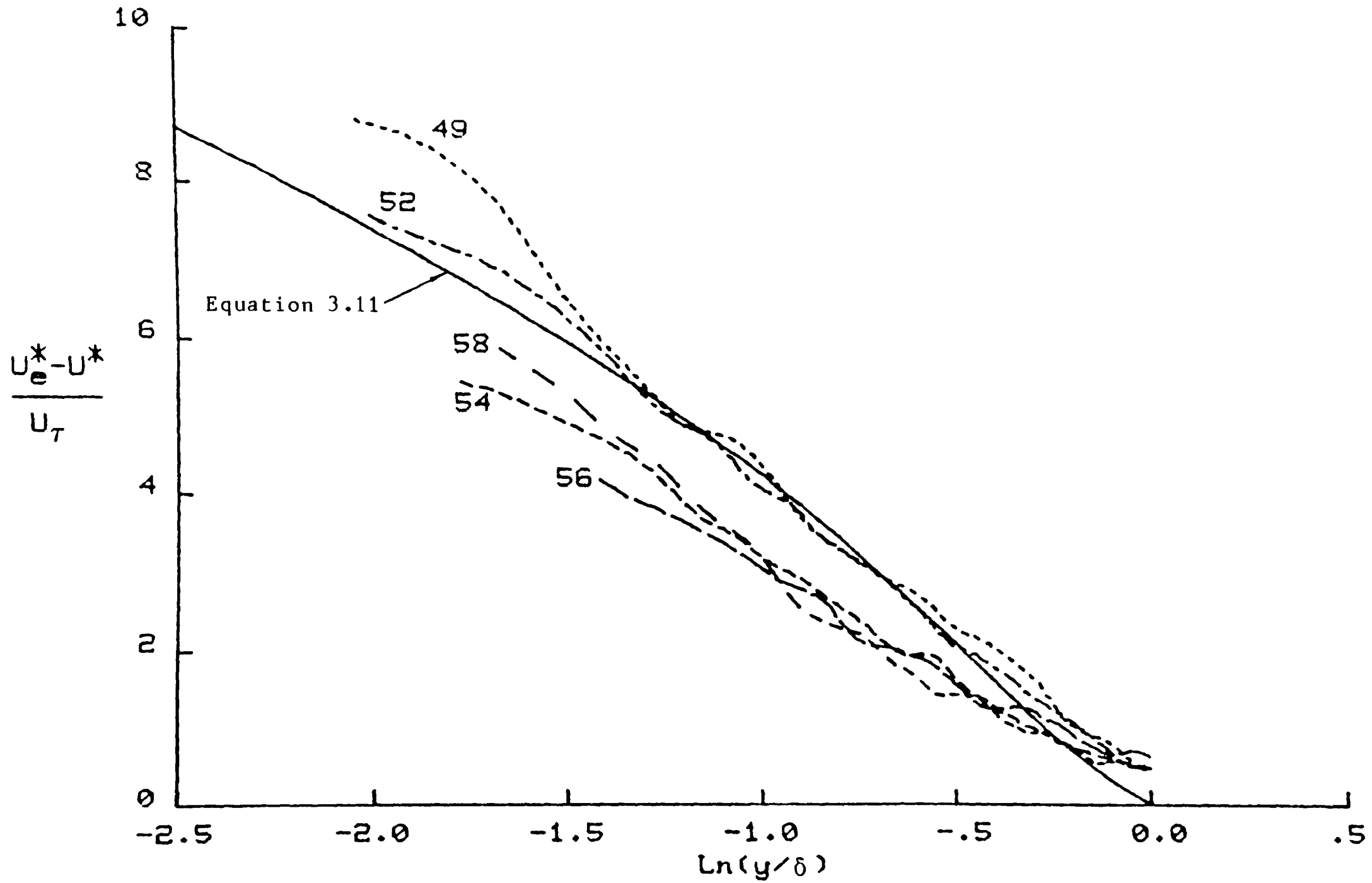

FIG. 5.57 EXP. DATA VS DEFECT LAW

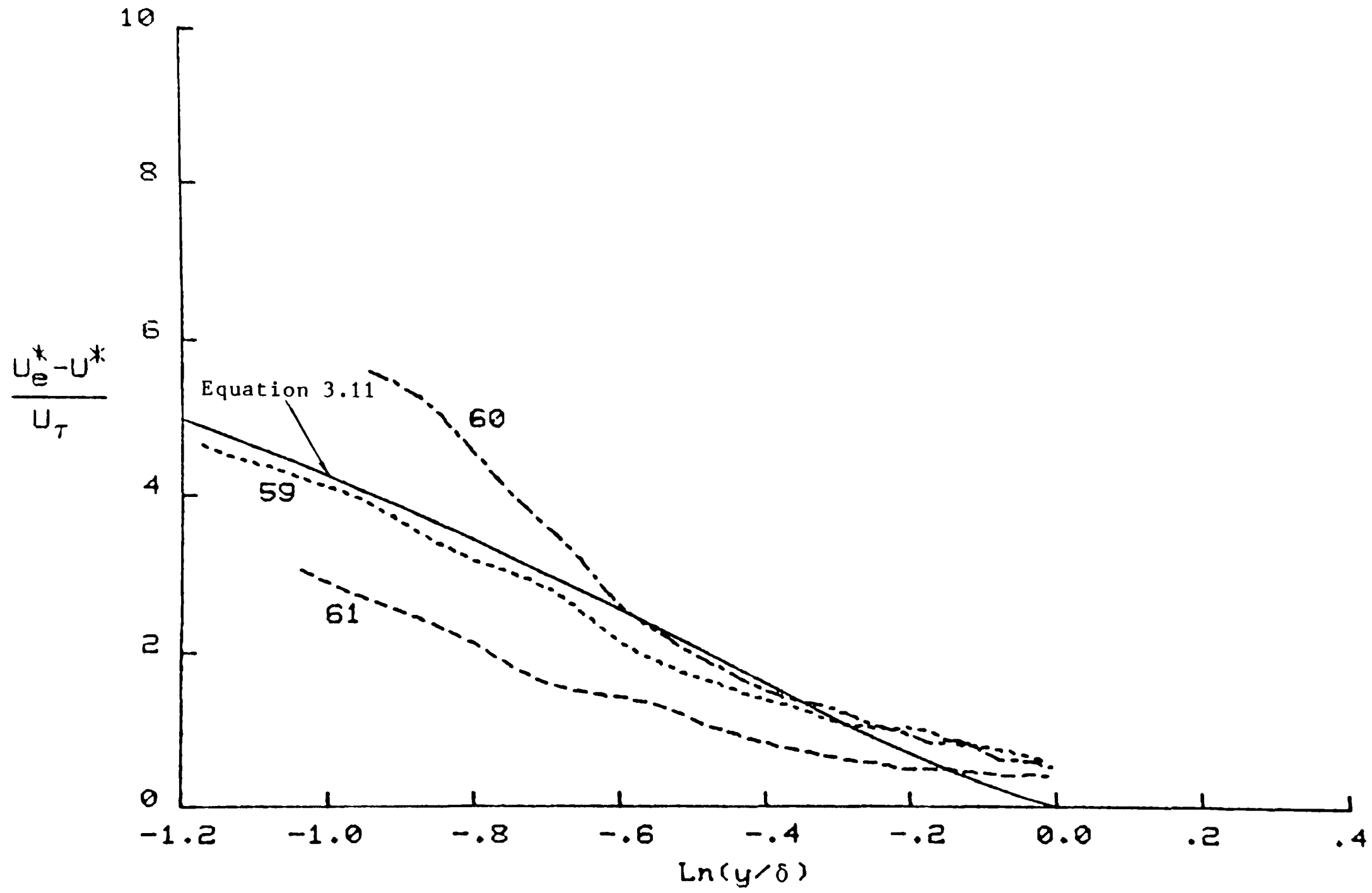

FIG. 5.58 EXP. DATA VS DEFECT LAW

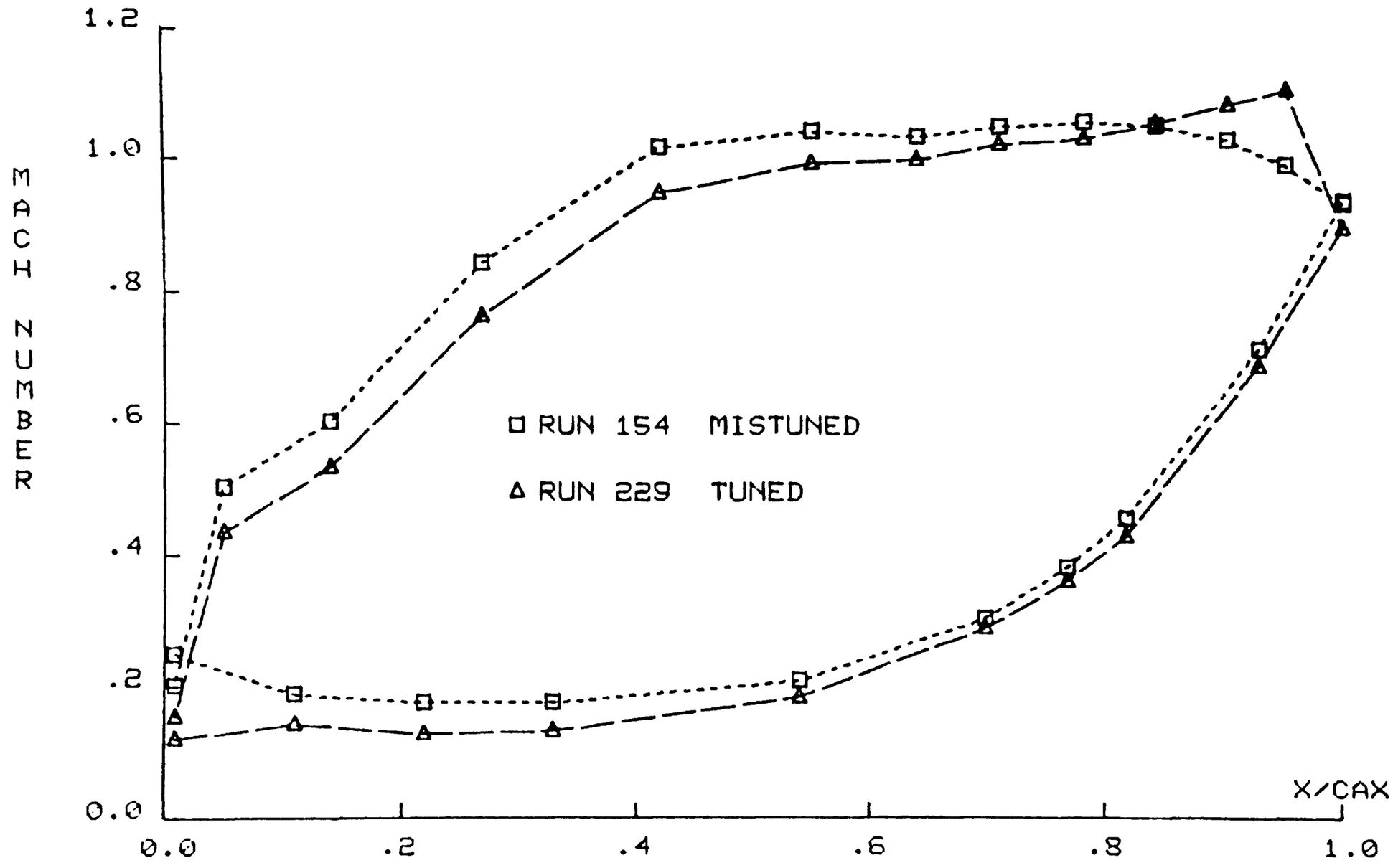

FIG.6.1 EFFECT OF TUNING ON SURFACE MACH NUMBERS